UCAM

UNIVERSIDAD CATÓLICA DE MURCIA

ESCUELA INTERNACIONAL DE DOCTORADO
Programa de Doctorado en Tecnologías de la Computación e Ingeniería Ambiental

Evaluación de la utilidad de datos de satélite para modelización hidrológica de cuencas no aforadas en América Central

Autor:

Pablo Blanco Gómez

Directores:

Dr. D. Javier Senent Aparicio

Dra. Dña. Patricia Jimeno Sáez

Murcia, septiembre de 2021

UCAM
UNIVERSIDAD CATÓLICA
DE MURCIA

ESCUELA INTERNACIONAL DE DOCTORADO
Programa de Doctorado en Tecnologías de la Computación e Ingeniería Ambiental

Evaluación de la utilidad de datos de satélite para modelización hidrológica de cuencas no aforadas en América Central

Autor:
Pablo Blanco Gómez

Directores:
Dr. D. Javier Senent Aparicio
Dra. Dña. Patricia Jimeno Sáez

Murcia, septiembre de 2021

AUTORIZACIÓN DEL DIRECTOR DE LA TESIS PARA SU PRESENTACIÓN

El Dr. D. Javier Senent Aparicio y la Dra. Dña. Patricia Jimeno Sáez como Directores de la Tesis Doctoral titulada "Evaluación de la utilidad de datos de satélite para modelización hidrológica de cuencas no aforadas en América Central" realizada por D. Pablo Blanco Gómez en el Programa de Doctorado en Tecnologías de la Computación e Ingeniería Ambiental, **autoriza su presentación a trámite** dado que reúne las condiciones necesarias para su defensa.

Lo que firmo, para dar cumplimiento al Real Decreto 99/2011 de 28 de enero, en Murcia a 25 de septiembre de 2021.

Firmado por JAVIER MELCHOR SENENT APARICIO - NIF:48394193P el día 28/09/2021 con un certificado emitido por ACCVCA-120

Firmado por JIMENO SAEZ PATRICIA - 48520499K el día 28/09/2021 con un certificado emitido por AC FNMT Usuarios

COMPENDIO DE PUBLICACIONES

Esta memoria se presenta en la modalidad de compendio de publicaciones. Los artículos publicados que integran la tesis son los siguientes:

- **Publicación 1:** Blanco-Gómez, P.; Jimeno-Sáez, P.; Senent-Aparicio, J.; Pérez-Sánchez, J. Impact of climate change on water balance components and droughts in the Guajoyo River Basin (El Salvador). Water 2019, 11, 2360. https://doi.org/10.3390/w11112360

- **Publicación 2:** Senent-Aparicio, J., Blanco-Gómez, P., López-Ballesteros, A., Jimeno-Sáez, P. (2021). Evaluating the Potential of GloFASERA5 River Discharge Reanalysis Data for Calibrating the SWAT Model in the Grande San Miguel River Basin (El Salvador). Remote Sens. 2021, 13, 3299. https://doi.org/10.3390/rs13163299

- **Publicación 3:** Jimeno-Sáez, P.; Blanco-Gómez, P.; Pérez-Sánchez, J.; Cecilia, J.M. and Senent-Aparicio, J. Impact Assessment of Gridded Precipitation Products on Streamflow Simulations over a Poorly Gauged Basin in El Salvador. Water 2021, 13, 2497. https://doi.org/10.3390/w13182497

AGRADECIMIENTOS

En primer lugar, me gustaría agradecer a mis directores de tesis, el Dr. Javier Senent Aparicio y la Dra. Patricia Jimeno Sáez, por su gran esfuerzo, apoyo y dedicación, sin los que esta tesis doctoral no habría sido posible.

De igual modo, es obligado el reconocimiento al Dr. José María Cecilia Canales por sus ánimos y empeño en la realización de este trabajo, que se ha desarrollado en colaboración entre la Universidad Católica de Murcia y la empresa Vielca Ingenieros, S.A. Las gracias más sinceras deben extenderse entre el resto de personas de ambas instituciones que han participado en la consecución de los objetivos de este trabajo.

Agradezco también el apoyo brindado desde el Ministerio de Medio Ambiente y Recursos Naturales (MARN) de El Salvador, facilitando una parte importante de la documentación de base de las investigaciones realizadas.

Finalmente, me gustaría agradecer a mi familia, en especial a Ramón, Santiago y María Pilar, por su apoyo y amor sin condiciones.

“El clima está cambiando, nosotros también deberíamos”.

ÍNDICE GENERAL

AUTORIZACIÓN DE LOS DIRECTORES
COMPENDIO DE PUBLICACIONES
AGRADECIMIENTOS
ÍNDICE GENERAL....13
SIGLAS Y ABREVIATURAS....15
ÍNDICE DE FIGURAS Y TABLAS....17
I- INTRODUCCIÓN....25
I.1 Justificación de la investigación....25
I.2 Objetivos....28
I.3 Estructura del documento....29
II- ANTECEDENTES Y ESTADO DEL ARTE....33
III- METODOLOGÍA DE INVESTIGACIÓN....43
III.1 Características de las zonas de estudio....43
III.2 Modelo hidrológico SWAT....48
III.2.1 Componentes hidrológicas del modelo SWAT....50
III.2.2 Análisis de sensibilidad, calibración y validación del modelo hidrológico SWAT....54
III.3 Manejo de escenarios de cambio climático....56
III.3.1 Herramienta de Cambio Climático (CCT)....57
III.3.2 Escenarios de cambio climático....59
III.4 Productos satelitales de precipitación y temperatura....65
III.4.1 ERA5....66
III.4.2 CHIRPS y CHIRTS....66
III.4.3 CFSR....67
III.4.4 MSWEP....68
III.4.5 PERSIANN-CDR....68
III.4.6 CMORPH....68
IV- PUBLICACIONES....71
IV.1 Publicación 1: Impact of Climate Change on Water Balance Components and Droughts in the Guajoyo River Basin (El Salvador)....73

IV.2 Publicación 2: Evaluating the Potential of GloFASERA5 River Discharge Reanalysis Data for Calibrating the SWAT Model in the Grande San Miguel River Basin (El Salvador) 99

IV.3 Publicación 3: Impact Assessment of Gridded Precipitation Products on Streamflow Simulations over a Poorly Gauged Basin in El Salvador 121

IV.4 Síntesis de resultados y discusión 147

IV.4.1 Impacto del cambio climático en las componentes del balance hídrico 147

IV.4.2 Uso de la serie de caudales de GloFAS-ERA5 para calibrar el modelo SWAT 154

IV.4.3 Impacto de los productos satelitales de precipitación en la simulación de caudales en cuencas con escasez de datos de aforo 161

IV.5 Conclusiones y líneas de investigación futura 168

V- REFERENCIAS BIBLIOGRAFICAS 175

APÉNDICE: CALIDAD DE LAS PUBLICACIONES 203

SIGLAS Y ABREVIATURAS

95PPU	95% de la sensibilidad de la predicción
BS	Puntuación de sesgo
CCT	Herramienta de Cambio Climático
CDF	Función de densidad acumulada
CFSR	Climate Forecast System Reanalysis
CHA	Estación hidrometeorológica Chapeltique
CHIRPS	Climate Hazards group Infrared Precipitation with Stations
CHIRTS	Climate Hazards group Infrared Temperature with Stations
CMIP5	Coupled Model Intercomparison Project Phase 5
CMORPH	Climate Prediction Center MORPHing method
CN	Número de curva
CSI	Índice de éxito crítico
DA_RCHG	Recarga acuífera
DEL	Estación hidrometeorológica El Delirio
DEM	Modelo Digital de Elevaciones
DRI	Daily Rainfall Intensity
ECMWF	European Center for Medium-Range Weather Forecasts
ERA5	ECMWF Re-Analysis 5
ESM	Modelos del Sistema Terrestre
FAR	Ratio de falsa alarma
GCM	Modelos de Circulación General
GIS	Sistemas de Información Geográfica
GloFAS-ERA5	Global Flood Awareness System-ERA5
GP	Gridded Precipitación
GRB	Cuenca del rio Guajoyo
GSM	Cuenca del río Grande de San Miguel
HadGEM2-ES	Hadley Centre Global Environmental Model version 2 Earth System configuration

HRU	Unidades de Respuesta Hidrológica
IPSL-CM5A-LR	Institut Pierre Simon Laplace Climate Model version 5A Low Resolution
MARN	Ministerio de Medio Ambiente y Recursos Naturales de El Salvador
MIG	Estación hidrometeorológica San Miguel
MIROC-ESM-CHEM	Model for Interdisciplinary Research on Climate Earth System Model with an atmospheric CHEMistry component
MSD	Mid-Summer Drought o Canícula
MSWEPv1.1	Multi-Source Weighted Ensembled Precipitation version 1.1
NCEP	National Center for Environmental Prediction
PERSIANN-CDR	Precipitation Estimate from Remotely Sensed Information using Artificial Neural Networks-Climate Data Records
POD	Probabilidad de detección
RCP	Representative Concentration Pathways
SCS	Soil Conservation Service
SPI	Standardized Precipitation Index
SRI	Standardized Runoff Index
SUFI-2	Sequential Uncertainty Fitting version 2
SWAT	Soil and Water Assessment Tool
SWAT-CUP	SWAT-Calibration Uncertainty Program
USGS	United States Geological Survey
VIL	Estación hidrometeorológica Villerías
WYLD	Producción total de agua

ÍNDICE DE FIGURAS Y TABLAS

ÍNDICE DE FIGURAS

Figura 1. Mapa de localización de la cuenca del río Guajoyo: (a) Ubicación de la República de El Salvador en Centroamérica; (b) Posición de la cuenca del río Guajoyo dentro de El Salvador; (c) Subcuencas, DEM, hidrografía y localización de estaciones hidrometeorológicas dentro de la cuenca 44

Figura 2. Localización de la cuenca del río Grande de San Miguel: (a) Posición de la cuenca del río GSM dentro de Centroamérica; (b) Subcuencas, DEM, hidrografía y localización de estaciones hidrometeorológicas dentro de la cuenca; (c) Mapa de suelos; (d) Mapa de usos del suelo.....47

Figura 3. Representación gráfica de la fase terrestre del ciclo hidrológico (Neitsch et al., 2011) 49

Figura 4. Proceso de trabajo de la Herramienta de Cambio Climático (CCT) (Vaguefi et al. 2017).....59

Figura 5. Regresión lineal de caudales observados y simulados para los periodos de (a) calibración (2006-2009), y (b) validación (2010-2012).....149

Figura 6. Comparativa de los valores medios mensuales de (a) precipitación y (b) temperatura entre el periodo histórico (1975-2005) y los escenarios de medio y largo término para RCP 4.5 y 8.5 del GCM HadGEM2-ES.....151

Figura 7. Distribución de la función de densidad de probabilidad por rangos para los productos satelitales y estaciones consideradas en el proyecto.....156

Figura 8. Comparación entre valores mensuales de precipitación de los productos ERA5, CHIRPS y CFSR y los valores observados, mediante gráficos de violín (izquierda), variaciones mensuales (centro) y dispersión (derecha).....157

Figura 9. Comparación entre valores mensuales de temperatura de los productos ERA5, CHIRTS y CFSR y los valores observados en MIG, mediante gráficos de violín (izquierda), variaciones mensuales (centro) y dispersión (derecha).....158

Figura 10. Comportamiento de los modelos sin calibrar con datos de ERA5, CHIRPS-CHIRTS y CFSR con los caudales mensuales observados.....159

Figura 11. Comportamiento de los modelos calibrados con datos de ERA5, CHIRPS-CHIRTS y CFSR con los caudales mensuales observados.....160

ÍNDICE DE TABLAS

Tabla 1. Parámetros de calibración del modelo SWAT en la cuenca GRB.....148

Tabla 2. Estadísticos de evaluación del modelo SWAT en las fases de calibración y validación 149

Tabla 3. Cálculo del índice Id para cada RCM.....150

Tabla 4. Variación de precipitación y temperatura respecto del periodo histórico para los escenarios RCP 4.5 y 8.5 152

Tabla 5. Análisis de tendencia para resultados mensuales y anuales de precipitación y temperatura para el periodo 2040-2099.....152

Tabla 6. Componentes del balance hídrico con SWAT para los distintos escenarios y periodos considerados 153

Tabla 7. Análisis de sequías en la cuenca GRB 154

Tabla 8. Comportamiento del modelo SWAT comparado con los datos de caudal de GloFAS.....160

Tabla 9. Índices de detección para los distintos GP en las estaciones hidrometeorológicas de referencia de la cuenca.....162

Tabla 10. Estadísticos diarios y mensuales de la comparativa entre GP y la precipitación observada en las estaciones PS-1 y PS-2.....163

Tabla 11. Clasificación de eventos de precipitación en función de su intensidad diaria (DRI, mm/día).....165

Tabla 12. Resultados del modelo SWAT calibrado con las estaciones hidrometeorológicas en las tres estaciones de aforos (SG-i) para los distintos GP evaluados.....166

Tabla 13. Resultados del modelo SWAT calibrado para cada GP en las tres estaciones de aforos (SG-i).....167

RESUMEN

La modelación hidrológica se emplea, entre otras razones, para conocer los caudales circulantes por los ríos, estableciendo los recursos disponibles para los distintos usos posibles del agua. Está basada en ecuaciones físicas que resuelven los problemas de las abstracciones iniciales – considerando dentro de ellas tanto la intercepción vegetal como la del terreno –, la infiltración, el proceso lluvia-escorrentía, en el que se determina la cantidad de agua que por cada unidad espacial se va aportando a los cauces principales y la propagación de caudales, por el que el agua se acumula y desplaza a través de los canales fluviales.

Las variables climáticas, junto con las características del terreno (orografía y tipo de suelo) y las coberturas vegetales o usos del suelo, resultan fundamentales para poder alimentar los modelos hidrológicos y obtener resultados que respondan de manera coherente al comportamiento de la cuenca. Para ello será necesario, adicionalmente, conocer los caudales circulantes por el río.

La falta de esta información tanto a nivel espacial como temporal constituye un limitante tradicional a este tipo de estudios y ha condicionado su aplicabilidad en cuencas no aforadas. Sin embargo, en la actualidad existen productos, basados en el reanálisis de imagen satelital, que ayudan a mejorar el conocimiento de alguna de estas variables de manera distribuida y con diferentes temporalidades, llegando en algunos casos a proveer series de más de 40 años y con variabilidad infradiaria.

En la presente investigación se ha empleado el modelo hidrológico semi-distribuido SWAT para simular los caudales diarios y mensuales en dos cuencas estratégicas de la República de El Salvador, en Centroamérica.

La primera de ellas, la cuenca del río Guajoyo (GRB), es una cuenca en estado natural afectada por importantes figuras de protección medioambiental que le confieren un especial interés para llevar a cabo el estudio de la afectación del cambio climático en este tipo de cuencas tanto por los problemas derivados de las inundaciones como los relativos a las sequías. A partir del estudio realizado se pudo observar como los incrementos de temperatura se asocian en estas latitudes con un descenso de la precipitación media anual, lo que conlleva una mayor duración e intensidad de las sequías.

Por otro lado, se han realizado dos estudios diferenciados en la cuenca del río Grande de San Miguel (GSM), uno dirigido a determinar la aplicabilidad de un

producto que establece los caudales medios diarios a partir de reanálisis de imagen satelital para la calibración de modelos y otro dedicado a evaluar la validez de cinco productos satelitales de precipitación para la modelación hidrológica de la cuenca.

Dentro de esta cuenca se utilizaron los registros de estaciones meteorológicas y de estaciones de aforo que permitieron calibrar y validar los modelos hidrológicos de ambos estudios, pudiendo comprobar la bondad de los distintos productos para cumplir con los objetivos marcados, que además de la determinación de caudales perseguían: establecer la capacidad de los mismos para detectar distintas intensidades de lluvia; ajustar los parámetros de los modelos hidrológicos y comprobar la validez del producto GloFAS para representar los caudales circulantes; así como, comparar los productos satelitales de precipitación entre sí y con los registros de las estaciones para determinar los que resultan más convenientes para modelar la cuenca.

Entre los distintos estudios se ha podido comprobar como los productos satelitales de precipitación tienden a sobreestimar el número y la intensidad de los eventos de precipitación; si existe una correlación entre las series de precipitación provenientes de reanálisis y los valores observados en la cuenca, los caudales provenientes de GloFAS son adecuados para la calibración de modelos hidrológicos; y, el empleo de productos satelitales de precipitación en la modelación hidrológica de cuencas fluviales presenta resultados aceptables en las cuencas de los ríos GRB y GSM.

Palabras clave: SWAT, modelación hidrológica, General Circulation Models, Gridded Precipitation, productos satelitales, Climate Change Toolkit, cambio climático.

ABSTRACT

Hydrological modelling is used to know the river discharge, among other reasons, and to establish the resources available for the different possible uses of water. It is based on physical equations that solve the problems of the initial abstractions –considering within them both the canopy and the soil surface interceptions –, the infiltration, the rainfall-runoff process, in which the amount of water contributed to the main channels per spatial unit is determined and the propagation of flows, by which the water accumulates and moves through the fluvial channels.

The climatic variables, together with terrain characteristics (orography and type of soil) and the vegetation cover or land uses, are essential to feed the hydrological models and obtain results that respond in a coherent way to the behaviour of the watershed. Additionally, it will be necessary to know the circulating flows to the main channel.

The lack of this information, both at a spatial and temporal level, constitutes a traditional limitation to this type of studies and has conditioned its applicability in non-gauged basins. However, currently there are products, based on satellite image reanalysis, that help to improve the knowledge of some of these variables in a distributed manner and with different temporalities, in some cases providing series of more than 40 years and with infraday variability.

In this research, SWAT semi-distributed hydrological model has been used to simulate daily and monthly flows in two strategic watersheds of the Republic of El Salvador, in Central America.

The first of them, the Guajoyo river basin (GRB), is a basin in a natural state affected by important environmental protection figures that give it a special interest to carry out the study of the impact of climate change in this type of basin both due to the problems derived from floods and those related to droughts. From the study carried out, it was possible to observe how temperature increases are associated in these latitudes with a decrease in average annual precipitation, which leads to a greater duration and intensity of droughts.

On the other hand, two differentiated studies have been carried out in the Rio Grande de San Miguel (GSM) basin, one aimed at determining the applicability of a satellite product that establishes the average daily flows from image reanalysis for the

calibration of models. and another dedicated to evaluating the validity of five satellite precipitation products for the hydrological modelling of the watershed.

Within this basin, the records of climate stations and stream gauges were used for calibrating and validating the hydrological models of both studies, being able to verify the goodness of fit of the different products to meet the objectives, which, besides the determination of discharges, pursued: to establish their capacity to detect different rainfall intensities; to adjust the hydrological models parameters and to check the validity of the GloFAS product to represent the main river discharges; and finally, to compare the GP products among them and with the records of the gauging and streamflow measurements stations to determine those that are more convenient to model the watershed.

From the different studies, it has been possible to verify how the gridded precipitation products tend to overestimate the number and intensity of precipitation events; if a correlation between the precipitation series from reanalysis and the values observed in the gauges of the watershed exists, the flows from GloFAS are suitable for the calibration of hydrological models; and, in the end, the use of satellite precipitation products in the hydrological modelling of river basins presents acceptable results in the GRB and GSM watersheds.

Keywords: SWAT, hydrological modelling, General Circulation Models, Gridded Precipitation, satellite products, Climate Change Toolkit, climate change.

I - INTRODUCCIÓN

I- INTRODUCCIÓN

I.1 JUSTIFICACIÓN DE LA INVESTIGACIÓN

La modelación hidrológica se utiliza para evaluar una serie de problemas relacionados con las masas de agua, como son el cambio climático, los cambios de usos del suelo, la predicción de eventos extremos de inundación y sequías, o la planificación y gestión de recursos hídricos (Pfannerstill, Guse y Fohrer, 2014).

La precipitación es un parámetro fundamental en la simulación numérica de la respuesta hidrológica de una cuenca fluvial. Una reproducción precisa de la variabilidad espacio-temporal de la misma es crucial para simular con precisión los procesos hidrológicos.

Sin embargo, en muchos casos la información hidrometeorológica no está disponible en la resolución y con la cantidad de registros necesaria, lo que puede conllevar una mala respuesta de los modelos hidrológicos para la evaluación de recursos hídricos. Este hecho es bastante frecuente en los países en vías de desarrollo y en las áreas remotas, donde la disponibilidad de estaciones de medición, tanto de variables climáticas como de caudales, es inferior a la necesaria o es inexistente. En estos casos, además, aunque existan datos, en muchas ocasiones son muy pobres o su acceso está restringido debido a una política de difusión muy estricta (Duan et al., 2019).

El método tradicional de obtención de series de precipitación es a través de la red convencional de estaciones hidrometeorológicas, que en regiones con baja cobertura de estaciones suelen requerir de interpolación para llevar a cabo la modelación hidrológica, lo que a menudo introduce mayor incertidumbre en los modelos (Woldemeskel, Sivakumar y Sharma, 2013) e incluso diferencias significativas entre la precipitación real y la estimada (Senent-Aparicio et al., 2018b). Adicionalmente, las estaciones hidrometeorológicas no siempre son dispositivos precisos en la medición de la precipitación real, pudiendo producirse desviaciones por la presencia de viento en el entorno del orificio de medición, defectos en la instalación del dispositivo, pérdidas por humectación y

evaporación en sus paredes y otro tipo de errores (Jimeno-Sáez et al., 2020; Sevruk, 1996). Por tanto, existe una necesidad evidente de mejorar la recolección de información y/o explorar alternativas más precisas que los registros terrestres.

En este contexto, una fuente de información alternativa que puede ser de especial utilidad en zonas con baja o nula cobertura de estaciones hidrometeorológicas son los productos globales de precipitación (GP, por sus siglas en inglés) que proveen registros continuos de precipitación con amplia cobertura espacial y mucha mejor resolución que las estaciones terrestres (Soo et al., 2019).

Tan y Yang (2020) demostraron que la ausencia de registros de precipitación en más de un 20% de la serie afectaba de manera significativa a la simulación de caudales en climas tropicales. Para contrarrestar la escasez y mala calidad de los registros de observación, un gran número de estudios han comparado los GP con los registros existentes para evaluar su aplicabilidad para la modelación hidrológica en cuencas hidrográficas alrededor del mundo (Dhanesh et al., 2020; Mazzoleni, Brandimarte y Amaranto, 2019; Yin et al., 2021; Usman et al., 2021).

De igual modo, de manera adicional a la precipitación, la consideración de la temperatura condiciona los resultados en la modelación hidrológica, debido, principalmente, a su relación directa con la evapotranspiración potencial. A pesar de ello, no son muchos los casos en los que se ha analizado esta variable en profundidad (Tan et al., 2021). Ejemplos de este tipo de estudios son Tan et al. (2017) en el Sudeste asiático; y Duan et al. (2019) en Etiopía, empleando en ambos casos registros satelitales de precipitación y temperatura para desarrollar la modelación hidrológica.

Tal y como se ha referido, contar con registros suficientemente extensos y con la adecuada cobertura espacial de las variables climáticas es fundamental para obtener buenos resultados en la modelación hidrológica, puesto que permiten obtener estimaciones más precisas de los parámetros del modelo durante los procesos de calibración y validación de este, comparando sus resultados con los caudales observados en el río.

Sin embargo, en muchas ocasiones los registros de caudales no están disponibles en muchos puntos de la cuenca, especialmente en países en vías de

desarrollo, en donde, además, el número de estaciones operativas decrece rápidamente por la falta de mantenimiento de las mismas.

En este contexto, la existencia de productos climáticos provenientes de sensores remotos como los referidos con anterioridad, ha permitido la modelación hidrológica a escala global y con ella, la proliferación de productos que estiman los caudales circulantes por los cauces principales (Harrigan et al., 2020; Ghiggi et al, 2021; Balsamo et al., 2011). Evaluar las condiciones de uso de este tipo de productos y su aplicabilidad en países en vías de desarrollo resulta de sumo interés para la calibración de modelos hidrológicos.

En otro orden de cosas, el último siglo ha experimentado un incremento dramático en las emisiones de gases de efecto invernadero. Estos incrementos en las concentraciones de dióxido de carbono y otros gases de efecto invernadero en la atmósfera terrestre afectan de manera directa a la temperatura (Verma et al., 2015) y, en consecuencia, el calentamiento global es causante de mayores tasas de evapotranspiración que conllevan cambios en los regímenes de precipitación a nivel global.

Un cambio climático de tal magnitud afecta de manera significativa al ciclo hidrológico y a los regímenes de caudales, especialmente a escala de cuenca (Zhang et al., 2016), lo que afecta de manera directa a los ecosistemas, la seguridad hídrica y las actividades económicas relacionadas con éstos, principalmente en los sectores agrícola, forestal y energético – a través de la producción hidroeléctrica.

Algunas de las consecuencias del cambio climático, tales como las inundaciones y sequías son inevitables (Chattopadhyay y Jha, 2016). Sin embargo, si que es posible cuantificar los impactos que el cambio climático puede tener sobre los recursos hídricos a escala de cuenca, para definir estrategias de adaptación y mitigación de los impactos negativos (Batha et al., 2019).

Según el Panel Intergubernamental del Cambio Climático (IPCC, 2007) se espera que casi todas las regiones del mundo experimenten impactos negativos debidos al cambio climático, siendo los países en vías de desarrollo más vulnerables que los países desarrollados, debido, entre otros motivos, a la dependencia de sus economías de la agricultura, la escasez de infraestructuras y

la falta de recursos para llevar a cabo medidas de adaptación (Fischer et al., 2005; Tubiello y Rosenzweig, 2008).

Tanto para validar el potencial de uso de los productos satelitales de precipitación, temperatura y caudal, como para explorar los potenciales efectos del cambio climático sobre los recursos hídricos, es necesario emplear un modelo hidrológico (Parajuli, 2010; Kiros, Shetty y Nandagiri, 2015; Krysanova y Srinivasan, 2015). El modelo Soil and Water Assessment Tool (SWAT) ha sido ampliamente empleado en estas tareas, por lo que se ha optado por su uso para llevar a cabo la presente investigación.

I.2 OBJETIVOS

Esta investigación se centra en la mejora creciente de los modelos hidrológicos con la disponibilidad de información climática proveniente de sensores remotos, lo que permite aumentar la precisión de sus resultados y con ella mejorar los estudios de planificación y gestión de recursos hídricos, especialmente en regiones con escasa cobertura de estaciones hidrometeorológicas.

Dentro de esta tesis se abordan dos temas principales: (1) el uso de productos satelitales de precipitación, temperatura y caudal para la calibración y validación de modelos hidrológicos; y (2) el estudio del impacto del cambio climático y las sequías.

Ambos asuntos se abordan en dos cuencas seleccionadas de la República de El Salvador – i.e. río Grande de San Miguel (GSM) y río Guajoyo (GRB) – en las que la cobertura espacio-temporal de las estaciones climáticas es escasa y los problemas derivados del cambio climático ponen en compromiso la forma de vida y las figuras de protección ambiental existentes en la actualidad.

En este contexto se presentan los siguientes objetivos generales de la investigación:

- Evaluar el comportamiento de los productos satelitales de precipitación y temperatura en la modelación hidrológica.
- Comprobar la capacidad que los productos satelitales de precipitación tienen para simular caudales mensuales observados.

- Investigar el potencial que el producto de caudales GloFAS-ERA5 proveniente de reanálisis de imagen satelital tiene para la calibración de modelos hidrológicos. Así como su relación con los productos satelitales de precipitación y temperatura.
- Evaluar los impactos del cambio climático sobre los procesos hidrológicos a partir de las proyecciones de temperatura y precipitación extraídas de GCM y para dos escenarios de emisiones, con ayuda de la herramienta CCT.
- Investigar el impacto del cambio climático sobre las sequías.

La modelación hidrológica se ha desarrollado con el modelo SWAT y la información necesaria para llevar a cabo la modelación, incluyendo los datos observados, ha sido facilitada por el Ministerio de Medio Ambiente y Recursos Naturales (MARN).

El trabajo englobado en la presente tesis aporta dos avances importantes a la modelación hidrológica: (1) el uso de productos satelitales de precipitación y temperatura para la calibración y validación de los modelos es de aplicación en Centroamérica, donde la cobertura de estaciones terrestres es escasa o inexistente; (2) el potencial que el registro de caudales proveniente de GloFAS-ERA5 tiene para la calibración de modelos en cuencas donde el acceso a registros convencionales es muy limitado.

I.3 ESTRUCTURA DEL DOCUMENTO

La presente tesis por compendio de publicaciones se estructura en seis capítulos diferenciados y un apéndice. El **Capítulo I**, comprende la introducción del documento en la que se incluye la justificación de la investigación y los objetivos principales; en el **Capítulo II** se presentan los antecedentes y estado del arte de la modelación hidrológica de recursos hídricos, los productos satelitales de precipitación y las herramientas de obtención de escenarios de cambio climático; en el **Capítulo III** se introducen las zonas de estudio y la metodología de trabajo; en el **Capítulo IV** se reproducen las tres publicaciones que integran la tesis, junto con una síntesis de los resultados principales y la discusión de los mismos; en el **Capítulo V** se exponen las conclusiones extraídas de la

investigación y se establecen las líneas futuras de trabajo; y en el **Capítulo VI** se reproducen las referencias bibliográficas que han sido manejadas durante la elaboración del documento.

De manera adicional se presenta en el **Apéndice** la información sobre la calidad de las revistas en las que han sido presentadas las tres publicaciones de la presente tesis.

II – ANTECEDENTES Y ESTADO DEL ARTE

II- ANTECEDENTES Y ESTADO DEL ARTE

El presente capítulo desarrolla la revisión bibliográfica que enmarca la teoría de la investigación realizada, incluyendo, tanto el estado del arte de la modelación hidrológica, como el relativo al uso de GCM y la herramienta de cambio climático CCT para usos compatibles con ella.

La modelación hidrológica se utiliza para evaluar la influencia que los cambios en el clima, los usos del suelo, la topografía, la geología, la cobertura vegetal y los suelos tienen sobre los procesos hidrológicos (Kiros, Shetty y Nandagiri, 2015; Krysanova y Srinivasan, 2014; Sing y Woolhiser, 2002). Todas estas variables comparten la característica de la no uniformidad en su distribución, temporalidad y respuesta, lo que acaba repercutiendo en la complejidad de los modelos físicos que persiguen explicar la hidrología de una cuenca (Srivastava et al., 2006; Singh y Woolhiser, 2002).

Su aplicación en el mundo de la ingeniería civil es diversa, ya que están relacionados con los problemas de gestión de recursos hídricos, tales como diseño de captaciones de agua potable y sistemas de riego, presas y embalses, canales y conducciones o sistemas de saneamiento, entre otros; y con el diseño de infraestructuras lineales, tales como carreteras y ferrocarriles, que precisan de obras de paso o puentes para salvar los cursos de agua.

Con anterioridad a la década de 1960, la modelización hidrológica estaba orientada al desarrollo de teorías y modelos que pudieran representar las componentes individuales del ciclo hidrológico, tales como la evaporación, la infiltración, el flujo superficial, o el flujo base (Singh y Woolhiser, 2002).

Desde entonces hasta la actualidad, se han desarrollado numerosos modelos, sus tipologías se han multiplicado, sus aplicaciones prácticas se han extendido, y la propia teoría de modelación ha sido objeto de avances sustanciales (Cabezas, 2015; Jodar-Abellán, Pla-Bru y Valdés-Abellán, 2019) gracias, en parte, a la proliferación de los ordenadores y al aumento de la potencia de cómputo. En este sentido, la situación se ha revertido por completo, pasando de aproximaciones someras de la realidad mediante modelos individuales de las distintas componentes del ciclo hidrológico, a contar con mayor capacidad de

cómputo que datos disponibles, lo que alienta a la necesidad de mejorar las redes y sistemas de recogida de datos para poder tener modelos más precisos y representativos de la realidad (Cabezas, 2015).

El primer ejemplo extendido de modelación conceptual del ciclo hidrológico fue el Stanford Watershed Model (Crawford y Linsley, 1966) y desde entonces, las dos siguientes décadas fueron muy prolíficas en su generación, destacando (según Arnold et al., 1998) los siguientes: SSARR (Rockwood, Davis y Anderson, 1972), el modelo Sacramento (Burnash, Ferral y McGuire, 1973), el modelo de tanque (Sugawara et al., 1976), HEC-1 (HEC, 1981), HYMO (Williams y Hann, 1973), RORB (Laurenson y Mein, 1983), TOPMODEL (Beven y Kirkby, 1979), CREAMS (Knisel, 1980), SHE (Abbott et al., 1986) y ARNO (Todini, 1996).

Con la mejora del poder de cálculo, las leyes físicas y las ecuaciones se han ido complicando, desde la resolución de ecuaciones diferenciales en diferencias finitas de leyes hidráulicas simplificadas o relaciones empíricas algebraicas, a la consideración de la variación dinámica de la humedad del suelo y su relación con la escorrentía superficial, o la mejora en la consideración del flujo subsuperficial. Y en este sentido han ido evolucionando los modelos anteriores.

Sin embargo, no ha sido hasta la llegada del S. XXI con las grandes mejoras en computación y desarrollo de software – en especial con la aparición de los Sistemas de Información Geográfica (GIS) y el desarrollo de bases de datos – cuando se ha logrado considerar la distribución espacial existente en el territorio, proliferando los modelos distribuidos físicamente basados.

Dentro de esta categoría, destaca a nivel científico – según Jodar-Abellán, Pla-Bru y Valdés-Abellán (2019) en 2017 el artículo de referencia contaba con 2,391 citas, quedando muy por encima de los artículos equivalentes de otros modelos hidrológicos – el modelo Soil and Water Assessment Tool (SWAT; Arnold et al., 1998), que fue desarrollado por el Servicio de Investigación Agrícola del USDA y en la actualidad cuenta con casos de estudios repartidos por todo el mundo sobre temáticas muy diversas, tales como la evaluación de recursos hídricos, calidad del agua, cambio de usos del suelo, o la evaluación del impacto del cambio climático (Krysanova & White, 2015).

Para alimentar estos modelos, tradicionalmente se ha obtenido la precipitación a partir de las estaciones meteorológicas existentes en el entorno de

la cuenca. Sin embargo, en áreas con baja densidad de las mismas, la interpolación de datos es necesaria con la correspondiente incertidumbre que ello conlleva (Woldemeskel, Sivakumar y Sharma, 2013) e incluso la no existencia de correlación entre la precipitación observada y la estimada (Senent-Aparicio et al., 2018b).

Adicionalmente, los pluviómetros no siempre son buenos instrumentos para medir la precipitación real, debido, entre otras cosas, a los efectos del viento sobre el dispositivo de medición, defectos en la instalación, imprecisiones por los procesos de humedad y evaporación en las paredes del dispositivo, y otro tipo de errores (Jimeno-Sáez et al., 2020; Sevruk, 1996; Centella-Artola et al., 2020). Por tanto, hay una necesidad evidente de mejora en la recopilación de datos y/o en la búsqueda de alternativas de información con una mayor representatividad espacial que las estaciones hidrometeorológicas.

En la región Centroamericana y Caribe, donde existen multitud de países e islas dispersas y en los que ha habido diferentes conflictos armados durante la segunda mitad del Siglo XX, la red de estaciones de precipitación no cuenta con registros continuos ni ha tenido el mantenimiento necesario, con lo que la necesidad de alternativas de información es muy evidente.

Sin embargo, hay muy pocos estudios que evalúen la precisión de los GP en el área de interés (Centella-Artola, et al. 2020). Jury (2009) estudió la habilidad de varios GP para representar la distribución espacial y la intensidad media de precipitación en el periodo 1979-2000; propuso una metodología para la comparación entre productos de precipitación basada en la identificación binaria (sí o no) de fenómenos conocidos y destacó que, a pesar de las diferencias existentes en la representación espacial de las precipitaciones en la mitad Este de las islas caribeñas según el producto utilizado, los productos satelitales de alta resolución eran razonablemente representativos. Desde entonces, muchos GP han sido actualizados y han aparecido otros con mayores resoluciones espacio-temporales.

Desde entonces, el uso de GP en los estudios de precipitaciones o su empleo en la modelación hidrológica parte de la premisa de que el producto satelital es el mejor disponible o el que más razonablemente representa el clima regional (Centella-Artola et al., 2020). Entre estos trabajos destaca la revisión realizada por

Jones et al. (2016), en la que se aborda la evolución de los estudios climatológicos desde mediados de la década de 1950 en la región Caribe, y como se ha pasado de la comparativa de valores medios mensuales de precipitación y el establecimiento de relaciones climáticas con valores observados en el resto del continente americano – e.g. Grandes llanuras de E.E.U.U., fenómeno de El Niño, etc. –, al uso de GP tanto para el estudio de la climatología como para la modelación hidrológica.

En la región Centroamericana, Jones et al. (2016) destaca el trabajo de Magaña, Amador y Medina (1999) en el que se elabora un producto de precipitación a partir de registros de estaciones para el periodo 1958-1995 con una resolución espacial de 1°x1° y con el que se pudo justificar la importancia del fenómeno de la canícula estival en la modulación del clima en Centroamérica.

En cuanto al uso de productos satelitales de precipitación en la modelación hidrológica son muchas las referencias existentes (e.g. Stisen y Sandholt, 2010; Bitew y Gebremichael, 2011; Skinner et al., 2015; Li et al., 2018; Zhu et al., 2018; Maggioni y Massari, 2018; Deng et al., 2019; Senent-Aparicio et al., 2021) y ofrecen una alternativa prometedora a los métodos tradicionales de monitoreo, con una escala global y resoluciones espacio-temporales cada vez de mayor detalle (Jiang y Wang, 2019).

En términos generales, la capacidad y el desempeño de los GP para la modelación hidrológica se ven muy afectadas por las diferencias existentes en la topografía, clima, estación del año, tamaño de la cuenca y la selección del modelo hidrológico y GP (Zhu et al., 2018; Maggioni y Massari, 2018; Bitew y Gebremichael, 2011). En este sentido, resulta fundamental la realización de un estudio estadístico que compruebe la coherencia de resultados entre productos y las estaciones climáticas existentes en las distintas épocas del año, detecte las desviaciones sistemáticas y los errores aleatorios y seleccione los productos satelitales que mejor se adapten a la zona de estudio (Stisen y Sandholt, 2010; Bitew y Gebremichael, 2011; Deng et al., 2019; Jiang y Wang, 2019; Senent-Aparicio et al., 2021).

Entre los ejemplos de uso de estos productos para la modelación hidrológica se tienen casos de estudio en África (Stisen y Sandholt, 2010; Bitew y

Gebremichael, 2011), China (Zhu et al., 2018; Deng et al., 2019), Europa (Senent-Aparicio et al., 2021) y América del Sur (Falk et al., 2015).

Sin embargo, hasta donde se tiene conocimiento, este tipo de productos no han sido empleados para realizar estudios de modelación hidrológica en la región Centroamericana.

Por otro lado, Harrigan et al. (2020) presenta la herramienta Global Flood Awareness System (GloFAS-ERA5) para la estimación de caudales a partir de reanálisis de imagen satelital. La gran novedad de este producto es que los datos están actualizados con tan sólo de dos a cinco días de retraso respecto del tiempo actual, lo que confiere a GloFAS la posibilidad de estudiar los eventos que se están produciendo en la actualidad.

La serie de GloFAS se inicia en enero de 1979, en consonancia con el producto satelital ERA5, del que extrae las condiciones climáticas para el cálculo de la escorrentía, aplica el modelo hidrológico LISFLOOD (Burek, van der Knijff y de Roo, 2013) para realizar el balance hídrico y obtiene la serie de caudales que constituyen el modelo GloFAS.

GloFAS realiza predicciones diarias con una escala temporal diaria e incluye dos productos principales: (1) GloFAS 30d, establece la probabilidad de excedencia de determinados caudales en una sección de cauce para los 30 próximos días; y (2) GloFAS-Seasonal que realiza proyecciones climáticas de 4 meses, que presenta una vez al mes y con una escala temporal semanal.

Aunque existen algunos ejemplos de aplicación de productos satelitales de precipitación en modelación hidrológica – Sikder et al. (2019) los emplearon para la gestión de cuencas transnacionales en el Sur y Sudeste asiático y Lakew et al. (2019) los aplicaron en un estudio de gestión de recursos hídricos en la cuenca del río Nilo, en Etiopía – GloFAS es un producto de reciente creación y su aplicación para la calibración de modelos hidrológicos no está documentada hasta la fecha.

Finalmente, Vaghefi et al. (2017) presenta la herramienta Climate Change Toolkit (CCT) para la reducción de escala y corrección del sesgo de los GCM seleccionados dentro del proyecto Inter-Sectoral Impact Model Intercomparison Project (ISI-MIP5), constituyéndose como una plataforma de referencia para la sistematización de estudios de cambio climático.

Durante la presentación del producto, Vaguefi et al. (2017) emplea como caso de estudio la Península de Baja California.

Magris et al. (2019) estudia la cuenca baja del río Doce, en el Sudeste de Brasil, donde en 2015 se produjo la rotura catastrófica de un embalse que produjo el vertido de lodos contaminados con metales pesados y utiliza la herramienta para extraer los escenarios de bajas emisiones (RCP2.6) y las proyecciones de corto plazo de las variables precipitación y temperatura.

Pérez-Sanchez et al. (2020) emplea la herramienta para la descarga y ajuste de escala de los distintos GCM en la cuenca del río Eo, en el Norte de España, para el estudio de los riesgos ecológicos e hidro-geomorfológicos para distintos escenarios temporales, teniendo en cuenta los escenarios de emisiones RCP4.5 y RCP8.5.

Gulakhmadov et al. (2020) estudia la influencia del cambio climático en la cuenca del río Vakhsh de Asia Central para el abastecimiento de agua a las poblaciones ubicadas a lo largo de su cauce. Se trata de un río de caudal condicionado por los aportes de la nieve al derretirse y que integra también la producción de energía dentro de sus usos. Los autores emplean SWAT para la simulación hidrológica de la cuenca vertiente y CCT para evaluar los escenarios de cambio climático, considerando los escenarios de emisiones RCP4.5 y RCP 8.5 para la evaluación del clima en los horizontes temporales 2022-2060 y 2061-2099.

López-Ballesteros et al. (2020) aplica el modelo SWAT de manera conjunta con el indicador de alteración hidrológica (IHA) en la cuenca del río Aracthos, al Noroeste de Grecia. El trabajo utiliza el periodo de largo plazo (2070-2099) para evaluar la influencia que el cambio climático tiene sobre el ciclo hidrológico de la cuenca, empleando para ello los escenarios de emisiones RCP4.5 y RCP8.5. Los datos climáticos regionalizados se obtienen con ayuda de la herramienta CCT.

Finalmente, Akoko, Kato y Tu (2020) estudia la influencia que el cambio climático va a tener en el cultivo de arroz en la cuenca del río Mwea en Kenia. Para ello, emplea la herramienta CCT para la extracción y ajuste de escala de los GCM seleccionados – i.e. GFDL-ESM2M, HadGEM2-ES y NorESM1-M –, obteniendo los valores para los periodos 2020-2060 y 2061-2099 y los escenarios de emisiones RCP2.6, RCP4.5, RCP6.0 y RCP8.5; SWAT como modelo hidrológico en

el que realizar la evaluación; y CropWat para evaluar los requerimientos de agua de los cultivos en los distintos espacios temporales y escenarios considerados.

Por tanto, al igual que en el caso de los productos GP, existen casos de estudio en diversos países a nivel mundial del uso de la herramienta Climate Change Toolkit (CCT) para la descarga, ajuste de escala y corrección del sesgo de los datos climáticos provenientes de los GCM seleccionados en el proyecto ISI-MIP5. Sin embargo, no se han encontrado ejemplos de aplicación de la herramienta para la obtención de proyecciones climáticas en Centroamérica, lo que convierte al presente estudio en pionero en ese sentido.

III – METODOLOGÍA DE INVESTIGACIÓN

III- METODOLOGÍA DE INVESTIGACIÓN

El presente capítulo de Metodología de investigación está organizado en cuatro apartados principales. En el apartado **III.1** se describen las características principales de las zonas de estudio. En el apartado **III.2** se presenta el modelo hidrológico SWAT, con el que se estudia la validez de los productos satelitales y la evaluación de recursos hídricos en las cuencas seleccionadas para escenarios de cambio climático. En el apartado **III.3** se introducen los escenarios de cambio climático considerados en la presente tesis – i.e. GFDL-ESM2M, HadGEM2-ES, IPSL-CM5A-LR, MIROC y NoerESM1-M – al tiempo que se presenta la Herramienta de Cambio Climático para la obtención y reducción de escala de los mismos. Finalmente, en el apartado **III.4** se presentan los productos satelitales de precipitación y temperatura empleados en las distintas publicaciones que integran esta tesis – i.e. CFSR, CHIRPS-CHIRTS, ERA5, MSWEPv1.1, PERSIANN-CDR y CMORPH.

III.1 CARACTERÍSTICAS DE LAS ZONAS DE ESTUDIO

La selección de las zonas de estudio se realizó de manera consensuada con el Ministerio de Medio Ambiente y Recursos Naturales (MARN) de El Salvador, dentro del convenio de colaboración suscrito con ellos por el que se puso a disposición del presente trabajo de investigación la siguiente información hidrológica:

- Mapas de usos del suelo.
- Modelo Digital de Elevaciones (DEM, por sus siglas en inglés).
- Registros de precipitación, temperatura y evapotranspiración.
- Estudio del Plan Nacional de Gestión Integrada del Recurso Hídrico de El Salvador, con Énfasis en Zonas Prioritarias, PNGIRH (2017).

Para el estudio de la disponibilidad de recursos hídricos y sequías bajo escenarios de cambio climático se seleccionó la cuenca del río Guajoyo (GRB), situada al Oeste de la República de El Salvador.

La cuenca tiene una superficie de 156 Km^2 aguas arriba de la estación foronómica de Piedra Cargada, empleada en la calibración del modelo hidrológico y que define el desagüe de la zona de estudio. La pendiente media es del 16% con valores de elevación que oscilan entre los 1,517 m y 425 m.

El río Guajoyo es tributario del río Lempa, una cuenca tri-nacional que se extiende en los territorios de Guatemala, Honduras y El Salvador, y constituye uno de los ríos más importantes de la Región Centroamericana, siendo el más importante en la República de El Salvador. Presenta un clima tropical con dos periodos bien diferenciados (MARN, 2017a), una estación seca – i.e. de Mayo a Octubre – y una estación húmeda – i.e. de Noviembre a Abril.

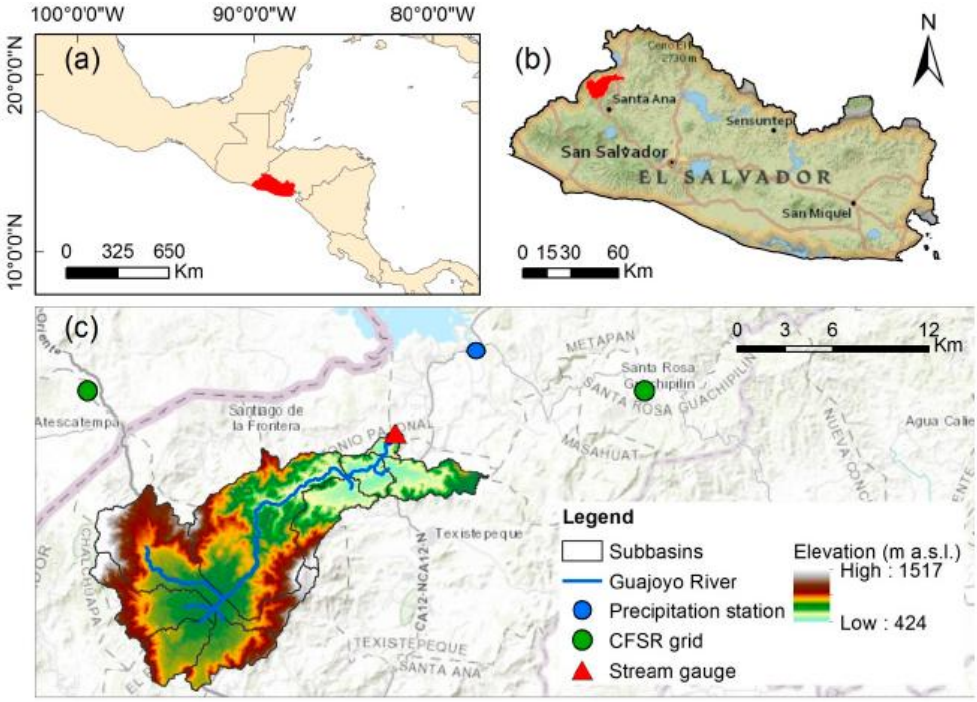

Figura 1. Mapa de localización de la cuenca del río Guajoyo: (a) Ubicación de la República de El Salvador en Centroamérica; (b) Posición de la cuenca del río Guajoyo dentro de El Salvador; (c) Subcuencas, DEM, hidrografía y localización de estaciones hidrometeorológicas dentro de la cuenca

La precipitación histórica anula varía entre los 863 y los 1,834 mm/año en el periodo de 1970 a 2017, con un valor medio de 1,373 mm/año. La variable temperatura varía principalmente con la altura, presentando pequeños cambios a lo largo del año – los valores máximos se alcanzan entre Marzo y Abril; y los valores mínimos entre Noviembre y Diciembre –, y un valor medio anual de 23 C.

En cuanto a tipología de suelos, dominan los andosoles, de origen volcánico, con alta permeabilidad y fértiles (Wada, 1985; Levard y Basile-Doelsch, 2016). De igual modo, en cuanto a tipología de usos del suelo destacan los terrenos de cultivo, que ocupan el 51% de la superficie de la cuenca; y los pastos, que cubren un 30% de la misma.

La cuenca GRB tiene especial interés desde el punto de vista medioambiental debido a las figuras de protección que presenta, tales como (1) El Complejo Güija, incluido en la lista Ramsar de la Convención de Humedales desde el año 2010, y que se ubica en la desembocadura del río Guajoyo, en su confluencia con el Río Desagüe; (2) El Área de Protección Natural La Montañita, conformada en 2010 en la parte alta de las quebradas Las Marías y San Marcos, tributarias del GRB, donde está presente el bosque tropical seco; y (3) La Reserva de la Biosfera de la UNESCO Trifinio Fraternidad, designada en 2011 y ubicada entre los países de El Salvador, Guatemala y Honduras, que garantiza el abastecimiento de agua a las comunidades locales, al tiempo que ejerce un papel principal en el desarrollo de la región a través del agroturismo y la plantación de cultivos como el café.

Y para los estudios del impacto que los productos satelitales de precipitación tienen en la simulación de caudales en cuencas con escasez de estaciones de aforo y el del análisis del potencial que el producto GloFAS-ERA5 de estimación de caudales por reanálisis de imagen satelital tiene para la calibración del modelo SWAT se seleccionó la cuenca del río Grande de San Miguel (GSM).

La cuenca del río GSM se encuentra en el este de la República de El Salvador y ocupa una superficie de 2,377 Km^2 hasta que alcanza el puno de desagüe del modelo. Se trata de una de las cuencas más grandes del país, con un

rango de altitudes que oscila entre el nivel del mar y valores superiores a los 2,000 m en el Volcán de San Miguel.

Al igual que en el caso de la cuenca GRB, la cuenca del río GSM está sometida a un clima tropical, con elevadas tasas de precipitación – con valores anuales medios de 1,700 mm –, distribuidas de manera muy diferenciada – en torno al 90% de la precipitación se produce entre Mayo y Octubre (Blanco-Gómez et al. (2019); Wobad y Jobel (1970) – en una época lluviosa y otra seca. Por su parte, las temperaturas oscilan entre los 17 °C y los 37 °C.

En lo relativo a la tipología de suelos, dominan los andosoles, phaeozems y regosoles. Los andosoles cubren la superficie alrededor del Volcán de San Miguel, son de origen volcánico, con alta permeabilidad y con condiciones ideales para el cultivo (Levard y Basile-Doelsch, 2016). Los regosoles están compuestos por material no consolidado, de granulometría fina, y son comunes en áreas montañosas; siendo dominantes en la parte Norte de la cuenca. Finalmente, los phaeozems son comunes en la parte Este de la cuenca y en ellos se albergan pastos húmedos y superficies boscosas por tratarse de materiales muy porosos y fértiles, lo que los convierte en un terreno excelente para la agricultura (FAO, 2008). De igual modo, en cuanto a tipología de usos del suelo destacan los pastos (43%), terrenos de cultivo (32%) y bosques (17%).

La ciudad de San Miguel, la segunda más habitada en El Salvador, se encuentra en el centro del área de estudio. La cuenca es muy sensible ecológicamente y algunos de sus ecosistemas poseen figuras de protección internacional. Tal es el caso de las zonas protegidas de Tecapa-San Miguel y la Bahía de Jiquilisco. La zona de Tecapa-San Miguel es conocida por sus plantaciones de café, sus lagunas costeras – algunas incluidas en la Convención Ramsar de Humedales – y sus cráteres volcánicos. Por su parte, desde 2005 la Bahía de Jiquilisco – situada en la desembocadura del río GSM – está catalogada como sitio Ramsar y una reserva mundial de la biosfera por la UNESCO.

Según MARN (2017a), la contaminación de las aguas y la necesidad potencial de aumentar la agricultura son las mayores presiones medioambientales en la cuenca del río GSM.

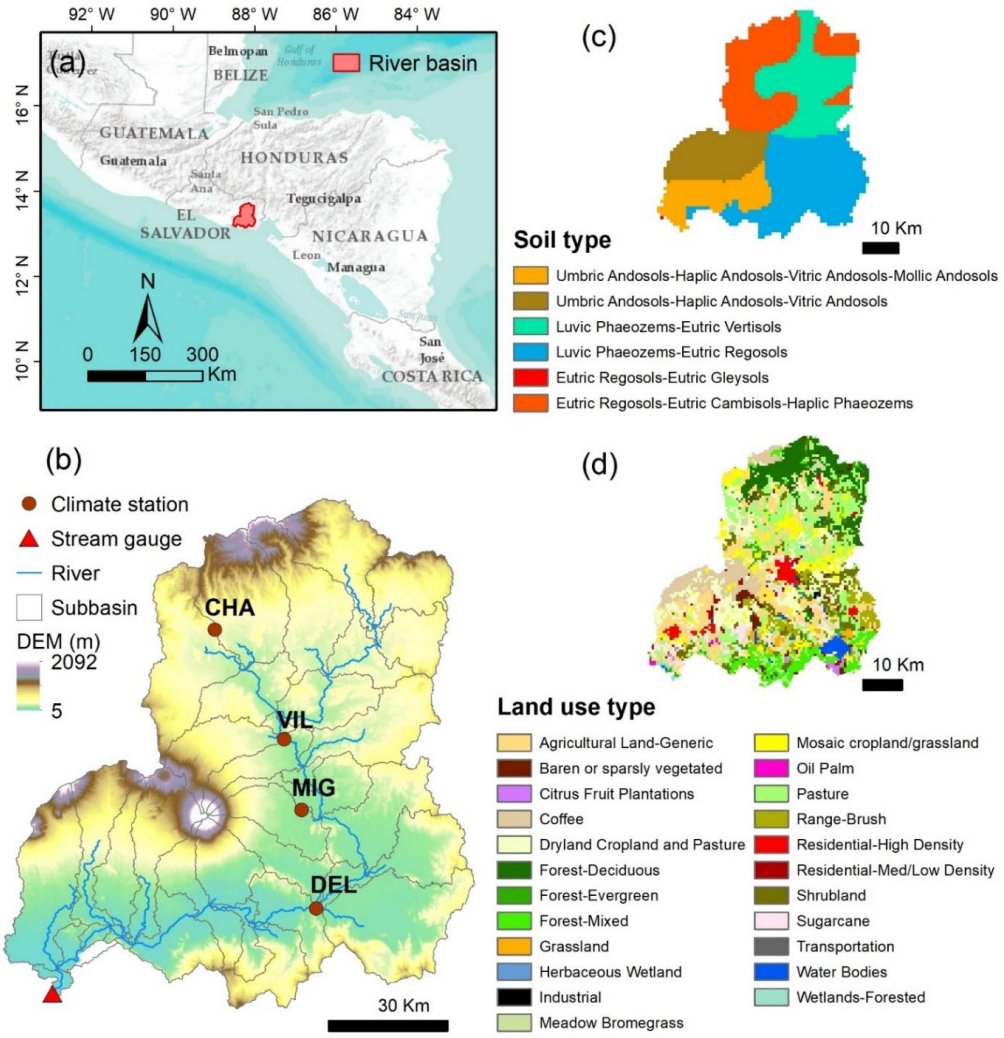

Figura 2. Localización de la cuenca del río Grande de San Miguel: (a) Posición de la cuenca del río GSM dentro de Centroamérica; (b) Subcuencas, DEM, hidrografía y localización de estaciones meteorológicas dentro de la cuenca; (c) Mapa de suelos; (d) Mapa de usos del suelo

III.2 MODELO HIDROLÓGICO SWAT

El Soil and Water Assessment Tool, SWAT (Arnold et al., 1998; Neitsch et al., 2011), es un modelo hidrológico a escala de cuenca físicamente basado, semi-distribuido y de simulación temporal continua – i.e. no está diseñado para la simulación de un evento de crecida o inundación. Fue desarrollado por el Dr. Jeff Arnold en el Departamento de Agricultura de los Estados Unidos con la Universidad de Texas a principios de la década de 1990.

SWAT precisa de un modelo digital de elevaciones (DEM, por sus siglas en inglés), un mapa de suelos y un mapa de usos del suelo para la división hidrológica de la cuenca. La integración de esta información espacial se realiza con ayuda de sistemas GIS, contando con complementos específicos en ArcGIS y QGIS.

En primer lugar se lleva a cabo el cálculo de la cuenca drenante a partir de la definición del punto de desagüe del modelo, el cálculo de la red hidrográfica y la división en subcuencas dependiendo de las ramificaciones de la red de drenaje. SWAT integra la información hidrográfica con las características del terreno y los usos del suelo a través de las unidades de respuesta hidrológica (HRU, por sus siglas en inglés), en las que se agrupan las superficies de terreno dentro de cada subcuenca con características homogéneas.

De acuerdo a Neitsch et al. (2011) la simulación hidrológica en SWAT distingue dos fases diferenciadas: (1) la fase terrestre o de producción y (2) la fase de propagación de caudales y transporte de materiales.

La fase de producción está fundamentada en el balance de agua y en ella se determina la cantidad de agua y las cargas de sedimentos, nutrientes y pesticidas que son aportadas al canal principal de cada una de las subcuencas.

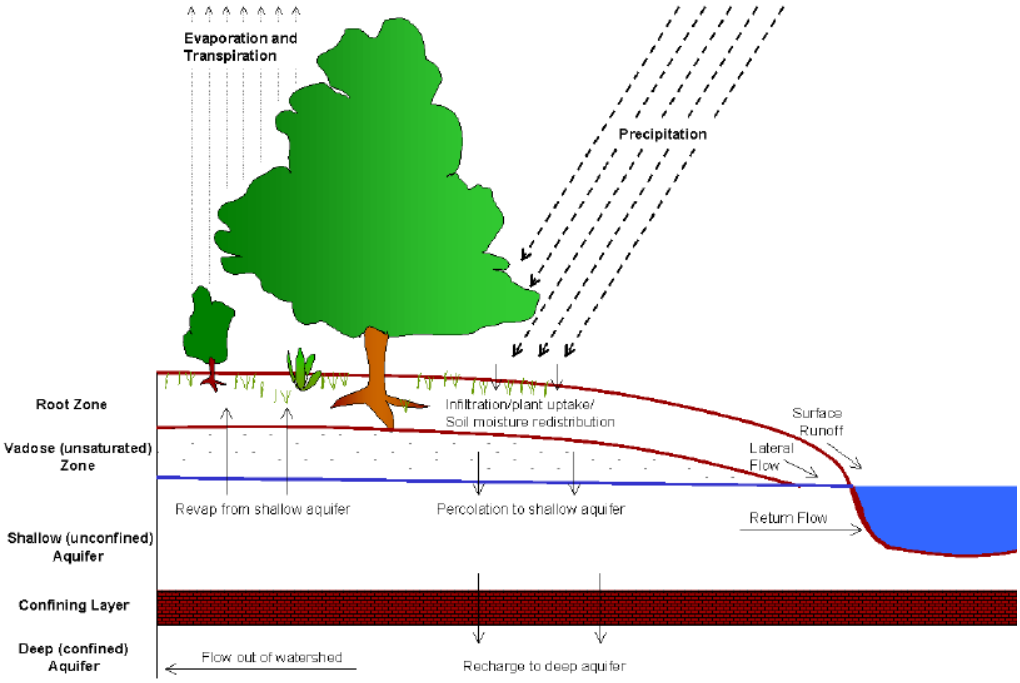

Figura 3. Representación gráfica de la fase terrestre del ciclo hidrológico (Neitsch et al., 2011)

Mientras que la fase de propagación de caudales queda definida por el movimiento del agua, el transporte de sedimentos, la transformación físico-química de las sustancias transportadas por la corriente y presentes en el fondo del cauce, etc. a lo largo de la red hidrográfica, entre cuencas, hasta alcanzar el punto de desagüe.

La ecuación fundamental del modelo se corresponde con el balance hídrico para cada HRU y tiene la siguiente expresión (Neitsch et al., 2011):

$$SW_t = SW_0 + \sum_{i=1}^{t} (R_{day} - Q_{surf} - E_a - W_{seep} - Q_{gw}) \qquad (1)$$

donde, SW_t es la cantidad final de agua en el suelo (mm), SW_0 es la cantidad inicial de agua en el suelo en el día i (mm), t es el tiempo (días), R_{day} es la precipitación del día i (mm), Q_{surf} es la escorrentía superficial en el día i (mm), E_a es la evapotranspiración del día i (mm), w_{seep} es la cantidad de agua que percola el día i (mm) y Q_{gw} es el flujo de retorno del día i (mm).

Los aportes de humedad y energía que controlan el balance hídrico se introducen a través del módulo de clima. Las variables climáticas definidas en los modelos de SWAT son la precipitación diaria, la temperatura máxima y mínima del aire, la radiación solar, la velocidad del viento y la humedad relativa.

Una vez evaluado el balance a nivel de HRU, se inicia la propagación de caudales a lo largo de los canales que definen la red de drenaje. SWAT plantea el transporte de agua a través de una red de canales trapezoidales en los que el agua circula en lámina libre. La velocidad de flujo se calcula mediante la ecuación de Manning y la propagación se realiza mediante el método de enrutamiento de almacenamiento variable o el método de Muskingum. De este modo, el flujo que se genera en cada HRU se agrega a lo largo de la red de drenaje hasta que alcanza el desagüe del modelo.

III.2.1 Componentes hidrológicas del modelo SWAT

El agua precipita desde la atmósfera y parte de ella es interceptada por la vegetación o queda retenida en la superficie terrestre. Otra parte, se infiltra a través del suelo alcanzando el acuífero subyacente o forma un flujo, superficial o subsuperficial, que por escorrentía alcanza los principales canales de agua, contribuyendo de este modo a aumentar el caudal de los ríos. Adicionalmente, parte del agua infiltrada quedará retenida en el suelo rellenando los huecos y ocupando parte de su capacidad de campo.

Todos estos procesos constituyen las componentes de la modelación hidrológica con SWAT, que seguidamente se describen en mayor detalle (Neitsch et al., 2011).

III.2.1.1 Escorrentía superficial

La escorrentía superficial se corresponde con la cantidad de agua precipitada que excede la capacidad de infiltración del suelo. En SWAT se puede calcular la escorrentía superficial aplicando dos métodos distintos: el método del número de curva (CN, por sus siglas en inglés) del Soil Conservation Service (SCS) de Estados Unidos (SCS) (USDA-SCS, 1972) y el método de infiltración de Green & Ampt (1911). En los modelos hidrológicos de la presente tesis se ha

empleado el método del número de curva para el cálculo de la escorrentía superficial.

El número de curva varía de forma no lineal con el contenido de humedad en el suelo y disminuye conforme el suelo se acerca al punto de marchitez permanente, de manera que valores cercanos a cero se corresponden con suelo con una muy alta permeabilidad y valores próximos a cien se corresponden con suelos saturados o muy impermeables.

III.2.1.2 Intercepción de agua en la superficie vegetal

El almacenamiento de agua en la cubierta vegetal está relacionado con el agua disponible para que se produzca la evaporación. Cuando se emplea el método del número de curva para el cálculo de la escorrentía superficial, la intercepción de agua en la superficie vegetal se emplea en el balance de escorrentía. En SWAT se define el valor máximo de agua que puede ser almacenada en la cubierta vegetal para cada tipo de cultivo, siendo esta agua la primera que desaparece cuando se considera la evaporación.

III.2.1.3 Infiltración

La infiltración es la cantidad de agua que entra en el suelo desde la superficie. Conforme el agua va penetrando en el terreno, éste se vuelve cada vez más húmedo, agotando su capacidad de almacenamiento de agua (o capacidad de campo) y disminuyendo la tasa de infiltración que se puede producir desde la superficie, hasta que alcanza un valor estable. La infiltración se determina como la diferencia entre la cantidad de precipitación y la de escorrentía superficial que se produce.

III.2.1.4 Evapotranspiración

La evapotranspiración comprende todos los procesos por los que el agua en estado líquido o sólido que se encuentra en la superficie terrestre o en sus proximidades, se convierte en vapor de agua. El concepto engloba tanto la evaporación proveniente del terreno desnudo o superficies vegetadas, o la provenientes de las aguas superficiales; la transpiración producida por la

superficie foliar de las plantas; y la sublimación de las superficies nevadas o heladas.

En SWAT es posible calcular la evapotranspiración potencial aplicando tres métodos distintos, a saber: Penman-Monteith (Monteith, 1965), Hargreaves (Hargreaves, Hargreaves, & Riley, 1985) y Priestley-Taylor (Priestley &Taylor, 1972).

En el caso del método de Penman-Monteith es necesario conocer la radiación solar, la temperatura del aire, la humedad relativa y la velocidad del viento para determinar la evapotranspiración. Por su parte, en el método de Priestley-Taylor son necesarios los datos de la radiación solar, la temperatura del aire y la humedad relativa; y finalmente, para el caso de Hargreaves sólo es requerida la temperatura del aire (temperatura máxima y mínima). Debido a la mayor facilidad de acceso a los datos de partida, es habitual el cálculo de la evapotranspiración mediante los métodos de Hargreaves y Penman-Monteith, como sucede en los modelos realizados en la presente tesis.

III.2.1.5 Flujo subsuperficial

El flujo subsuperficial se origina en la zona no saturada, generalmente en los dos primeros metros de suelo y constituye una aportación directa al caudal de los cauces de aguas superficiales. En SWAT se calcula mediante un modelo de almacenamiento cinemático en cada una de las capas que constituyen la zona no saturada conforme al modelo de Sloan et al. (1983).

III.2.1.6 Percolación profunda

La percolación profunda, al igual que el flujo subsuperficial, es calculada para cada capa del suelo en la zona no saturada. El flujo gravitacional, o percolación, se produce cuando la capacidad de campo de cada capa del suelo se ve excedida – i.e. se satura – y la capa subyacente no está saturada, de manera que el movimiento del agua está gobernado por la conductividad saturada de cada perfil del suelo.

La temperatura es un factor determinante en este proceso, de manera que, para temperaturas inferiores a 0 C, el agua del terreno está congelada y no se produce el flujo.

III.2.1.7 Estanques

Los estanques son estructuras de almacenamiento de agua ubicadas en una subcuenca y que interceptan la escorrentía superficial. Se ubican fuera de la red de canales principales y no reciben agua de ellos.

III.2.1.8 Canales

Se consideran dos tipos distintos de canales en SWAT: (1) la red de canales principales; (2) los canales tributarios o secundarios. Los canales tributarios se encargan de recoger las escorrentías superficiales de una porción de las subcuencas y conducirla a la red de canales principales. El flujo subsuperficial en SWAT se conecta directamente con la red principal.

De igual modo, los atributos de los canales secundarios se emplean para calcular el tiempo de concentración de cada una de las subcuencas.

Para determinar las pérdidas a través del lecho del cauce, SWAT emplea el método de Lane descrito en USDA-SCS (2007), en el que las pérdidas de agua son función de la forma (ancho y largo) del canal y del tiempo de flujo.

III.2.1.9 Recarga acuífera

El flujo base es el aporte de caudal a las aguas superficiales proveniente de las aguas subterráneas. SWAT divide las aguas subterráneas en dos sistemas acuíferos: (1) un acuífero poco profundo y no confinado, que aporta el flujo base a las corrientes superficiales de la cuenca; y (2) un acuífero profundo y confinado que aporta el flujo base a las corrientes superficiales fuera de la cuenca (Arnold, Allen, & Bernhardt, 1993).

De manera adicional al flujo base, el agua almacenada en el acuífero poco profundo contribuye a la reposición de humedad en el perfil del suelo en condiciones muy secas o es consumida por la vegetación.

III.2.2 Análisis de sensibilidad, calibración y validación del modelo hidrológico SWAT

El ajuste de los parámetros definitorios del ciclo hidrológico en SWAT se realiza a través de un procedimiento de calibración consistente en tres etapas diferenciadas: (1) análisis de sensibilidad, (2) calibración y (3) validación.

Al tratarse SWAT de un modelo con multitud de parámetros es recomendable la calibración automática y para ello se ha empleado en los distintos modelos desarrollados en la presente tesis el algoritmo SUFI-2 implementado en el paquete de software SWAT-CUP.

Llegados a este punto, cabe destacar que la calibración de los modelos de cuenca es subjetiva y que ningún algoritmo de calibración puede reemplazar el conocimiento de un hidrólogo y su análisis de la hidrología de la cuenca y del proceso de calibración (Abbaspour et al., 2015). Por ello no debería de realizarse ningún proceso de calibración sin haber realizado un análisis de la sensibilidad de los parámetros del modelo.

El proceso de calibración del algoritmo SUFI-2 queda descrito en los siguientes pasos (Abbaspour, Johnson and van Genuchten, 2004):

1. Definición de la función objetivo dependiente de los objetivos del proyecto – e.g. buena representación de los caudales punta y del flujo base, consideración de varias variables al unísono, tales como flujo y concentración, etc.
2. Establecimiento de los rangos de variación de los parámetros en base a las características físicas de los mismos.
3. Análisis de sensibilidad de los parámetros seleccionados en el modelo. Para cada parámetro se fija el resto en un valor realista y se divide el rango de variación del mismo en diez intervalos iguales, de manera que cada uno de los intervalos evalúe su respuesta en el modelo hidrológico y se representen sus resultados frente a los valores observados, valorando de este modo la sensibilidad del parámetro.
4. Asignación de los valores iniciales de los parámetros de calibración.

5. Ejecución de *n* simulaciones (siendo *n* un valor relativamente alto: 1,000-2,000), guardando los resultados del modelo para cada una de ellos, incluyendo los siguientes pasos:
    a. Cálculo de estadísticos – i.e. RMSE –, pesos y función objetivo de cada simulación.
    b. Desviación típica, intervalos de confianza del 95% y sensibilidad relativa (cuando el resto de parámetros también varían) para cada parámetro.
    c. Cálculo del 95% de la sensibilidad de la predicción (95PPU), resultando un modelo satisfactorio cuando el 90% de los datos medidos se encuentran en el intervalo 95PPU, la distancia media entre el valor más alto y más bajo de 95PPU es menor que la desviación típica y R^2 es mayor que 0.8.
6. Definición del nuevo rango de parámetros y repetición de las simulaciones hasta conseguir el ajuste deseado.

El algoritmo SUFI-2 emplea el estadístico *p*-value en el análisis de sensibilidad de cada uno de los parámetros, de manera que en el correspondiente análisis de regresión múltiple se comprueba la veracidad de la hipótesis nula por la que el coeficiente de regresión es igual a cero. De manera que, cuanto menor es el estadístico *p*-value (valores inferiores a 0.05), más sensible es el parámetro considerado (Abbaspour et al., 2007).

Una vez detectados los parámetros más sensibles se inicia el proceso de calibración y validación de parámetros, dependiendo en muchos casos los resultados de los valores iniciales de los mismos. Para reducir la influencia de éstos, se emplea el tiempo de calentamiento, en el que durante un periodo inicial se evalúa el modelo buscando su estabilización, adoptando como valores iniciales los alcanzados por los parámetros al final del periodo de calentamiento.

El modelo se calibra de manera automática con ayuda del algoritmo SUFI-2 y se obtienen los valores alcanzados por los parámetros definitorios del problema.

Finalmente, se seleccionan datos de entrada y de salida – e.g. series climáticas y caudales de salida, respectivamente – de un periodo distinto al considerado en la fase de calibración y se valida el comportamiento del modelo

con los parámetros obtenidos en la calibración. De este modo se garantiza la validez del modelo en condiciones distintas a las de la fase de calibración.

III.3 MANEJO DE ESCENARIOS DE CAMBIO CLIMÁTICO

Según IPCC-AR6 (2021) los científicos están observando cambios en el clima de la Tierra en todas las regiones y en el sistema climático en su conjunto. Muchos de los cambios observados en el clima no tienen precedentes en miles, sino en cientos de miles de años, y algunos de los cambios que ya se están produciendo, como el aumento continuo del nivel del mar, no se podrán revertir hasta dentro de varios siglos o milenios.

Los Modelos del Sistema Terrestre (ESM, por sus siglas en inglés) constituyen actualmente los modelos más complejos que contribuyen a los estudios de cambio climático (IPCC-AR6, 2021). Se fundamentan en las ecuaciones matemáticas de las leyes naturales que gobiernan la evolución del clima, tales como: atmósfera, océanos, criosfera, tierra, biosfera y el ciclo del carbono (Flato, 2011).

El núcleo central de cada ESM está compuesto por Modelos de Circulación General (GCM, por sus siglas en inglés) que se encargan de la representación de las dinámicas de los sistemas atmosférico y oceánico (IPCC-AR6, 2021). El desempeño de los GCM no está limitado a la modelación a escala Global, sino que su uso es de aplicación en modelos a escala regional, donde fenómenos locales – e.g. condiciones de contorno, orografía, etc. – condicionan el comportamiento de los modelos.

Por tanto, los estudios de cambio climático requieren del procesado de enormes bases de datos con gran resolución espacial y largas series temporales (Ahmed et al., 2013). Esta información precisa de su adaptación a los sitios de estudio mediante la corrección del sesgo y la reducción de escala de los GCM, lo que convierte los estudios de cambio climático en repetitivos y tediosos (van Vuuren y Carter, 2014).

La Herramienta de Cambio Climático (CCT, por sus siglas en inglés) fue desarrollada por Vaghefi et al. (2017) para sistematizar el proceso de reducción de escala de los modelos GCM y poder emplearlos en los modelos hidrológicos

desarrollados con SWAT. Los principales objetivos para los que fue concebida son:

1. Manejo de grandes series de datos, como las que son requeridas en los estudios de cambio climático, sobre todo cuando se trata de estudios de gran escala y con largas series temporales.
2. Facilitar y sistematizar el proceso de adaptación de la información para los estudios de cambio climático, tales como el formateo de los datos, interpolación, reducción de escala y corrección del sesgo.
3. Proyección futura de eventos históricos extremos mediante el reconocimiento de patrones de eventos pasados.

III.3.1 Herramienta de Cambio Climático (CCT)

La Herramienta de Cambio Climático funciona en MS Windows y está compuesta por 6 módulos diferenciados con las siguientes características (Vaguefi et al., 2017):

- Descarga de información. Disponible desde la siguiente web (http://www.2w2e.com/, consultado el 18 de agosto de 2021) el usuario define las coordenadas de descarga de la información y obtiene la información climática disponible en un base de datos de formato MS Access.
- Extracción de información. En este módulo se selecciona un polígono que esté contenido en los datos descargados, y en caso de querer emplear datos observados, los GCM deben regionalizarse a las coordenadas de observación, para lo que la herramienta requiere de la ejecución en dos pasos, una para el periodo seleccionado de datos históricos (GCM-historical) y otra para el periodo de datos futuros (GCM-future).
- Gestión de la información climática Global (GCDM, por sus siglas en inglés). En este módulo se realizan los siguientes cálculos:
    - Medias mensuales y anuales de las variables climáticas seleccionadas.

    - Medias a largo plazo y detección de anomalías en las estaciones climáticas.

- Corrección del sesgo usando reducción estadística de escala (BCSD, por sus siglas en inglés). En este módulo se realiza la reducción de escala por corrección del sesgo de los datos en la región seleccionada. Es aquí donde los datos correspondientes al periodo futuro (GCM-future) corrigen su sesgo respecto de los datos observados.
- Interpolación espacial de datos climáticos. Los datos son interpolados en el polígono seleccionado por el método de Ponderación de Distancia Inversa (IDW, por sus siglas en inglés) para adaptarlos al tamaño seleccionado de malla.
- Analizador de días consecutivos críticos (CCDA, por sus siglas en inglés). Emplea un enfoque personalizado de minería de datos para reconocer patrones en determinadas variables climáticas – i.e. temperatura, precipitación y humedad del suelo – para identificar la frecuencia de ocurrencia simultánea en un determinado periodo. De igual modo, el CCDA puede ser emplea para identificar eventos hidrológicos extremos mediante el cálculo continuo de los periodos de días secos y húmedos.

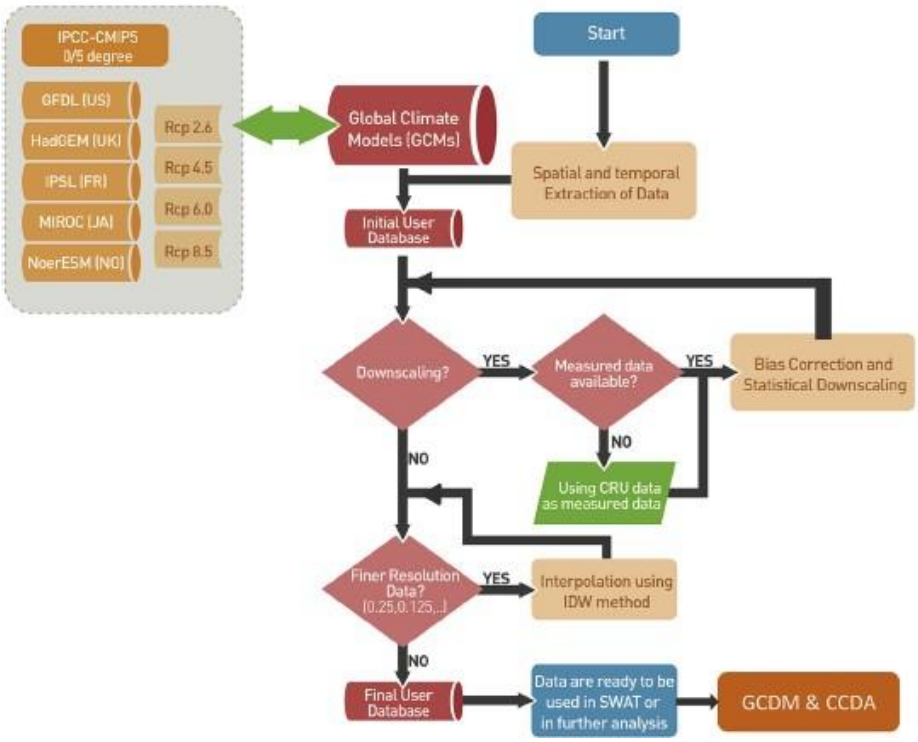

Figura 4. Proceso de trabajo de la Herramienta de Cambio Climático (CCT) (Vaguefi et al. 2017)

III.3.2 Escenarios de cambio climático

La comprensión científica del sistema climático terrestre, incluido su comportamiento frente a las perturbaciones ocasionadas por la actividad humana, queda capturada en los GCM y ESM (Jones et al., 2011).

En la fase 5 del Coupled Model Intercomparison Project (CMIP5) se estableció un protocolo experimental estándar para el estudio de los resultados de los modelos de circulación general (GCM) en los que se evaluaba de manera conjunta el comportamiento oceánico y atmosférico – en inglés, coupled ocean-atmosphere GCM. CMIP5 proveía una infraestructura de soporte para el diagnóstico, validación, comparación, documentación y acceso a los datos de los modelos climáticos que surgió como respuesta de las cuestiones científicas del Cuarto Informe de Asesoría del IPCC (AR4) y sirvió para la realización de los

modelos de cambio climático del Quinto Informe de Asesoría del IPCC (AR5). Los objetivos de la modelación de CMIP5 eran (Jones et al., 2011):

- Evaluar cuán realistas eran los modelos en la simulación del pasado reciente.
- Desarrollar proyecciones futuras de cambio climático para dos escalas temporales diferenciadas: (1) corto término (hasta el entorno de 2035); y (2) largo término (hasta 2100 o posterior).
- Entender algunos de los factores responsables de las diferencias entre las proyecciones de los modelos, incluyendo la cuantificación de factores relevantes como los relacionados con las nubes y el ciclo del carbono.

Algunos de los experimentos propuestos en CMIP5 fueron novedosos respecto de los estudios antecedentes, incluyendo la consideración de escenarios de emisiones provenientes del ciclo de carbono en los ESM.

Posteriormente, se planteó el proyecto Inter-Sectoral Impact Model Intercomparison Model (ISI-MIP) para definir un protocolo común intersectorial – i.e. disponibilidad de agua, inundaciones fluviales, inundaciones costeras, agricultura, ecosistemas y demanda energética – para la medición de los impactos del cambio climático. Los objetivos específicos de ISI-MIP son (Warszawski et al., 2014):

- El análisis cuantitativo de los impactos del cambio climático a nivel global de manera consistente para diversos sectores.
- Estimación de la sensibilidad de los modelos basada en la cuantificación de las variaciones para los GCM y los modelos de impacto globales.
- Iniciar el desarrollo coordinado de la mejora en la modelación y evaluación de impactos.

El producto se lanzó a tiempo para que el IPCC contase con los primeros resultados para la elaboración del Quinto Informe de Asesoría (AR5). En la actualidad cumple con la doble función de facilitar el conocimiento y la capacidad de modelación de impactos entre la comunidad científica y arrojar resultados cuantitativos disponibles para los actores relevantes y la sociedad en general.

Los datos del producto ISI-MIP5 contienen una corrección diaria del sesgo para las variables consideradas (Hempel et al., 2013) – i.e. temperatura media, máxima y mínima; precipitación total; nieve; radiación de onda corta y larga; viento (velocidad y dirección); presión superficial. Se seleccionaron los cinco modelos de cambio climático que disponían de información para las variables objetivo en el periodo 1950-2099 dentro del proyecto CMIP5 – incluyendo tanto los datos históricos como los referentes a todos los Representative Concentration Pathway (RCP), relativos al escenario de emisiones correspondiente (Moss et al., 2010).

Los datos climáticos disponibles se interpolaron espacialmente hasta conseguir una malla de 0.5° x 0.5°, al igual que los datos temporales, con los que se obtuvieron los valores diarios de toda la serie. Los GCM que integran el proyecto ISI-MIP5 son:

- HadGEM2-ES.
- IPSL-CM5A-LR.
- MIROC-ESM-CHEM.
- GFDL-ESM2M.
- NorESM1-M.

En la presente tesis se ha realizado una descarga de esta información con ayuda de la herramienta CCT para el estudio del impacto del cambio climático y sequías en la cuenca GRB. A continuación, se describen las características principales de los GCM integrados en ISI-MIP5:

III.3.2.1 HadGEM2-ES

El modelo Hadley Centre Global Environmental Model version 2 Earth System configuration (HadGEM2-ES) tiene una resolución espacial de 1.25 x 1.875 en la componente atmosférica y 38 niveles verticales y una resolución de 1 en el océano (Good et al., 2013). Las componentes principales del modelo son (Collins et al., 2011):

- Ciclo de carbono terrestre, mediante el esquema dinámico TRIFFID de vegetación.

- Ciclo de carbono oceánico, mediante el esquema biológico diat-HadOCC.
- Química atmosférica, mediante el esquema UKCA de la troposfera.
- Aerosoles, considerando el carbono orgánico derivado de combustibles fósiles, amonio, polvo, aerosoles orgánicos biogénicos.

III.3.2.2 IPSL-CM5A-LR

El modelo Institut Pierre Simon Laplace Climate Model version 5A Low Resolution (IPSL-CM5A-LR) tiene una resolución espacial de 3.75 x 1.875 y sus componentes principales son (Dufresne et al., 2013):

- Ciclo de carbono terrestre, mediante el modelo ORCHIDEE de suelo y vegetación.
- Ciclo de carbono oceánico, mediante la combinación de los modelos NEMO y PISCES.
- Química atmosférica, basada en el GCM atmosférico LMDZ5 y considerando las variables químicas mediante el modelo REPROBUS.
- Aerosoles, mediante el modelo INCA.

III.3.2.3 MIROC-ESM-CHEM

El modelo Model for Interdisciplinary Research on Climate Earth System Model with an atmospheric CHEMistry component (MIROC-ESM-CHEM) tiene una resolución espacial de 2.8125 x 2.7906 y sus componentes principales son (Watanabe et al., 2011):

- Ciclo de carbono terrestre, mediante el modelo SEIB-DGVM de suelo y vegetación.
- Ciclo de carbono oceánico, mediante el modelo ocean GCM.
- Química atmosférica, mediante el modelo COCO.
- Aerosoles, mediante el módulo SPRINTARS.

III.3.2.4 GFDL-ESM2M

El modelo Geophysical Fluid Dynamics Laboratory Earth System Model version 2M (GFDL-ESM2M) tiene una resolución espacial de 2.5 x 2.0225 y sus componentes principales son (Dunne et al., 2012 y 2013):

- Ciclo de carbono terrestre, mediante el modelo Land Model version 3.0 (LM3.0) de suelo y vegetación.
- Ciclo de carbono oceánico, mediante el modelo Climate Model version 2.1(CM2.1).
- Química atmosférica, mediante el modelo TOPAZ2.

III.3.2.5 NorESM1-M

El modelo Norwegian Earth System Model (Nor-ESM1-M) tiene una resolución espacial de 2.5 x 1.8947 y sus componentes principales son (Iversen et al., 2013):

- Ciclo de carbono terrestre, mediante el modelo CCSM4 de suelo y vegetación.
- Ciclo de carbono oceánico, basado en el modelo MICOM.
- Química atmosférica, mediante el modelo CAM4.
- Aerosoles, mediante el modelo CAM4-Oslo.

Finalmente, los estudios climáticos requieren de unos escenarios comunes de emisiones, concentraciones y usos del suelo que permitan evaluar los costes y beneficios de las distintas medidas que se puedan plantear, en definitiva el planteamiento de los Representative Concentration Pathways (RCP).

Para su establecimiento el IPCC requirió a la comunidad científica su desarrollo, quedando fuera de los objetivos del panel. Los criterios que se establecieron para la definición de escenarios fueron los siguientes (van Vuuren et al., 2011):

- Los RCP deben basarse en escenarios existentes en la literatura, desarrollados de manera independiente entre los distintos grupos de modelación y ser representativos en términos de emisiones y concentraciones – estableciendo a su vez una descripción del futuro plausible y consistente.

- Los RCP deben presentar información de las distintas componentes de esfuerzos radiactivos necesarias para la modelación climática y de la química atmosférica – i.e. emisión de gases de efecto invernadero, contaminantes del aire y usos del suelo. La información generada deberá estar disponible geográficamente.
- Los RCP deben partir de una base común de asunciones para las emisiones y los usos del suelo para tener una transición suave entre los análisis de datos históricos y los periodos futuros.
- Los RCP deben cubrir hasta el año 2100, aunque la información debe estar disponible para los siglos venideros.

En base a estas premisas se seleccionaron distintos escenarios de la literatura que fueron procesados para obtener los RCP de manera secuencial: (1) selección de cuatro escenarios de la literatura disponible; (2) actualización de escenarios para homogeneizar los periodos de emisión y la información de usos del suelo; (3) armonización de usos del suelo y reducción de escala; (4) idem para los datos de emisiones; (5) conversión de los datos de emisión en datos de concentración mediante el modelado del ciclo de carbono para los gases de efecto invernadero y un modelo químico de la atmósfera para las sustancias reactivas de corta duración; (6) extensión simple de los RCP en el periodo 2100-2300; y (7) disponibilidad de la información a través de un repositorio.

Los RCP reciben su nombre en función del nivel de energía radioactiva para 2100 en relación a los valores previos a la Revolución Industrial. Los escenarios finalmente establecidos son:

- RCP2.6, referente a un nivel de energía muy bajo que alcanza lo 3 W/m^2 antes de finalizar el S.XXI y desciende hasta 2.6 W/m^2 en 2100.
- RCP4.5, escenario de estabilización bajo que alcanza los 4.5 W/m^2 en 2100.
- RCP6, escenario de estabilización medio que alcanza los 6 W/m^2 en 2100.
- RCP8.5, referente a un nivel de energía muy alto que alcanza los 8.5 W/m^2 en 2100.

En la presente tesis se seleccionaron los RCP 4.5 y 8.5 para evaluar el cambio climático en la cuenca del rio GRB en El Salvador.

Para seleccionar los GCM que mejor representan los datos climatológicos históricos se emplea el indicador Id, que mide la bondad del ajuste del GCM regionalizado a partir del análisis de la media y la desviación típica. La formulación empleada es la siguiente:

$$\mathrm{Id}_i = \sum_{n,m=1}^{2} \mathrm{Id}_i(V_n S_m)$$
$$\mathrm{Id}_i(V_n S_m) = \sum_{j=1}^{12} \left[(V_n S_m)_i^j - (V_n S_m)_{Hist}^j \right] / (V_n S_m)_{Hist}^j \qquad (2)$$

donde el subíndice *i* hace referencia al producto GCM regionalizado y el subíndice *j* al mes correspondiente del año medio de estudio. V_1 es la variable precipitación y V_2 es la variable temperatura, siendo S_1 el valor medio mensual y S_2 la desviación típica de cada GCM regionalizado.

Del mismo modo, tanto los registros de los GCM como los valores observados en las estaciones climáticas fueron sometidos a test de Mann-Kendall y Sen para analizar las tendencias anuales y mensuales de las variables precipitación y temperatura, empleando para ello la hoja de MS Excel MAKESENS (Version 1.0).

III.4 PRODUCTOS SATELITALES DE PRECIPITACIÓN Y TEMPERATURA

Las variables climáticas de precipitación y temperatura son el parámetro principal de entrada de los modelos hidrológicos y los estudios de cambio climático.

Tradicionalmente, la obtención de ambos datos se ha realizado a partir de estaciones meteorológicas, que permiten registrar – tanto de manera manual como automática – las variables climáticas con diferentes frecuencias de escritura. Sin embargo, este tipo de registros presenta limitaciones espaciales y temporales, ya que la heterogeneidad espacial de los fenómenos climatológicos es muy grande y los registros tradicionales tienen una cadencia temporal insuficiente para el estudio de determinados fenómenos hidrológicos – i.e. en muchos casos

no es posible realizar estudios de crecidas a partir de datos diarios de precipitación.

Posteriormente, a partir de la Segunda Guerra Mundial comenzaron a desarrollarse los primeros dispositivos basados en sensores remotos, en este caso, el radar meteorológico, que ha tenido una implantación adecuada en los países más desarrollados, como Estados Unidos o China, pero que sigue presentando problemas de coberturas inadecuadas y de falta de implantación en los países en vías de desarrollo.

En este contexto, tiene especial relevancia el uso de productos satelitales para la observación de las variables climáticas, puesto que amplían la cobertura espacial y temporal de los productos referidos con anterioridad y el recabado de su información se produce de manera continua y uniforme.

A continuación, se describen las características principales de los productos satelitales de precipitación y temperatura que han sido empleados en la modelación hidrológica de los distintos artículos que componen esta tesis.

III.4.1 ERA5

El producto satelital del Centro Europeo de Predicciones Meteorológicas a Plazo Medio (ECMWF, por sus siglas en inglés) es el ERA5. Se trata de un producto reciente que mejora y sustituye a ERA-Interim, que se mantuvo en producción hasta el 31 de agosto de 2019. La resolución espacial es de 31 Km y el producto incluye una gran cantidad de variables climáticas desde enero de 1950 hasta la actualidad (Hersbach et al., 2020).

Dentro de la presente tesis se han empleado las series horarias de precipitación y temperatura descargadas desde la aplicación del Copernicus Climate Data Store (CCDS, disponible en https://cds.climate.copernicus.eu, accedido el 3 de septiembre de 2021) y agregados a valores diarios.

III.4.2 CHIRPS y CHIRTS

La información del producto satelital del Climate Hazards group Infrared Precipitation (Temperature) with Stations (CHIRPS/CHIRTS) es resultado de la colaboración entre el USGS y la Universidad de California. La malla de referencia

tiene una resolución especial de 0.05° y combina información satelital con datos recabados en estaciones hidrometeorológicas existentes.

La base de datos fue creada a partir de las siguientes fuentes de datos (Funk et al., 2015):

- El producto Tropical Rainfall Measuring Mission (TRMM) 3B42 de la NASA.
- La precipitación mensual climatológica (CHPClim).
- El modelo atmosférico de campos de precipitación del National Oceanic and Atmospheric Administration (NOAA) Climate Forecast System version 2 (CFSv2).
- Las observaciones satelitales geoestacionarias de infrarrojo de dos Fuentes de la NOAA.
- Precipitación observada in situ.

De manera más reciente, un producto satelital con valores de temperatura ha sido desarrollado a escala diaria con idéntica resolución que CHIRPS, para ello parte de los valores mensuales y desagrega sus valores empleando las temperaturas de ERA5 para obtener los valores diarios (Verdin et al., 2020). CHIRPS v2.0 y CHIRTS v1.0 pueden obtenerse desde la web del Climate Hazards Group (https://www.chc.ucsb.edu/data/, accedido el 5 de septiembre de 2021).

III.4.3 CFSR

El producto satelital Climate Forecast System Reanalysis (CFSR) fue desarrollado por NCEP (Saha et al., 2014) y combina métodos avanzados de asimilación de datos e información proveniente de una red global de estaciones climáticas y productos satelitales. La información de CFSR tiene una resolución espacial de 0.30 y está disponible desde 1979 hasta 2014, pudiendo descargarse desde la web de SWAT (https://globalweather.tamu.edu/, accedido el 5 de septiembre de 2021).

III.4.4 MSWEP

El producto Multi-Source Weighted-Ensemble Precipitation (MSWEP) fue desarrollado por GloH2O (Beck et al., 2017), tiene una resolución temporal de 3 h y proviene de la combinación de información proveniente de estaciones meteorológicas, datos satelitales y datos provenientes de reanálisis. La información de MSWEP v1.1 tiene una resolución espacial de 0.25 y está disponible desde 1979 hasta 2015 (www.gloh2o.org, accedido el 6 de septiembre de 2021).

III.4.5 PERSIANN-CDR

El producto satelital Precipitation Estimation from Remotely Sensed Information using Artificial Neural Networks – Climate Data Record (PERSIANN-CDR) fue desarrollado por la NOAA (Ashouri et al., 2015) y es un producto de precipitación a partir de reanálisis que presenta los resultados a escala diaria con una resolución especial de 0.25 , estando disponible desde 1982 hasta la actualidad (https://www.ncei.noaa.gov/data/precipitation-persiann/access/, accedido el 6 de septiembre de 2021).

III.4.6 CMORPH

El producto satelital Climate Prediction Center (CPC) MORPHing method (CMORPH) fue desarrollado por la NOAA (Joyce et al., 2004) y estima la precipitación a partir de microondas observadas a partir de satélites geoestacionarios de datos infrarrojos. La resolución espacial es de 0.0728 y la temporal es de 30 min. Sus datos están disponibles desde 1998 hasta la actualidad (https://www.ncei.noaa.gov/data/cmorph-high-resolution-global-precipitation-estimates/access/, accedido el 6 de septiembre de 2021).

IV – PUBLICACIONES

IV- PUBLICACIONES

Dentro de este capítulo se encuentran las publicaciones que integran la presente tesis. Se trata de una secuencia de tres etapas, en la que cada una de ellas concluye con un artículo publicado. El denominador común de todas ellas es el empleo del modelo SWAT para la evaluación de recursos hídricos en cuencas en un contexto tropical y con escasez de información climatológica y foronómica.

- **Publicación 1:** El inicio de esta investigación se orientó a la evaluación que los cambios en temperatura y precipitación tienen sobre la disponibilidad del recurso hídrico y las sequías. SWAT se empleó por primera vez en El Salvador para el estudio del cambio climático en la cuenca GRB, que presenta un alto interés ecológico y medioambiental. El software CCT se utiliza para preparar la información de los productos GCM de precipitación y temperatura con la corrección estadística del sesgo para la escala de cuenca. De entre los GCM evaluados, se seleccionó el modelo HadGEM2-ES para los escenarios climáticos de emisiones RCP 4.5 y 8.5 por ser el que mejor reproduce el clima histórico (1975-2004). Los resultados de este periodo fueron comparados con los obtenidos por los escenarios climáticos para los periodos futuros 2040-2069 y 2070-2099. A partir de un análisis de tendencia se puede comprobar como en ambos horizontes se produce un descenso en la precipitación y un incremento en la temperatura, más acusados en el escenario de emisiones RCP 8.5, que conllevarán un impacto negativo en la disponibilidad de recursos hídricos debido al cambio climático. Adicionalmente se emplearon los índices SPI y SRI para medir el impacto del cambio climático sobre las sequías, observando como en un futuro las sequías serán más pronunciadas que las actuales, destacando por su mayor intensidad y duración.
- **Publicación 2:** La siguiente etapa de esta tesis se centra en la aplicabilidad que los datos de descargas del producto satelital GloFAS tienen para la calibración de modelos hidrológicos en

regiones en las que la información climática y de aforos de caudal es escasa o inexistente, siempre y cuando existe una buena correlación entre la temperatura y precipitación proveniente de reanálisis y las observadas en la zona de estudio. El estudio se llevó a cabo en la cuenca del río GSM y evaluó los productos de reanálisis ERA5, CHIRPS-CHIRTS y CFSR, que demostraron una capacidad aceptable para detectar la producción de precipitación y, en algunos casos, excelente para representar a la temperatura. De manera que los tres modelos climáticos quedaron habilitados para realizar el estudio hidrológico empleando los caudales de GloFAS como valores de calibración. Tras emplear los caudales provenientes de GloFAS para la calibración de los modelos hidrológicos se pudo comprobar el buen desempeño de los mismos respecto de los realizados con los caudales observados – para ello se emplearon los estadísticos R^2, NSE, PBIAS y KGE.

- **Publicación 3:** Finalmente, la última etapa de esta tesis se centra en profundizar sobre los productos satelitales de precipitación (GP) como datos de entrada en la modelación hidrológica con SWAT. Para ello se emplea nuevamente la cuenca del río GSM para la evaluación de cinco GP. En primer lugar, se realizó una comparativa entre ellos y las mediciones observadas en las estaciones climatológicas de la zona de estudio. Seguidamente se realizó un modelo SWAT con cada uno de ellos como dato de entrada y se comprobó como en todos los casos se conseguía simular adecuadamente los caudales observados, lo que demuestra el potencial de los GP para la simulación hidrológica en regiones en las que hay escasez de información.

IV.1 PUBLICACIÓN 1: IMPACT OF CLIMATE CHANGE ON WATER BALANCE COMPONENTS AND DROUGHTS IN THE GUAJOYO RIVER BASIN (EL SALVADOR)

Blanco-Gómez, P.; Jimeno-Sáez, P.; Senent-Aparicio, J.; Pérez-Sánchez, J. Impact of climate change on water balance components and droughts in the Guajoyo River Basin (El Salvador). *Water* **2019**, *11*, 2360.

https://doi.org/10.3390/w11112360

water

MDPI

Article

Impact of Climate Change on Water Balance Components and Droughts in the Guajoyo River Basin (El Salvador)

Pablo Blanco-Gómez, Patricia Jimeno-Sáez *, Javier Senent-Aparicio and Julio Pérez-Sánchez

Department of Civil Engineering, Catholic University of San Antonio, Campus de los Jerónimos s/n, Guadalupe, 30107 Murcia, Spain

* Correspondence: pjimeno@ucam.edu; Tel.: +34-968-278-818

Received: 27 September 2019; Accepted: 8 November 2019; Published: 11 November 2019

check for updates

Abstract: This study assessed how changes in terms of temperature and precipitation might translate into changes in water availability and droughts in an area in a developing country with environmental interest. The hydrological model Soil and Water Assessment Tool (SWAT) was applied to analyze the impacts of climate change on water resources of the Guajoyo River Basin in El Salvador. El Salvador is in one of the most vulnerable regions in Latin America to the effects of climate change. The predicted future climate change by two climate change scenarios (RCP 4.5 and RCP 8.5) and five general circulation models (GCMs) were considered. A statistical analysis was performed to identify which GCM was better in terms of goodness of fit to variation in means and standard deviations of the historical series. A significant decreasing trend in precipitation and a significant increase in annual average temperatures were projected by the middle and the end of the twenty–first century. The results indicated a decreasing trend of the amount of water available and more severe droughts for future climate scenarios with respect to the base period (1975–2004). These findings will provide local water management authorities useful information in the face of climate change to help decision making.

Keywords: SWAT; hydrological modeling; climate change; Guajoyo River; El Salvador

1. Introduction

The last century has seen a dramatic increase in greenhouse gas emissions. These higher concentrations of carbon dioxide and other greenhouse gases in the Earth's atmosphere increase the greenhouse effect and directly affect global temperature [1]. Consequently, global warming has caused higher evapotranspiration rates leading to changes in precipitation worldwide. Such global climate change significantly affects the hydrological cycle and streamflow regimes, especially at the basin scale [2], which directly affects ecosystems, water security and economic activity, mainly in the agricultural sector, in forestry and energy generation by hydroelectricity. Some of the consequences of climate change, such as an increase in extreme floods and droughts, maybe unavoidable [3]. Therefore, quantifying the climate change impact on water availability is essential to watershed management as well as to the formulation of adaptation strategies to mitigate its negative impacts [4].

According to the Intergovernmental Panel on Climate Change (IPCC) [5], it is expected that almost all regions of the world will experience a negative impact on climate change. Specifically, developing countries are more vulnerable to climate change than developed countries, due to increased exposure to extreme hydrometeorological events, the predominance of agriculture in their economies, poor infrastructure and less capital for developing adaptation measures [6,7]. This study explores local responses to climate change-related perturbations through one case study in a rural area of El Salvador,

the Guajoyo River Basin. El Salvador is in one of the most vulnerable regions in Latin America to the effects of climate change, as it is located within a band of hurricanes and low-lying coastal areas, among other particularities [5,8]. Numerous publications have evaluated the impact of climate changes on the hydrological cycle in Latin America and the rest of the world. However, few studies focused on the evaluation of streamflow changes in El Salvador. Maurer et al. [9] studied the hydrologic impacts of climate change to the Lempa River Basin, one of the largest basins in Central America, covering portions of Guatemala, Honduras, and El Salvador. Imbach et al. [10] evaluated the likelihood and magnitude of the impacts of climate change on potential vegetation and the water cycle in El Salvador and the rest of Central America. Other studies that analyzed climate change near the study area, albeit without focusing on the study of water availability, were: Campos et al. [8] explored local adaptation strategies to mitigate climate change-related perturbations through two case studies in rural areas of Mexico and El Salvador; and Aguilar et al. [11] assessed climate vulnerability and adaptation to climate change of rural inhabitants in the central coastal plain of El Salvador.

Hydrological models are the principal tools used to explore the potential effects of climate change on water resources [12]. The hydrological model Soil and Water Assessment Tool (SWAT) has been successfully and widely used all over the world to simulate basin hydrology under different climate change scenarios [13–15]. However, to the best of our knowledge, no previous works have been found applying the SWAT model in El Salvador and so far no study has been carried out in the Guajoyo River Basin in relation to the impact of climate change on water resource availability under climate change conditions in particular.

The Guajoyo River Basin presents an environmental interest in terms of international protection figures, such as (1) the Complejo Güija, part of the Ramsar List of the Convention of Wetlands since 2010, located in the mouth of the river Guajoyo where it flows into the river Desagüe; (2) the Montañita Protected Natural Area, designated in 2010, in the upper part of the tributary catchments Quebrada Las Marias and Quebrada San Marcos, where the dry tropical forest stands; and (3) the Trifinio Fraternidad area designated as a Biosphere Reserve by UNESCO in 2011 and located between El Salvador, Guatemala and Honduras, which guarantees water supply for local communities, whilst playing a key role in regional development through agro–tourism and coffee activities.

As a result of its environmental interest, the hydrologic balance of the Guajoyo River Basin becomes crucial in order to maintain or enhance the sustainability of the area while coping with the human and climate change pressures. Therefore, the main objective of this paper is to assess the impacts of climate change on hydrological processes, such as water balance components of the basin, using five future general circulation models (GCMs) climate projections of temperatures and precipitation under different emission climate scenarios, downscaled for use as an input in a SWAT model of the Guajoyo River Basin, located in northwest El Salvador. Also, the potential impacts of climate change on droughts in this basin were evaluated. The results obtained in this study are expected to provide more insight into the future water availability in this developing country, where these types of studies are scarce, to help local water management authorities make wise and rational decisions to meet and overcome water challenges and plan water resources management in the basin in the context of climate change.

2. Materials and Methods

2.1. Study Area

The headwaters of Guajoyo River Basin are situated in the West of El Salvador and cover about 156 km^2, with terrain elevations of between 425 and 1517 m (Figure 1). The average slope in the basin is 16%, with steep slopes characterizing the highlands and relatively gentle slopes being predominant in the lowlands. The Guajoyo River is a tributary of the Lempa River, the largest and most important river in El Salvador. The studied basin, as the region in general, has a tropical climate and experiences a wet season followed by a dry season [16].

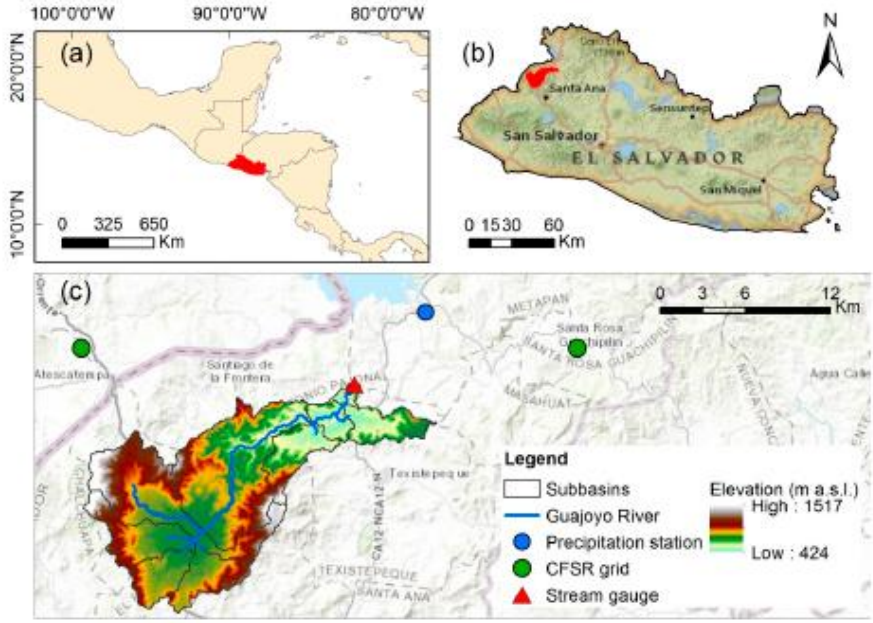

Figure 1. Location map: (**a**) Location of El Salvador in Central America; (**b**) Location of the Guajoyo River Basin in El Salvador; (**c**) Subbasins, Digital Elevation Data (DEM), river and hydro-meteorological stations of Guajoyo River Basin.

The annual historical precipitation in this area ranges from 862 to 1834 mm/year, with the average annual precipitation from 1970 to 2017 being 1373 mm/year. The wet period from May to October is clearly distinguishable, with an average rainfall of 1249 mm, equivalent to 91% of the total annual rainfall, and the dry period from November to April with a rainfall of 124 mm representing 9%. Temperature values vary mainly with elevation and show few seasonal changes, with maximum values in the months of March and April and minimum values in the months of November and December. The average annual temperature in the basin is 23 °C. The dominant soils are andosols, which are of volcanic origin, highly permeable and fertile [17,18]. The basin is covered by sixteen land use types (Table 1), being dominated by cropland, which accounts for 51% of the total area, and by pastureland (30%).

Table 1. Land use type of the Guajoyo River Basin.

Land Use Type	Area (km^2)	% Coverage
Commercial	0.66	0.42
Sugarcane	0.68	0.43
Range–Grasses	0.97	0.62
Residential–High Density	1.70	1.09
Forest–Deciduous	2.00	1.28
Forest–Mixed	2.35	1.50
Southwestern US (Arid) Range	3.22	2.06
Meadow Bromegrass	3.22	2.06
Forest–Evergreen	3.84	2.46
Residential–Medium Density	4.27	2.74
Coffee	5.75	3.69
Shrubland	11.51	7.38
Pasture	12.47	7.99
Range–Grasses	31.44	20.15
Dryland cropland and pasture	34.44	22.07
Agricultural Land–Generic	37.52	24.05

2.2. *Data Sources*

The SWAT model requires input of Digital Elevation Data (DEM), land use, soils, and meteorological data, such as daily precipitation, maximum and minimum temperatures, solar radiation, relative humidity and wind speed. The terrain data were obtained from the Advanced Spaceborne Thermal Emission and Reflection Radiometer (ASTER) Global Digital Elevation Model (GDEM) version 2, with a resolution of 30 × 30 m [19]. Land use maps, precipitation and streamflow data were obtained from Ministry for the Environment and Natural Resources of El Salvador (MARN). The rainfall station is located on Lake Güija at an altitude of 485 m a.s.l. The streamflow data are monthly data from 2006 to 2012 for a gauge station called Piedra–Cargada that is located at the outlet of the basin. Soil data were taken from the Harmonized World Soil Database [20]. Due to the poor quality and scarcity of measured data, other weather data (maximum, and minimum air temperatures, average wind speed, solar radiation, and relative humidity) were derived from the Climate Forecast System Reanalysis (CFSR) data set developed by the National Centers for Environmental Prediction (NCEP) in the USA [21], with a grid data of size 38 by 38 km (see Supplementary Materials, Tables S1 and S2). The CFSR data were obtained from the SWAT team at Texas A&M University (https://globalweather.tamu.edu/). Global atmospheric reanalysis such as CFSR are commonly used to provide basin–scale hydrological simulations with the required climate data, especially where measured data are scarce [22].

In this study, the software Climate Change Toolkit (CCT) (described by Vaghefi et al. [23]) had been used to prepare the data for the climate change scenarios. CCT is a platform which allows the user to extract and prepare data needed in a climate change study for application to hydrology. Data for different climate change scenarios were prepared using the CCT software. CCT database involves five sets of global 0.5° × 0.5° grid GCM data from Inter-Sectoral Impact Model Inter comparison Project (ISI-MIP5) [24]. Historical (1975–2005) and future data (2006–2099) for temperature (°C) and precipitation (mm) from five GCMs (GFDL–ESM2M, HadGEM2–ES, IPSL–CM5A–LR, MIROC, and NoerESM1–M) were downloaded (made available at http://www.2w2e.com). CCT software uses a statistical bias correction method to downscale meteorological variables from GCMs. The RCP 4.5 and 8.5 emission scenarios were used to quantify climate change on the hydrologic regime of Guajoyo River Basin.

2.3. *Conceptual Model*

The aim of this study is to quantify the future climate and its impact on the streamflow of the Guajoyo River Basin. A SWAT model was used to develop different model setup scenarios.

Under different climatic conditions in the future, specifically with respect to rainfall and temperature, the response of the basin was evaluated. The potential impact of climate change on hydrology is analyzed in two different time horizons: mid future (2040–2069), and far future (2070–2099). The 30-year period from 1975–2004 was used as a baseline. The methodology used in this study is presented in Figure 2. It includes the following steps: (1) configuration, calibration and validation of hydrological model using SWAT; (2) spatial and temporal extraction of GCMs data, bias correction and statistical downscaling of these data using CCT software; (3) analysis and comparative assessment of downscaled GCM projections according to their ability to reproduce historical climatology for the selection of GCM; (4) obtaining the results in SWAT for each scenario considered; (5) assessment of the impact of climate change in the basin by simulating the new climate conditions in the calibrated SWAT model and drought analysis.

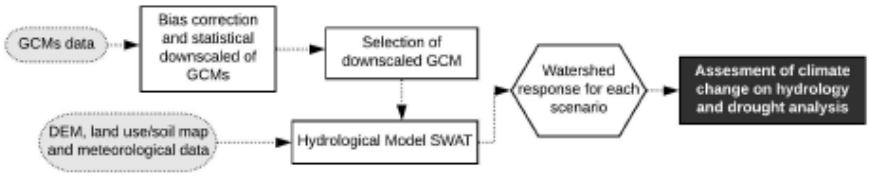

Figure 2. Flowchart for the methodology adopted in the present study.

2.4. *The SWAT Hydrological Model*

The hydrological modelling of Guajoyo River Basin was carried out using SWAT. The SWAT model is a semi-distributed physically based hydrological model, operating on a daily time step and used for continuous long-term simulations of a variety of processes. The major simulated hydrological variables of the SWAT model consist of surface runoff, soil and root zone infiltration, evapotranspiration, soil and snow evaporation, and return flow [25].

The SWAT model works on the principle of dividing the basin into a multiple sub-basins based on the river network and topography; subsequently, sub–basins are divided into hydrologic response units (HRUs) which have unique soil, slope and land use properties [26]. SWAT simulates the hydrological cycle based on the water balance using the following equation:

$$SW_t = SW_{init} + \sum_{i=1}^{t} \left(R_{day}(i) - Q_{surf}(i) - E_a(i) - W_{seep}(i) - Q_{gw}(i) \right) \quad (1)$$

where SW_t is the final soil water content (mm), SW_{init} is the initial soil water content (mm), t is the time in days, $R_{day}(i)$ is the amount of precipitation on day i (mm), $Q_{surf}(i)$ is the surface runoff (mm), $E_a(i)$ is the evapotranspiration (mm), $W_{seep}(i)$ is the percolation (mm) and $G_{gw}(i)$ is the return flow (mm).

2.4.1. Model Setup

The SWAT model requires three physically based inputs to characterize a watershed: a soil map, a land cover/use map, and a DEM. The first step in SWAT model setup for a particular area are defining the watershed boundaries and analyze the drainage patterns of the terrain using a DEM of 30 m × 30 m grid size. The landuse data contains use and crop specific digital layers, suitable for use in Geographic Information System (GIS) and are one of the most important factors that control events such as runoff, evapotranspiration, sediment deposition and soil erosion [27]. The area under each landuse type and SWAT classification system are presented in Table 1. Soil maps were used to characterize each soil type from information on soil texture, hydraulic conductivity and available water content, among others, and includes one type of soil for the study area. Due to high elevation differences in the basin, four categories of slope were defined (0–5%, 5–10%, 10–20% and >20%) which cover 23, 9, 18, and 50% of

the watershed, respectively. In SWAT, land use, soil and slope maps were overlaid to create the HRUs. To have a better estimation of streamflow of the basin and so as to avoid unnecessary large number of HRUs, a threshold level of 10% was established to simplify model processing and remove minor slopes, soils and land uses for each sub–basin. Finally, the Guajoyo River Basin has been divided into 11 sub-basins and 85 HRUs.

The main required climate inputs for SWAT are temperatures and precipitation, which are the ultimate climate drivers of the runoff process [28]. In this study, the SCS curve number method developed by the Soil Conservation Service [29] was used to estimate surface runoff from precipitation. The FAO Penman–Monteith method [30] was adopted to calculate the daily potential evapotranspiration. The Penman–Monteith method is recommended as the sole standard method by the United Nations Food and Agriculture Organization (FAO) and requires solar radiation, air temperature, relative humidity and wind speed [31]. Finally, once the meteorological data were loaded, the SWAT model run was started.

2.4.2. Model Calibration and Validation Procedures

The SWAT model has been calibrated and validated against observed discharge data from a gauging station using the SUFI–2 algorithm of SWAT–CUP (Calibration and Uncertainty Programs) [32]. Eleven widely used flow calibration parameters and their ranges were selected based on available literature and our previous experience, incorporating aspects of groundwater flow, runoff and soil data. To reach an acceptable calibration, three iterations (each iteration representing 500 simulations) were performed as recommended by Alemayehu et al. [33] and Pomeón et al. [34]. The parameter ranges were updated after each iteration. Among the incomplete and non-continuous measured streamflow data and considering five years as warm-up, the periods 2006–2009 and 2010–2012 were selected as the calibration and validation periods, respectively. Following the recommendations of Arnold et al. [35], the selected calibration period includes dry and wet periods to ensure that it reflects the range of conditions under which the model is expected to operate.

The model was evaluated on a monthly scale and the Nash–Sutcliffe Efficiency (NSE) was chosen as the objective function. The performance of the model for the monthly flow was evaluated according to the recommendation and performance ratings proposed by Moriasi et al. [36]. Further efficiency criteria used in this study were the R^2, *PBIAS*, *RMSE*, and *RSR*. These statistics are defined in Table 2.

Table 2. Performance metrics [36,37].

Performance Metric	Equation	Range
Nash–Sutcliffe efficiency coefficient (*NSE*)	$NSE = 1 - \frac{\sum_{i=1}^{n}(O_i - S_i)^2}{\sum_{i=1}^{n}(O_i - \overline{O})^2}$	$[-\infty, 1]$
Coefficient of determination (R^2)	$R^2 = \left[\frac{\sum_{i=1}^{n}(O_i - \overline{O})\cdot(S_i - \overline{S})}{\left[\sum_{i=1}^{n}(O_i - \overline{O})^2\right]^{0.5}\cdot\left[\sum_{i=1}^{n}(S_i - \overline{S})^2\right]^{0.5}}\right]^2$	[0, 1]
Percent bias (*PBIAS*)	$PBIAS = \frac{\sum_{i=1}^{n}(O_i - S_i)\cdot 100}{\sum_{i=1}^{n}(O_i)}$	$[-\infty, \infty]$
Root mean squared error (*RMSE*)	$RMSE = \sqrt{\frac{\sum_{i=1}^{n}(O_i - S_i)^2}{n}}$	$[0, \infty]$
RMSE–observations standard deviation ratio (*RSR*)	$RSR = \frac{\sqrt{\sum_{i=1}^{n}(O_i - S_i)^2}}{\sqrt{\sum_{i=1}^{n}(O_i - \overline{S})^2}}$	$[0, \infty]$

O_i is the i-th observed data, $\overline{O}$ is the mean of the observed data, S_i is the i-th simulated data, $\overline{S}$ is the mean of the simulated data and n is the total number of observations.

2.5. Climate Change Scenarios and Predictions

After the SWAT model was calibrated and validated under current conditions, the simulation of streamflow corresponding to future climate change were carried for future periods in two time horizons, mid future (2040–2069), and far future (2070–2099), for both RCP 4.5 and RCP 8.5 climate scenarios.

Firstly, historical and future GCMs climate data was extracted from GFDL–ESM2M, HadGEM2–ES, IPSL–CM5A–LR, MIROC, and NoerESM1–M models. Second, it was necessary that GCMs products be regionalized to a specific area to obtain a meaningful interpretation of the impacts of climate change on a local scale. In addition, biases need to be corrected to eliminate existing biases in climate data [38]. In this study bias correction using statistical downscaling was used for the GCM future data, which were bias corrected against the observed data. The performance of statistical bias correction methods to downscale the meteorological variables of the GCMs is considered satisfactory in different hydro-climatological studies [39]. The observed data for the period 1975–2004 used as the base period were also corrected according to Sofaer et al. [40] (see Supplementary Materials, Tables S3 and S4). Data download, spatial downscaling and bias correction of GCMs and the observed data were carried out in the CCT software. The CCT downscaling module searches for the measured data stations and finds the one closest to the GCM grids to apply the correction factor. In this method, an additive and multiplicative correction factor has been applied to each month for temperature and precipitation, respectively.

The next step in this study was to perform a comparative analysis of GCMs products, previously downscaled and bias corrected, to select the better model according to their ability to reproduce historical climatology of the study area. The methodology used in this task is the one proposed by Pulido-Velazquez et al. [41]. This method consists of comparing means and standard deviations for a mean year on a monthly basis for historical precipitation and temperature time series and control series derived from the regionalized GCM (RCM) over the same period, in this study from 1980 to 2004. For this purpose, an indicator (Id) given by Equation (2) measures the goodness of adjustment obtained using each RCM for two statistics, mean and standard deviation, of both climatic variables:

$$\begin{aligned} \mathrm{Id}_i &= \sum_{n,m=1}^{2} \mathrm{Id}_i(V_n S_m) \\ \mathrm{Id}_i(V_n S_m) &= \sum_{j=1}^{12} \left[(V_n S_m)_i^j - (V_n S_m)_{Hist}^j \right] / (V_n S_m)_{Hist}^j \end{aligned} \tag{2}$$

where the subindex i is employed for a specific RCM and superscript j for the months for a mean year. V_1 is the precipitation variable, V_2 is the mean temperature variable, S_1 the mean monthly value, S_2 the monthly standard deviation for a specific RCM$_i$.

Afterward, once the four Id indicators have been obtained for each RCM, corresponding to the mean and standard deviation of both series, the best models in terms of goodness of fit to the observed time series were selected. Finally, the simulation results from the selected RCMs such as daily precipitation, and maximum and minimum temperature data of both scenarios were used as input for the SWAT model to generate the future flows.

Trend Analysis Methods

In this study, the Mann–Kendall test for the detection of trends of annual and monthly precipitation and mean temperature, and Sen's method for estimating of the slope of linear trends were used. Both non-parametric methods have been applied using the Microsoft Excel template application MAKESENS (Version 1.0) (more details can be found in Salmi et al. [42]). The Mann–Kendall test is one of the most widely used non–parametric tests for detecting trends in hydroclimatic series, which, contrary to parametric methods, it does not require the data to be normally distributed, requires only that it the data be independent. In addition, it has a low sensitivity to abrupt peaks due to inhomogeneous time series [43]. The presence of a statistically significant trend is evaluated using the test statistic Z. A positive value of Z indicates an upward trend and a negative value indicates a downward trend. In MAKESENS, the tested significance levels are 0.001, 0.01, 0.05 and 0.1. Details about the formulation of Mann-Kendall test can be found in Partal and Kahya [44]. The Sen's

method [45] is another very useful index that estimates the magnitude of the trend and is given for the sample of N pairs of data by:

$$Q_i = median\left(\frac{x_j - x_k}{j-k}\right) for\ i = 1, \ldots, N \quad (3)$$

where x_j and x_k are the data values at time j and k ($j > k$), respectively.

2.6. Drought Analysis

In this study, the standardized precipitation index (SPI) [46] and the standardized runoff index (SRI) [47] were used to characterize the meteorological and hydrological droughts, using observed precipitation and model derived runoff data for the baseline period and future simulation periods. In this study, 12-month SPI (SPI–12) and 12-month SRI (SRI–12) values were calculated using SPI Generator software developed by National Drought Mitigation Center (NDMC) [48]. A drought event is a period where SPI or SRI values are continuously negative. A drought event begins when the SPI or SRI reaches an intensity of −1.0 or less and ends when the SPI or SRI reaches a positive value. The duration of a drought event is the total number of months from the beginning to the end of the episode. The intensity of the drought event is calculated as the mean of all absolute monthly SPI or SRI values over that duration [49].

3. Results and Discussion

3.1. Performance of the SWAT Model

As discussed in the previous section, a total of 11 SWAT–parameters were optimized using the SUFI–2 algorithm of SWAT–CUP. The calibration was performed over a period of 4 years, from 2006 to 2009. The final ranges used and the final fitted values of these parameters are given in Table 3.

Table 3. Calibration of SWAT parameters for the Guajoyo River Basin.

Parameter [1]	Description	Final Range Used in Calibration	Fitted Value	Final Value
r_CN2.mgt	SCS runoff curve number	−0.2 to 0.2	−0.09	[63.40–75.17] [2]
v_ALPHA_BE.gw	Baseflow alpha factor (days−1)	0 to 0.65	0.09	0.09
a_GW_DELAY.gw	Groundwater delay time (days)	−10 to 60	−2.90	28.07
a_GWQMN.gw	Threshold depth of water in the shallow aquifer for return flow to occur (mm)	200 to 1500	1407.70	2407.70
v_GW_REVAP.gw	Groundwater revap coefficient	0.02 to 0.15	0.13	0.13
a_RCHRG_DP.gw	Deep aquifer percolation fraction	−0.02 to 0.03	0.02	0.07
a_REVAPMN.gw	Threshold depth of water in the shallow aquifer for revap or percolation to the deep aquifer to occur (mm)	−150 to 150	−85.50	664.5
v_CANMX.hru	Maximum canopy storage (mm)	1 to 10	4.47	4.47
v_EPCO.bsn	Plant uptake compensation factor	0.5 to 1	0.87	0.87
v_ESCO.bsn	Soil evaporation compensation factor	0.3 to 0.9	0.79	0.79
r_SOL_AWC.sol	Available water capacity of the soil layer (mm H_2O/mm soil)	−0.02 to 0.02	−0.01	[0.06–0.10] [3]

[1] The qualifier (r_) refers to relative change, i.e., the current parameter must be multiplied by (1 + the value obtained in calibration), (v_) means that the value of the existing parameter must be replaced by the value obtained in calibration, and (a_) refers to absolute change, i.e., the fitted value must be added to the existing value of the parameter. [2] Varies by HRU. [3] Varies by soil layer.

Figure 3 shows the results of the SWAT model plotted against the observed values of streamflow during model calibration and validation. As seen in the regression graphs (Figure 3), the model results showed that a systematic error of the SWAT model was the inability to simulate the peak flows. This problem seems to be common in many studies [50–52] and is a source of uncertainty that has

been taken into account. Despite this drawback, model calibration and validation provided globally satisfactory performance statistics (Table 4), according to the criteria given by Moriasi et al. [36].

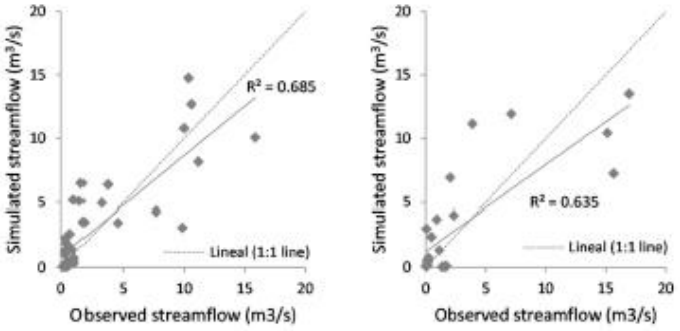

Figure 3. Regression plots of observed versus simulated monthly streamflows for the (**a**) calibration period (2006–2009), and (**b**) validation period (2010–2012).

Table 4. SWAT model performance of calibration and validation.

Performance Metric	Calibration	Validation
NSE	0.67	0.63
R^2	0.69	0.64
PBIAS (%)	−9.04	−8.80
RMSE (m^3/s)	2.35	3.12
RSR	0.58	0.61

The model performance of the monthly streamflow simulation was summarized in Table 4. For the calibration period, the SWAT model simulated the streamflow reasonably well, and also proved satisfactory for the validation period. For both periods, a *NSE* greater than 0.5, a *PBIAS* less than 25% and an *RSR* less than 0.7, indicated a suitable calibration and validation with respect to the water balance [36]. Values of R^2 greater than 0.6 also showed an acceptable model fit. These reasonable results in monthly streamflow simulation, considering the scarcity of data available in the area, allowed the SWAT model to be considered suitable for assessing hydrological responses to medium- and long-term climate change in the Guajoyo River Basin. This evaluation will be presented in the following sections. In order to demonstrate the model's goodness-of-fit, the calibrated model was run using CHIRPS (Climate Hazards Group InfraRed Precipitation with Stations) rainfall satellite data for the period 2006–2012. The CHIRPS dataset was acquired through website (http://chg.geog.ucsb.edu/data/chirps/) and has a spatial resolution of 0.05°. With these data, good statistics were also obtained for the period 2006–2012: a *NSE* of 0.74, a R^2 of 0.78, a *PBIAS* of −23.55, a *RMSE* of 2.29 and a *RSR* of 0.51.

3.2. Selection of Climate Change Models

Once the information was extracted and prepared for the study area of the five GCMs (GFDL–ESM2M, HadGEM2–ES, IPSL–CM5A–LR, MIROC, and NoerESM1–M) using CCT software, the model that best reproduced the changes for the average year for the key monthly statistics was selected. To make this selection, the Id index, defined as the sum of the absolute value of the relative difference between the statistics of the historical series and the control scenario during the 12 months of an average year, was calculated. Table 5 shows the Id_i index of each RCM_i on a monthly scale in the period 1980–2004. Each Id_i represents the distance between the means (Δx) and the standard deviations ($\Delta\sigma$) of

the historical and control scenarios. The models with higher Id are inferior in terms of goodness–of–fit to the observed time series. Of the five regionalized GCMs, the HadGEM2–ES model obtained a smaller Id ($Id_2 = 12.10$) so fitted better to the historical series of precipitation and temperature. Using this validation-based approach, we are assuming that a model's ability to simulate an observed baseline climate will be representative of the same model's ability to project future climate. The selection of GCMs has been analyzed in a number of studies (e.g., [41,53,54]). However, there is not yet sufficient scientific consensus with respect to both the identification of unsatisfactory models, and the relation between apparently poor performance to the plausibility of future projections [55]. As discussed by Overland et al. [56], the elimination of some GCMs may narrow the range of uncertainty represented by the remaining models, but it is also true that a falsely narrow range of projections may lead to over confidence and maladaptation. In this study, and due to the big differences between the fit of this model and the others, only the HadGEM2–ES model was selected for the evaluation of the impacts of climate change.

Table 5. Id index of each RCM.

	RCMs	Monthly Series				
		Precipitation		Temperature		Id
		Id (Δx)	Id (Δσ)	Id (Δx)	Id (Δσ)	
1	GFDL–ESM2M	2.14	11.18	1.22	3.76	18.30
2	HadGEM2–ES	1.78	5.95	1.63	2.74	12.10
3	IPSL–CM5A–LR	1.51	10.93	1.23	4.15	17.82
4	MIROC	2.65	9.30	1.21	9.17	22.33
5	NoerESM1–M	1.52	8.13	1.23	5.45	16.33

3.3. Changes in Climate Variables under RCP Scenarios

Changes in average monthly streamflows attributed to climate change, such as temperature and precipitation changes, in the mid-century and late-century periods, as compared to the baseline period for the Guajoyo River Basin for the HadGEM2–ES model, are presented in Figure 4.

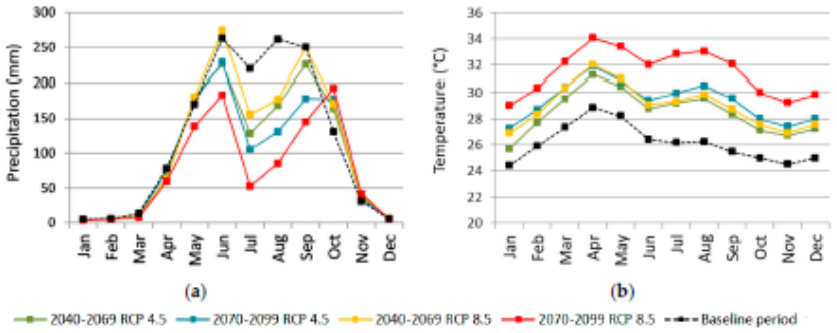

Figure 4. Comparison of monthly mean (a) precipitation and (b) temperature between baseline period (1975–2004) and mid and far future under RCP 4.5 and 8.5 for the HadGEM2–ES model.

Figure 4a shows the bimodal distribution of precipitation of the rainy summer season for the baseline and future periods, with the maximum values in the months of June and September–October and the relative minimums in July and August. This relative minimum is known as the "Mid–Summer Drought" (MSD) [57] which is considered one of the most important regional climate variability modulators [58]. On a monthly scale, considering the dry season, precipitation is expected to increase in

both scenarios and in both future periods for November and December. Specifically, for the regionalized HadGEM2–ES model, precipitation will increase by around 20% in November. However, during the rainy season (between May and October), the changes obtained show decreases in precipitation, except in October, when precipitation is expected to increase by around 27% in the medium term and 41% by the end of the century. The results show that the decrease in precipitation during the months of the wet season could occur with greater intensity in the months of July and August, with reductions of about 35% in the medium term and 61% in the long term, producing an intensification of the MSD. On the other hand, Figure 4b shows the results for the average temperature. The greatest increases in mean temperature were obtained during the summer months (July, August and September), with average increases of 3.1 °C (RCP 4.5) and 3.3 °C (RCP 8.5) by mid-century and 4 °C (RCP4.5) and 6.7 °C (RCP 8.5) by the end of the century. Similar trends of these climatic variables in El Salvador were found in the work carried out by the MARN (2017) [58].

Table 6 summarizes average annual climate variables for the baseline as well as under both emissions scenarios and both future periods of the HadGEM2–ES model. On an annual scale, the results show that precipitation will follow a decreasing trend under future conditions, whilst average temperatures will follow an increasing trend. Overall, the maximum decrease in precipitation of up to 36% is expected under RCP 8.5 in late century compared to the baseline precipitation of 1435.60 mm/year, in accord with the study of CEPAL (2010) [59], in which it was predicted that rainfall in El Salvador will decrease between 27% and 32%. In addition, the highest average temperatures are expected at the end of the century, with temperatures 12% and 21% higher than the base temperature of 26.12 °C for RCP 4.5 and 8.5 respectively. The results obtained are consistent with the findings of Conde–Álvarez and Saldaña–Zorrilla [60], which indicated that warming in Latin America by the end of the century, according to different models, will be from 1 to 6 °C for different emission scenarios.

Table 6. Average climate variables changes.

Model	Scenario	Time Period	Precipitation (mm)		Temperature (°C)	
			Value	Change with Respect to Baseline	Value	Change with Respect to Baseline
Baseline		1975–2004	1435.60	–	26.12	–
HadGEM2–ES	RCP 4.5	2040–2069	1219.12	−216.48 (−15%)	28.45	+2.33 (+9%)
		2070–2099	1129.62	−305.98 (−21%)	29.30	+3.19 (+12%)
	RCP 8.5	2040–2069	1332.64	−102.96 (−7%)	28.95	+2.84 (+11%)
		2070–2099	919.07	−516.53 (−36%)	31.49	+5.38 (+21%)

Figure 5 shows the average yearly precipitation and temperature in the basin from 2040 to 2099. Figure 5a shows how the future trend of precipitation is decreasing. In the medium term, the predicted decrease is greater in the RCP 4.5. However, in the long term, the predicted decrease in precipitation is higher for RCP 8.5, as shown in Table 6. Future temperature trends (Figure 5b) show that Guajoyo River Basin will likely experience warmer conditions in the future, the largest increase being for the RCP 8.5 scenario.

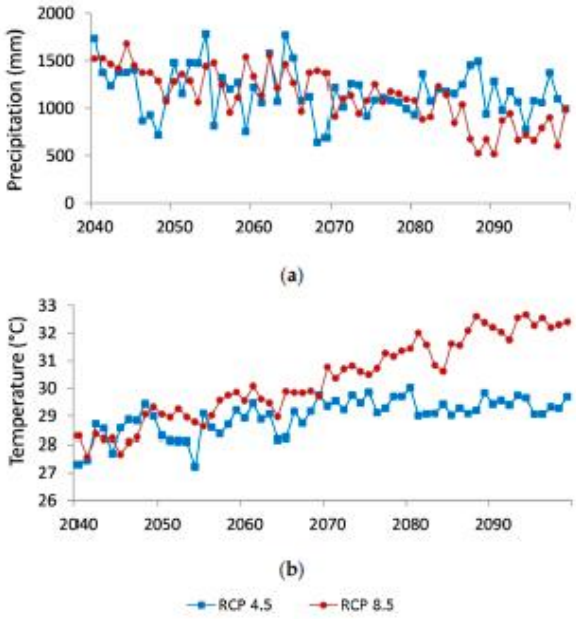

Figure 5. Temporal variations of the projected climatic variables under RCP 4.5 and 8.5: (**a**) precipitation for 2040–2099 and (**b**) temperature for 2040–2099.

Trends in the Climatic Variables

The results of the Mann-Kendall and Sen's slope analysis of precipitation and mean temperature for the period 2040–2099 are provided in Table 7. As shown, the majority of the trends in the monthly precipitation series were downward, with a significant decrease in the summer months. In the case of monthly temperatures, the majority of months showed significant upward trends in both scenarios.

Table 7. Trend analysis results for monthly and annual precipitation and mean temperature.

Month	Precipitation RCP 4.5			Temperature RCP 4.5			Precipitation RCP 8.5			Temperature RCP 8.5		
	Test Z	Sig.	Q_i	Test Z	Sig.	Q_i	Test Z	Sig.	Q_i	Test Z	Sig.	Q_i
January	−0.49		−0.01	3.78	***	0.03	0.16		0.00	7.79	***	0.07
February	0.10		0.00	4.98	***	0.03	−0.56		−0.01	7.57	***	0.07
March	−0.17		−0.01	4.02	***	0.02	−0.84		−0.03	8.12	***	0.07
April	0.91		0.27	3.31	***	0.02	−0.43		−0.10	7.53	***	0.07
May	−0.07		−0.05	1.10		0.01	−2.38	*	−1.19	6.96	***	0.07
June	−0.12		−0.09	2.98	**	0.02	−3.50	***	−2.46	7.67	***	0.09
July	−1.91	+	−0.90	2.56	*	0.03	−5.83	***	−2.53	8.41	***	0.11
August	−1.55		−0.94	3.91	***	0.03	−5.35	***	−2.92	9.29	***	0.10
September	−2.53	*	−1.34	4.46	***	0.03	−5.02	***	−3.66	9.00	***	0.11
October	0.94		0.42	4.11	***	0.03	1.24		0.75	8.09	***	0.08
November	−0.47		−0.04	3.17	**	0.02	1.17		0.18	7.83	***	0.07
December	1.00		0.02	4.45	***	0.02	−0.32		−0.01	7.69	***	0.07
Annual	−1.79	+	−3.70	5.24	***	0.02	−6.8	***	−13.17	9.34	***	0.08

Test Z is the Mann–Kendall (MK) test statistic; Q_i is the Sen's slope estimator; + indicates a significance level of 0.1; * indicates a significance level of 0.05; ** indicates a significance level of 0.01; *** indicates a significance level of 0.001.

The trend analysis showed a decrease in annual precipitation of 3.70 mm/year with a significance level of 0.1 and 13.17 mm/year with a significance level of 0.001 for RCP 4.5 and RCP 8.5 scenarios, respectively. The annual mean temperature indicated a significant upward trend (0.001 level of

significance). The temperature increased 0.02 °C/year for the RCP 4.5 scenario and 0.08 °C/year for the RCP 8.5 scenario.

3.4. Changes in Water Balance under RCP Scenarios

The impact of climate change on water availability was assessed according to the climate change scenarios for the basin. In this study, it was assumed that future land use change was constant in order to investigate the impact with respect to change in climate variables, keeping all other factors constant. After the SWAT hydrological model was calibrated and validated, the downscaled future precipitation and temperature predictions of the HadGEM2–ES model under two emission scenarios were used as input to explore streamflow responses to projected future climate change scenarios. Table 8 summarizes the response of basin's water balance components (precipitation, evapotranspiration, total water yield and groundwater recharge) under two RCP scenarios in terms of average annual values and percentage change from the baseline condition.

Table 8. Annual SWAT water balance components for Guajoyo River Basin

Scenario	Time Period	P (mm)	ET (mm)	ET/P	WYLD (mm)	DA_RCHG (mm)
Baseline	1975–2004	1435.6	523.9	0.36	720.72	27.95
RCP 4.5	2040–2069	1219.12 (−15%)	608.70 (+16%)	0.50	450.33 (−37%)	15.85 (−43%)
	2070–2099	1129.62 (−21%)	613.80 (+17%)	0.54	359.47 (−50%)	12.55 (−55%)
RCP 8.5	2040–2069	1332.64 (−7%)	626.40 (+19%)	0.47	522.18 (−27%)	18.66 (−33%)
	2070–2099	919.07 (−36%)	547.00 (+4%)	0.60	268.87 (−63%)	8.19 (−71%)

P = precipitation, ET = evapotranspiration, ET/P = evapotranspiration/precipitation, WYLD = the net amount of water that contributes to streamflow (surface runoff contribution to streamflow + lateral flow + groundwater contribution to streamflow − transmission losses) and DA_RCHG = amount of water entering deep aquifer from root zone.

It was apparent from this table that with an increase in temperature and a decrease in precipitation, there will be an increasing trend in the ET and in the ET/P ratio but a decreasing trend in the WYLD and DA_RCHG. ET will increase in both future scenarios. As a consequence of climate warming, the midcentury ratio of ET/P could be between 0.47 and 0.50, and at the end of century could be between 0.54 and 0.60. The annual water yield for the basin for baseline period was 720.72 mm. The WYLD for midcentury is likely to decrease under the projected climate scenarios and it could vary between 450.33 mm and 522.18 mm. Also, a considerable reduction in recharges to deep aquifers is also predicted. On the other hand, end-of-century water yield can be predicted as a drastic decrease of approximately 50% (359.47 mm) and 63% (268.87 mm) for the RCP 4.5 and RCP 8.5 scenarios. The results obtained in this study were in accord with previous researches such as the study of CEPAL (2010) [59], in which it was predicted that the total availability of renewable water could decrease between 35% and 63% by the end of the century, with El Salvador being one of the most affected countries. Maurer et al. [9] projected an increase of the average temperature and a reduction of average precipitation that imply a reduction, on average by 13 to 24%, in inflows to major reservoirs of the Lempa River Basin for end of the 21st century. Also, a decreasing runoff across all Central America, even in areas where precipitation increases, was obtained in the work of Imbach et al. [10].

3.5. Future Projections of Drought

The SPI–12 and SRI–12 values are given in Table 9 and were calculated to quantify the effects of observed changes under historical climate variability and projected future climate change on meteorological and hydrological drought.

Table 9. Drought analysis of the Guajoyo River Basin.

Characteristics of drought	Baseline (1975–2004)		RCP 4.5				RCP 8.5			
			2040–2069		2070–2099		2040–2069		2070–2099	
	SPI	SRI	SPI	SRI	SPI	SRI	SPI	SRI	SPI	SRI
Number of drought events	9	5	4	4	10	6	7	7	3	3
Longest duration of drought events (months)	26	36	47	46	34	34	22	24	54	53
Average duration of drought events (months)	12	14	22	27	13	14	15	14	36	36
Average drought intensity	1.60	1.95	2.15	2.01	1.47	1.85	1.93	1.53	1.98	1.90
Maximum drought intensity	2.52	2.64	2.68	2.49	2.44	2.15	2.42	2.68	2.74	2.58

The number of meteorological and hydrological drought events was 9 and 5, with an average duration of 12 and 14 months, and an average intensity of 1.60 and 1.95 respectively for the baseline period. The mid-century RCP 4.5 scenario indicated that the number of meteorological and hydrological drought events will be fewer but will be of greater duration and intensity. For this scenario, the number of drought events will increase for both types of drought in the long term, but with less intensity than for the baseline period. In the case of meteorological droughts, drought events will be longer. In RCP 8.5 scenario, the number of drought events was lower, but with an increase of duration in both meteorological and hydrological droughts, and the intensity only in the meteorological type. This is consistent with the study of Esquivel et al. [61] which indicates that future droughts will be more pronounced than current droughts, both in terms of the amount of resources available and the duration of events. Also, the IPCC-AR5 (2014) [62] reported that long-term changes in rainfall in Latin America will cause longer periods of drought.

4. Conclusions

The Guajoyo River Basin is located in an area of environmental interest in terms of international protection figures which guarantees water supply for local communities, as well as being important in regional development through agro-tourism and coffee activities. In the present study, the impacts of a climate change on meteorological variables (i.e., precipitation and temperature) have been analyzed, as well as on the main hydrological variables (i.e., ET, WYLD and DA_RCHG) and on the droughts of the Guajoyo River Basin. The future projections of precipitation and temperature of five GCMs (GFDL–ESM2M, HadGEM2–ES, IPSL–CM5A–LR, MIROC, and NoerESM1–M) were considered. After the analysis and comparative evaluation of these projections, the best model was selected according to its ability to reproduce the historical climate. The physically based semi-distributed SWAT model was employed to quantify the impacts of future climate variations on the hydrological processes driven by a regionalized HadGEM2–ES for RCP 4.5 and RCP 8.5 climate scenarios. SWAT acceptably simulated monthly streamflow despite data scarcity, and the results in the basin for the historic baseline were compared with future periods (2040–2069 and 2070–2099).

The results of this analysis indicated an annual decrease in precipitation of 15% (RCP 4.5) and 7% (RCP 8.5) during mid-century and 21% (RCP 4.5) and 36% (RCP 8.5) during the end of the century with respect to the base period (1975–2004). The annual mean temperature showed an increase for the midcentury period of 9% and 11% and an increase of 12% and 21% for the late century period, under RCP 4.5 and RCP 8.5 scenarios, respectively. The Mann–Kendall analysis indicated for the future period (2040–2099) a significant downward trend in annual precipitation and a significant upward trend in annual mean temperatures for both emission scenarios. For the hydrological cycle, the results suggested that the impact of climate change will be negative in the medium and long term. The availability of water will experience a decrease. As for WYLD, a decrease of 37% (RCP 4.5)

and 27% (RCP 8.5) was obtained for the medium term and 50% (RCP 4.5) and 63% (RCP 8.5) for the end of the century. Similarly, a reduction of aquifer recharge was predicted by 43% and 33% for the middle of the century and by 55% and 71% at the end of the century, under RCP 4.5 and RCP 8.5 respectively. The ET/P ratio showed an increasing trend, going from 0.36 in the base period to 0.54 (RCP 4.5) and 0.6 (RCP 8.5) in the long term. Additionally, the impact of climate change on droughts has been analyzed using two drought indexes, SPI and SRI. In both studied scenarios it was obtained that in the future the droughts will be more pronounced than current droughts, being more intense and of longer duration.

This study supports and raises awareness of the possible future impacts of climate change on the water balance and on the droughts of this river basin. The results show that the availability of water will be significantly affected in the medium and long term, and therefore, policies must be developed to adapt to climate change to ensure environmental and economic sustainability of this area.

Supplementary Materials: The following are available online at http://www.mdpi.com/2073-4441/11/11/2360/s1, Table S1: Climatic stations used in the basin, Table S2: Monthly data used for model calibration and validation (2001–2012), Table S3: Modelled past data. Annual data for baseline period (1975–2004), Table S4: Modelled future data. Annual data for future period 2040–2099.

Author Contributions: All authors contributed significantly to the development of the methodology applied in this study. P.B.-G. and P.J.-S. designed the experiments and wrote the article. J.S.-A. provided technical assistance and reviewed and helped to prepare this paper for publication. J.P.-S. provided many important advices on the concept of methodology and reviewed this manuscript.

Funding: This research received no external funding.

Acknowledgments: We thank the Ministry for the Environment and Natural Resources (MARN) of El Salvador for their available data. We also would like to thank Jethro David Howard for proof-reading the text.

Conflicts of Interest: The authors declare no conflict of interest.

References

1. Verma, S.; Bhattarai, R.; Bosch, N.S.; Cooke, R.C.; Kalita, P.K.; Markus, M. Climate change impacts on flow, sediment and nutrient export in a Great Lakes watershed using SWAT. *Clean Soil Air Water* **2015**, *43*, 1464–1474. [CrossRef]
2. Zhang, Y.; You, Q.; Chen, C.; Ge, J. Impacts of climate change on streamflows under RCP scenarios: A case study in Xin River Basin, China. *Atmos. Res.* **2016**, *178*, 521–534. [CrossRef]
3. Chattopadhyay, S.; Jha, M.K. Hydrological response due to projected climate variability in Haw River watershed, North Carolina, USA. *Hydrol. Sci. J.* **2016**, *61*, 495–506. [CrossRef]
4. Bhatta, B.; Shrestha, S.; Shrestha, P.K.; Talchabhadel, R. Evaluation and application of a SWAT model to assess the climate change impact on the hydrology of the Himalayan River Basin. *Catena* **2019**, *181*, 104082. [CrossRef]
5. Parry, M.L.; Canziani, O.F.; Palutikof, J.P.; Van der Linden, P.J.; Hanson, C.E. *IPCC, 2007. Climate Change 2007: Impacts, Adaptation and Vulnerability. Contribution of Working Group II to the Fourth Assessment Report of the Intergovernmental Panel on Climate Change*; Cambridge University Press: Cambridge, UK, 2007; p. 976.
6. Fischer, G.; Shah, M.; Tubiello, F.N.; Van Velhuizen, H. Socio–economic and climate change impacts on agriculture: An integrated assessment, 1990–2080. *Philos. T. Roy. Soc. B* **2005**, *360*, 2067–2083. [CrossRef] [PubMed]
7. Tubiello, F.N.; Rosenzweig, C. Developing climate change impact metrics for agriculture. *Integrat. Assess.* **2008**, *8*, 165–184.
8. Campos, M.; Herrador, D.; Manuel, C.; McCall, M.K. Estrategias de adaptación al cambio climático en dos comunidades rurales de México y El Salvador. *BAGE* **2013**, *61*, 329–349.
9. Maurer, E.P.; Adam, J.C.; Wood, A.W. Climate model based consensus on the hydrologic impacts of climate change to the Rio Lempa basin of Central America. *Hydrol. Earth Syst. Sci.* **2009**, *13*, 183–194. [CrossRef]
10. Imbach, P.; Molina, L.; Locatelli, B.; Roupsard, O.; Mahé, G.; Neilson, R.; Corrales, L.; Scholze, M.; Ciais, P. Modeling potential equilibrium states of vegetation and terrestrial water cycle of mesoamerica under climate change scenarios. *J. Hydrometeorol.* **2012**, *13*, 665–680. [CrossRef]

11. Aguilar, M.Y.; Pacheco, T.R.; Tobar, J.M.; Quiñónez, J.C. Vulnerability and adaptation to climate change of rural inhabitants in the central coastal plain of El Salvador. *Clim. Res.* **2009**, *40*, 187–198. [CrossRef]
12. Parajuli, P.B. Assessing sensitivity of hydrologic responses to climate change from forested watershed in Mississippi. *Hydrol. Process.* **2010**, *24*, 3785–3797. [CrossRef]
13. Zhang, X.; Xu, Y.; Hao, F.; Li, C.; Wang, X. Hydrological components variability under the impact of climate change in a semi–arid river basin. *Water* **2019**, *11*, 1122. [CrossRef]
14. Ji, L.; Duan, K. What is the main driving force of hydrological cycle variations in the semiarid and semi–humid Weihe River Basin, China? *Sci. Total Environ.* **2019**, *684*, 254–264. [CrossRef] [PubMed]
15. Senent–Aparicio, J.; Pérez–Sánchez, J.; Carrillo–García, J.; Soto, J. Using SWAT and fuzzy TOPSIS to assess the impact of climate change in the headwaters of the segura river Basin (SE Spain). *Water* **2017**, *9*, 149. [CrossRef]
16. MARN. *Plan Nacional de Gestión Integrada del Recurso Hídrico de El Salvador, con Énfasis en Zonas Prioritarias*, 1st ed.; Ministerio de Medio Ambiente y Recursos Naturales: San Salvador, El Salvador, 2017. Available online: http://www.marn.gob.sv/plan-nacional-de-gestion-integrada-del-recurso-hidrico/ (accessed on 1 May 2019).
17. Wada, K. The distinctive properties of Andosols. In *Advances in Soil Science*; Springer: New York, NY, USA, 1985; pp. 173–229. [CrossRef]
18. Levard, C.; Basile–Doelsch, I. Geology and mineralogy of imogolite–type materials. In *Nanosized Tubular Clay Minerals*; Elsevier: Amsterdam, The Netherlands, 2016; pp. 49–65. [CrossRef]
19. ASTER Global Digital Elevation Map. Available online: https://asterweb.jpl.nasa.gov/gdem.asp (accessed on 20 May 2019).
20. Fischer, G.; Nachtergaele, F.; Prieler, S.; Velthuizenvan, H.; Verelst, L.; Wiberg, D. *Global Agro–Ecological Zones Assessment for Agriculture (GAEZ 2008)*; IIASA: Laxenburg, Austria; FAO: Rome, Italy, 2008.
21. Saha, S.; Moorthi, S.; Pan, H.L.; Wu, X.; Wang, J.; Nadiga, S.; Tripp, P.; Kistler, R.; Woollen, J.; Behringer, D.; et al. The NCEP climate forecast system reanalysis. *B. Am. Meteorol. Soc.* **2010**, *91*, 1015–1057. [CrossRef]
22. Tarawneh, E.; Bridge, J.; Macdonald, N. A pre–calibration approach to select optimum inputs for hydrological models in data–scarce regions. *Hydrol. Earth Syst. Sci.* **2016**, *70*, 4391–4407. [CrossRef]
23. Vaghefi, S.A.; Abbaspour, N.; Kamali, B.; Abbaspour, K.C. A toolkit for climate change analysis and pattern recognition for extreme weather conditions—Case study: California–Baja California peninsula. *Environ. Model. Softw.* **2017**, *96*, 181–198. [CrossRef]
24. Hempel, S.; Frieler, K.; Warszawski, L.; Schewe, J.; Piontek, F. A trend-preserving bias correction—The isi-mip approach. *Earth Syst. Dynam.* **2013**, *4*, 219–236. [CrossRef]
25. Arnold, J.G.; Srinivasan, R.; Muttiah, R.S.; Williams, J.R. Large area hydrologic modeling and assessment Part I: Model development. *J. Am. Water Resour. Assoc.* **1998**, *34*, 73–89. [CrossRef]
26. Arnold, J.G.; Kiniry, J.R.; Srinivasan, R.; Williams, J.R.; Haney, E.B.; Neitsch, S.L. *Soil & Water Assessment Tool—Input/Output Documentation*; Version 2012; Texas Water Resources Institute: College Station, TX, USA, 2012; p. 650. Available online: https://swat.tamu.edu/docs/ (accessed on 20 May 2019).
27. Singh, V.; Bankar, N.; Salunkhe, S.S.; Bera, A.K.; Sharma, J.R. Hydrological stream flow modelling on Tungabhadra catchment: Parameterization and uncertainty analysis using SWAT CUP. *Curr. Sci. India* **2013**, *104*, 1187–1199.
28. Emami, F.; Koch, M. Modeling the impact of climate change on water availability in the Zarrine River Basin and inflow to the Boukan Dam, Iran. *Climate* **2019**, *7*, 51. [CrossRef]
29. USDA, SCS. Hydrology. In *National Engineering Handbook, Section 4*; USDA Soil Conservation Service: Washington, DC, USA, 1972.
30. Monteith, J.L. Evaporation and environment. *Symp. Soc. Exp. Biol.* **1965**, *19*, 205–234. [PubMed]
31. Allen, R.G.; Pereira, L.S.; Raes, D.; Smith, M. *Crop Evapotranspiration: Guidelines for Computing Crop Water Requirements*; Food and Agriculture Organization of the United Nations: Rome, Italy, 1998.
32. Abbaspour, K.C.; Vejdani, M.; Haghighat, S. SWAT–CUP calibration and uncertainty programs for SWAT. In Proceedings of the Modsim 2007: International Congress on Modelling and Simulation, Christchurch, New Zealand, 3–8 December 2007; pp. 1603–1609.
33. Alemayehu, T.; van Griensven, A.; Bauwens, W. Evaluating CFSR and WATCH data as input to swat for the estimation of the potential evapotranspiration in a data–scarce Eastern–African catchment. *J. Hydrol. Eng.* **2016**, *21*, 16. [CrossRef]

34. Poméon, T.; Diekkrüger, B.; Springer, A.; Kusche, J.; Eicker, A. Multi–objective validation of SWAT for sparsely–gauged West African River basins—A remote sensing approach. *Water* **2018**, *10*, 451. [CrossRef]
35. Arnold, J.G.; Moriasi, D.; Gassman, P.W.; Abbaspour, K.C.; White, M.J.; Srinivasan, R.; Santhi, C.; Harmel, R.D.; van Griensven, A.; Van Liew, M.W.; et al. SWAT: Model use, calibration, and validation. *Trans. ASABE* **2012**, *55*, 1491–1508. [CrossRef]
36. Moriasi, D.N.; Arnold, J.G.; van Liew, M.W.; Bingner, R.L.; Harmel, R.D.; Veith, T.L. Model evaluation guidelines for systematic quantification of accuracy in watershed simulations. *Trans. ASABE* **2007**, *50*, 885–900. [CrossRef]
37. Gupta, H.V.; Kling, H.; Yilmaz, K.K.; Martinez, G.F. Decomposition of the mean squared error and NSE performance criteria: Implications for improving hydrological modelling. *J. Hydrol.* **2009**, *377*, 80–91. [CrossRef]
38. Chen, J.; Brissette, F.P.; Chaumont, D.; Braun, M. Performance and uncertainty evaluation of empirical downscaling methods in quantifying the climate change impacts on hydrology over two North American river basins. *J. Hydrol.* **2013**, *479*, 200–214. [CrossRef]
39. Vaghefi, S.A.; Iravani, M.; Sauchyn, D.; Andreichuk, Y.; Goss, G.; Faramarzi, M. Regionalization and parameterization of a hydrologic model significantly affect the cascade of uncertainty in climate–impact projections. *Clim. Dyn.* **2019**, *53*, 2861–2886. [CrossRef]
40. Sofaer, H.R.; Barsugli, J.J.; Jarnevich, C.S.; Abatzoglou, J.T.; Talbert, M.K.; Miller, B.W.; Morisette, J.T. Designing ecological climate change impact assessments to reflect key climatic drivers. *Glob. Change Biol.* **2017**, *23*, 2537–2553. [CrossRef] [PubMed]
41. Pulido–Velazquez, D.; García–Aróstegui, J.L.; Molina, J.L.; Pulido–Velazquez, M. Assessment of future groundwater recharge in semi–arid regions under climate change scenarios (Serral–Salinas aquifer, SE Spain). Could increased rainfall variability increase the recharge rate? *Hydrol. Process.* **2015**, *29*, 828–844. [CrossRef]
42. Salmi, T.; Maatta, A.; Anttila, P.; Airola, T.R.; Amnell, T. *Detecting Trends of Annual Values of Atmospheric Pollutants by the Mann–Kendal Test and Sen's Slope Estimates—The Excel Template Application MAKESENS*; User Manual; Air Quality, Finish Meteorological Institute: Helsinki, Finland, 2002; p. 35.
43. Senent-Aparicio, J.; Liu, S.; Pérez-Sánchez, J.; López-Ballesteros, A.; Jimeno-Sáez, P. Assessing impacts of climate variability and reforestation activities on water resources in the headwaters of the Segura River Basin (SE Spain). *Sustainability* **2018**, *10*, 3277. [CrossRef]
44. Partal, T.; Kahya, E. Trend analysis in Turkish precipitation data. *Hydrol. Process.* **2006**, *20*, 2011–2026. [CrossRef]
45. Sen, P.K. Estimates of the regression coefficient based on Kendall's tau. *J. Am. Stat. Assoc.* **1968**, *63*, 1379–1389. [CrossRef]
46. McKee, T.B.; Doesken, N.J.; Kleist, J. The relationship of drought frequency and duration to time scales. In Proceedings of the 8th Conference on Applied Climatology, Anaheim, CA, USA, 17–22 January 1993; pp. 179–184.
47. Shukla, S.; Wood, A.W. Use of a standardized runoff index for characterizing hydrologic drought. *Geophys. Res. Lett.* **2008**, *35*, L02405. [CrossRef]
48. NDMC. SPI Generator Software. University of Nebraska–Lincoln, USA. 2019. Available online: https://drought.unl.edu/droughtmonitoring/SPI/SPIProgram.aspx (accessed on 23 July 2019).
49. WMO. *Standardized Precipitation Index User Guide*; WMO–No. 1090; WMO: Geveva, Switzerland, 2012; Available online: https://library.wmo.int/doc_num.php?explnum_id=7768 (accessed on 23 July 2019).
50. Jimeno–Sáez, P.; Senent–Aparicio, J.; Pérez–Sánchez, J.; Pulido–Velazquez, D. A Comparison of SWAT and ANN models for daily runoff simulation in different climatic zones of Peninsular Spain. *Water* **2018**, *10*, 192. [CrossRef]
51. Spellman, P.; Webster, V.; Watkins, D. Bias correcting instantaneous peak flows generated using a continuous, semi–distributed hydrologic model. *J. Flood Risk Manag.* **2018**, *11*, e12342. [CrossRef]
52. Čerkasova, N.; Umgiesser, G.; Ertürk, A. Assessing climate change impacts on streamflow, sediment and nutrient loadings of the Minija River (Lithuania): A hillslope watershed discretization application with high–resolution spatial inputs. *Water* **2019**, *11*, 676. [CrossRef]
53. McSweeney, C.F.; Jones, R.G.; Lee, R.W.; Rowell, D.P. Selecting CMIP5 GCMs for downscaling over multiple regions. *Clim. Dyn.* **2015**, *44*, 3237–3260. [CrossRef]

54. Ahmed, K.; Sachindra, D.A.; Shahid, S.; Demirel, M.C.; Chung, E.S. Selection of multi-model ensemble of GCMs for the simulation of precipitation based on spatial assessment metrics. *Hydrol. Earth Syst. Sci.* **2019**. Discuss, in review. [CrossRef]
55. Knutti, R.; Furrer, R.; Tebaldi, C.; Cermak, J.; Meehl, G.A. Challenges in combining projections from multiple climate models. *J. Clim.* **2010**, *23*, 2739–2758. [CrossRef]
56. Overland, J.E.; Wang, M.; Bond, N.A.; Walsh, J.E.; Kattsov, V.M.; Chapman, W.L. Considerations in the selection of global climate models for regional climate projections: The Arctic as a case study. *J. Clim.* **2011**, *24*, 1583–1597. [CrossRef]
57. Magaña, V.; Amador, J.A.; Medina, S. The midsummer drought over Mexico and Central America. *J. Clim.* **1999**, *12*, 1577–1588. [CrossRef]
58. MARN. *Modelos de Simulación y Escenarios Climáticos para El Salvador (Nacional, Regional y Local)*; Ministerio de Medio Ambiente y Recursos Naturales, Centro del Agua del Trópico Húmedo para América Latina y el Caribe: San Salvador, El Salvador, 2017. Available online: http://rcc.marn.gob.sv/xmlui/handle/123456789/347 (accessed on 15 August 2019).
59. CEPAL. *La Economía del Cambio Climático en Centroamérica—Síntesis 2010*; Comisión Económica para América Latina y El Caribe (CEPAL): Naciones Unidas, México, 2010.
60. Conde–Álvarez, C.; Saldaña–Zorrilla, O. Cambio climático en América Latina y el Caribe: Impactos, vulnerabilidad y adaptación. *Revista Ambiente y Desarrollo* **2007**, *23*, 23–30.
61. Esquivel, M.; Grünwaldt, A.; Paredes, J.R.; Rodríguez–Flores, E. *Vulnerabilidad al Cambio Climático de los Sistemas de Producción Hidroeléctrica en Centroamérica y sus Opciones de Adaptación, Resumen Ejecutivo*; Sector de Cambio Climático y Sector de Energía, Banco Interamericano de Desarrollo (BID): Madrid, Spain, 2016; Available online: http://expertosenred.olade.org/wp-content/uploads/sites/8/2017/01/Vulnerabilidad-al-cambio-climatico-de-los-sistemas-de-produccion-hidroelectrica-en-Centroamerica-y-sus-opciones-de-adaptacion-1.pdf (accessed on 23 August 2019).
62. IPCC–AR5. *Climate change 2013, The Physical Science Basis, Working Group I Contribution to the Fifth Assessment Report of the Intergovernmental Panel on Climate Change*; Cambridge University Press: Cambridge, UK, 2014; ISBN 978-1-107-66182-0.

Supplementary material

Impact of Climate Change on Water Balance Components and Droughts in the Guajoyo River Basin (El Salvador)

Pablo Blanco-Gómez, Patricia Jimeno-Sáez*, Javier Senent-Aparicio and Julio Pérez-Sánchez

Department of Civil Engineering, Catholic University of San Antonio, Campus de los Jerónimos s/n, 30107, Guadalupe, Murcia, Spain

* Correspondence: pjimeno@ucam.edu; Tel.: +34–968–278–818

Supplementary Table S1. Climatic stations used in the basin.

No.	Station Name	Latitude (°N)	Longitude (°W)	Elevation (m)	Category	Number of sub-basins using the station
1	Güija	14.23	-89.47	485	R	11
2	t142-894	14.21	-89.38	446	T	2
3	t142-897	14.21	-89.69	585	T	9

Note: The alphabets of R and T stand for rain gauge station and CFSR temperature data, respectively.

Supplementary Table S2. Monthly data used for model calibration and validation (2001-2012).

Date	Station				
	Güija	t142-894		t142-897	
	P (mm)	Tmax (°C)	Tmin (°C)	Tmax (°C)	Tmin (°C)
Jan-01	1.4	26.1	15.4	26.4	14.8
Feb-01	0	27.5	18.1	27.6	17.3
Mar-01	0	31.8	15.2	32.0	14.9
Apr-01	69	33.6	19.2	34.2	18.6
May-01	147.4	32.4	18.9	31.9	18.8
Jun-01	35.9	29.5	18.5	28.9	18.4
Jul-01	263.5	30.1	18.3	28.9	17.8
Aug-01	136.2	29.9	19.0	29.2	18.6
Sep-01	247	27.4	17.1	26.8	17.2
Oct-01	188.8	27.1	18.0	27.1	17.7
Nov-01	0	27.7	16.6	27.9	16.0
Dec-01	0	28.5	17.8	28.8	17.1
Jan-02	0	28.8	17.0	29.2	16.4
Feb-02	4.6	30.2	17.3	30.2	16.6
Mar-02	0.5	33.1	17.4	32.9	16.7
Apr-02	29.2	33.0	19.0	33.8	18.1
May-02	262.8	30.8	19.6	30.6	19.1
Jun-02	227.4	28.9	18.6	28.3	18.4
Jul-02	205.9	28.8	18.9	29.1	18.4
Aug-02	205.4	29.9	18.8	30.1	18.3
Sep-02	252.3	27.2	17.6	26.4	17.5
Oct-02	81.7	26.5	18.0	26.5	17.5
Nov-02	6.8	24.9	16.9	24.7	16.5
Dec-02	0	26.7	17.2	26.7	16.6
Jan-03	0	23.8	16.2	24.0	15.7
Feb-03	0	31.1	17.0	30.8	16.4
Mar-03	50.7	32.3	17.6	31.8	17.2

2

Apr-03	12	34.3	18.3	34.8	17.8
May-03	141.1	32.8	19.4	32.7	19.1
Jun-03	163.3	27.8	17.8	27.3	17.8
Jul-03	234.4	27.4	18.5	27.5	18.1
Aug-03	248.2	28.7	18.4	28.6	18.0
Sep-03	343.7	27.6	18.4	27.2	17.9
Oct-03	120.9	26.6	17.9	26.7	17.6
Nov-03	13.9	26.7	17.6	27.3	17.1
Dec-03	0	24.6	15.4	25.5	15.0
Jan-04	0	27.1	15.9	27.5	15.6
Feb-04		30.3	16.5	30.2	16.0
Mar-04	0	30.9	18.5	31.0	18.0
Apr-04	31.6	32.6	17.7	32.7	17.4
May-04	140.9	30.3	19.8	29.9	19.4
Jun-04	187.4	28.1	18.9	27.8	18.7
Jul-04	160.3	28.1	18.2	27.7	17.7
Aug-04	181.4	30.0	18.8	29.4	18.3
Sep-04	294.8	29.9	18.0	29.5	17.5
Oct-04	119.2	27.2	17.5	27.0	17.2
Nov-04	7.1	26.3	17.4	26.4	16.8
Dec-04	0	26.2	16.8	26.3	16.3
Jan-05	0	26.5	15.9	26.6	15.2
Feb-05	0	31.0	16.5	30.7	15.9
Mar-05	4.1	32.5	18.1	32.0	17.5
Apr-05	19.3	34.1	19.4	34.5	19.0
May-05	181.4	31.5	19.4	31.1	19.2
Jun-05	427.4	29.1	18.9	28.4	18.7
Jul-05	213.2	27.4	18.1	26.9	18.1
Aug-05	211.8	27.4	18.4	27.1	18.1
Sep-05	350.12	26.8	18.4	26.4	18.3
Oct-05	208.3	24.2	17.6	23.9	17.2
Nov-05	9	24.2	16.5	24.3	16.1
Dec-05	5	27.0	16.8	26.9	16.3
Jan-06	0	26.6	16.7	26.5	16.1
Feb-06	0.3	28.4	16.4	28.6	15.9
Mar-06	11.9	32.3	16.8	32.1	16.0
Apr-06	61.4	32.6	17.6	33.0	17.3
May-06	241.8	31.2	19.3	30.6	19.0
Jun-06	367.5	26.3	18.9	26.0	18.5
Jul-06	316.7	27.6	19.0	27.2	18.6
Aug-06	116.9	28.3	18.9	27.9	18.4
Sep-06	201.44	27.6	18.6	26.8	18.2
Oct-06	179.2	27.6	17.9	27.7	17.6
Nov-06	120.7	25.8	16.6	25.6	16.1
Dec-06	2	26.8	17.7	26.9	17.1
Jan-07	0	27.3	18.0	27.5	17.3
Feb-07	0	31.5	17.1	31.0	16.4
Mar-07	0.6	31.3	18.1	31.4	17.3
Apr-07	139.1	34.3	18.8	34.7	18.5
May-07	96.5	33.6	19.4	33.2	19.2
Jun-07	127.4	29.2	19.0	28.4	18.6
Jul-07	162	29.7	18.3	29.2	17.9
Aug-07	173.2	28.1	17.7	27.5	17.4
Sep-07	314.9	27.1	17.8	26.7	17.4
Oct-07	77.2	24.9	16.7	24.5	16.5
Nov-07	0	23.6	17.4	23.5	16.8
Dec-07	0	26.2	16.4	26.4	15.8

3

Jan-08	0.8	26.8	16.5	26.9	16.0
Feb-08	11.5	30.5	16.8	30.4	16.3
Mar-08	23	31.2	17.0	31.1	16.5
Apr-08	86.7	33.3	18.2	34.0	17.8
May-08	124	31.3	18.8	31.0	18.6
Jun-08	376.5	27.6	18.4	26.9	18.3
Jul-08	386	27.1	18.2	26.4	18.1
Aug-08	240	27.8	17.5	27.3	17.4
Sep-08	385	26.9	17.4	26.2	17.2
Oct-08	201.3	23.9	17.5	23.7	17.1
Nov-08	0	24.1	15.3	23.9	15.0
Dec-08	0	24.7	16.2	24.8	15.5
Jan-09	10.2	26.5	16.2	26.5	15.5
Feb-09	3.1	26.9	16.7	26.9	16.0
Mar-09	0.7	29.6	16.2	29.6	15.4
Apr-09	6.6	33.5	18.3	33.6	17.7
May-09	298.73	29.8	19.2	29.3	18.9
Jun-09	194.3	28.5	17.5	27.6	17.5
Jul-09	216.7	28.3	18.9	27.7	18.5
Aug-09	173.1	28.2	18.9	27.7	18.3
Sep-09	125.1	28.5	18.3	28.0	18.0
Oct-09	95.8	28.3	17.3	27.9	16.9
Nov-09	114.5	27.1	17.1	26.9	16.7
Dec-09	7.5	28.7	16.2	28.4	15.9
Jan-10	0	27.3	15.5	27.0	15.1
Feb-10	0	31.2	16.5	30.5	16.4
Mar-10	0.1	33.9	17.0	33.9	16.7
Apr-10	95.2	32.7	19.5	32.9	19.1
May-10	399.8	30.6	20.1	30.0	19.8
Jun-10	330.6	27.1	18.9	26.5	18.7
Jul-10	211.3	26.8	17.8	26.2	17.5
Aug-10	350.9	26.3	17.8	25.7	17.9
Sep-10	269.1	25.2	17.8	24.6	17.7
Oct-10	34.9	25.0	16.8	24.9	16.3
Nov-10	2.4	25.9	15.5	25.8	15.0
Dec-10	0	25.0	14.4	24.9	13.8
Jan-11	0.2	28.8	14.6	29.2	16.1
Feb-11	5.5	29.8	15.0	30.1	16.3
Mar-11	8.8	30.3	14.8	30.4	16.3
Apr-11	38.7	31.2	17.3	30.0	18.2
May-11	193.8	27.4	18.2	27.6	19.0
Jun-11	265.1	24.8	17.9	24.9	18.6
Jul-11	254.8	25.3	16.7	25.2	17.7
Aug-11	260.7	25.3	16.7	25.1	17.7
Sep-11	262.6	24.6	16.7	25.0	17.6
Oct-11	284	22.6	16.2	23.5	17.0
Nov-11	19.1	24.6	15.3	25.9	16.4
Dec-11	0	25.7	15.1	27.2	16.5
Jan-12	0.3	27.5	14.9	28.6	16.2
Feb-12	0.3	29.6	15.8	30.8	17.1
Mar-12	0	31.5	15.6	31.3	17.0
Apr-12	129	30.3	17.1	30.0	18.2
May-12	208	26.4	18.3	26.1	19.0
Jun-12	118.5	25.4	17.0	25.8	17.5
Jul-12	219.5	26.9	16.3	27.7	17.2
Aug-12	370.4	25.4	16.3	25.5	17.4
Sep-12	235.7	25.7	16.3	26.3	17.3

4

Oct-12	176.2	24.8	16.4	25.7	17.2
Nov-12	0	24.5	15.2	26.0	16.5
Dec-12	1	27.8	14.9	28.3	16.1

Supplementary Table S3. Modelled past data. Annual data for baseline period (1975-2004).

Date	Station				
	Güija	t142-894		t142-897	
	P (mm)	Tmax (°C)	Tmin (°C)	Tmax (°C)	Tmin (°C)
1975	1602.5	32.4	19.7	32.1	19.3
1976	1412.3	32.6	19.4	32.3	19.0
1977	1206.6	33.2	19.8	32.9	19.4
1978	1752.2	32.3	20.0	32.1	19.6
1979	1675.2	32.4	19.7	32.2	19.3
1980	1604.4	32.5	19.1	32.3	18.7
1981	1525.2	32.1	19.1	31.9	18.7
1982	1169.7	33.8	19.3	33.6	18.9
1983	1499.3	32.0	19.2	31.7	18.8
1984	1080.4	33.3	19.6	33.1	19.2
1985	1394.0	33.5	20.1	33.2	19.7
1986	1362.0	33.2	20.1	32.9	19.7
1987	1322.2	33.5	19.8	33.2	19.4
1988	1517.2	33.1	19.9	32.8	19.5
1989	1141.0	33.2	19.8	33.0	19.4
1990	924.4	33.9	19.6	33.6	19.2
1991	1422.2	32.8	19.5	32.6	19.1
1992	1489.2	32.1	19.6	31.8	19.2
1993	1148.2	33.6	19.6	33.3	19.2
1994	1661.8	32.4	19.6	32.2	19.2
1995	1551.7	32.7	19.9	32.5	19.5
1996	964.9	34.1	19.9	33.9	19.5
1997	1692.7	32.6	19.8	32.4	19.4
1998	1437.8	33.2	19.9	33.0	19.5
1999	1766.4	32.6	20.1	32.4	19.7
2000	1385.8	33.2	20.1	32.9	19.7
2001	1539.5	34.0	20.1	33.7	19.7
2002	1769.7	33.1	20.5	32.8	20.1
2003	1619.3	33.0	20.0	32.7	19.6
2004	1405.7	33.1	19.9	32.9	19.5

Supplementary Table S4. Modelled future data. Annual data for future period 2040-2099.

Date	Station									
	Güija		t142-894				t142-897			
	P (mm)		Tmax (°C)		Tmin (°C)		Tmax (°C)		Tmin (°C)	
	RCP 4.5	RCP 8.5	RCP 4.5	RCP 8.5	RCP 4.5	RCP 8.5	RCP 4.5	RCP 8.5	RCP 4.5	RCP 8.5
2040	1732.8	1519.1	33.6	35.0	21.3	21.9	33.4	34.7	20.9	21.5
2041	1372.8	1523.0	34.1	34.1	21.1	21.4	33.9	33.8	20.7	21.0
2042	1232.6	1463.3	35.6	35.0	22.2	22.0	35.4	34.8	21.8	21.6
2043	1375.1	1417.4	35.3	34.7	22.1	22.0	35.1	34.4	21.7	21.6
2044	1374.1	1676.8	34.3	34.7	21.4	22.1	34.0	34.4	21.0	21.7
2045	1403.8	1447.9	35.4	34.1	22.0	21.5	35.2	33.8	21.6	21.2
2046	866.7	1372.6	36.2	34.6	21.9	21.9	36.0	34.3	21.5	21.5
2047	927.0	1373.6	36.0	34.8	22.0	22.0	35.7	34.6	21.6	21.6
2048	715.4	1286.2	37.1	36.1	22.1	22.3	36.8	35.9	21.7	21.9
2049	1089.4	1072.0	36.0	36.4	22.3	22.6	35.7	36.2	21.9	22.2
2050	1478.2	1279.3	35.0	35.7	21.9	22.7	34.8	35.5	21.5	22.3

5

2051	1154.4	1358.2	35.0	35.6	21.6	22.6	34.7	35.4	21.2	22.2
2052	1478.1	1286.7	34.9	36.1	21.6	22.7	34.7	35.9	21.2	22.3
2053	1472.3	1062.5	34.8	36.0	21.8	22.2	34.5	35.8	21.4	21.8
2054	1779.3	1439.1	33.3	35.3	21.4	22.5	33.1	35.1	21.1	22.2
2055	812.9	1476.8	36.3	35.2	22.2	22.4	36.1	34.9	21.8	22.0
2056	1320.6	1244.1	35.3	35.8	22.2	22.6	35.1	35.5	21.8	22.2
2057	1199.1	955.3	35.2	36.5	21.9	23.0	34.9	36.2	21.5	22.6
2058	1269.7	1112.6	35.5	36.8	22.2	23.1	35.2	36.5	21.8	22.7
2059	753.5	1536.1	36.6	36.7	22.1	23.3	36.4	36.5	21.7	22.9
2060	1220.7	1332.5	35.8	36.2	22.4	23.2	35.5	36.0	22.0	22.8
2061	1055.0	1132.5	36.7	37.1	22.5	23.4	36.5	36.8	22.1	23.0
2062	1580.7	1553.9	35.5	36.0	22.6	23.5	35.2	35.8	22.2	23.1
2063	1070.6	1209.6	35.9	36.3	22.5	22.9	35.7	36.1	22.1	22.5
2064	1769.3	1459.3	34.5	35.4	22.2	22.8	34.2	35.2	21.8	22.4
2065	1526.2	1268.5	34.6	36.7	22.2	23.4	34.3	36.4	21.8	23.0
2066	1077.9	966.0	36.1	36.8	22.6	23.2	35.8	36.5	22.2	22.8
2067	1119.9	1371.9	35.8	36.5	22.0	23.5	35.6	36.3	21.6	23.1
2068	639.9	1393.6	36.7	36.4	22.0	23.7	36.4	36.1	21.6	23.4
2069	687.5	1368.1	37.2	36.1	22.6	23.6	37.0	35.8	22.2	23.2
2070	1218.2	913.6	36.1	37.9	22.9	24.0	35.8	37.6	22.5	23.6
2071	1012.5	1100.0	36.6	37.4	22.9	23.6	36.3	37.2	22.5	23.2
2072	1258.7	1132.1	36.0	37.6	22.7	24.2	35.8	37.3	22.3	23.8
2073	1245.3	942.6	36.7	37.8	23.1	24.1	36.4	37.5	22.7	23.7
2074	914.7	1080.3	36.5	37.6	22.7	23.9	36.3	37.3	22.3	23.6
2075	1086.0	1250.3	37.1	37.4	22.9	24.0	36.9	37.1	22.5	23.6
2076	1108.9	1065.9	36.0	37.6	22.5	24.2	35.7	37.3	22.2	23.8
2077	1082.7	1175.2	36.2	38.3	22.7	24.6	35.9	38.0	22.3	24.2
2078	1063.1	1152.2	36.7	38.0	23.0	24.6	36.5	37.8	22.6	24.2
2079	990.6	1094.5	36.9	38.2	22.8	24.8	36.7	38.0	22.4	24.4
2080	928.2	1079.9	37.2	38.5	23.1	24.7	37.0	38.3	22.7	24.3
2081	1360.2	881.3	35.6	39.1	22.7	25.2	35.4	38.9	22.3	24.8
2082	1072.5	908.6	35.8	38.6	22.7	24.8	35.5	38.4	22.3	24.4
2083	1202.3	1229.7	35.8	37.5	22.6	24.5	35.6	37.3	22.2	24.1
2084	1176.4	1142.3	36.4	37.2	22.7	24.3	36.2	37.0	22.3	23.9
2085	1150.7	845.3	35.8	38.9	22.5	24.7	35.6	38.6	22.1	24.3
2086	1248.5	1036.4	36.1	38.4	22.8	25.0	35.8	38.2	22.4	24.6
2087	1449.8	675.8	35.8	39.3	22.7	25.2	35.6	39.0	22.3	24.8
2088	1489.7	524.4	35.8	40.1	22.9	25.5	35.6	39.8	22.5	25.1
2089	937.7	670.0	36.9	39.6	23.1	25.5	36.7	39.3	22.7	25.1
2090	1283.0	516.8	36.2	39.7	23.0	25.0	35.9	39.5	22.6	24.6
2091	976.9	869.4	36.7	38.9	22.7	25.5	36.5	38.7	22.3	25.1
2092	1176.4	942.0	36.4	38.7	22.7	25.2	36.2	38.4	22.3	24.8
2093	1067.1	664.7	36.7	39.9	23.1	25.5	36.5	39.6	22.7	25.1
2094	774.2	717.9	37.0	39.9	22.7	25.8	36.7	39.6	22.3	25.4
2095	1077.7	660.5	35.9	39.7	22.5	25.2	35.7	39.4	22.1	24.8
2096	1057.1	789.6	36.0	39.7	22.4	25.8	35.8	39.4	22.1	25.4
2097	1370.9	901.9	36.1	39.1	22.9	25.6	35.8	38.9	22.5	25.2
2098	1097.1	605.6	36.2	39.6	22.7	25.4	35.9	39.3	22.3	25.0
2099	992.1	986.9	36.9	39.3	22.8	25.8	36.7	39.1	22.4	25.4

IV.2 PUBLICACIÓN 2: EVALUATING THE POTENTIAL OF GLOFASERA5 RIVER DISCHARGE REANALYSIS DATA FOR CALIBRATING THE SWAT MODEL IN THE GRANDE SAN MIGUEL RIVER BASIN (EL SALVADOR)

Senent-Aparicio, J.; Blanco-Gómez, P.; López-Ballesteros, A.; Jimeno-Sáez, P. Evaluating the Potential of GloFASERA5 River Discharge Reanalysis Data for Calibrating the SWAT Model in the Grande San Miguel River Basin (El Salvador). Remote Sens. 2021, 13, 3299.

https://doi.org/10.3390/rs13163299

remote sensing

MDPI

Article

Evaluating the Potential of GloFAS-ERA5 River Discharge Reanalysis Data for Calibrating the SWAT Model in the Grande San Miguel River Basin (El Salvador)

Javier Senent-Aparicio [1,*], Pablo Blanco-Gómez [1], Adrián López-Ballesteros [1], Patricia Jimeno-Sáez [1] and Julio Pérez-Sánchez [1,2]

[1] Department of Civil Engineering, Universidad Católica San Antonio de Murcia, Campus de Los Jerónimos s/n, 30107 Murcia, Spain; pblanco4@alu.ucam.edu (P.B.-G.); alopez6@ucam.edu (A.L.-B.); pjimeno@ucam.edu (P.J.-S.); jperez058@ucam.edu (J.P.-S.)
[2] Department of Civil Engineering, Universidad de Las Palmas de Gran Canaria, Campus de Tafira, 35017 Las Palmas de Gran Canaria, Spain
* Correspondence: jsenent@ucam.edu; Tel.: +34-968-278-769

Abstract: Hydrological modelling requires accurate climate data with high spatial-temporal resolution, which is often unavailable in certain parts of the world—such as Central America. Numerous studies have previously demonstrated that in hydrological modelling, global weather reanalysis data provides a viable alternative to observed data. However, calibrating and validating models requires the use of observed discharge data, which is also frequently unavailable. Recent, global-scale applications have been developed based on weather data from reanalysis; these applications allow streamflows with satisfactory resolution to be obtained. An example is the Global Flood Awareness System (GloFAS), which uses the fifth generation of reanalysis data produced by the European Centre for Medium-Range Weather Forecasts (ERA5) as input. It provides discharge data from 1979 to the present with a resolution of 0.1°. This study assesses the potential of GloFAS for calibrating hydrological models in ungauged basins. For this purpose, the quality of data from ERA5 and from the Climate Hazards Group InfraRed Precipitation and Temperature with Station as well as the Climate Forecast System Reanalysis (CFSR) was analysed. The focus was on flow simulation using the Soil and Water Assessment Tool (SWAT) model. The models were calibrated using GloFAS discharge data. Our results indicate that all the reanalysis datasets displayed an acceptable fit with the observed precipitation and temperature data. The correlation coefficient (CC) between the reanalysis data and the observed data indicates a strong relationship at the monthly level all of the analysed stations (CC > 0.80). The Kling–Gupta Efficiency (KGE) also showed the acceptable performance of the calibrated SWAT models (KGE > 0.74). We concluded that GloFAS data has substantial potential for calibrating hydrological models that estimate the monthly streamflow in ungauged watersheds. This approach can aid water resource management.

Keywords: SWAT; satellite weather dataset; ERA-5; GloFAS; hydrological modelling; El Salvador

Citation: Senent-Aparicio, J.; Blanco-Gómez, P.; López-Ballesteros, A.; Jimeno-Sáez, P.; Pérez-Sánchez, J. Evaluating the Potential of GloFAS-ERA5 River Discharge Reanalysis Data for Calibrating the SWAT Model in the Grande San Miguel River Basin (El Salvador). *Remote Sens.* **2021**, *13*, 3299. https://doi.org/10.3390/rs13163299

Academic Editors: Sandra G. García Galiano, Fulgencio Cánovas García and Juan Diego Giraldo-Osorio

Received: 12 July 2021
Accepted: 18 August 2021
Published: 20 August 2021

1. Introduction

Hydrological models are commonly used to understand changes in hydrological processes due to changes in the climatic or the land use [1,2]. Such changes in land use and climatic conditions are especially important in Central America. Recent studies have highlighted deforestation as the main land-use change in this area [3]. However, climate change can also strongly affect the hydrological cycle by altering the timing and intensity of rainfall, recharge and runoff. This change has intensified the mid-summer drought characteristic of Central America's weather [4].

In addition to forecasting and estimating the quantity and quality of water for decision-makers, hydrological models can assist local authorities in forecasting the effects of natural

and anthropogenic changes on water resources. Furthermore, they can characterise the temporal and spatial availability of water resources to enable the design of appropriate strategies to mitigate water-related hazards. These includes droughts, floods and the discharge of pollutants.

Several conceptual and semi-distributed models have been applied at grid scale in tropical climatology. Srivastava et al. (2017) [5] successfully implemented the variable infiltration capacity (VIC) model for the Kangsabati River Basin and obtained satisfactory evapotranspiration estimates at the monthly scale. Srivastava et al. (2020) [6] compared two models, namely VIC and the model for the identification of unit hydrograph and components flows from rainfall, evapotranspiration and streamflow (IHACRES). They concluded that IHACRES is a very useful model for data-scarce regions. Paul et al. (2018) [7] similarly reported the successful implementation of a modified time-variant spatially distributed hydrograph technique integrated into the satellite-based hydrological model (SHM) for the Kabini River Basin.

The distributed Soil and Water Assessment Tool (SWAT) model has also been widely used in tropical basins [8]. Darbandsari and Coulibaly (2020) [9] demonstrated the usefulness of lumped hydrological models for simulating hydrological processes in data-scarce watersheds. However, in the current study, the distributed SWAT model is used, because once calibrated, it allows further analyses related to land-use changes. SWAT is one of several models employed to assess the influence of land use and land management changes on water resources [10].

Accuracy in simulating a basin's water resources fundamentally depends on the input data used for modelling and on the capability of the hydrological model. Primary input data are meteorological and geographical data (e.g., precipitation and temperature as well as data from digital elevation models and land-use and soil maps). In recent years, several ready-to-use global-scale maps have been developed that provide good results and make the SWAT model application easier [11].

The application of hydrological models is usually limited by the sparse distribution of rainfall observation stations. In most watersheds, the actual density of a rainfall network is notably lower than the values recommended by the World Meteorological Organization. Ground-based precipitation observation is also unevenly distributed in many countries due to economic constraints [12], and this issue can affect model estimates of streamflow performance. Missing values in rainfall data negatively affect the quality of hydrological modelling. Tan and Yang (2020) [13] demonstrated that missing values of more than 20% significantly affected the streamflow simulation for tropical climates. To overcome limitations arising from the scarcity of data or from poor-quality observations, numerous studies have compared gridded rainfall datasets with local datasets. The aim is to assess their suitability of those datasets in various hydrological models [14–17] for watersheds around the world.

The influence of temperature data on hydrological balance and discharge in simulated river basins has rarely been analysed (Tan et al., 2021). In Southeast Asia, Tan et al. (2017) [18] recommended combining the Asian Precipitation Highly Resolved Observational Data Integration Towards Evaluation (APHRODITE) dataset [19] with the maximum and minimum temperatures from the Climate Forecast System Reanalysis (CFSR) dataset [20]. The objective was to model ungauged or gauge-limited catchments. In Ethiopia, Duan et al. (2019) [21] recommended the use of Climate Hazards Group Infrared Precipitation with Stations (CHIRPS) data [22] together with temperature data from CFSR for hydrological modelling.

Due to advances in satellite technology, many satellite weather products have been developed to monitor weather conditions on a global scale. Some are called reanalysis products; they combine satellite data with observed data to improve weather representation. An example is the CFSR dataset. It is widely used for hydrological modelling in the SWAT model, because—in addition to precipitation—it includes other meteorological variables that are easily downloadable from the SWAT website [23]. Additional reanalysis

datasets that include precipitation and temperature data for simulations have recently been launched. For example, the CHIRPS precipitation dataset has recently been complemented with temperature data to yield the Climate Hazards Center InfraRed Temperature with Stations CHIRTS [24]. This data is available for the global scale at a spatial resolution of 0.05°.

Another recently launched dataset that includes precipitation and temperature is the ERA5 global reanalysis dataset [25]. It provides data from 1950 to the present at a spatial resolution of 31 km. It was released recently and has not yet been tested in hydrological modelling for several areas of the world. However, Tarek et al. (2020) [26] tested the potential of ERA5 in hydrological modelling across North America. Their results highlighted many advantages over the previous dataset, ERA-Interim, and demonstrated a level of efficiency similar to that obtained in hydrological models that use observed data for most of the territory analysed. Kolluru et al. (2020) [27] concluded that ERA5 is efficient for detecting rainfall patterns, whereas CHIRPS dysplays better flow simulation. Jiang et al. (2021) [28] obtained highly varying results depending on the regions analysed and identified the general underestimation of extreme rainfall.

Model calibration and validation are key steps for obtaining accurate estimates of streamflow from hydrological models. These steps are generally performed using observed data [29]. However, in situ flow data are commonly unavailable for much of the land area, especially in developing countries, and the number of operational stations is decreasing rapidly. The recent availability of global-scale remote sensing climate products (such as those discussed above) has led to the development of hydrological models that provide discharge estimates at a global scale [30–32].

One such application is the Global Flood Awareness System (GloFAS), developed by the European Centre for Medium-Range Weather Forecasts (ECMWF) in collaboration with the University of Reading and the Joint Research Centre of the European Commission. This system couples the Hydrology Tiled ECMWF Scheme for Surface Exchanges over Land (HTESSEL) [33] and LISFLOOD models [34]; it provides streamflow estimates at a global scale from 1979 to the present, using ERA5 as the climatological input data. Global hydrological models are powerful tools for reconstructing components of the water balance because they generate continuous data, which can be used in applications such as hydrological model calibration [35]. Given the recent release of GloFAS, its potential has not been fully explored.

Central America is an area in which remotely sensed data can be highly useful for hydrological modelling to improve estimates of water resources [36]. Tan et al. (2021) [37] reviewed 123 articles regarding the use of alternative climate products in SWAT modelling. The authors found only one study conducted in Mexico and no precedents of this type of study for Central America.

In light of the above, this work may be of interest to stakeholders who model watersheds located in Central America. We selected the Grande San Miguel (GSM) River Basin as a case study, because many of the problems discussed above occur there. These include a low density of stations that provide precipitation and temperature records, a substantial percentage of missing data, and difficulty in obtaining streamflow data to enable model calibration. Using monthly flow data provided by the Ministry of Environment and Natural Resources in El Salvador for the period 2005–2010, we explored the potential of the GLoFAS-ERA5 river discharge reanalysis dataset for calibrating hydrological models in ungauged watersheds. The use of remotely sensed rainfall data for hydrological simulation is common in recent literature [37]. However, the use of globally generated flow data from remotely sensed data for calibrating a hydrological models is very novel because the release of these products is so recent [38,39].

This paper addresses the following objectives: (1) to evaluate the performance of precipitation and temperature variables using satellite reanalysis data such as CFSR, CHIRPS and ERA5 throughout the GSM River Basin; and (2) to assess the GLoFAS-ERA5 river discharge reanalysis dataset's potential for calibrating hydrological models and its relation

to precipitation and temperature reanalysis data used as input data. To date, few studies [21,40] have analysed the effectiveness of reanalysis data that includes temperature for simulating hydrological processes in a watershed. Most studies have considered only precipitation data.

2. Study Area and Weather Data Sources

2.1. Study Area

The GSM River Basin is geographically located in the east of El Salvador; it covers 2377 km^2 up to the outlet control point (Figure 1). The basin is among the largest in El Salvador. The city of San Miguel is situated at its core and is El Salvador's second most populous city. The basin is ecologically sensitive in terms of international protection, such as the protected zones of Tepaca-San Miguel and Jiquilisco Bay. Tecapa-San Miguel is known for its coffee plantations, coastal plain wetlands, and volcanic craters; the area includes several lagoons listed under the Ramsar Convention on Wetlands. Since 2005, the Jiquilisco Bay—which is located at the mouth of the Grande de San Miguel River—has been designated as a Ramsar site and a UNESCO biosphere reserve.

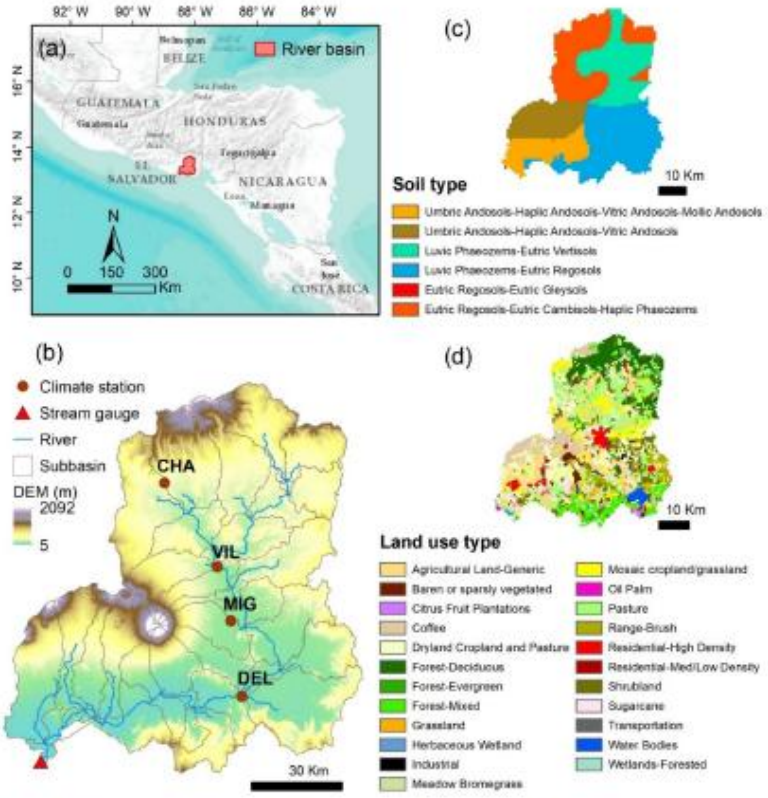

Figure 1. The study area location: (**a**) location of the Grande San Miguel river basin in Central America, (**b**) digital elevation model (DEM), sub-basins, and river stream delineation in the Grande San Miguel river basin, (**c**) soil map, and (**d**) land-use map.

Polluted water and the potential need for agricultural water are the two most pressing challenges in the GSM River Basin. [41]. To propose effective governance methods to mitigate the effect of these stress factors, the precise simulation of hydrological processes at the basin scale is crucial.

This region's climate is tropical, with high annual precipitation rates. However, the intra-annual distribution is uneven, with 90% of precipitation falling during the rainy season between May and October and scattered showers occurring during the dry season between November and April [36,42]. According to weather station measurements, the average annual precipitation is 1700 mm. The wettest months are from May to October and the driest months are from November to April. The basin is occasionally crossed by hurricanes, especially in September and October, which cause substantial flooding. Maximum temperatures are as high as 37 °C, and minimum temperatures drop to 17 °C. The altitude ranges from sea level to higher than 2000 m at the San Miguel Volcano.

Andosols, phaeozems, and regosols are the three most common soil types in the area (Figure 1c). The andosols that cover the area around the San Miguel Volcano are volcanic soils, which are highly permeable and have ideal agricultural qualities [43]. Regosols are unconsolidated materials with fine granulometry, common in mountainous areas. This is the dominant soil type at the northern boundaries. By contrast, phaeozem soils are abundant in the eastern part of the basin; they accommodate wet grasslands and forest regions because they are porous and fertile, and they provide excellent agricultural land (FAO, 2008). Grassland and pasture (43%), crops (32%), and forest (17%) are the most common land uses. The land-use map of the basin is shown in Figure 1d.

2.2. *In Situ Rainfall and Temperature Data*

Figure 1 shows the spatial distribution of rainfall stations in the GSM River Basin. Most of the existing weather stations are located in the lowlands, between 100 m and 200 m above sea level. As indicated in Table 1, three of the four available meteorological stations had more than 20% of data missing during the period under study (2005–2010). According to Tan and Yang (2020) [13], missing data of more than 20% significantly affects the simulation of flows in tropical climates. Given this fact and the low density of available stations, we used observed data to analyse the performance of the rainfall and temperature reanalysis data, but we did not simulate flows based on observed data.

Table 1. Summary of the weather stations used in this study.

Code	Station	Latitude (°)	Longitude (°)	Elevation (m)	Missing Data (%) [1]
MIG	San Miguel	13.4690	−88.1590	98	11.3/1.2
CHA	Chapeltique	13.6424	−88.2608	207	25.4
DEL	El Delirio	13.3274	−88.1416	92	41.4
VIL	Villerías	13.5187	−88.1795	109	51.7

[1] At San Miguel station, daily precipitation and temperature data are obtained. The percentages of missing data on precipitation and temperature data are 11.3% and 1.2% respectively.

2.3. *Reanalysis Precipitation and Temperature Datasets Used in This Study*

2.3.1. ERA5 Reanalysis Dataset

The ECMWF's most advanced reanalysis output is ERA5. This output was recently released with a resolution of roughly 30 km and can be used to compute many atmospheric variables from January 1950 to near real-time [25]. In the current study, the ERA5 hourly rainfall and temperature were extracted from the toolbox available on the Copernicus Climate Data Store website (https://cds.climate.copernicus.eu, accessed on 1 April 2021) and aggregated to the daily time step.

2.3.2. CHIRPS and CHIRTS

The CHIRPS dataset is the result of a collaboration between the United States Geological Survey and the University of California. It consists of a rainfall grid with a geographical resolution of 0.05° that combines data from satellites with data from on-site rainfall stations. The dataset was created using the following sources [22]:

- the Tropical Rainfall Measuring Mission (TRMM) 3B42 product from NASA
- the monthly precipitation climatology (CHPClim)
- atmospheric model rainfall fields from the National Oceanic and Atmospheric Administration (NOAA) Climate Forecast System version 2 (CFSv2)
- quasi-global geostationary thermal infrared (IR) satellite observations from two NOAA sources
- in situ rainfall observations

More recently, a temperature dataset with the same spatial resolution as CHIRPS has been developed on a daily scale. It entailed merging the monthly CHIRTS and disaggregating the monthly data using daily temperatures from ERA5 [24]. On the Climate Hazards Group website (https://www.chc.ucsb.edu/data/, accessed on 5 April 2021), users can obtain daily CHIRPS v2.0 and CHIRTS v1.0 data.

2.3.3. CFSR

The CFSR product was developed by the National Centers for Environmental Prediction (NCEP) [44]. It uses advanced data-assimilation methods and data from a global network of weather stations and satellite-based products; it also draws on complex atmospheric, oceanic, and surface modelling elements coupled with a resolution of 0.30° and covering any land location in the world [20]. The available CFSR data is available for 1979 to 2014 and can be downloaded from the SWAT website (https://globalweather.tamu.edu/, accessed on 5 April 2021).

2.4. GloFAS River Discharge Reanalysis Dataset

The GloFAS is part of the Copernicus Emergency Management Service (CEMS). The dataset was developed through collaboration between the ECMWF, the Joint Research Centre of the European Commission and the University of Reading (www.globalfloods.eu, accessed on 22 March 2021). The GLoFAS river discharge reanalysis dataset is a product of CEMS and is produced by coupling surface and subsurface runoff data from the HTESSEL surface model used forced by ERA5 reanalysis data [25] with the Distributed Water Balance and Flood Simulation (LISFLOOD) hydrological and channel routing model [34].

The model was calibrated using more than a thousand flow stations located in 66 different countries. It achieved a median Kling–Gupta efficiency (KGE) values of 0.67 and a correlation value of 0.80 [35]. The river discharge reanalysis, with daily time steps and 0.1° spatial resolution, is freely available to download for the period 1979 until near-present through the Copernicus Climate Data Store (https://cds.climate.copernicus.eu, accessed on 1 April 2021).

3. Materials and Methods

The methodological approach followed in this study is illustrated in Figure 2. It consisted of two main steps: (1) a comparison of rainfall and temperature data from reanalysis products with observed weather gauge data; and (2) an evaluation of the applicability of the flow data available in GLoFAS for the calibration of the SWAT hydrological model on a monthly scale. In the latter step, the weather input data used were ERA5, CHIRPS-CHIRTS and CFSR.

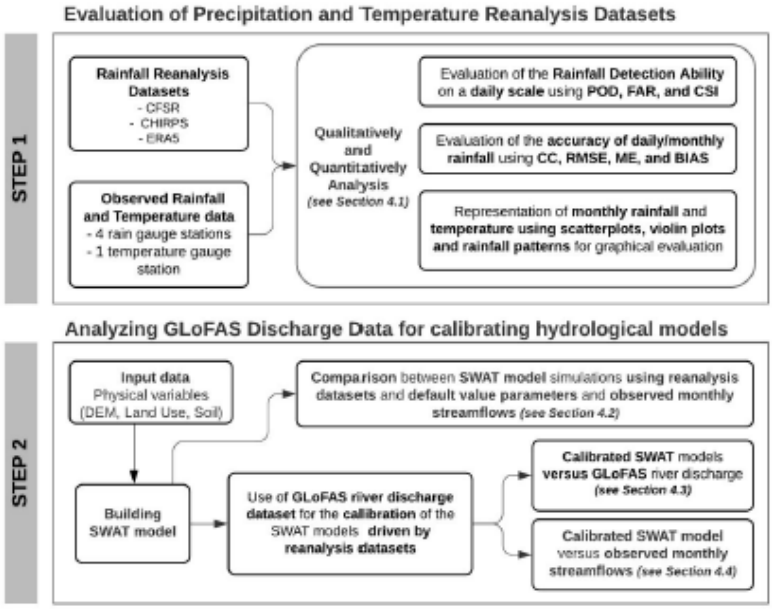

Figure 2. Flowchart of the methodological approach used in this study.

To perform the evaluation, streamflows were first assessed using each of the reanalysis products as input values; the monthly streamflows were simulated from the default values of the parameters in the SWAT model. Second, each simulation was calibrated independently using the GLoFAS data as the observed data. Finally, the accuracy of the GLoFAS-calibrated models for reproducing the observed monthly flows was assessed.

3.1. SWAT Model Description

The SWAT model is a physically based and distributed, and continuous, time model. It is used to model rainfall runoff at the basin scale [10]. Several global studies have applied the SWAT model to investigate hydrological and water quality processes [45–47], the impact of human pressure on water resources [48–50], and the consequences of climate change [36,51–53]. The model's GIS interface [54] allows for simple and quick data processing, such as watershed delineation and spatial and tabular data handling.

A watershed is divided into multiple sub-watersheds by SWAT. These are further subdivided into hydrological response units (HRUs), which include homogeneous land use, soil, and land slope. Water balance components, sediment flow, plant development and nutrient loss are some of the major processes that the model can replicate. To simulate the water balance components, SWAT solves the following equation:

$$SW_t = SW_0 + \sum_{i=1}^{t} \left(R_{day} - Q_{surf} - E_a - W_{seep} - Q_{gw} \right), \quad (1)$$

where SW_t is the final soil water content (mm), SW_0 is the initial soil water content (mm), t is the time in days, R_{day} is the precipitation (mm), Q_{surf} is the surface runoff (mm), E_a is the evapotranspiration (mm), W_{seep} is the percolation (mm) and Q_{gw} is the return flow (mm). Neitsch et al. (2012) [55] provide more information on the operation of the SWAT hydrological model.

3.2. SWAT Model Setup

We used the QGIS interface for SWAT, namely QSWAT version 3 [54], to build the model with publicly available information. In this study, the spatial data for the SWAT model includes a digital terrain model, land-use map, and soil map. For basin delineation, we acquired the Advanced Spaceborne Thermal Emission and Reflection Radiometer Global Digital Elevation Model (ASTER GDEM) from the official website, with a resolution of 30 m (Figure 1b). The Harmonized World Soil Database, published by the United Nations Food and Agriculture Organization (using a grid size of 1 km × 1 km) was used to extract soil data (Figure 1c). El Salvador's Ministry of Environment and Natural Resources provided the land-use map (Figure 1d). Potential evapotranspiration rates were calculated using the Hargreaves method [56] because it requires only temperature data.

3.3. SWAT Model Calibration

To evaluate the remote-sensing precipitation and temperature data and the monthly flow simulation, we selected the periods 2005–2008 and 2009–2010 were selected as the calibration and validation periods, respectively. Precipitation and temperature data from ERA5, CHIRPS-CHIRTS, and CFSR were available for a longer period, which allowed us to use a three-year warming period (2002–2004) to drive the SWAT model to a steady state. Twelve regularly used flow calibration parameters and their ranges were chosen, based on past experiences with similar watersheds [36] to integrate the components of surface runoff, groundwater, and soil data. The SWAT Calibration and Uncertainty Program (SWATCUP) [57] includes the Sequential Uncertainty Fitting Procedure version 2 (SUFI-2) optimisation method. We used this to perform monthly automatic calibration. The Nash–Sutcliffe model efficiency coefficient (NSE) was employed as the objective function, and 2000 simulations were performed.

Table 2 shows the list of adjusted SWAT parameters. The range of variation and the final values were determined after calibration, as a function of the gridded dataset.

Table 2. Sensitivity analysis of SWAT model parameters for the GSM River Basin.

Parameter	Description	ERA5		CHIRPS-CHIRTS		CFSR	
		Ranking	*p*-Value	Ranking	*p*-Value	Ranking	*p*-Value
CN2.mgt	SCS runoff curve number	1	0.000	1	0.000	1	0.000
ALPHA_BF.gw	Baseflow alpha factor (day^{-1})	10	0.551	11	0.799	7	0.552
GWQMN.gw	Threshold depth of water in the shallow aquifer for return flow to occur (mm)	2	0.003	4	0.024	2	0.002
GW_REVAP.gw	Groundwater revap coefficient	5	0.114	8	0.229	4	0.068
RCHRG_DP.gw	Deep aquifer percolation fraction	11	0.555	6	0.100	3	0.032
REVAPMN.gw	Threshold depth of water in shallow aquifer for revap or percolation to deep aquifer to occur (mm)	9	0.531	10	0.704	10	0.637
CANMX.hru	Maximum canopy storage (mm)	12	0.573	12	0.909	8	0.564
EPCO.bsn	Plant uptake compensation factor	8	0.451	7	0.186	6	0.531
ESCO.bsn	Soil evaporation compensation factor	4	0.015	2	0.000	5	0.32
SOL_AWC.sol	Available water capacity of the soil layer (mm H_2O/mm soil)	7	0.202	5	0.037	11	0.672
LAT_TTIME.hru	Lateral flow travel time (day)	6	0.175	9	0.489	12	0.806
SLSOIL.hru	Slope length for lateral subsurface flow (m)	3	0.012	3	0.006	9	0.610

3.4. Performance Evaluation of the Reanalysis Datasets and Simulated Streamflow

Our aim was to qualitatively compare the ERA5, CHIRPS, and CFSR reanalysis datasets with the rain gauge observations. The following statistical indices for validation were used: the correlation coefficient (CC or R^2), mean (M), standard deviation (SD), mean error (ME), root-mean square error (RMSE), and relative bias (BIAS). The linear correlation is indicated by CC, the average difference is shown by RMSE, and the average error magnitude between the reanalysis precipitation and observed rain gauge data is shown by ME. The systematic bias of the satellite precipitation is described by BIAS.

Rainfall detection capability was analysed using three categorical statistical indices: (1) the probability of detection (POD); (2) the false alarm rate (FAR); and (3) the critical success index (CSI). The POD is also known as the hit rate. This is the ratio of total rainfall events that are successfully recognised by the reanalysis datasets. The FAR indicates the percentage of falsely warned rainfall events among all warnings. The most balanced and accurate detection statistic is the CSI, which is a function of POD and FAR [58]. The POD, FAR, and CSI scores range between 0 and 1, with 1 being a perfect score for POD and CSI and 0 for FAR. The formulas and further details about the indices appear in Jiang et al. (2018) [59].

To assess the SWAT model's accuracy, we included the coefficient of determination (R^2), the Nash–Sutcliffe efficiency ratio (NSE), percentage bias (PBIAS), observed data SD ratio (RSR), and the Kling–Gupta efficiency ratio (KGE). These statistics are extensively used in hydrological research [60]. At the monthly scale, when the PBIAS is below 25% and the NSE and KGE are above 0.5, and the RSR is below 0.7, the model's performance is considered to be adequate [61,62].

4. Results and Discussion

4.1. Comparison between Observed and Reanalysis Datasets

Precipitation data from the three reanalysis datasets (CFSR, ERA5, and CHIRPSv2.0) were directly compared to precipitation data from rainfall stations in the GSM River Basin. Daily precipitation data was collected from the reanalysis data grid cells closest to the available weather stations; days with no observed data were omitted from the comparative analysis. To enable conclusions regarding the flow simulation, we used the same period to evaluate the accuracy of the precipitation data as the period for which the flow data was available (2005–2010).

The validation statistics for the GSM River Basin are presented in Table 3. Among the three reanalysis datasets, the CHIRPS was more accurate; it yielded low ME values together with higher CC and CSI values. Hence, it performed best in both accuracy and detection capability. The results obtained from ERA5 and CFSR were also acceptable. In the case of ERA5, the correlation with observed data was slightly lower than that yielded by CHIRPS. Of the three reanalysis datasets, ERA5 achieved a monthly SD most similar to that of the observed data. However, ERA5 presented the highest BIAS of the three reanalysis datasets analysed, overestimating the rainfall values at some weather stations by more than 40%. The higher amount of rainfall explained why ERA5 yielded relatively high POD and FAR values.

The CFSR yielded a smaller correlation with the observed data than CHIRPS and ERA5. Conversely, the BIAS was lower than that shown by ERA5, which signified overestimation or underestimation of the rainfall depending on the station analysed. The lower BIAS value was related to a lower POD and FAR compared to the results obtained with ERA5. On average, CSI was similar for both CFSR and ERA5, which implies a similar detection capability.

Table 3. Comparison of various validation statistics for the different reanalysis products covering the GSM River Basin. Daily and monthly statistics are shown on the left and right sides of a/symbol. Gaps in gauge observation records result in different daily and monthly BIAS. Only months with complete daily data were compared.

Station	Dataset	M	SD	CC	RMSE (mm)	ME (mm)	BIAS (%)	POD	FAR	CSI
MIG	Observed	1469	274	-	-	-	-	-	-	-
	ERA5	2105	303	0.43/0.85	13.54/115.23	6.04/72.05	38.32/40.60	0.91	0.50	0.48
	CHIRPS	1752	285	0.52/0.93	10.71/61.44	4.55/41.87	13.33/15.69	0.79	0.35	0.54
	CFSR	1441	356	0.27/0.84	12.91/71.01	5.70/51.54	−4.64/−4.75	0.79	0.48	0.44
CHA	Observed	1561	470	-	-	-	-	-	-	-
	ERA5	2204	495	0.38/0.80	15.55/124.38	6.87/78.05	18.95/25.19	0.92	0.42	0.55
	CHIRPS	1991	268	0.55/0.88	11.56/82.54	5.38/54.25	6.70/10.01	0.82	0.27	0.63
	CFSR	1441	356	0.34/0.85	13.54/94.53	6.25/62.46	−21.73/−20.47	0.79	0.41	0.51
DEL	Observed	1136	731	-	-	-	-	-	-	-
	ERA5	1994	549	0.49/0.83	14.33/123.69	5.97/82.61	46.89/48.62	0.89	0.53	0.45
	CHIRPS	1821	341	0.62/0.86	11.13/97.85	5.06/63.11	31.66/33.74	0.80	0.40	0.52
	CFSR	1817	385	0.38/0.86	13.56/92.77	5.97/65.00	27.86/30.30	0.89	0.54	0.43
VIL	Observed	1023	627	-	-	-	-	-	-	-
	ERA5	2106	519	0.41/0.86	12.53/103.13	5.56/69.76	49.77/48.90	0.91	0.49	0.48
	CHIRPS	1785	263	0.51/0.91	9.73/76.38	4.48/50.54	30.86/31.97	0.79	0.36	0.54
	CFSR	1441	356	0.27/0.84	11.50/62.68	5.03/40.79	−0.07/0.78	0.75	0.48	0.44

Figure 3 shows the probability density function of rainfall events on a daily scale. It is evident that all the remote-sensing data we analysed missed some rain events and CHIRPS was most similar to the observed data in this regard. ERA5 clearly overestimated the amount of light and medium rainfall events (where 'light' refers to daily rainfall of 1–5 mm) and medium refers to daily rainfall of 5–20 mm). CFSR, despite overestimating these rainfall events, was the reanalysis dataset that most closely reflected the observed data for medium rainfall events. Among the three reanalysis datasets, CHIRPS best represented light rainfall events, but it significantly overestimated medium rainfall events. Regarding the highest intensity events (daily rainfall over 20 mm), the three reanalysis datasets yielded similar performances.

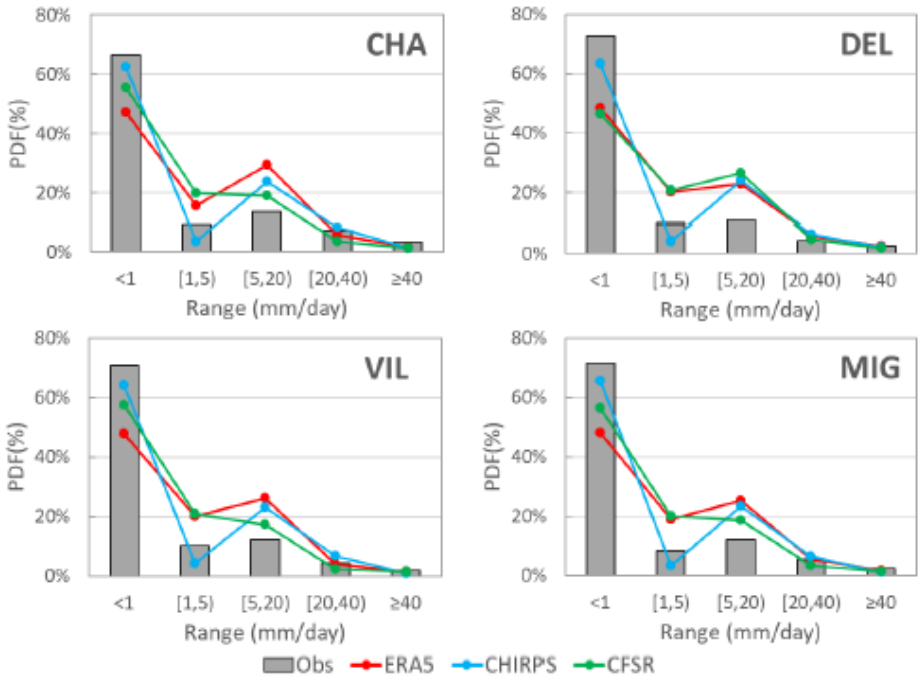

Figure 3. Description of different rainfall intensities of the probability density function of rainfall events on a daily scale.

The general overestimation of the number of rainfall events and the volume of rainfall may be due to the ability of satellites to detect strong convective events while having more difficulty in detecting shallow and warm rains. In addition, the bias correction techniques generally used to correct satellite data often inflate the volume of rainfall in the detected events to compensate for the missed events [63].

As evident in Figure 4, monthly observed rainfall and variations in rainfall patterns were also analysed. In the left column, violin plots combine box plots and a kernel density plot to simultaneously represent the data distribution and probability density. Except for MIG, the density distribution displayed a consistently more accurate adjustment when using the CHIRPS data. The median prediction is shown as a white dot in the graphs, and significant differences were detected. In general, ERA5 overestimated the median value, except at the CHA station (located at the highest altitude), where the reanalysis data resulted in an underestimated median value. Similarly, ERA5, CHIRPS and CFSR adequately reflected the inter-annual variation in precipitation; they indicated the existence of a dry period from November to April and a wet period from May to October.

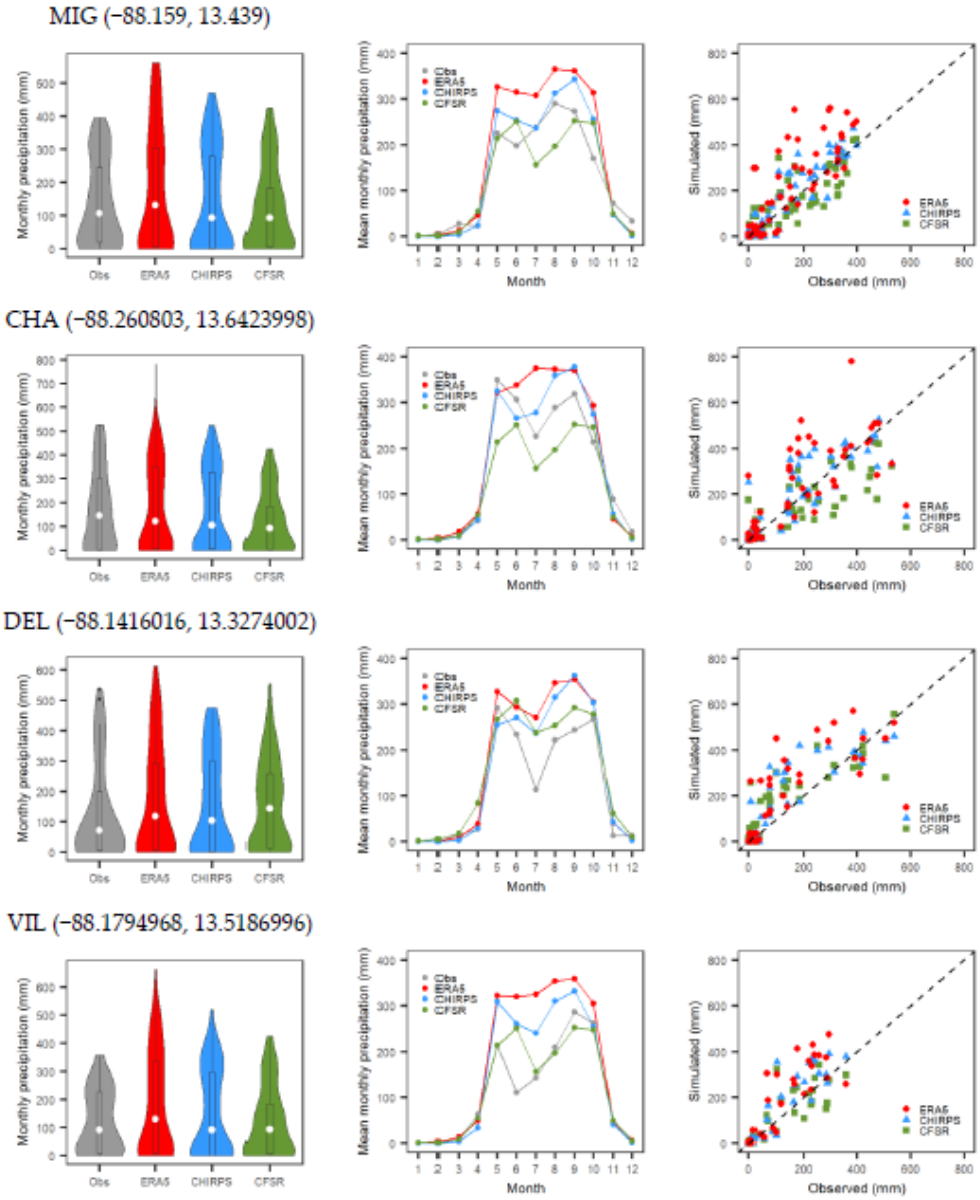

Figure 4. Comparison of average monthly observed precipitation with ERA5, CHIRTS, and CFSR datasets using violin plots (**left** column), variations in rainfall patterns (**central** column) and scatterplots (**right** column).

A characteristic aspects of the climate in the study area is a maximum monthly rainfall that occurs between June and September, interrupted by a typical mid-summer drought during the month of July [36,64]. This pattern was detected by all the products we assessed. In addition, unlike CFSR, the ERA5 and CHIRPS datasets overestimated

the average monthly rainfall reported during the rainy season. We also found that the scatterplots suggested a higher performance for the CHIRPS data, with an overall closer fit with the observations. This finding was supported by the calculated CC values. Using the CHIRPS data, the CC values for the tested weather stations ranged from 0.86 to 0.93. By contrast, for the CFSR and ERA5 datasets, the CC values ranged from 0.84 to 0.86 and 0.80 to 0.86, respectively.

The observed monthly temperatures were compared to data from ERA5, CHIRTS, and CFSR, as discussed in the previous section (Figure 5). Although the shape of the density distribution and the monthly variations showed a good fit, we noted a significant overestimation of CHIRTS temperatures by 2–3 °C, depending on the month considered, over the year. For CFSR, an overestimation of the monthly mean temperature was also detected for all months, which was far lower than that observed in CHIRTS. At the MIG station, which was the only station for which temperature data was available, the data from ERA5 provided the best fit.

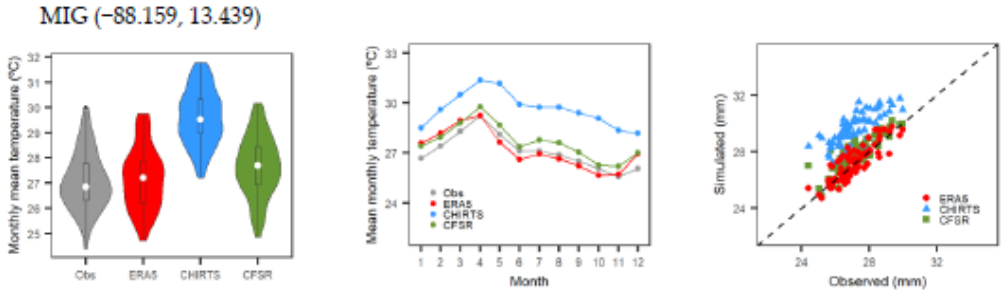

Figure 5. Comparison of average monthly observed temperature with ERA5, CHIRTS, and CFSR datasets using violin plots (**left** column), variations in rainfall patterns (**central** column) and scatterplots (**right** column).

4.2. Model Performance before Calibration

When data is missing from observations, the performance of an uncalibrated model is an important indicator of how well the model performs [65]. The main purpose for which the SWAT model was conceived was to model ungauged rural watersheds [10]. The suitability of the different reanalysis datasets was evaluated by simulating flows within the SWAT model framework using default parameters.

Figure 6 shows the observed and simulated monthly runoff in the GSM River Basin for the period 2005–2010. The criteria for evaluating the model performance are indicated in Figure 5, from which it is evident that CFSR yielded the best results. This was as expected, since this dataset contained the least biased reanalysis data. However, it is important to note that on a monthly scale, all the reanalysis datasets yielded adequate CCs, which ranged between 0.64 and 0.74. These results suggest that after calibrating the most sensitive parameters, the overall performance of the models may be acceptable.

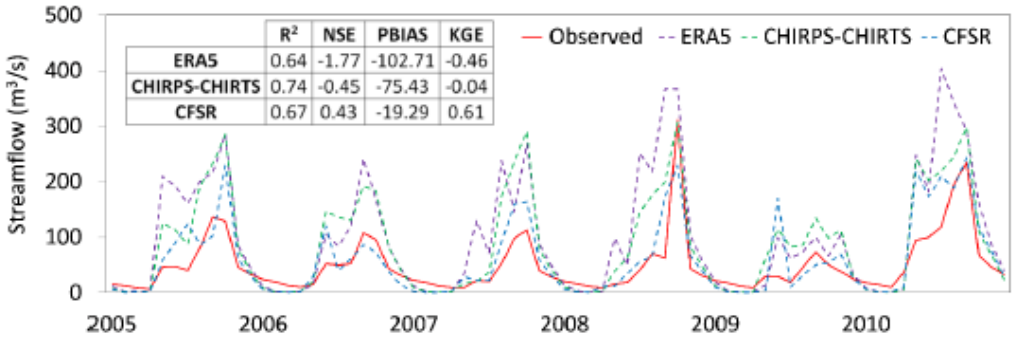

Figure 6. Model performance comparison for the default SWAT model using ERA5, CHIRPS-CHIRTS, and CFSR datasets for the input data together with monthly observed streamflows.

4.3. Model Calibration Using GLoFAS Discharge Data

As shown in Figure 2, we first compared the observed rainfall and temperature data and the reanalysis data. Then we evaluated the performance of three datasets as inputs for the SWAT model to simulate the observed flow in the GSM River Basin. For this purpose, the SWAT model was calibrated for each of the reanalysis products, including both precipitation and temperature. The SUFI-2 algorithm included in the SWATCUP software was used to optimise 12 SWAT parameters. Parameter selection was based on previous studies in nearby catchments in El Salvador [36], as mentioned in Section 3.3.

In addition, a sensitivity analysis was conducted to determine the most sensitive parameters using each of the reanalysis datasets as input data and performing 500 model runs. As shown in Table 3, regardless of the reanalysis data used, CN2 was the most sensitive parameter, followed by GWQMN and ESCO; these parameters obtained the lowest *p*-values. The *p*-value for each parameter represents a test of the null hypothesis that the regression coefficient is equal to zero. According to Abbaspour et al. (2007) [66], the more sensitive the parameter, the smaller the *p*-value.

Table 4 shows the parameter ranges and the final calibrated values for each of the reanalysis products. Among the calibrated parameters—and as demonstrated by the sensitivity analysis, CN2 was one of the most sensitive parameters as it is directly related to runoff generation [67,68]. We thus expected that the calibrated CN2 values would be substantially reduced to correct the overestimation of precipitation as detected using the reanalysis data, with the expected reduction being between 11.7% and 19.9%.

Table 4. Calibrated parameter values.

Parameter	Range	Calibrated Value		
		ERA5	CHIRPS-CHIRTS	CFSR
CN2.mgt	−0.2 to 0.2	−0.199	−0.117	−0.157
ALPHA_BF.gw	0.01 to 1	0.85555	0.5099	0.24333
GWQMN.gw	0 to 5000	4765	3675	195
GW_REVAP.gw	0.02 to 0.2	0.1167	0.1026	0.0846
RCHRG_DP.gw	0 to 1	0.315	0.065	0.785
REVAPMN.gw	0 to 500	356.5	302.5	320.5
CANMX.hru	0 to 100	90.9	95.7	29.5
EPCO.bsn	0 to 1	0.499	0.819	0.365
ESCO.bsn	0 to 1	0.8155	0.801	0.861
SOL_AWC.sol	−0.3 to 0.3	0.055	−0.1974	−0.213
LAT_TTIME.hru	0 to 180	48.06	108.90	15.3
SLSOIL.hru	0 to 150	43.35	38.55	35.25

In addition, ESCO was also reduced from the default value of 0.95 to values between 0.80 and 0.86, which represents an increase in evaporation generated by the model. These ESCO values are in line with those obtained in other tropical areas [36,69]. The largest discrepancies between the fitted values and the reanalysis data were noted for the groundwater parameters (ALPHA_BF, GWQMN, GW_REVAP, RCHRG_DP and REVAPMN). This result might be attributable to the inherent complexity of the volcanic aquifers in Central America; the aquifers display high permeability and fissure flows, making them very complicated to study [70]. However, ALPHA_BF varied from 0.24 (for CFSR) to 0.85 (for ERA5). The latter value indicates a faster recharge response [71], which is consistent with the volcanic aquifers in the study area.

The performance of the calibrated model for each of the input datasets is summarised in Table 5. The statistics show that the SWAT model simulated the GloFAS discharge flows reasonably well for both calibration (2005–2008) and validation (2009–2010) periods. This result was independent of the reanalysis data, since all the simulations had a CC ranging between 0.76 and 0.85, an NSE greater than 0.50, and a KGE value between 0.84 and 0.86. As expected, the best results were obtained using data from ERA5, which is used to obtain the global-scale flows in GloFAS.

Table 5. SWAT model performance compared with GloFAS discharge data.

Parameter	Dataset					
	ERA5		CHIRPS-CHIRTS		CFSR	
	Calibration	Validation	Calibration	Validation	Calibration	Validation
R^2	0.88	0.82	0.78	0.78	0.82	0.60
NSE	0.87	0.81	0.77	0.70	0.81	0.54
PBIAS (%)	−11.68	−13.36	7.34	−30.70	−3.29	−32.31
KGE	0.86	0.81	0.85	0.65	0.88	0.47

4.4. Evaluation of the Simulated Monthly Streamflows for Various Scenarios

Finally, the simulated monthly scale flows obtained from the GloFAS calibration were compared with the observed flows. The simulations performed using CHIRPS-CHIRTS data showed the best fit, as evident in Figure 7. Nonetheless, all three simulations performed using ERA5, CHIRPS-CHIRTS, and CFSR data showed an acceptable fit with the observed streamflows.

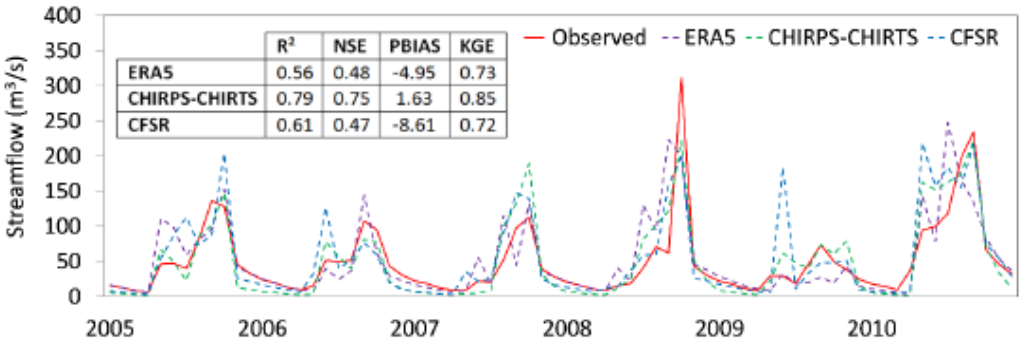

Figure 7. Model performance comparison between simulated and observed monthly streamflows after calibration using GLoFAS discharge data.

These results demonstrate that when the ERA5 reanalysis data show an adequate fit, GloFAS discharge data could potentially be used to simulate the hydrological processes of ungauged catchments at the monthly scale. This would allow the use of distributed hydrological models such as SWAT to analyse fundamental aspects in water resource management—such as the impact of changes in land use or the climate. Similar to our findings, Eini et al. (2019) [72] reported that when precipitation reanalysis data represented well-observed precipitation (R^2 higher than 0.6) in a semi-arid basin in Iran, the result was reasonable simulations for river discharge. However, these results should be viewed with caution as they depend on the quality of the GloFAS adjustment to the observed flows. In this regard, Harrigan et al. (2020) [30] demonstrated that the quality of the GloFAS adjustment increased substantially along with the size of the catchment. We thus recommend that the methodology followed in our study should be replicated in larger catchments.

4.5. Limitations and Future Research Directions

This study demonstrates that when remotely sensed weather data are accurate with respect to observed climatological data, flow simulation is often accurate. Hence, the use of discharge data, such as GLoFAS, contributes to the correct simulation of the hydrological processes in a basin. However, several limitations need to be considered. Firstly, data from a single flow-gauging station at the outlet of the basin was used to calibrate the model. This means there is the possibility of equifinality issues with some parameters having optimal values that are physically unrealistic. Future research should include additional calibration with other variables that are available through remote sensing, such as evapotranspiration.

Second, NSE has been used as the objective function. This coefficient usually presents the problem of being weighted towards higher flows. The use of other objective functions would return different results, and it would be interesting to study the effect of the selected objective function on the results obtained.

Third, only the SWAT model was employed to test the methodological approach used in this work. Future research and performance testing with different hydrological models could help to clarify the limitations and strengths of our methodological approach. Finally, if observed data is available, future studies could assess the performance of GLoFAS discharge data on a daily and sub-daily basis.

5. Conclusions

This study evaluates the application of GLoFAS discharge data in model calibration in El Salvador, Central America. This is a country in which climatological input data and observed flow data for calibrating hydrological models is scarce or unavailable. GLoFAS determines the streamflow by applying a global-scale hydrological model that uses ERA5 reanalysis data as the input data. This work tested whether the streamflow data from GLoFAS provided a suitable option for calibrating hydrological models in ungauged catchments, as long as there is a good fit between reanalysis precipitation and temperature data and observed climatological data. Climatological reanalysis data (CHIRPS-CHIRTS and CFSR) were also evaluated. The following conclusions are presented:

(1) The statistical indicators (CC, RMSE, ME, and BIAS) allowed the accuracy of the reanalysis data to be quantitatively evaluated. We found that CHIRPS performed best in reproducing the observed precipitation, despite consistently overestimating the rainfall.

(2) In terms of rain detection ability, CHIRPS (CSI ranging from 0.52 to 0.63) displayed the greatest daily accuracy in detecting the precipitation occurrences. The next best were ERA5 and then CFSR. However, all three reanalysis datasets showed acceptable rainfall detection capability.

(3) Among the three temperature reanalysis products, the performance of CHIRTS was the least accurate; it repeatedly overestimated mean temperature by 2–3 °C. By contrast, ERA5 and CFSR presented excellent agreement with the observed data.

(4) Models that were calibrated using GloFAS data as the observed data, independently of the precipitation and temperature data (ERA5, CHIRPS-CHIRTS and CFSR) showed acceptable model performance. This point was evident in the KGE values, which ranged from 0.74 to 0.79, and the R^2 values of between 0.57 and 0.78.

Overall, these findings demonstrate that reanalysis rainfall products can improve hydrological process modelling for Central American watersheds, where poorly gauged or ungauged watersheds are common. This research also highlights the GLoFAS dataset's potential for model calibration in catchments where the availability of streamflow data is limited. The availability of a calibrated hydrological model that adequately reflects the hydrological processes of a basin provides decision-makers with a tool to quantify the availability of water resources. The modelalso provides the basis for estimating the impact of land use changes or climate change on water resources.

Author Contributions: J.S.-A. and P.B.-G. conceived and designed the experiments; P.B.-G., P.J.-S. and A.L.-B. performed the experiments and analysed the data; J.P.-S. provided reviews and suggestions; J.S.-A. prepared the manuscript with contributions from all co-authors. All authors have read and agreed to the published version of the manuscript.

Funding: This research was funded by the European Union's Horizon 2020 research and innovation programme within the framework of the project SMARTLAGOON, grant agreement number 101017861.

Acknowledgments: The authors acknowledge Scribbr editing services for proofreading the manuscript.

Conflicts of Interest: The authors declare no conflict of interest.

References

1. Kiros, G.; Shetty, A.; Nandagiri, L. Performance evaluation of SWAT model for land use and land cover changes under different climatic conditions: A review. *J. Waste Water Treat. Anal.* **2015**, *6*, 1–6. [CrossRef]
2. Krysanova, V.; Srinivasan, R. Assessment of climate and land use change impacts with SWAT. *Reg. Environ. Chang.* **2014**, *15*, 431–434. [CrossRef]
3. Kok, K.; Winograd, M. Modelling land-use change for Central America, with special reference to the impact of hurricane mitch. *Ecol. Model.* **2002**, *149*, 53–69. [CrossRef]
4. Hidalgo, H.G.; Amador, J.A.; Alfaro, E.J.; Quesada, B. Hydrological climate change projections for Central America. *J. Hydrol.* **2013**, *495*, 94–112. [CrossRef]
5. Srivastava, A.; Sahoo, B.; Raghuwanshi, N.S.; Singh, R. Evaluation of variable-infiltration capacity model and modis-terra satellite-derived grid-scale evapotranspiration estimates in a river basin with tropical monsoon-type climatology. *J. Irrig. Drain. Eng.* **2017**, *143*, 04017028. [CrossRef]
6. Srivastava, A.; Deb, P.; Kumari, N. Multi-Model approach to assess the dynamics of hydrologic components in a tropical ecosystem. *Water Resour. Manag.* **2020**, *34*, 327–341. [CrossRef]
7. Paul, P.K.; Kumari, N.; Panigrahi, N.; Mishra, A.; Singh, R. Implementation of cell-to-cell routing scheme in a large scale conceptual hydrological model. *Environ. Model. Softw.* **2018**, *101*, 23–33. [CrossRef]
8. Fukunaga, D.C.; Cecílio, R.; Zanetti, S.S.; Oliveira, L.T.; Caiado, M.A.C. Application of the SWAT hydrologic model to a tropical watershed at Brazil. *Catena* **2015**, *125*, 206–213. [CrossRef]
9. Darbandsari, P.; Coulibaly, P. Inter-comparison of lumped hydrological models in data-scarce watersheds using different precipitation forcing data sets: Case study of Northern Ontario, Canada. *J. Hydrol. Reg. Stud.* **2020**, *31*, 100730. [CrossRef]
10. Arnold, J.G.; Srinivasan, R.; Muttiah, R.S.; Williams, J.R. Large area hydrologic modeling and assessment part I: Model development. *JAWRA J. Am. Water Resour. Assoc.* **1998**, *34*, 73–89. [CrossRef]
11. Abbaspour, K.C.; Vaghefi, S.A.; Yang, H.; Srinivasan, R. Global soil, landuse, evapotranspiration, historical and future weather databases for SWAT Applications. *Sci. Data* **2019**, *6*, 1–11. [CrossRef] [PubMed]
12. Hughes, D.A. Comparison of satellite rainfall data with observations from gauging station networks. *J. Hydrol.* **2006**, *327*, 399–410. [CrossRef]
13. Tan, M.L.; Yang, X. Effect of rainfall station density, distribution and missing values on SWAT outputs in tropical region. *J. Hydrol.* **2020**, *584*, 124660. [CrossRef]
14. Dhanesh, Y.; Bindhu, V.; Senent-Aparicio, J.; Brighenti, T.; Ayana, E.; Smitha, P.; Fei, C.; Srinivasan, R. A comparative evaluation of the performance of CHIRPS and CFSR data for different climate zones using the SWAT model. *Remote Sens.* **2020**, *12*, 3088. [CrossRef]
15. Mazzoleni, M.; Brandimarte, L.; Amaranto, A. Evaluating precipitation datasets for large-scale distributed hydrological modelling. *J. Hydrol.* **2019**, *578*, 124076. [CrossRef]

16. Yin, J.; Guo, S.; Gu, L.; Zeng, Z.; Liu, D.; Chen, J.; Shen, Y.; Xu, C.-Y. Blending multi-satellite, atmospheric reanalysis and gauge precipitation products to facilitate hydrological modelling. *J. Hydrol.* **2021**, *593*, 125878. [CrossRef]
17. Usman, M.; Ndehedehe, C.E.; Ahmad, B.; Manzanas, R.; Adeyeri, O.E. Modeling streamflow using multiple precipitation products in a topographically complex catchment. *Model. Earth Syst. Environ.* **2021**, 1–11. [CrossRef]
18. Tan, M.L.; Gassman, P.W.; Cracknell, A.P. Assessment of three long-term gridded climate products for hydro-climatic simulations in tropical river basins. *Water* **2017**, *9*, 229. [CrossRef]
19. Yatagai, A.; Kamiguchi, K.; Arakawa, O.; Hamada, A.; Yasutomi, N.; Kitoh, A. Aphrodite: Constructing a long-term daily gridded precipitation dataset for Asia based on a dense network of rain gauges. *Bull. Am. Meteorol. Soc.* **2012**, *93*, 1401–1415. [CrossRef]
20. Saha, S.; Moorthi, S.; Pan, H.-L.; Wu, X.; Wang, J.; Nadiga, S.; Tripp, P.; Kistler, R.; Woollen, J.; Behringer, D.; et al. The NCEP climate forecast system reanalysis. *Bull. Am. Meteorol. Soc.* **2010**, *91*, 1015–1058. [CrossRef]
21. Duan, Z.; Tuo, Y.; Liu, J.; Gao, H.; Song, X.; Zhang, Z.; Yang, L.; Mekonnen, D.F. Hydrological evaluation of open-access precipitation and air temperature datasets using SWAT in a poorly gauged basin in Ethiopia. *J. Hydrol.* **2019**, *569*, 612–626. [CrossRef]
22. Funk, C.; Peterson, P.; Landsfeld, M.; Pedreros, D.; Verdin, J.; Shukla, S.; Husak, G.; Rowland, J.; Harrison, L.; Hoell, A.; et al. The climate hazards infrared precipitation with stations—A new environmental record for monitoring extremes. *Sci. Data* **2015**, *2*, 150066. [CrossRef]
23. Senent-Aparicio, J.; Jimeno-Sáez, P.; López-Ballesteros, A.; Giménez, J.G.; Pérez-Sánchez, J.; Cecilia, J.M.; Srinivasan, R. Impacts of SWAT weather generator statistics from high-resolution datasets on monthly streamflow simulation over Peninsular Spain. *J. Hydrol. Reg. Stud.* **2021**, *35*, 100826. [CrossRef]
24. Verdin, A.; Funk, C.; Peterson, P.; Landsfeld, M.; Tuholske, C.; Grace, K. Development and validation of the chirts-daily quasi-global high-resolution daily temperature data set. *Sci. Data* **2020**, *7*, 1–14. [CrossRef]
25. Hersbach, H.; Bell, B.; Berrisford, P.; Hirahara, S.; Horanyi, A.; Muñoz-Sabater, J.; Nicolas, J.; Peubey, C.; Radu, R.; Schepers, D.; et al. The ERA5 global reanalysis. *Q. J. R. Meteorol. Soc.* **2020**, *146*, 1999–2049. [CrossRef]
26. Tarek, M.; Brissette, F.P.; Arsenault, R. Evaluation of the ERA5 reanalysis as a potential reference dataset for hydrological modelling over North America. *Hydrol. Earth Syst. Sci.* **2020**, *24*, 2527–2544. [CrossRef]
27. Kolluru, V.; Kolluru, S.; Konkathi, P. Evaluation and integration of reanalysis rainfall products under contrasting climatic conditions in India. *Atmos. Res.* **2020**, *246*, 105121. [CrossRef]
28. Jiang, Q.; Li, W.; Fan, Z.; He, X.; Sun, W.; Chen, S.; Wen, J.; Gao, J.; Wang, J. Evaluation of the ERA5 reanalysis precipitation 45dataset over Chinese Mainland. *J. Hydrol.* **2021**, *595*, 125660. [CrossRef]
29. Revilla-Romero, B.; Beck, H.E.; Burek, P.; Salamon, P.; de Roo, A.; Thielen, J. Filling the gaps: Calibrating a rainfall-runoff model using satellite-derived surface water extent. *Remote Sens. Environ.* **2015**, *171*, 118–131. [CrossRef]
30. Harrigan, S.; Zsoter, E.; Alfieri, L.; Prudhomme, C.; Salamon, P.; Wetterhall, F.; Barnard, C.; Cloke, H.; Pappenberger, F. GloFAS-ERA5 operational global river discharge reanalysis 1979–present. *Earth Syst. Sci. Data* **2020**, *12*, 2043–2060. [CrossRef]
31. Ghiggi, G.; Humphrey, V.; Seneviratne, S.I.; Gudmundsson, L. G-RUN ensemble: A multi-forcing observation-based global runoff reanalysis. *Water Resour. Res.* **2021**, *57*. [CrossRef]
32. He, X.; Pan, M.; Wei, Z.; Wood, E.F.; Sheffield, J. A global drought and flood catalogue from 1950 to 2016. *Bull. Am. Meteorol. Soc.* **2020**, *101*, E508–E535. [CrossRef]
33. Balsamo, G.; Pappenberger, F.; Dutra, E.; Viterbo, P.; Hurk, B.V.D. A revised land hydrology in the ECMWF model: A step towards daily water flux prediction in a fully-closed water cycle. *Hydrol. Process.* **2011**, *25*, 1046–1054. [CrossRef]
34. van der Knijff, J.; Younis, J.; De Roo, A.P.J. LISFLOOD: A GIS-based distributed model for river basin scale water balance and flood simulation. *Int. J. Geogr. Inf. Sci.* **2010**, *24*, 189–212. [CrossRef]
35. Alfieri, L.; Lorini, V.; Hirpa, F.A.; Harrigan, S.; Zsoter, E.; Prudhomme, C.; Salamon, P. A global streamflow reanalysis for 1980–2018. *J. Hydrol. X* **2020**, *6*, 100049. [CrossRef] [PubMed]
36. Blanco-Gómez, P.; Jimeno-Sáez, P.; Senent-Aparicio, J.; Pérez-Sánchez, J. Impact of climate change on water balance components and droughts in the Guajoyo River Basin (El Salvador). *Water* **2019**, *11*, 2360. [CrossRef]
37. Tan, M.L.; Gassman, P.W.; Liang, J.; Haywood, J.M. A review of alternative climate products for SWAT modelling: Sources, assessment and future directions. *Sci. Total. Environ.* **2021**, *795*, 148915. [CrossRef] [PubMed]
38. Sikder, S.; David, C.; Allen, G.H.; Qiao, X.; Nelson, E.J.; Matin, M.A. Evaluation of available global runoff datasets through a river model in support of transboundary water management in South and Southeast Asia. *Front. Environ. Sci.* **2019**, *7*, 171. [CrossRef]
39. Lakew, H.B.; Moges, S.A.; Anagnostou, E.N.; Nikolopoulos, E.I.; Asfaw, D.H. Evaluation of global water resources reanalysis runoff products for local water resources applications: Case study-upper blue Nile basin of Ethiopia. *Water Resour. Manag.* **2019**, *34*, 2157–2177. [CrossRef]
40. Yen, H.; Wang, R.; Feng, Q.; Young, C.-C.; Chen, S.-T.; Tseng, W.-H.; Wolfe III, J.E.; White, M.J.; Arnold, J.G. Input uncertainty on watershed modeling_ evaluation of precipitation and air temperature data by latent variables using SWAT. *Ecol. Eng.* **2018**, *122*, 16–26. [CrossRef]
41. MARN Plan Nacional de Gestión Integrada Del Recurso Hídrico de El Salvador, Con Énfasis En Zonas Prioritarias. *Minist. De Medio Ambiente Y Recur. Nat.* 2017. Available online: https://cidoc.marn.gob.sv/documentos/plan-nacional-de-gestion-integrada-del-recurso-hidrico-de-el-salvador-con-enfasis-en-zonas-prioritarias/ (accessed on 11 July 2021).

42. Wozab, D.; Jovel, J.R. Hydrological analysis of volcanic terrane: Lower basin of the rio grande de san miguel el salvador. *Int. Assoc. Sci. Hydrol. Bull.* **1970**, *15*, 47–66. [CrossRef]
43. Levard, C.; Basile-Doelsch, I. Geology and mineralogy of imogolite-type materials. In *Developments in Clay Science*; Elsevier BV: Amsterdam, The Netherlands, 2016; Volume 7, pp. 49–65.
44. Saha, S.; Moorthi, S.; Wu, X.; Wang, J.; Nadiga, S.; Tripp, P.; Behringer, D.; Hou, Y.-T.; Chuang, H.-Y.; Iredell, M.; et al. The NCEP climate forecast system version 2. *J. Clim.* **2014**, *27*, 2185–2208. [CrossRef]
45. Krysanova, V.; Arnold, J.G. Advances in ecohydrological modelling with SWAT—A review. *Hydrol. Sci. J.* **2008**, *53*, 939–947. [CrossRef]
46. Senent-Aparicio, J.; Alcalá, F.J.; Liu, S.; Jimeno-Sáez, P. Coupling SWAT model and CMB method for modeling of high-permeability bedrock basins receiving inter basin groundwater flow. *Water* **2020**, *12*, 657. [CrossRef]
47. Yasir, M.; Hu, T.; Hakeem, S.A. Impending hydrological regime of lhasa river as subjected to hydraulic interventions—a SWAT model manifestation. *Remote Sens.* **2021**, *13*, 1382. [CrossRef]
48. Senent-Aparicio, J.; Liu, S.; Pérez-Sánchez, J.; López-Ballesteros, A.; Jimeno-Sáez, P. Assessing impacts of climate variability and reforestation activities on water resources in the headwaters of the Segura River Basin (SE Spain). *Sustainability* **2018**, *10*, 3277. [CrossRef]
49. Woldesenbet, T.A.; Elagib, N.; Ribbe, L.; Heinrich, J. Hydrological responses to land use/cover changes in the source region of the upper blue Nile Basin, Ethiopia. *Sci. Total Environ.* **2017**, *575*, 724–741. [CrossRef] [PubMed]
50. Yang, L.; Feng, Q.; Yin, Z.; Wen, X.; Si, J.; Li, C.; Deo, R. Identifying separate impacts of climate and land use/cover change on hydrological processes in upper stream of Heihe River, Northwest China. *Hydrol. Process.* **2017**, *31*, 1100–1112. [CrossRef]
51. López-Ballesteros, A.; Senent-Aparicio, J.; Martínez, C.; Pérez-Sánchez, J. Assessment of future hydrologic alteration due to climate change in the Aracthos River basin (NW Greece). *Sci. Total. Environ.* **2020**, *733*, 139299. [CrossRef] [PubMed]
52. Senent-Aparicio, J.; Pérez-Sánchez, J.; Carrillo-García, J.; Soto, J. Using SWAT and Fuzzy TOPSIS to assess the impact of climate change in the headwaters of the Segura River Basin (SE Spain). *Water* **2017**, *9*, 149. [CrossRef]
53. Aznarez, C.; Jimeno-Sáez, P.; López-Ballesteros, A.; Pacheco, J.; Senent-Aparicio, J. Analysing the impact of climate change on hydrological ecosystem services in Laguna del Sauce (Uruguay) using the SWAT model and remote sensing data. *Remote Sens.* **2021**, *13*, 2014. [CrossRef]
54. Dile, Y.T.; Daggupati, P.; George, C.; Srinivasan, R.; Arnold, J. Introducing a new open source GIS user interface for the SWAT model. *Environ. Model. Softw.* **2016**, *85*, 129–138. [CrossRef]
55. Neitsch, S.L.; Arnold, J.G.; Kiniry, J.R.; Williams, J.R. *Soil and Water Assessment Tool Theoretical Documentation Version 2009*; Texas Water Resources Institute: College Station, TX, USA, 2011.
56. Hargreaves, G.H. Defining and using reference evapotranspiration. *J. Irrig. Drain. Eng.* **1994**, *120*, 1132–1139. [CrossRef]
57. Abbaspour, K.C. *User Manual for SWAT-Cup, SWAT Calibration and Uncertainty Analysis Programs*; Swiss Federal Institute of Aquatic Science and Technology, Eawag: Duebendorf, Switzerland, 2007.
58. Le, M.-H.; Lakshmi, V.; Bolten, J.; Du Bui, D. Adequacy of satellite-derived precipitation estimate for hydrological modeling in Vietnam Basins. *J. Hydrol.* **2020**, *586*, 124820. [CrossRef]
59. Jiang, S.; Ren, L.; Xu, C.-Y.; Yong, B.; Yuan, F.; Liu, Y.; Yang, X.; Zeng, X. Statistical and hydrological evaluation of the latest Integrated Multi-satellitE Retrievals for GPM (IMERG) over a midlatitude humid basin in South China. *Atmos. Res.* **2018**, *214*, 418–429. [CrossRef]
60. Jimeno-Sáez, P.; Senent-Aparicio, J.; Pérez-Sánchez, J.; Pulido-Velazquez, D. A comparison of SWAT and ANN models for daily runoff simulation in different climatic zones of Peninsular Spain. *Water* **2018**, *10*, 192. [CrossRef]
61. Moriasi, D.N.; Arnold, J.G.; Van Liew, M.W.; Bingner, R.L.; Harmel, R.D.; Veith, T.L. Model evaluation guidelines for systematic quantification of accuracy in watershed simulations. *Trans. ASABE* **2007**, *50*, 885–900. [CrossRef]
62. Brighenti, T.M.; Bonumá, N.B.; Grison, F.; Mota, A.D.A.; Kobiyama, M.; Chaffe, P.L.B. Two calibration methods for modeling streamflow and suspended sediment with the SWAT model. *Ecol. Eng.* **2019**, *127*, 103–113. [CrossRef]
63. Tian, Y.; Peters-Lidard, C.D.; Choudhury, B.J.; Garcia, M. Multitemporal Analysis of TRMM-based satellite precipitation products for land data assimilation applications. *J. Hydrometeorol.* **2007**, *8*, 1165–1183. [CrossRef]
64. Magaña, V.; Amador, J.A.; Medina, S. The midsummer drought over Mexico and Central America. *J. Clim.* **1999**, *12*, 1577–1588. [CrossRef]
65. Peterson, J.R.; Hamlett, J.M. Hydrologic calibration of the SWAT model in a watershed containing fragipan soils. *JAWRA J. Am. Water Resour. Assoc.* **1998**, *34*, 531–544. [CrossRef]
66. Abbaspour, K.C.; Yang, J.; Maximov, I.; Siber, R.; Bogner, K.; Mieleitner, J.; Zobrist, J.; Srinivasan, R. Modelling hydrology and water quality in the pre-alpine/alpine Thur watershed using SWAT. *J. Hydrol.* **2007**, *333*, 413–430. [CrossRef]
67. Arnold, J.; Muttiah, R.; Srinivasan, R.; Allen, P. Regional estimation of base flow and groundwater recharge in the Upper Mississippi river basin. *J. Hydrol.* **2000**, *227*, 21–40. [CrossRef]
68. Marin, M.; Clinciu, I.; Tudose, N.C.; Ungurean, C.; Adorjani, A.; Mihalache, A.L.; Davidescu, A.A.; Davidescu, Ș.O.; Dinca, L.; Cacovean, H. Assessing the vulnerability of water resources in the context of climate changes in a small forested watershed using SWAT: A review. *Environ. Res.* **2020**, *184*, 109330. [CrossRef] [PubMed]
69. da Silva, R.M.; Dantas, J.C.; Beltrão, J.D.A.; Santos, C.A.G. Hydrological simulation in a tropical humid basin in the Cerrado biome using the SWAT model. *Hydrol. Res.* **2018**, *49*, 908–923. [CrossRef]

70. Sánchez-Murillo, R.; Esquivel-Hernández, G.; Corrales-Salazar, L.; Castro-Chacón, L.; Durán-Quesada, A.; Guerrero-Hernández, M.; Delgado, V.; Barberena, J.; Montenegro-Rayo, K.; Calderón, H.; et al. Tracer hydrology of the data-scarce and heterogeneous Central American Isthmus. *Hydrol. Process.* **2020**, 2660–2675. [CrossRef]
71. Jang, W.S.; Engel, B.; Ryu, J. Efficient flow calibration method for accurate estimation of baseflow using a watershed scale hydrological model (SWAT). *Ecol. Eng.* **2018**, *125*, 50–67. [CrossRef]
72. Eini, M.R.; Javadi, S.; Delavar, M.; Monteiro, J.; Darand, M. High accuracy of precipitation reanalyses resulted in good river discharge simulations in a semi-arid basin. *Ecol. Eng.* **2019**, *131*, 107–119. [CrossRef]

IV.3 PUBLICACIÓN 3: IMPACT ASSESSMENT OF GRIDDED PRECIPITATION PRODUCTS ON STREAMFLOW SIMULATIONS OVER A POORLY GAUGED BASIN IN EL SALVADOR

Jimeno-Sáez, P.; Blanco-Gómez, P.; Pérez-Sánchez, J.; Cecilia, J.M. and Senent-Aparicio, J. Impact Assessment of Gridded Precipitation Products on Streamflow Simulations over a Poorly Gauged Basin in El Salvador. Water 2021, 13, 2497.

https://doi.org/10.3390/w13182497

water

MDPI

Article

Impact Assessment of Gridded Precipitation Products on Streamflow Simulations over a Poorly Gauged Basin in El Salvador

Patricia Jimeno-Sáez [1,*], Pablo Blanco-Gómez [1], Julio Pérez-Sánchez [1,2], José M. Cecilia [3] and Javier Senent-Aparicio [1]

[1] Department of Civil Engineering, Universidad Católica San Antonio de Murcia, Campus de Los Jerónimos s/n, 30107 Murcia, Spain; pblanco4@alu.ucam.edu (P.B.-G.); jperez058@ucam.edu or julio.sanchez@ulpgc.es (J.P.-S.); jsenent@ucam.edu (J.S.-A.)
[2] Department of Civil Engineering, Universidad de Las Palmas de Gran Canaria, Campus de Tafira, 35017 Las Palmas de Gran Canaria, Spain
[3] Department of Computer Engineering (DISCA), Universitat Politécnica de Valencia (UPV), 46022 Valencia, Spain; jmcecilia@disca.upv.es
* Correspondence: pjimeno@ucam.edu

Abstract: In this study, five open access gridded precipitation (GP) products (CFSR, MSWEPv1.1, PERSIANN-CDR, CMORPH, and CHIRPSv2.0) and local climate data were evaluated over the Grande de San Miguel (GSM) River Basin in El Salvador. The main purpose was to identify optional data sources of precipitation for hydrological modelling given that ground-based precipitation gauges in El Salvador are scarce and their data includes important temporal and spatial gaps. Firstly, a direct comparison was made between the precipitation data from the five GP products and from the rain gauges. Secondly, the SWAT model was used to simulate the streamflow regimen based on the precipitation datasets. The analysis of results showed that the models produced correct predictions, and the accuracy increased as models were calibrated to each specific precipitation product. Overall, PERSIANN-CDR produced the best simulation results, including streamflow predictions in the GSM basin, and outperformed other GP products and also the results obtained from data precipitation gauges. The findings of this research support the hydrological modelling based on open-access GP products, particularly when the data from precipitation gauges are scarce and poor.

Keywords: gridded precipitation products; data-scarce regions; hydrological modelling; SWAT; streamflow; El Salvador

Citation: Jimeno-Sáez, P.; Blanco-Gómez, P.; Pérez-Sánchez, J.; Cecilia, J.M.; Senent-Aparicio, J. Impact Assessment of Gridded Precipitation Products on Streamflow Simulations over a Poorly Gauged Basin in El Salvador. *Water* **2021**, *13*, 2497. https://doi.org/10.3390/w13182497

Academic Editor: Momcilo Markus

Received: 16 July 2021
Accepted: 8 September 2021
Published: 11 September 2021

1. Introduction

Precipitation is a vital input in the numerical simulation of the hydrological responses in a river basin. A precise reproduction of the spatiotemporal variability of precipitation is crucial to accurately simulate hydrological processes. However, the limited availability of observed hydro-meteorological data often hinders streamflow modelling efforts, particularly in developing countries and in remote areas where measured data are unavailable or non-existent. Even when measured data exist, their quality can be very poor and free access to them may be limited due to a strict data transfer policy [1].

The traditional method of obtaining spatial precipitation data is through ground observations from a network of rain gauges. However, in poorly monitored areas, data interpolation is necessary and may produce uncertainty [2] and even significant mismatches between actual and estimated precipitation [3]. Furthermore, rain gauges are not always accurate devices for measuring real precipitation. Specifically, disparities between the measurements and real values of precipitation may be caused by the effects of wind above the gauge orifice, flaws in the rain gauge installation, losses by wetting and evaporation on the inside walls of the rain gauge, and other random and systematic errors [4,5]. Therefore,

there is an evident need to enhance data collection and/or explore more accurate alternatives to ground-based data from rain gauges. One useful alternative source of data for poorly gauged and/or ungauged basins is the global gridded precipitation (GP) products that provide continuous precipitation with extensive spatial coverage and much finer spatial resolutions than terrestrial rain gauges [6].

Several GP data are operationally available and provide precipitation maps with different ranges of spatial resolutions (from 0.05° × 0.05° to 1° × 1°) and time scales (hourly, daily, and monthly). The following are some of the most widely used products based on satellite data in the hydrology field: Multi-Source Weighted-Ensemble Precipitation (MSWEP) [7], Precipitation Estimate from Remotely Sensed Information using Artificial Neural Networks-Climate Data Records (PERSIANN-CDR) [8], National Oceanic and Atmospheric Administration Climate Prediction Center morphing technique product (CMORPH) [9] and the Climate Hazards group Infrared Precipitation with Stations dataset (CHIRPS) [10]. Other gridded meteorological products that have been widely used in hydrological modelling include global reanalysis data, such as the Climate Prediction System Reanalysis (CFSR) [11].

The values of the precipitation grids may be subjected to various sources of error including atmospheric effects that change the radiation field, limited correlation between remote sensing signals and precipitation rates or gaps [12]. Therefore, exhaustive validation is required, and in this sense numerous studies of precipitation grids have been conducted to improve its use. Furthermore, efforts to deepen the knowledge on their uncertainties have been carried out over different regions, increasing the accuracy of hydrological modelling using these precipitation data products. The validation of GP products can be conducted in two ways: by directly comparing the data with gauge rainfall [3,13–17] and by analyzing their ability to reproduce observed streamflow using hydrologic models [3,15,17].

The Soil and Water Assessment Tool (SWAT) model [18] is one of the most popular models used at the basin scale. SWAT has been widely applied in numerous studies around the world to resolve several processes, such as water balance, climate and land-use changes, agricultural pollution from nonpoint sources, and land management [19–24]. Recent SWAT studies [1,17,25,26] showed a growing trend towards the use of alternatives to rain gauge networks. The calibration of hydrological models is subject to the type of precipitation data source. In previous research conducted in a different area of El Salvador [27], good statistics were obtained in the SWAT hydrological model using CHIRPS as input. Many previous studies [28,29] calibrated SWAT parameters with the monitored rainfall, and they subsequently executed simulations with GP using these parameter values without any additional calibration. However, if the observed data are not reliable, then the calibrated model will be inaccurate. Other studies [25,30–32] considered the impact on the calibration of each data source and the sensitivity of the associated parameters by calibrating the SWAT model with each different precipitation source. However, the parameters forced on each set of data may hide data errors. Notwithstanding, very few studies have used both methodologies to validate the different precipitation products [33,34].

Despite the numerous studies around the world, knowledge about the abilities and limitations of GP products in Latin America, a region where the scarcity of weather stations is the norm, remains scarce and limited. Dinku et al. [14] found that the GP products were poor at estimating the amount of daily precipitation but good at detecting the occurrence of precipitation events over Colombia, with relatively good performance for CMORPH and a low performance using PERSIANN and TRMM 3B42RT. Blacutt et al. [35] assessed two reanalysis datasets (Modern-Era Retrospective Analysis for Research and Applications (MERRA) [36] and CFSR), a satellite product (TRMM3B42) [37], and a combined product (CoSch), which successfully eliminates satellite bias, in four areas of Bolivia.. Melo et al. [38] found a low performance of TRMM 3B42v6 and 3B42v7 in daily and seasonal analysis over Brazil. Zambrano-Bigiarini et al. [39] evaluated seven satellite products for the Chilean territory and found that CHIRPSv2.0, TRMM 3B42v7, and MSWEPv1.1 provided relatively good results. Baez-Villanueva et al. [13] evaluated six satellite-based rainfall

datasets (TRMM 3B42v7, TRMM 3B42RT, CHIRPSv2.0, CMORPH, PERSIANN-CDR, and MSWEPv2) over three different basins in Latin America (Colombia, Chile, and Brazil), and they showed that for the basin in Brazil, MSWEPv2 offered the best performance, while CHIRPSv2.0 performed the best for the basin in Colombia, and MSWEPv2 and CHIRPSv2.0 performed the best in Chile. Even fewer studies in Latin America evaluate the ability of different GP products to reproduce the observed streamflow. Oliveira et al. [40] used rainfall data from TRMM3B42V6 and V7 to evaluate the water balance of a Brazilian region, and they found that the precipitation from 3B42V7 provided a lower overestimate of stream discharge compared to the 3B42V6 dataset. However, the use of alternative climate products for hydrological purposes is widespread worldwide [41], such as in data-scarce countries in Asia [17,42–44] or Africa [1,26,31,45,46].

This study provides an overview of the quality of different sources of precipitation for hydrological applications in a poorly gauged Central American basin. In addition to evaluating the replication of the streamflow regimen, a direct comparison was made between the precipitation data from the five GP products and the precipitation data from the rain gauges. This will also contribute to contrasting not only the disparities between ground-based data and GP products, but also the resulting water balances and the quality and accuracy of the precipitation data products studied. Specifically, the goals of this study are (1) to assess the spatiotemporal performance of five high-resolution precipitation products and compare them with monitored precipitation data in a tropical climate basin in El Salvador at different time scales, and (2) to assess the ability of these precipitation datasets to simulate monthly observed streamflow in SWAT using two calibration strategies: (a) calibrating with data from the observed precipitation and then running the simulations using the GP, and (b) calibrating the SWAT parameters with each of the precipitation sources.

2. Materials and Methods

The methodology used for this comparative study of the different sources of precipitation is shown below and summarized in Figure 1, as described previously.

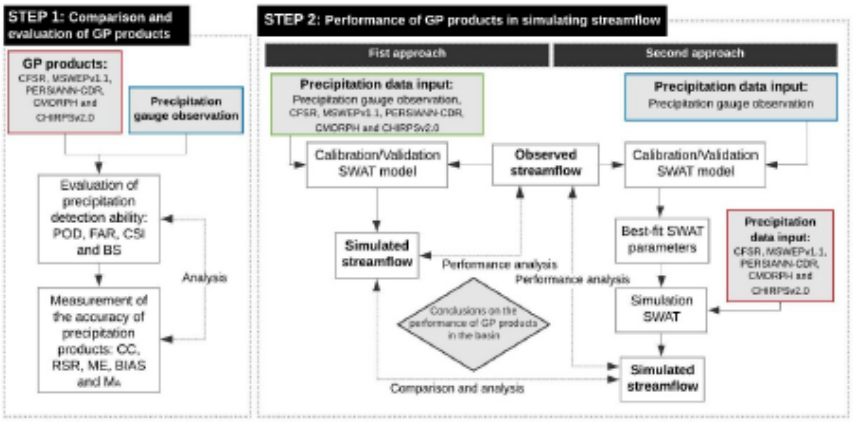

Figure 1. Flowchart for comparative study.

2.1. Study Area

The GSM River Basin is located in eastern El Salvador and covers an area of 2377 km^2 up to the outlet control point (Figure 2). This basin is one of the most important and largest river basins in El Salvador. The city of San Miguel is located at its centre and is considered demographically to be the second most important city in El Salvador. The GSM River Basin is regarded as a priority area (PA) within the National Plan of Integrated Water Resources

Management of El Salvador [47]. Each PA is the object of special measures regarding water resource management due to the hydrological problems identified. Specifically, the major problems in the GSM River Basin are the pollution of surface water and the high irrigation water demand, creating substantial stress on water resources [47]. An accurate understanding of the hydrological processes at the basin scale is necessary to propose efficient management strategies to minimize the effect of these stress factors. Furthermore, the city of San Miguel has attracted environmental interest in terms of international protection figures, such as the Tepaca-San Miguel and Jiquilisco Bay conservation areas. Tecapa-San Miguel is characterized by shade-grown coffee plantations, an abundance of coastal plain wetlands, and volcanic craters, including multiple protected areas such as the San Miguel Volcano and the El Jocotal and Olomega lagoons, both of which are part of the Ramsar List of the Convention of Wetlands. The Jiquilisco Bay located in the mouth of the Grande de San Miguel River has been recognized as a Ramsar site since 2005 and as a UNESCO biosphere reserve since 2007.

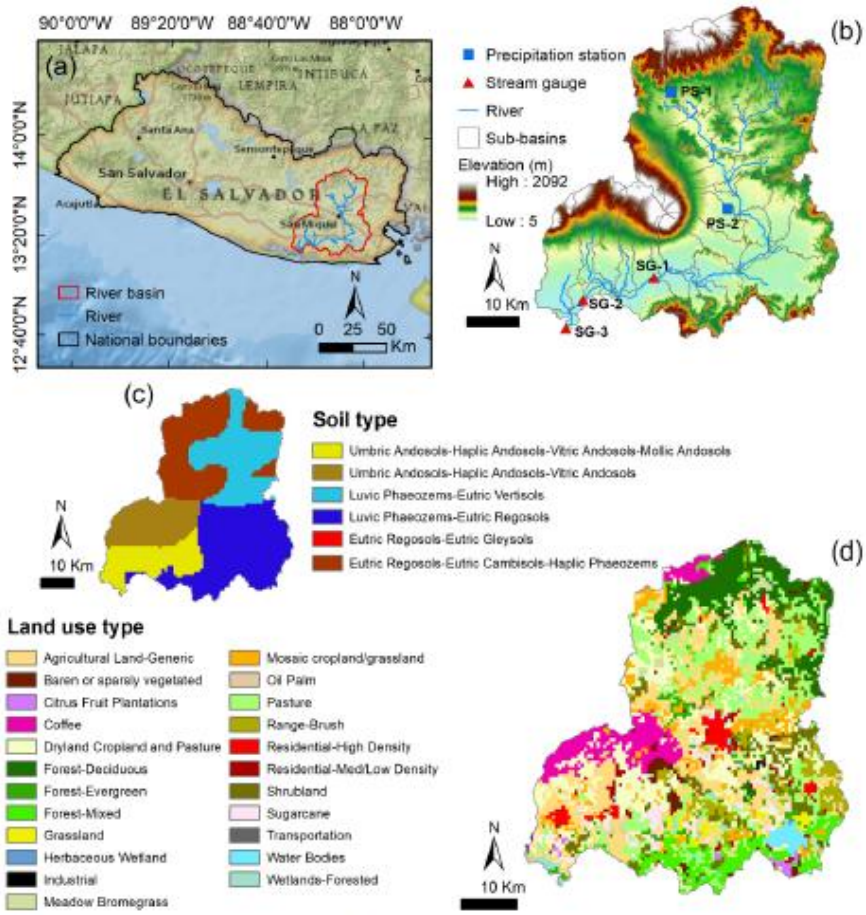

Figure 2. (a) Location of GSM River Basin in El Salvador; (b) topography of the basin and location of hydro-meteorological stations; (c) soil map of the basin and (d) land use map of the basin.

While the region has a tropical climate with high annual rates of precipitation, the intra-annual distribution is uneven. Specifically, 90% of the precipitation falls during the wet season between May and October, and only scattered showers occur during the dry season between November and April [27,48]. According to observations of the weather stations and the GP analysed, the mean annual precipitation is around 1700–2000 mm, which is consistent with previous studies [48]. The wettest months are August and September, with average monthly rainfall values of 290 and 298 mm. January and February have the lowest rainfall, with an average monthly rainfall of 2 mm. The average annual temperature in the basin is 28 °C, with maximum and minimum values of 33 and 22 °C, respectively. The dominant soil groups in the region are classified as andosols, phaeozems, and regosols (Figure 2c). The andosols that cover the area associated with the San Miguel volcano are volcanic soils and have favourable properties for agriculture [49]. The dominant soil types at the northern boundaries are regosols, unconsolidated materials with fine granulometry common in mountainous areas, whilst throughout the eastern part of the basin, phaeozem soils are abundant and accommodate wet grasslands and forest regions as they are characteristically porous, fertile, and excellent agricultural land [50]. Regarding the basin hydrogeology, previous studies [51] indicate high permeability, fissure flows and a faster recharge response [52]. The main land-use types are grassland and pasture (43%), cropland (32%), and forest (17%). The land use map of the basin shown in Figure 2d is based on RapidEye imagery satellite at 5 m spatial resolution [53].

2.2. Precipitation Datasets

In this study, six datasets were selected. Table 1 summarizes the list of precipitation products used, their spatial and temporal resolution, their available period, and their spatial coverage. These precipitation datasets can be grouped into three categories: (1) one observed precipitation dataset from ground precipitation gauges located within the GSM River Basin; (2) one reanalysis gridded product (CFSR); and (3) four gridded satellite-based precipitation datasets (MSWEPv1.1, PERSIANN-CDR, CMORPH, and CHIRPSv2.0).

Table 1. List of precipitation datasets used.

Product	Spatial Resolution	Time-Step	Available Period	Spatial Coverage
Gauge observation	Point	Daily	2005–2010	Study area
CFSR	0.30° × 0.30° (~38 km)	Daily	1979–2014	Global
MSWEPv1.1	0.25° × 0.25° (~30 km)	Daily	1979–2015	Global
PERSIANN-CDR	0.25° × 0.25° (~30 km)	Daily	1983–present	Latitude band 60° N-S
CMORPH	0.25° × 0.25° (~30 km)	Daily	1998–present	Latitude band 60° N-S
CHIRPSv2.0	0.05° × 0.05° (~5.3 km)	Daily	1981–present	Latitude band 50° N-S

After intensive analyses of measured precipitation data, two stations within the basin (PS-1 and PS-2 in Figure 2b) were selected from six existing stations in the area for the study period (2005–2010). Four stations were excluded following the Tan and Yang [54] criterion for tropical basins, which states that rainfall gauges with more than 20% missing data would significantly affect streamflow simulation. The missing values in PS-1 and PS-2 were 16% and 8%, respectively. The hydrological model filled the missing weather data automatically using SWAT's built-in weather generator. The gaps and scarcity of data in this country, as mentioned in a previous study [27], was the main driver for this research to explore the potential of open access alternative precipitation data. Details on the GP products are available in the Supplementary Material.

2.3. Precipitation Comparison

Daily precipitation information was extracted from the grid cells that contained the gauge observation stations, and the days without observed data were excluded from the gridded data in the comparative study. We evaluated the closest grid cell of each GP

product to the respective rain gauge. It is to be noted that this is a limitation of the study, as the different resolution of the GP products penalises the coarser datasets and may bias the assessment. The period from 2005 to 2010 was selected to assess the accuracy of the precipitation datasets.

The ability to detect the occurrence of rainfall events of each precipitation product was assessed by using four categorical indexes: (1) the probability of detection (POD); (2) false alarm ratio (FAR); (3) critical success index (CSI); and (4) bias score (BS). The POD provides the capability of precipitation products to accurately capture the actual precipitation occurrence. FAR assesses the fraction of false alarms detected by the products of precipitation. The ability of the data to comprehensively detect true precipitation events is measured by CSI. CSI is an accurate and balanced detection metric and is based on POD and FAR. BS is the ratio of the estimated to observed rain. Five quantitative performance metrics were employed to measure the accuracy of the precipitation datasets in terms of the amount of rain and time dynamics (three time scales: day, month, and year): (1) correlation coefficient (CC); (2) RMSE-observations standard deviation ratio (RSR); (3) mean error (ME); (4) relative bias (BIAS); and (5) annual mean precipitation (M_A). The CC explains the degree of linear correlation between gauge observations and GP products. RSR incorporates the benefits of error index statistics and includes a normalization factor. ME provides an assessment of the bias in the estimates, while BIAS indicates the degree to which the observed value is overestimated or underestimated as a percentage. The formulae and optimal values for each precipitation performance metric are presented in Table 2.

Table 2. Precipitation performance metrics.

Statistic	Equation [1]	Unit	Optimal Value
POD	$\frac{N_{11}}{N_{11}+N_{01}}$	-	1
FAR	$\frac{N_{10}}{N_{11}+N_{10}}$	-	0
CSI	$\frac{N_{11}}{N_{11}+N_{01}+N_{10}}$	-	1
BS	$\frac{N_{11}+N_{10}}{N_{11}+N_{01}}$	-	1
CC	$\frac{\sum_{i=1}^{n}(O_i-\overline{O})(G_i-\overline{G})}{\sqrt{\sum_{i=1}^{n}(O_i-\overline{O})^2}\cdot\sqrt{\sum_{i=1}^{n}(G_i-\overline{G})^2}}$	-	1
RSR	$\frac{\sqrt{\sum_{i=1}^{n}(O_i-G_i)^2}}{\sqrt{\sum_{i=1}^{n}(O_i-\overline{O})^2}}$	-	0
ME	$\frac{\sum_{i=1}^{n}(G_i-O_i)}{n}$	mm	0
BIAS	$\frac{\sum_{i=1}^{n}(G_i-O_i)}{\sum_{i=1}^{n}O_i}\cdot 100$	%	0

[1] Note: N_{11} represents the observed precipitation that was correctly detected; N_{01} is the observed precipitation not detected; N_{10} is the precipitation detected but not observed; O_i and G_i are observed and GP; i is the index of data and n is the total number of measurements; $\overline{O}$ and $\overline{G}$ is the mean value of observed and GP.

Additionally, the cumulative density function (CDF) of the daily precipitation distribution was computed for the six datasets. The cumulative frequency was evaluated based on the precipitation event classification of the World Meteorological Organization (WMO) standard [55] as presented in Table 3.

Table 3. Precipitation event classification based on daily rainfall intensity.

Type of Event	Daily Rainfall Intensity (mm/Day)
Tiny rain	<1
Light rain	[1, 2)
Low modeerate rain	[2, 5)
High moderate rain	[5, 10)
Heavy rain	[10, 50)
Violent rain	≥50

2.4. Precipitation Performance in Simulating Streamflow

Since the results presented in the previous section were sensitive to the quality of the observed data (which was questionable and of poor quality in this study area), a second analysis was performed based on the simulation of streamflow.

In this study, the SWAT hydrological model was used to assess the reliability of precipitation products in predicting the observed streamflow. The model assessed how the different precipitation sources might affect the model calibrations and its performance and the hydrological coherence of precipitation datasets with hydrological observations.

2.4.1. SWAT Hydrological Model

SWAT is a physically based hydrological model that operates on a watershed scale in a semi-distributed way and simulates the main components of the water balance continuously on a daily scale [18]. SWAT divides river basins into sub-basins according to topography and the network of rivers; subsequently, sub-basins are subdivided into hydrologic response units (HRUs). HRUs group land areas with unique combinations of land use, soil, and slope, describing the spatial heterogeneity within a watershed [56]. SWAT simulates the hydrological cycle by calculating the runoff of each HRU individually and then aggregating it to the sub-basin level based on the water balance.

2.4.2. Model Set-Up and Sensitivity Analysis

The open-source QSWAT version 2012 [56], a QGIS interface for SWAT, was employed to construct a model of the GSM River Basin. Multiple datasets were needed to model, calibrate and validate the SWAT model, including daily climatic data (precipitation, maximum and minimum air temperature), geographic information (digital elevation model (DEM), soil properties, and land use/land cover data (LULC)), and hydrological datasets. The six selected sources of precipitation are described in the previous section. The SWAT model distributes the meteorological data to the sub-basins using the data from a single station or cell data that are closest to the centroid of each sub-basin [57]. Figure 3 presents the spatial resolution of the GP products with the centroids of the sub-basins of the SWAT model. Due to the scarcity of measured data in this region, daily temperature records were derived from the CFSR dataset. The topography of the basin was defined from the DEM to delineate the basin boundary, determine the stream network, and establish sub-basins. The DEM (Figure 2b) used in this study had a resolution of 30 m and was downloaded from the Advanced Spaceborne Thermal Emission and Reflection Radiometer Global Digital Elevation Model version 2 (ASTER GDEM v2) by NASA (https://asterweb.jpl.nasa.gov/gdem.asp (accessed on 5 May 2021)). The soil and LULC data were important to define the HRUs. Soil data (Figure 2c) were taken from the Harmonized World Soil Database (HWSD) and can be downloaded from http://www.fao.org/land-water/databases-and-software/hwsd/en/ (accessed on 5 May 2021). The LULC map (Figure 2d) and observed discharges were acquired from the Ministry for the Environment and Natural Resources of El Salvador (MARN). Using these data, the GSM River Basin was divided into 41 sub-basins (Figure 2b) and 579 HRU. The data of the monthly observed discharges are available from 1970 to 2012 in three hydrological stations (SG-1, SG-2, and SG-3), the locations of which are shown in Figure 2b. The Hargreaves method [58] was used to calculate the potential evapotranspiration using maximum and minimum daily air temperatures as input data. The curve number (CN) method of the Soil Conservation Service (SCS) [59] was used to compute the surface runoff and infiltration for each HRU using daily precipitation. After rigorous analysis of the observed data, the period 2005 to 2010 was selected, for which all the necessary data for SWAT calibration and validation were available. A two-year period was used to warm up the model.

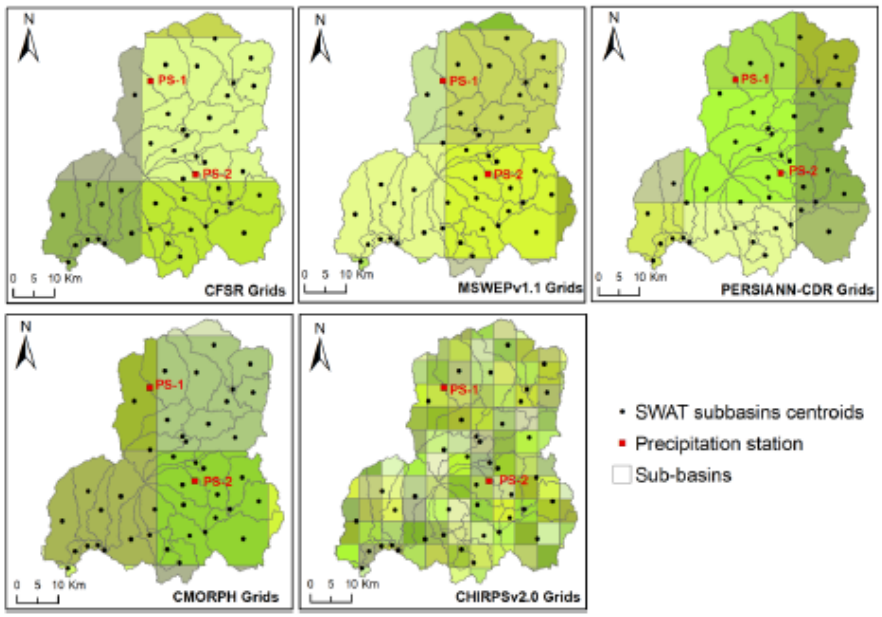

Figure 3. Precipitation grids with the sub-basin centroids.

2.4.3. Model Calibration and Validation

The performance of SWAT models was assessed for each GP product with two different strategies to consider the effect of each data source on the process of calibration and sensitivity of the associated parameters. The first approach entailed the calibration of the SWAT model using gauge observations, and then the best-fitted parameters found were used with each GP product as input without additional calibration. The second approach was the calibration and validation of the SWAT model using each of the different precipitation sources (Figure 1).

The calibration of models was performed using the SUFI-2 algorithm [60] in the SWAT-CUP software [61]. The models were calibrated from 2005 to 2007 and validated for the 2008 to 2010 period. According to the recommendations of Arnold et al. [62], the period of calibration and validation contained both dry and wet periods to ensure that they reflected the range of conditions under which the model was expected to operate. Based on the authors' previous experience and the available literature [27,28], some sensitive hydrological parameters in the simulation of streamflow, and which incorporated aspects of soil, groundwater, and surface water, were selected. Firstly, 500 model runs with the gauge observation precipitation dataset were conducted and the least sensitive parameters were excluded. Thereafter, two iterations of 1000 simulations were executed with the 16 most sensitive parameters (Table 4), using the corresponding precipitation dataset as input, and adjusting the range of parameters in the second iteration. The same 16 parameters were used to calibrate all SWAT models, using the same initial range (Table 4) for each of them to allow a correct comparison and starting point.

The parameters were calibrated by comparing simulated streamflow with monitored streamflow in the three stream gauges (Figure 2b), and the Nash-Sutcliffe Efficiency (NSE) [63] was used as the objective function. Four model performance metrics defined in Table 5 were calculated to assess the performance of monthly streamflow simulation for each SWAT model following the criteria and performance ratings suggested by Moriasi et al. [64].

Table 4. SWAT calibration parameters.

Type	Parameter [1]	Description	Initial Range
Management	r_CN2	SCS runoff curve number	[−0.2, 0.2]
Groundwater	v_ALPHA_BF	Baseflow alpha factor (days−1)	[0, 1]
Groundwater	v_GWQMN	Threshold depth of water in the shallow aquifer for return flow to occur (mm)	[0, 5000]
Groundwater	v_GW_REVAP	Groundwater "revap" coefficient	[0.02, 0.20]
Groundwater	v_RCHRG_DP	Deep aquifer percolation fraction	[0, 1]
Groundwater	v_SHALLST	Initial depth of water in the shallow aquifer (mm)	[0, 1500]
HRU	v_CANMX	Maximum canopy storage (mm)	[0, 50]
HRU	r_SLSUBBSN	Average slope length	[−0.5, 0.5]
HRU	r_HRU_SLP	Average slope steepness	[−0.5, 0.5]
Basin	v_ESCO	Soil evaporation compensation factor	[0.1, 1]
Basin	v_SURLAG	Surface runoff lag time	[0.05, 24]
Routing	v_CH_N2	Manning's "n" value for the main channel	[−0.01, 0.3]
Routing	v_CH_K2	Effective hydraulic conductivity in main channel alluvium	[0.01, 150]
Soil	r_SOL_AWC	Available water capacity of the soil layer (mm H_2O/mm soil)	[−0.3, 0.3]
Soil	r_SOL_BD	Moist bulk density	[−0.3, 0.3]
Soil	r_SOL_Z	Depth from soil surface to bottom of layer	[−0.3, 0.3]

[1] r_ denotes the relative change (the current value must be multiplied by 1 + the value obtained in calibration), and v_ indicates that the existing value is replaced by the value obtained in the calibration.

Table 5. Model performance metrics.

Performance Metric	Equation [1]	Range
Coefficient of determination (R^2)	$\left[\frac{\sum_{i=1}^{n}(O_i-\overline{O})\cdot(S_i-\overline{S})}{\left[\sum_{i=1}^{n}(O_i-\overline{O})^2\right]^{0.5}\cdot\left[\sum_{i=1}^{n}(S_i-\overline{S})^2\right]^{0.5}}\right]^2$	[0, 1]
Nash-Sutcliffe Efficiency (NSE)	$1-\frac{\sum_{i=1}^{n}(O_i-S_i)^2}{\sum_{i=1}^{n}(O_i-\overline{O})^2}$	[−∞, 1]
Percent bias (PBIAS)	$\frac{\sum_{i=1}^{n}(O_i-S_i)\cdot 100}{\sum_{i=1}^{n}(O_i)}$	[−∞, ∞]
RMSE-observations standard deviation ratio (RSR)	$\frac{\sqrt{\sum_{i=1}^{n}(O_i-S_i)^2}}{\sqrt{\sum_{i=1}^{n}(O_i-\overline{O})^2}}$	[0, ∞]

[1] O_i is the ith observed streamflow value, $\overline{O}$ is the mean of the observed data, S_i is the ith simulated streamflow value, $\overline{O}$ is the mean of the observed data and n is the total number of observations.

3. Results and Discussion

3.1. Comparison and Evaluation of GP Products

Regarding precipitation detection ability assessment, Table 6 provides precipitation detection metrics (POD, FAR, CSI, and BS) for each GP product computed using a 1 mm/day threshold.

Table 6. Precipitation detection metrics based on comparison with gauge observation at PS-1 station and at PS-2 station.

Precipitation Dataset	PS-1 Station				PS-2 Station			
	POD	FAR	CSI	BS	POD	FAR	CSI	BS
CFSR	0.78	0.40	0.51	1.31	0.79	0.48	0.46	1.53
MSWEPv1.1	0.93	0.41	0.57	1.57	0.91	0.46	0.51	1.69
PERSIANN-CDR	0.93	0.41	0.57	1.58	0.92	0.47	0.51	1.74
CMORPH	0.80	0.31	0.59	1.16	0.79	0.30	0.59	1.13
CHIRPSv2.0	0.81	0.27	0.62	1.11	0.79	0.35	0.55	1.22

POD values for all GP products were higher than 0.78. MSWEPv1.1 and PERSIANN-CDR demonstrated the highest POD values due to their high number of rainy days against the monitored data (Table 6). In the case of FAR, the values range from 0.27 to 0.48.

CHIRPSv2.0 and CMORPH precipitation data provided lower values of FAR. CSI values showed a range of 0.51 to 0.62 for the PS-1 station and 0.46 to 0.59 for the PS-2 station. As shown in Table 7, these low CSI values were obtained due to the high number of rainy days detected by all GP products compared to the observed data.

Table 7. Total number of days in which precipitation exceeds 1 (PD1) or 10 (PD10) mm in the period of study (2005–2010).

Precipitation Dataset	PS-1 Station		PS-2 Station	
	PD1	PD10	PD1	PD10
Gauge observations	600	339	558	282
CFSR	788	236	854	248
MSWEPv1.1	942	369	944	339
PERSIANN-CDR	946	409	973	424
CMORPH	696	315	628	289
CHIRPSv2.0	666	439	678	409

The BS result, ranging from 1.11 to 1.74, suggests that all GP products overestimate the total number of observed precipitation events. CHIRPSv2.0 and CMORPH showed the best BS values for both stations. When the threshold was adjusted to 10 mm, the detection ability of all GP products for these heavy precipitation events demonstrated better agreement with the observed data. In conclusion, no GP datasets are highlighted for their ability to detect precipitation events in the studied basin.

Table 8 summarizes statistical indices for daily and monthly precipitation products against gauge observation in both stations and the M_A value for each precipitation dataset.

Table 8. Daily and monthly statistical indices of precipitation products against gauge observation at stations PS-1 and PS-2.

Station/Precipitation Dataset	CC		RSR		ME		BIAS [1]		M_A (mm)
	Daily	Monthly	Daily	Monthly	Daily	Monthly	Daily	Monthly	
PS-1									
Gauge observations	-	-	-	-	-	-	-	-	1833.55
CFSR	0.32	0.84	1.05	0.60	−1.15	−34.64	−19.83	−19.83	1526.50
MSWEPv1.1	0.51	0.82	0.88	0.59	0.11	3.39	1.94	1.94	1867.66
PERSIANN-CDR	0.48	0.83	0.89	0.56	−0.03	−1.09	−0.58	−0.63	1813.24
CMORPH	0.50	0.87	0.96	0.50	−0.03	−0.96	−0.55	−0.55	1805.05
CHIRPSv2.0	0.55	0.89	0.88	0.50	0.50	15.05	8.62	8.62	2058.75
PS-2									
Gauge observations	-		-	-	-	-	-	-	1553.04
CFSR	0.27	0.86	1.10	0.52	−0.25	−5.38	−5.49	−5.38	1537.81
MSWEPv1.1	0.52	0.88	0.90	0.57	0.55	12.26	12.13	12.26	1752.64
PERSIANN-CDR	0.47	0.90	0.91	0.53	0.82	17.98	17.88	17.98	1827.73
CMORPH	0.47	0.84	1.03	0.60	0.02	0.85	0.73	0.85	1588.88
CHIRPSv2.0	0.53	0.94	0.91	0.45	0.61	13.48	13.34	13.48	1847.27

[1] Note: Differences between daily and monthly BIAS are due to gaps in gauge observation datasets. Only months with all daily data available were compared.

Both stations showed daily CC values of approximately 0.5 and demonstrated that CC values of all precipitation datasets improved significantly on a monthly scale. High monthly correlations to observation were obtained, with values in the range of 0.82 to 0.94. The best daily and monthly CC values were found for CHIRPSv2.0 precipitation at both stations. A noticeable difference between the daily and monthly scales was observed for RSR. The monthly RSR values of CHIRPSv2.0 were smaller than for the other GP products in both stations. For the PS-1 station, the best ME and BIAS values were demonstrated by CMORPH (daily ME of -0.03 mm, monthly ME of -0.96 mm, and BIAS of −0.55%), followed by PERSIANN-CDR with similar values (daily ME of −0.03 mm, monthly ME of −1.09 mm, daily BIAS of −0.58% and monthly BIAS of −0.63%). For the PS-2 station,

the CMORPH again demonstrated the best values (daily ME of 0.02 mm, monthly ME of 0.85 mm, daily BIAS of 0.73%, and monthly BIAS of 0.85%). The ME and BIAS values for CFSR and PERSIANN-CDR showed the greatest discrepancies with the observations of the PS-1 station and PS-2 station, respectively. Regarding M_A values, the greatest differences compared to the observed data were obtained by CFSR (−307 mm), followed by CHIRPSv2.0 (+225 mm) for the PS-1 station and by CHIRPSv2.0 (+294 mm) and PERSIANN-CDR (+275 mm) for the PS-2 station. Monthly precipitations were computed from GP datasets and gauge observations to assess inter-annual variability. Figure 4 presents the box plot comparison of monthly precipitation from gauge observations, CFSR, MSWEPv1.1, PERSIANN-CDR, CMORPH, and CHIRPSv2.0 for the selected precipitation stations.

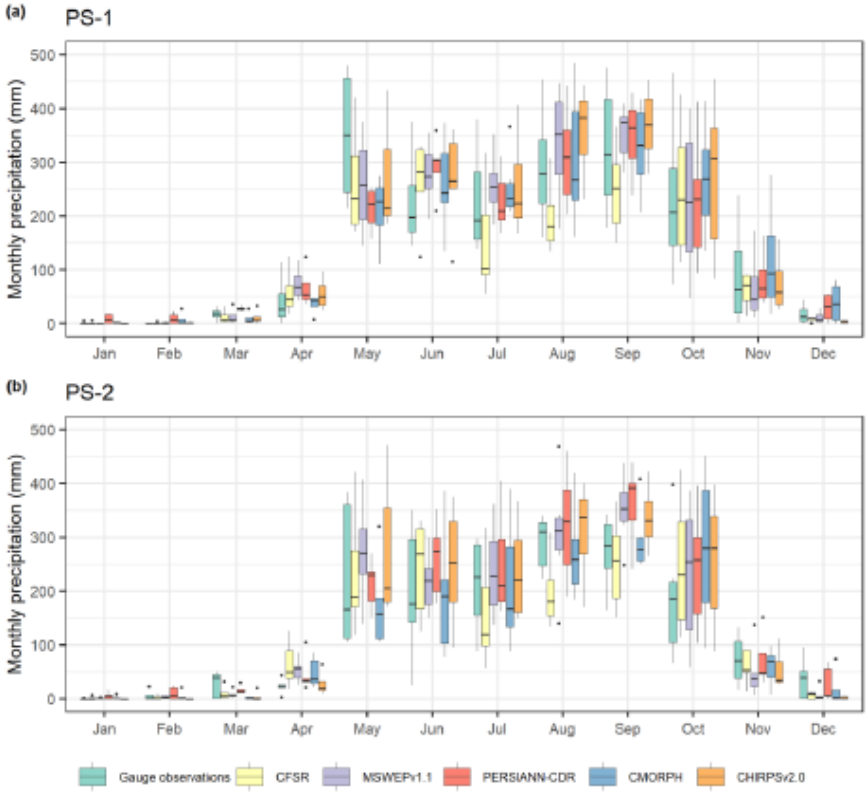

Figure 4. Box plot with the temporal distribution of the monthly precipitation of the gauge observations and of different GP products in (**a**) PS-1 station and (**b**) PS-2 station. Dots denote outliers.

GP products were similar to the gauge observations in both stations, reflecting the inter-annual variation of precipitation with a clearly distinguishable wet period from May to October and a dry period from November to April. Figure 4a,b also show the bimodal distribution of the rainy summer season for most of the precipitation data, with maximum mean values in June and September and a relative minimum in July known as "Mid-Summer Drought" (MSD) [65], which is recognised as one of the most significant modulators of regional climate variability [27]. GP products, except for CFSR, generally overestimate the mean monthly precipitation observed in the wet season.

Figures 5 and 6 show the CDF of daily precipitation in PS1 and PS2, respectively, for the observed values versus the six GP studied. Regarding the probability of dry days (rain = 0 mm), both gauge stations and CHIRPSv2.0 provided a similar probability, of approximately 65%. However, the other five GPs displayed lower probabilities that ranged from 32 to 36% (PS1–PS2, respectively) in the cases of CFSR and MSWEPv1.1 to 48 to 56% (PS1–PS2) for CMORPH, which is an increase in the number of rainy events compared to PS data. In fact, the CDFs in both stations were greater than the GP curves for precipitations below 10–20 mm due to the high percentage of days with no rain in PS1 and PS2. While minimal rain (lower than 1 mm) did not reach 1% in PS1, MSWEPv1.1 and CMORPH exceeded 10% (13.4 % and 12%, respectively), and 20.5% was achieved with CFSR, However, CHIRPSv2.0 did not register minimal rain with either PS1 or PS2. Similar values were provided by GP in PS2, although the registered data in this station exceeded 6%. Differences in light rain (between 1 and 2 mm) were reduced to around 1% between the observed data in both stations and GP, except for CHIRPSv2.0, which rarely showed precipitation of this amount (0.2% and 0.3% in PS1 and PS2, respectively). The disparities between PS and PERSIANN-CDR, CFSR and MSWEPv1.1 were doubled with moderate rain (between 2 and 10 mm), while CHIRPSv2.0 and CMORPH values remained relatively similar to observed data. CMORPH and CFSR reached similar values to PS (16% and 13% for PS1 and PS2, respectively) for heavy rain (between 10 and 50 mm), while the remaining GPs increased observed values at approximately 50%. Violent rain (above 50 mm) was underestimated for all GPs studied, except in the case of MORPH, which halved observed percentages in PS1 and PS2 (18% and 12%, respectively) or even without detecting them, as in the case of PERSIANN-CDR. On the assumption that the observed data in PS1 and PS2 are accurate, GP tended to underestimate extreme events on dry days except for CHIRPSv2.0 and in extremely high rainfall except for MORPH. These percentage differences also resulted in disparities in the remaining event ranges considered. However, GP performance varied substantially depending both on the segment of the amount of rain and the dataset considered. CMORPH appeared to be the best fit GP for precipitation above 1 mm. PERSIANN-CDR, CHIRPSv2.0 and MSWEPv1.1 overestimated precipitation in moderate and heavy rain events. CFSR did not follow a specific pattern with regard to the precipitation event classification, as shown in Table 3.

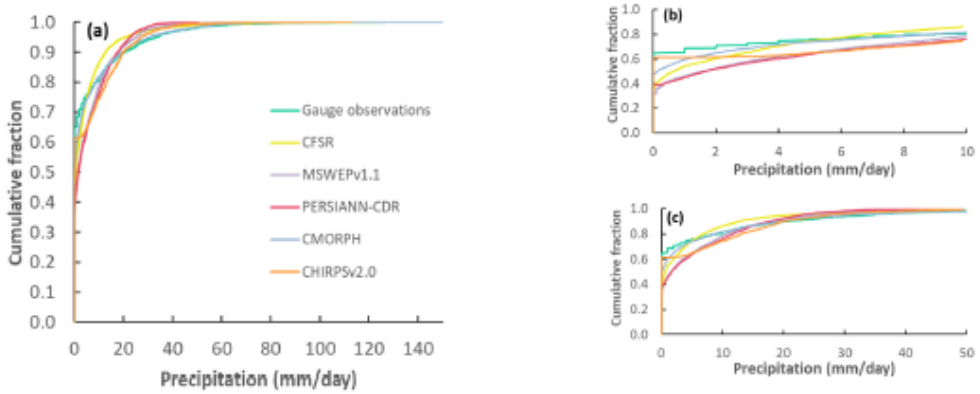

Figure 5. Distribution of daily precipitation values of the six precipitation inputs at PS-1: (**a**) distribution of all precipitation values; (**b**) distribution of precipitation < 10 mm; (**c**) distribution of 10 mm ≤ precipitation ≤ 50 mm.

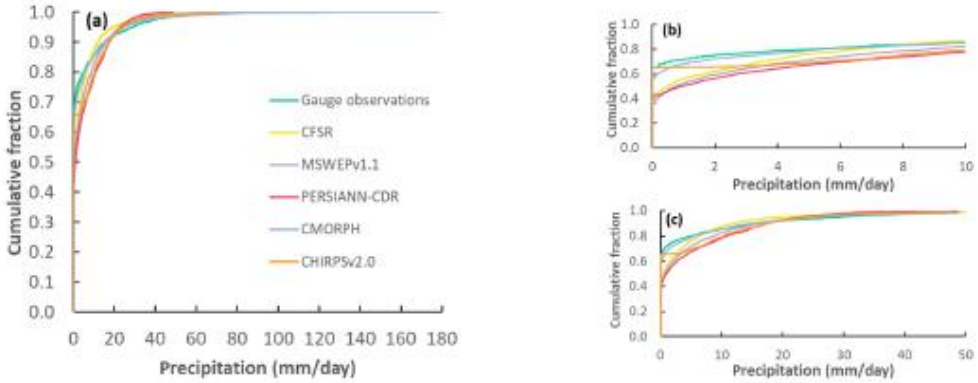

Figure 6. Distribution of daily precipitation values of the six precipitation inputs at PS-2: (**a**) distribution of all precipitation values; (**b**) distribution of precipitation < 10 mm; (**c**) distribution of 10 mm ≤ precipitation ≤ 50 mm.

The annual variability of the different datasets is shown in Figure 7. The results of annual precipitation again show that CMORPH presented the smallest deviation from the observed data, whilst CFSR was the dataset with the lowest precipitation for both precipitation stations. The annual variability between the years 2005 and 2006, 2007 and 2008, and 2009 and 2010 were similar to those observed at station PS-1. At station PS-2, the period 2007–2010 showed the same variability as the observed data. CMORPH showed the same annual variability in all years as the observed data at station PS-1 and PERSIANN-CDR and CHIRPSv2.0 at station PS-2. In the case of PS-2, 2009 was the driest year in all cases. In contrast, the wettest year was 2010 for all data and both stations, except for MSWEPv1.1 in the case of PS-2, where it was 2008.

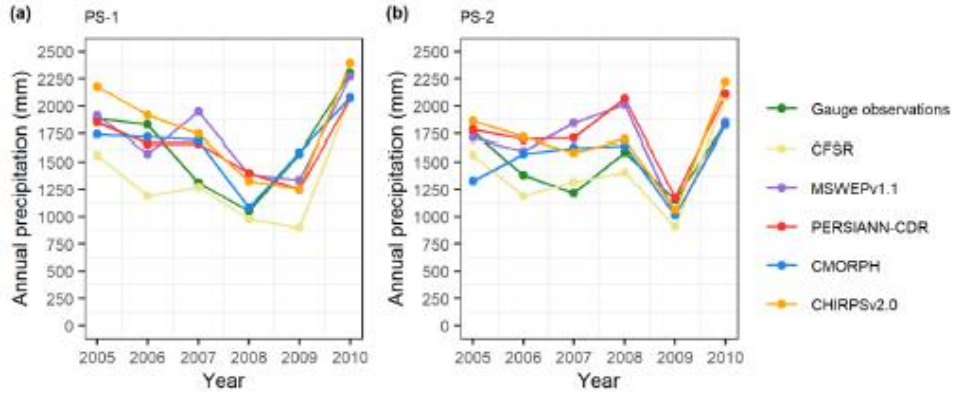

Figure 7. Annual precipitation in: (**a**) PS-1 station and (**b**) PS-2 station.

The divergent results of the different global precipitation products demonstrate that no particular GP product performs better in general. In other words, more research is needed in the different hydro-climatic regions to explore and assess their usefulness as an alternative to the observed data in data-scarce regions. Therefore, the different GP products must be validated for each case study, which means that the simulation of streamflow is mandatory in regions with poor data.

3.2. Performance of GP Products in Simulating Streamflow

During the second stage, the performances of the five GP products and the data from the ground gauges were evaluated as an input to the SWAT model to simulate the observed streamflow in the three stream gauges (SG-1, SG-2, and SG-3). In the first approach of this study, the best-fit parameters found for the SWAT model with the precipitation gauge observation data were used to simulate the streamflow with each GP product as an input, and the results are illustrated in Table 9.

Table 9. Performance of SWAT simulations on a monthly scale derived with the best-fitted parameters calibrated with precipitation gauge stations for calibration (2005–2007) and validation (2008–2010) for three gauge stations.

Stream Gauge/Criteria	CFSR	MSWEPv1.1	PERSIANN-CDR	CMORPH	CHIRPSv2.0
SG-1 calibration (validation)					
R^2	0.54 (0.68)	0.75 (0.65)	0.76 (0.72)	0.63 (0.60)	0.80 (0.82)
NSE	0.39 (0.63)	0.67 (0.64)	0.69 (0.71)	0.36 (0.58)	0.51 (0.80)
PBIAS	31.97 (25.56)	11.92 (11.57)	18.71 (6.03)	1.70 (0.78)	−10.49 (−6.30)
RSR	0.78 (0.61)	0.57 (0.60)	0.56 (0.54)	0.80 (0.65)	0.70 (0.45)
SG-2 calibration (validation)					
R^2	0.60 (0.69)	0.77 (0.66)	0.78 (0.70)	0.63 (0.60)	0.80 (0.82)
NSE	0.42 (0.62)	0.67 (0.63)	0.68 (0.68)	0.34 (0.58)	0.50 (0.80)
PBIAS	33.99 (26.73)	15.49 (16.46)	24.43 (12.31)	8.24 (7.21)	−5.06 (−3.20)
RSR	0.76 (0.62)	0.57 (0.61)	0.57 (0.56)	0.81 (0.65)	0.70 (0.45)
SG-3 calibration (validation)					
R^2	0.62 (0.67)	0.78 (0.65)	0.79 (0.71)	0.65 (0.59)	0.82 (0.81)
NSE	0.44 (0.61)	0.67 (0.63)	0.68 (0.69)	0.34 (0.57)	0.53 (0.79)
PBIAS	34.19 (25.79)	16.08 (16.58)	25.56 (12.63)	9.53 (7.46)	−3.47 (−3.24)
RSR	0.75 (0.63)	0.57 (0.61)	0.57 (0.56)	0.82 (0.66)	0.69 (0.46)

No relevant disparities in water balance were found between GPs and the baseline model using the best-adjusted parameters for gauge observations input. The mean ratio of annually observed streamflow to annual precipitation was 0.28 to compensate for the GP overestimating precipitation. Most of the total streamflow in all the GP (around 87%) came from surface runoff, while aquifer recharge accounted for less than 2.5% of total precipitation, reproducing the baseline model, with 2%. The mean ratio ET to total precipitation was similar for all the GPs at approximately 0.45.

In the case of models that use CFSR and CMORPH as the input, the indexes did not deliver good results, despite the good statistics obtained with CMORPH when comparing precipitation data. PBIAS for PERSIIAN-CDR and RSR for CHIRPS worsened considerably in the calibration phase. CFSR presented the worst values of PBIAS against the other GP products. MSWEPv1.1 showed better performance in terms of R^2, NSE, and RSR in the validation period. Based on the criteria of Moriasi et al. [64], the models simulated with CFSR and CMORPH were unsatisfactory according to the NSE and RSR indexes. However, models driven by MSWEPv1.1, PERSIANN-CDR, and CHIRPSv2.0 were satisfactory except for the PBIAS statistic with PERSIANN-CDR at station SG-3 which reached the limit value of 25% in the calibration period. In conclusion, in the first approach, PERSIANN-CDR and CHIRPSv2.0 were the precipitation products that performed best in the streamflow simulations during the validation period. Given the large number of parameters involved in model calibration, a second approach was additionally used to evaluate the GP products. In this second approach, the SWAT model was calibrated for each of the precipitation products. The values of the calibrated parameters in each case are shown in Table 10. Most of the parameters show significant differences depending on the dataset used. While CN2 remained almost unchanged for CMORPH, there was a slight decrease in the initial value for gauge stations and CFSR and reductions higher than 10% for MSWEPv1.1, CHIRPSv2.0 and PERSIAN-CDR. The latter reached 19%, characterizing the basin as having high permeability. According to the ALPHA_BF values, the response to aquifer recharge is

very low for gauge stations, CFSR, CMORPH and CHIRPSv2.0, unlike MSWEPv1.1 and PERSIANN-CDR, which is in line with the hydrology of the basin. Similar conclusions can be drawn when analysing RCHRG_DP fitted values. Parameters related to HRUs' slope (SLSUBBSN and HRU_SLP) showed significant differences between datasets, which varied in a wide range (−0.48–0.42). The resistance to flood flows in the main channel measured by CH_N2 contributes (together with its hydraulic conductivity (CH_K2)) to water transfer mechanisms and surface runoff. CMORPH and CHIRPSv2.0 provide abnormally low roughness values (0.01). Furthermore, MSWEPv1.1 and PERSIANN-CDR show a moderate loss rate, according to Lane et al. [66] (hydraulic conductivity below 25 mm/h), and CMORPH and CHIRPSv2.0 reach values above 75 mm/h, which indicate a high loss rate. While this should correspond with clean sand and gravel as a bed material in the channel, it does not reflect the riverbed's reality. Soil parameters were also significantly different depending on the GP. Thus, SOL_AWC increased the initial value in all datasets but CFSR and MSWEPv1.1, and decreased the stream flow due to the ability of soil to retain more water [67].

Table 10. SWAT parameter values calibrated with each of the precipitation sources.

Parameter	Parameter Values					
	Precipitation Gauge Data	CFSR	MSWEPv1.1	PERSIANN-CDR	CMORPH	CHIRPSv2.0
r_CN2	−0.06	−0.07	−0.14	−0.19	−0.02	−0.11
v_ALPHA_BF	0.14	0.03	0.82	0.47	0.02	0.02
v_GWQMN	3568.33	3313	4425	3737.5	4712.5	3385
v_GW_REVAP	0.12	0.12	0.10	0.15	0.08	0.12
v_RCHRG_DP	0.09	0.15	0.54	0.44	0.02	0.01
v_SHALLST	92.33	594.25	657	521.5	937.5	1062.5
v_CANMX	28.38	28.55	29.05	16.57	32.58	19.55
r_SLSUBBSN	0.42	0.23	−0.24	0.25	−0.28	−0.18
r_HRU_SLP	−0.48	−0.21	−0.45	−0.01	0.31	0.24
v_ESCO	0.85	0.58	0.40	0.56	0.75	0.73
v_SURLAG	12.86	7.96	15.15	7.74	9.26	5.79
v_CH_N2	0.13	0.03	0.24	0.10	0.01	0.01
v_CH_K2	39.65	44.24	8.65	16.15	116.93	77.95
r_SOL_AWC	0.07	−0.08	−0.02	0.02	0.16	0.07
r_SOL_BD	−0.08	0.03	0.09	0.02	−0.13	−0.06
r_SOL_Z	−0.24	0.13	−0.27	−0.16	0.22	0.04

Concerning the balance models obtained, the mean ratio of annual observed streamflow to annually precipitation for the studied period (2005–2010) was 0.32, ranging from 0.21 to 0.40 for PERSIANN-CDR and CMORPH, respectively. In the case of the SWAT model for the precipitation gauge data, this ratio was 0.35 and 91% of the total flow came from surface run-off. The proportion between surface run-off and base flow was more balanced in PERSIANN-CDR, CHIRPSv2.0 and MSWEPv1.1, where the percentages were around 60% and 40%, respectively. Consequently, the highest differences in models were found in the recharge to the aquifer, which was almost 0% in all models except in PERSIANN-CDR and MSWEPv1.1, where the ratio of deep recharge to total precipitation was 0.15 and 0.19, respectively. The latter is consistent with previous hydrogeological studies in Central American aquifers [52,53], which indicated high permeability and faster response recharge. No discrepancies were found regarding the ratio ET to total precipitation, which varied from 0.42 (gauge station and CHIRPSv2.0) to 0.50 (CFSR), highlighting the relevance of precipitation data in water balance.

Table 11 shows the calibration and validation model results on a monthly scale with each precipitation dataset. In general, SWAT simulations based on the best-fit parameters for each GP product showed a better performance in terms of R^2, NSE, PBIAS, and RSR compared to the simulation results using GP products with the best-adjusted parameters for gauge observations input. The performance indices were better in calibration and

validation, except for the PBIAS index using CHIRPSv2.0. In concrete terms, the NSE values increased slightly in calibration (approximately 0.15) and had minimal variation in validation for the model driven by PERSIANN-CDR. On the other hand, in the model driven by CHIRPSv2.0, there was a significant increase in the NSE values of about 0.31 in calibration and a slight increase (about 0.08) in validation. Similar results were obtained by Bitew et al. [33], who revealed significant improvements in the simulations when the models were calibrated with each of the precipitation products rather than with observed data. In terms of R^2, NSE, and RSR, the SWAT model with PERSIANN-CDR and CHIRPSv2.0 as inputs simulated the streamflow with the best results in both the calibration and validation for the three stream gauges.

Table 11. Performance of SWAT simulations at a monthly scale based on the input of different precipitation products for calibration (2005–2007) and validation (2008–2010) for three stream gauges.

Stream Gauge/Criteria	Precipitation Gauge Data	CFSR	MSWEPv1.1	PERSIANN-CDR	CMORPH	CHIRPSv2.0
			SG-1 calibration (validation)			
R^2	0.73 (0.61)	0.68 (0.79)	0.76 (0.59)	0.83 (0.71)	0.58 (0.62)	0.82 (0.90)
NSE	0.70 (0.60)	0.62 (0.77)	0.71 (0.57)	0.82 (0.69)	0.56 (0.57)	0.79 (0.87)
PBIAS	−7.48 (10.37)	−1.03 (−6.41)	−16.63 (−15.10)	−4.76 (−13.66)	−13.36 (−13.58)	−14.52 (−12.15)
RSR	0.55 (0.63)	0.62 (0.48)	0.54 (0.66)	0.43 (0.56)	0.67 (0.66)	0.46 (0.37)
			SG-2 calibration (validation)			
R^2	0.77 (0.63)	0.74 (0.79)	0.78 (0.57)	0.85 (0.70)	0.60 (0.62)	0.84 (0.91)
NSE	0.76 (0.61)	0.67 (0.76)	0.72 (0.56)	0.84 (0.69)	0.60 (0.58)	0.83 (0.88)
PBIAS	1.13 (16.85)	0.20 (−6.26)	−13.82 (−11.52)	1.03 (−7.75)	−5.60 (−7.37)	−8.50 (−12.53)
RSR	0.49 (0.63)	0.58 (0.49)	0.53 (0.66)	0.39 (0.55)	0.63 (0.65)	0.41 (0.35)
			SG-3 calibration (validation)			
R^2	0.77 (0.62)	0.76 (0.78)	0.78 (0.57)	0.85 (0.71)	0.62 (0.61)	0.85 (0.91)
NSE	0.76 (0.59)	0.67 (0.73)	0.72 (0.56)	0.84 (0.70)	0.62 (0.58)	0.84 (0.88)
PBIAS	3.11 (17.34)	−0.10 (−8.11)	−13.59 (−12.31)	2.14 (−7.67)	−3.99 (−7.20)	−6.39 (−14.24)
RSR	0.49 (0.64)	0.57 (0.52)	0.53 (0.67)	0.39 (0.54)	0.62 (0.65)	0.40 (0.34)

The CFSR-driven simulation obtained the lowest PBIAS values for all three gauges, except for SG-3 in the validation period, where the best results were obtained using the PERSIANN-CDR and CMORPH datasets. The simulated streamflow driven by the MSWEPv1.1 and CMORPH datasets obtained the poorest fits with the observed streamflow. In accordance with NSE, PBIAS, and RSR, SWAT's performances for all precipitation inputs were satisfactory (defined as NSE > 0.5, PBIAS < ±25, and RSR ≤ 0.7 [52]), in both the calibration and validation periods. Very good model performances (defined as NSE > 0.75) were obtained for PERSIANN-CDR and CHIRPSv2.0. Based on the results of the four indexes, it is concluded that the results of the streamflow simulation on a monthly scale driven by the PERSIANN-CDR and CHIRPSv2.0 products were better than those obtained with the observed precipitation data, meaning that the use of PERSIANN-CDR and CHIRPSv2.0 was advantageous for the observed data. Notwithstanding, comparative techniques similar to those undertaken must be carried out to avoid parameter overfitting. Furthermore, water balance analysis revealed that there was not aquifer recharge with CHIRPSv2.0, which is inconsistent with hydrological characteristics of the basin. Thus, PERSIANN-CDR was the most stable and appropriate product to simulate the streamflow in the GSM River Basin. Figure 8 presents a comparison of the streamflow simulations using the best-fit parameters for the precipitation gauge observations data for the calibration (2005–2007) and validation (2008–2009) periods. The streamflow simulation conducted by CFSR, MSWEPv1.1, and PERSIANN-CDR resulted in reduced wet and dry season flows, underestimating the observed streamflow as shown in the PBIAS (Table 9).

Figure 9 shows the comparison of the streamflow simulations for each precipitation dataset input with observed monthly streamflow using model parameters calibrated for each dataset.

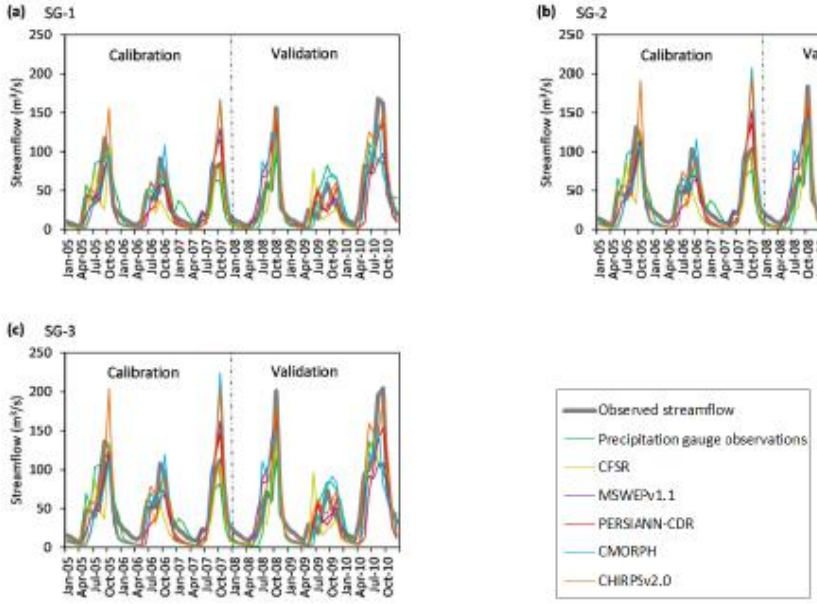

Figure 8. Comparison of simulated streamflow for different precipitation sources and observed monthly streamflow using Table 1. (**a**) SG-1, (**b**) SG-2, and (**c**) SG-3.

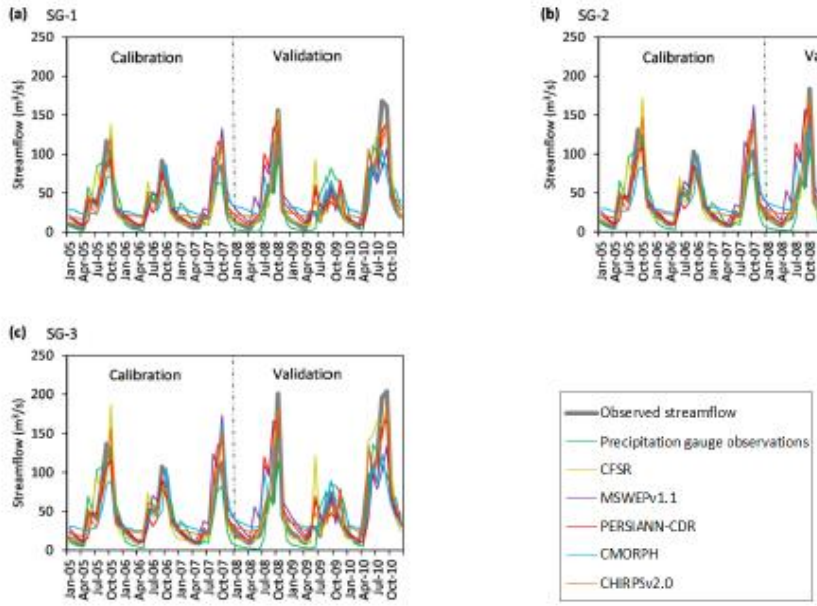

Figure 9. Comparison of simulated streamflow for different precipitation sources and observed monthly streamflow using model parameters calibrated for each dataset in (**a**) SG-1, (**b**) SG-2, and (**c**) SG-3.

The simulation based on precipitation gauge data input overlooked the highest peak flows in the calibration and validation periods, which suggests that this dataset was not able to capture the precipitation events that produced these peaks. Moreover, the streamflow simulated with the data from the precipitation gauges was lower than the observed streamflow and the GP products. In all the simulations, the observed highest peak flows of the validation period were not reached. The maximum peak flows simulated with GP products are produced by CFSR and CHIRPSv2.0 for all three gauges. Regarding the modelling of low flows for the dry season, CFSR, MSWEPv1.1, and PERSIANN-CDR modelled them well in general. However, CMORPH and CHIRPSv2.0 overestimated these flows. The streamflow simulated with the CMORPH and CHIRPSv2.0 products indicated an increase in peak flows and a decrease in low flows compared with the first approach, decreasing the differences with respect to the observed flows, as reflected in a decline in PBIAS (Tables 9 and 11).

The advantage of using gridded versus the point data shown in the present study may be due to the following [3]: (1) observed historical data were scarce and poor in the basin; (2) these data may also be subject to error due to malfunctioning of installed equipment; and (3) there are often significant differences between point scale meter information and actual rainfall in an area. It is therefore advisable to use gridded datasets rather than a few point scale meters.

4. Conclusions

The spatial and temporal accuracy of precipitation data is crucial for the reliable simulation of hydrological processes. Streamflow simulation in El Salvador basins is a challenging task due to very sparse and unreliable ground-based precipitation information. This study assessed the capacity of five high-resolution GP products to provide reliable precipitation information for the application of streamflow simulation in this region.

After a comprehensive analysis, the following conclusions were drawn: (1) concerning the comparison of precipitation sources, the divergent results demonstrate that no particular GP product performs better in general; (2) in terms of the ability of the different datasets to simulate streamflow, the simulations using the selected GP products provided realistic and acceptable models; (3) the results of the simulation of the streamflow driven by PERSIANN-CDR and CHIRPSv2.0 products fitted better than those obtained from the data of the precipitation gauges; (4) PERSIANN-CDR was the most adequate and stable dataset to simulate the streamflow in the GSM River Basin; (5) the type of GP dataset significantly influences model performance; (6) GP products have potential use for hydrology purposes; (7) the performance of the models improves when they are calibrated with the specific precipitation instead of a rain gauge input.

Despite the satisfactory results for most of the precipitation products evaluated in this studied area, it is recommended to evaluate the datasets before using them for hydrological studies in other specific sites. In future research, other and newer GP products can be analyzed to determine whether the results can be improved. Moreover, lower timescales of both precipitation and streamflow could be assessed.

The contribution of this study was particularly relevant, since it was the first assessment of the accuracy of GP datasets in the hydrological modelling of a poorly gauged basin in El Salvador in Central America Water management, and climate change studies could be more accurately conducted in data-poor regions with calibrated and validated GP. This research can be performed in areas or countries with a similar problem relating to the non-availability of data.

Supplementary Materials: The following are available online at https://www.mdpi.com/article/10.3390/w13182497/s1.

Author Contributions: Conceptualization, P.J.-S., J.S.-A. and P.B.-G.; Formal analysis, P.J.-S., J.S.-A. and P.B.-G.; Funding acquisition, J.M.C.; Investigation, J.S.-A.; Methodology, P.J.-S. and P.B.-G.;

Software, P.J.-S.; Supervision, J.P.-S. and J.M.C.; Validation, J.P.-S.; Writing—review and editing, P.J.-S., J.P.-S., J.S.-A. and P.B.-G. All authors have read and agreed to the published version of the manuscript.

Funding: This research was funded by Ministerio de Ciencia e Innovación de España (grant numbers RTI2018-096384-B-I00, RTC-2017-6389-5 and RTC2019-007159-5) and by Ramon y Cajal Program (grant number RYC2018-025580-I).

Institutional Review Board Statement: Not applicable.

Informed Consent Statement: Not applicable.

Data Availability Statement: Not applicable.

Acknowledgments: The authors are grateful to Ministerio de Medio Ambiente y Recursos Naturales (MARN) of El Salvador for providing the data necessary for this study, and also to Scribbr editing services for proofreading the text.

Conflicts of Interest: The authors declare no conflict of interest.

References

1. Duan, Z.; Tuo, Y.; Liu, J.; Gao, H.; Song, X.; Zhang, Z.; Yang, L.; Mekonnen, D.F. Hydrological Evaluation of Open-Access Precipitation and Air Temperature Datasets Using SWAT in a Poorly Gauged Basin in Ethiopia. *J. Hydrol.* **2019**, *569*, 612–626. [CrossRef]
2. Woldemeskel, F.M.; Sivakumar, B.; Sharma, A. Merging Gauge and Satellite Rainfall with Specification of Associated Uncertainty across Australia. *J. Hydrol.* **2013**, *499*, 167–176. [CrossRef]
3. Serrat-Aparicio, J.; López-Ballesteros, A.; Pérez-Sánchez, J.; Segura-Méndez, F.; Pulido-Velazquez, D. Using Multiple Monthly Water Balance Models to Evaluate Gridded Precipitation Products over Peninsular Spain. *Remote Sens.* **2018**, *10*, 922. [CrossRef]
4. Jimeno-Sáez, P.; Pulido-Velazquez, D.; Collados-Lara, A.-J.; Pardo-Igúzquiza, E.; Serrat-Aparicio, J.; Baena-Ruiz, L. A Preliminary Assessment of the "Undercatching" and the Precipitation Pattern in an Alpine Basin. *Water* **2020**, *12*, 1061. [CrossRef]
5. Sevruk, B. Adjustment of Tipping-Bucket Precipitation Gauge Measurements. *Atmos. Res.* **1996**, *42*, 237–246. [CrossRef]
6. Soo, E.Z.X.; Jaafar, W.Z.W.; Lai, S.H.; Islam, T.; Srivastava, P. Evaluation of Satellite Precipitation Products for Extreme Flood Events: Case Study in Peninsular Malaysia. *J. Water Clim. Chang.* **2019**, *10*, 871–892. [CrossRef]
7. Beck, H.E.; van Dijk, A.I.J.M.; Levizzani, V.; Schellekens, J.; Miralles, D.G.; Martens, B.; de Roo, A. MSWEP: 3-Hourly 0.25° Global Gridded Precipitation (1979–2015) by Merging Gauge, Satellite, and Reanalysis Data. *Hydrol. Earth Syst. Sci.* **2017**, *21*, 589–615. [CrossRef]
8. Ashouri, H.; Hsu, K.-L.; Sorooshian, S.; Braithwaite, D.K.; Knapp, K.R.; Cecil, L.D.; Nelson, B.R.; Prat, O.P. PERSIANN-CDR: Daily Precipitation Climate Data Record from Multisatellite Observations for Hydrological and Climate Studies. *Bull. Amer. Meteorol. Soc.* **2015**, *96*, 69–83. [CrossRef]
9. Joyce, R.J.; Janowiak, J.E.; Arkin, P.A.; Xie, P. CMORPH: A Method That Produces Global Precipitation Estimates from Passive Microwave and Infrared Data at High Spatial and Temporal Resolution. *J. Hydrometeorol.* **2004**, *5*, 17. [CrossRef]
10. Funk, C.; Peterson, P.; Landsfeld, M.; Pedreros, D.; Verdin, J.; Shukla, S.; Husak, G.; Rowland, J.; Harrison, L.; Hoell, A.; et al. The Climate Hazards Infrared Precipitation with Stations—A New Environmental Record for Monitoring Extremes. *Sci. Data* **2015**, *2*, 150066. [CrossRef] [PubMed]
11. Saha, S.; Moorthi, S.; Wu, X.; Wang, J.; Nadiga, S.; Tripp, P.; Behringer, D.; Hou, Y.-T.; Chuang, H.; Iredell, M.; et al. The NCEP Climate Forecast System Version 2. *J. Clim.* **2014**, *27*, 2185–2208. [CrossRef]
12. Bitew, M.M.; Gebremichael, M. Assessment of Satellite Rainfall Products for Streamflow Simulation in Medium Watersheds of the Ethiopian Highlands. *Hydrol. Earth Syst. Sci.* **2011**, *15*, 1147–1155. [CrossRef]
13. Baez-Villanueva, O.M.; Zambrano-Bigiarini, M.; Ribbe, L.; Nauditt, A.; Giraldo-Osorio, J.D.; Thinh, N.X. Temporal and Spatial Evaluation of Satellite Rainfall Estimates over Different Regions in Latin-America. *Atmos. Res.* **2018**, *213*, 34–50. [CrossRef]
14. Dinku, T.; Ruiz, F.; Connor, S.J.; Ceccato, P. Validation and Intercomparison of Satellite Rainfall Estimates over Colombia. *J. Appl. Meteorol. Climatol.* **2010**, *49*, 1004–1014. [CrossRef]
15. Elgamal, A.; Reggiani, P.; Jonoski, A. Impact Analysis of Satellite Rainfall Products on Flow Simulations in the Magdalena River Basin, Colombia. *J. Hydrol. Reg. Stud.* **2017**, *9*, 85–103. [CrossRef]
16. Hirpa, F.A.; Gebremichael, M.; Hopson, T. Evaluation of High-Resolution Satellite Precipitation Products over Very Complex Terrain in Ethiopia. *J. Appl. Meteorol. Climatol.* **2010**, *49*, 1044–1051. [CrossRef]
17. Le, M.-H.; Lakshmi, V.; Bolten, J.; Bui, D.D. Adequacy of Satellite-Derived Precipitation Estimate for Hydrological Modeling in Vietnam Basins. *J. Hydrol.* **2020**, *586*, 124820. [CrossRef]
18. Arnold, J.G.; Srinivasan, R.; Muttiah, R.S.; Williams, J.R. Large Area Hydrologic Modeling and Assessment Part I: Model Development. *J. Am. Water Resour. Assoc.* **1998**, *34*, 73–89. [CrossRef]
19. Liu, R.; Xu, F.; Zhang, P.; Yu, W.; Men, C. Identifying Non-Point Source Critical Source Areas Based on Multi-Factors at a Basin Scale with SWAT. *J. Hydrol.* **2016**, *533*, 379–388. [CrossRef]

20. Liu, Y.; Wang, R.; Guo, T.; Engel, B.A.; Flanagan, D.C.; Lee, J.G.; Li, S.; Pijanowski, B.C.; Collingsworth, P.D.; Wallace, C.W. Evaluating Efficiencies and Cost-Effectiveness of Best Management Practices in Improving Agricultural Water Quality Using Integrated SWAT and Cost Evaluation Tool. *J. Hydrol.* **2019**, *577*, 123965. [CrossRef]
21. López-Ballesteros, A.; Senent-Aparicio, J.; Martínez, C.; Pérez-Sánchez, J. Assessment of Future Hydrologic Alteration Due to Climate Change in the Aracthos River Basin (NW Greece). *Sci. Total Environ.* **2020**, *733*, 139299. [CrossRef]
22. Pérez-Sánchez, J.; Senent-Aparicio, J.; Martínez Santa-María, C.; López-Ballesteros, A. Assessment of Ecological and Hydro-Geomorphological Alterations under Climate Change Using SWAT and IAHRIS in the Eo River in Northern Spain. *Water* **2020**, *12*, 1745. [CrossRef]
23. Senent-Aparicio, J.; Alcalá, F.J.; Liu, S.; Jimeno-Sáez, P. Coupling SWAT Model and CMB Method for Modeling of High-Permeability Bedrock Basins Receiving Interbasin Groundwater Flow. *Water* **2020**, *12*, 657. [CrossRef]
24. Worku, T.; Khare, D.; Tripathi, S.K. Modeling Runoff–Sediment Response to Land Use/Land Cover Changes Using Integrated GIS and SWAT Model in the Beressa Watershed. *Environ. Earth Sci.* **2017**, *76*, 550. [CrossRef]
25. Muche, M.E.; Sinnathamby, S.; Parmar, R.; Knightes, C.D.; Johnston, J.M.; Wolfe, K.; Purucker, S.T.; Cyterski, M.J.; Smith, D. Comparison and Evaluation of Gridded Precipitation Datasets in a Kansas Agricultural Watershed Using SWAT. *J. Am. Water Resour. Assoc.* **2020**, *56*, 486–506. [CrossRef]
26. Tolera, M.; Chung, I.-M.; Chang, S. Evaluation of the Climate Forecast System Reanalysis Weather Data for Watershed Modeling in Upper Awash Basin, Ethiopia. *Water* **2018**, *10*, 725. [CrossRef]
27. Blanco-Gómez, P.; Jimeno-Sáez, P.; Senent-Aparicio, J.; Pérez-Sánchez, J. Impact of Climate Change on Water Balance Components and Droughts in the Guajoyo River Basin (El Salvador). *Water* **2019**, *11*, 2360. [CrossRef]
28. Gao, J.; Sheshukov, A.Y.; Yen, H.; White, M.J. Impacts of Alternative Climate Information on Hydrologic Processes with SWAT: A Comparison of NCDC, PRISM and NEXRAD Datasets. *Catena* **2017**, *156*, 353–364. [CrossRef]
29. Wang, N.; Liu, W.; Sun, F.; Yao, Z.; Wang, H.; Liu, W. Evaluating Satellite-Based and Reanalysis Precipitation Datasets with Gauge-Observed Data and Hydrological Modeling in the Xihe River Basin, China. *Atmos. Res.* **2020**, *234*, 104746. [CrossRef]
30. Dhanesh, Y.; Bindhu, V.M.; Senent-Aparicio, J.; Brighenti, T.M.; Ayana, E.; Smitha, P.S.; Fei, C.; Srinivasan, R. A Comparative Evaluation of the Performance of CHIRPS and CFSR Data for Different Climate Zones Using the SWAT Model. *Remote Sens.* **2020**, *12*, 3088. [CrossRef]
31. Mararakanye, N.; Le Roux, J.J.; Franke, A.C. Using Satellite-Based Weather Data as Input to SWAT in a Data Poor Catchment. *Phys. Chem. Earth* **2020**, *117*, 102871. [CrossRef]
32. Radcliffe, D.E.; Mukundan, R. PRISM vs. CFSR Precipitation Data Effects on Calibration and Validation of SWAT Models. *J. Am. Water Resour. Assoc.* **2017**, *53*, 89–100. [CrossRef]
33. Bitew, M.M.; Gebremichael, M.; Ghebremichael, L.T.; Bayissa, Y.A. Evaluation of High-Resolution Satellite Rainfall Products through Streamflow Simulation in a Hydrological Modeling of a Small Mountainous Watershed in Ethiopia. *J. Hydrometeorol.* **2012**, *13*, 338–350. [CrossRef]
34. Zhu, H.; Li, Y.; Huang, Y.; Li, Y.; Hou, C.; Shi, X. Evaluation and Hydrological Application of Satellite-Based Precipitation Datasets in Driving Hydrological Models over the Huifa River Basin in Northeast China. *Atmos. Res.* **2018**, *207*, 28–41. [CrossRef]
35. Blacutt, L.A.; Herdies, D.L.; de Gonçalves, L.G.G.; Vila, D.A.; Andrade, M. Precipitation Comparison for the CFSR, MERRA, TRMM3B42 and Combined Scheme Datasets in Bolivia. *Atmos. Res.* **2015**, *163*, 117–131. [CrossRef]
36. Rienecker, M.M.; Suarez, M.J.; Gelaro, R.; Todling, R.; Bacmeister, J.; Liu, E.; Bosilovich, M.G.; Schubert, S.D.; Takacs, L.; Kim, G.-K.; et al. MERRA: NASA's Modern-Era Retrospective Analysis for Research and Applications. *J. Clim.* **2011**, *24*, 3624–3648. [CrossRef]
37. Huffman, G.J.; Bolvin, D.T.; Nelkin, E.J.; Wolff, D.B.; Adler, R.F.; Gu, G.; Hong, Y.; Bowman, K.P.; Stocker, E.F. The TRMM Multisatellite Precipitation Analysis (TMPA): Quasi-Global, Multiyear, Combined-Sensor Precipitation Estimates at Fine Scales. *J. Hydrometeorol.* **2007**, *8*, 38–55. [CrossRef]
38. Melo, D.d.C.D.; Xavier, A.C.; Bianchi, T.; Oliveira, P.T.S.; Scanlon, B.R.; Lucas, M.C.; Wendland, E. Performance Evaluation of Rainfall Estimates by TRMM Multi-satellite Precipitation Analysis 3B42V6 and V7 over Brazil. *J. Geophys. Res. Atmos.* **2015**, *120*, 9426–9436. [CrossRef]
39. Zambrano-Bigiarini, M.; Nauditt, A.; Birkel, C.; Verbist, K.; Ribbe, L. Temporal and Spatial Evaluation of Satellite-Based Rainfall Estimates across the Complex Topographical and Climatic Gradients of Chile. *Hydrol. Earth Syst. Sci.* **2017**, *21*, 1295–1320. [CrossRef]
40. Oliveira, P.T.S.; Nearing, M.A.; Moran, M.S.; Goodrich, D.C.; Wendland, E.; Gupta, H.V. Trends in Water Balance Components across the Brazilian Cerrado. *Water Resour. Res.* **2014**, *50*, 7100–7114. [CrossRef]
41. Tan, M.L.; Gassman, P.W.; Liang, J.; Haywood, J.M. A Review of Alternative Climate Products for SWAT Modelling: Sources, Assessment and Future Directions. *Sci. Total Environ.* **2021**, *795*, 148915. [CrossRef] [PubMed]
42. Dinh, K.D.; Anh, T.N.; Nguyen, N.Y.; Bui, D.D.; Srinivasan, R. Evaluation of grid-based rainfall products and water balances over the Mekong River basin. *Remote Sens.* **2020**, *12*, 1858. [CrossRef]
43. Tang, X.; Zhang, J.; Gao, C.; Ruben, G.B.; Wang, G. Assessing the uncertainties of four precipitation products for swatmodeling in Mekong River basin. *Remote Sens.* **2019**, *11*, 304. [CrossRef]
44. Dutta, P.; Sarma, A.K. Hydrological modeling as a tool for water resources management of the data-scarce Brahmaputra basin. *J. Water Clim. Change* **2020**, *12*, 152–165. [CrossRef]

45. Dile, Y.T.; Srinivasan, R. Evaluation of CFSR climate data for hydrologic prediction in data-scarce watersheds: An application in the Blue Nile River Basin. *JAWRA J. Am. Water Resour. Assoc.* **2014**, *50*, 1226–1241. [CrossRef]
46. Musie, M.; Sen, S.; Srivastava, P. Comparison and evaluation of gridded precipitation datasets for streamflow simulation in data scarce watersheds of Ethiopia. *J. Hydrol.* **2019**, *579*, 124168. [CrossRef]
47. MARN. Plan Nacional de Gestión Integrada del Recurso Hídrico de El Salvador, Con Énfasis en Zonas Prioritarias. Ministerio de Medio Ambiente y Recursos Naturales. Available online: http://rcc.marn.gob.sv/xmlui/handle/123456789/52 (accessed on 1 March 2021).
48. Wozab, D.; Jovel, J.R. Hydrological Analysis of Volcanic Terrane: Lower Basin of the Rio Grande de San Miguel, El Salvador. *Hydrol. Sci. J.* **1970**, *15*, 47–66. [CrossRef]
49. Levard, C.; Basile-Doelsch, I. Geology and Mineralogy of Imogolite-Type Materials. In *Developments in Clay Science*; Elsevier: Amsterdam, The Netherlands, 2016; Volume 7, pp. 49–65. ISBN 978-0-08-100293-3.
50. FAO. Base Referencial Mundial Del Recurso Suelo: Un Marco Conceptual Para Clasificación, Correlación y Comunicación Internacional. *Roma, Italy.* 2008. Available online: http://www.fao.org/3/a0510s/a0510s.pdf (accessed on 15 June 2021).
51. Sánchez-Murillo, R.; Esquivel-Hernández, G.; Corrales-Salazar, J.L.; Castro-Chacón, L.; Durán-Quesada, A.M.; Guerrero-Hernández, M.; Delgado, V.; Barberena, J.; Montenegro-Rayo, K.; Calderón, H.; et al. Tracer Hydrology of the Data-scarce and Heterogeneous Central American Isthmus. *Hydrol. Process.* **2020**, *34*, 2660–2675. [CrossRef]
52. Jang, W.S.; Engel, B.; Ryu, J. Efficient Flow Calibration Method for Accurate Estimation of Baseflow Using a Watershed Scale Hydrological Model (SWAT). *Ecol. Eng.* **2018**, *125*, 50–67. [CrossRef]
53. Sierra Alcocer, R.; Zenteno-Jimenez, E.D.; Barrios, J. Automatic Land Use and Land Cover Classification Using RapidEye Imagery in Mexico. In Proceedings of the AAAI Workshops Workshops at the Twenty-Ninth AAAI Conference on Artificial Intelligence, Austin, TX, USA, 25–26 January 2015. [CrossRef]
54. Tan, M.L.; Yang, X. Effect of Rainfall Station Density, Distribution and Missing Values on SWAT Outputs in Tropical Region. *J. Hydrol.* **2020**, *584*, 124660. [CrossRef]
55. World Meteorological Organization. Chapter 14; Observation of present and past weather; state of the ground. In *Guide to Meteorological Instruments and Methods of Observation*; WMO: Geneva, Switzerland, 2012; pp. I.14–I.19. Available online: http://www.posmet.ufv.br/wp-content/uploads/2016/09/MET-474-WMO-Guide.pdf (accessed on 12 August 2021).
56. Dile, Y.T.; Daggupati, P.; George, C.; Srinivasan, R.; Arnold, J. Introducing a New Open Source GIS User Interface for the SWAT Model. *Environ. Modell. Softw.* **2016**, *85*, 129–138. [CrossRef]
57. Tuo, Y.; Duan, Z.; Disse, M.; Chiogna, G. Evaluation of Precipitation Input for SWAT Modeling in Alpine Catchment: A Case Study in the Adige River Basin (Italy). *Sci. Total Environ.* **2016**, *573*, 66–82. [CrossRef]
58. Hargreaves, G.H. Defining and Using Reference Evapotranspiration. *J. Irrig. Drain. Eng.* **1994**, *120*, 1132–1139. [CrossRef]
59. USDA. *National Engineering Handbook, Section 4: Hydrology*; US Soil Conservation Service: Washington, DC, USA, 1972.
60. Abbaspour, K.C.; Johnson, C.A.; van Genuchten, M.T. Estimating Uncertain Flow and Transport Parameters Using a Sequential Uncertainty Fitting Procedure. *Vadose Zone J.* **2004**, *3*, 1340–1352. [CrossRef]
61. Abbaspour, K.C. *SWAT Calibration and Uncertainty Program—A User Manual. SWAT-CUP-2012*, 2012th ed.; Swiss Federal Institute of Aquatic Science and Technology: Dubendorf, Switzerland, 2012.
62. Arnold, J.G.; Moriasi, D.N.; Gassman, P.W.; Abbaspour, K.C.; White, M.J.; Srinivasan, R.; Santhi, C.; Harmel, R.D.; van Griensven, A.; Van Liew, M.W.; et al. SWAT: Model Use, Calibration, and Validation. *Trans. ASABE* **2012**, *55*, 1491–1508. [CrossRef]
63. Nash, J.E.; Sutcliffe, J.V. River Flow Forecasting through Conceptual Models Part I—A Discussion of Principles. *J. Hydrol.* **1970**, *10*, 282–290. [CrossRef]
64. Moriasi, D.N.; Arnold, J.G.; Liew, M.W.V.; Bingner, R.L.; Harmel, R.D.; Veith, T.L. Model Evaluation Guidelines for Systematic Quantification of Accuracy in Watershed Simulations. *Trans. ASABE* **2007**, *50*, 885–900. [CrossRef]
65. Magaña, V.; Amador, J.A.; Medina, S. The Midsummer Drought over Mexico and Central America. *J. Clim.* **1999**, *12*, 1577–1588. [CrossRef]
66. Lane, L.J.; Ferreira, V.A.; Shirley, E.D. Estimating transmission losses in ephemeral stream channels. In *Hydrology and Water Resources in Arizona and the Southwest*; Arizona-Nevada Academy of Science: Las Vegas, NV, USA, 1980.
67. Opere, A.O.; Okello, B.N. Hydrologic analysis for river Nyando using SWAT. *Hydrol. Earth Syst. Sci. Discuss.* **2011**, *8*, 1765–1797. [CrossRef]

water

MDPI

Article

Impact assessment of gridded precipitation products on streamflow simulations over a poorly gauged basin in El Salvador

Patricia Jimeno-Sáez[1,*], Pablo Blanco-Gómez[1], Julio Pérez-Sánchez[1,2], José M. Cecilia[3] and Javier Senent-Aparicio[1].

[1] Department of Civil Engineering, Universidad Católica San Antonio de Murcia, Campus de Los Jerónimos s/n, 30107 Guadalupe, Murcia, Spain; pjimeno@ucam.edu, jsenent@ucam.edu, pblanco4@alu.ucam.edu, jperez058@ucam.edu

[2] Department of Civil Engineering, Universidad de Las Palmas de Gran Canaria, Campus de Tafira, 35017 Las Palmas de Gran Canaria, Spain, julio.sanchez@ulpgc.es

[3] Department of Computer Engineering (DISCA), Universitat Politécnica de Valencia (UPV), 46022 Valencia, Spain; jmcecilia@disca.upv.es

[*] Correspondence: pjimeno@ucam.edu;

Supplementary material

Gridded Precipitation products

1.1. CFSR product

CFSR product was developed by the National Centers for Environmental Prediction (NCEP) [1]. CFSR was developed through advanced data-assimilation methods using data from a global network of weather stations and satellite-based products, as well as very complex atmospheric, oceanic and surface modeling elements coupled with a resolution of 0.30° resolution and covering any land location in the world [2]. The data available from the CFSR cover the period 1979-2014 and is accessible in Global Weather Data for the SWAT data portal (https://globalweather.tamu.edu/).

1.2. MSWEP product

MSWEPv1.1 is a global precipitation database available for the period 1979 to 2015 with a time step of 3 hours and a spatial resolution of 0.25° and specifically developed for hydrological modeling. MSWEP merges the highest quality precipitation data sources available based on time scale and location and was generated as a data weighted combination of seven datasets: was generated as a data weighted combination of seven datasets: two products from reanalysis of numerical weather prediction models, three derived from satellite remote sensing (CMORPH, GSMaP-MVK, and TMPA 3B42RT) and two based on interpolated gauge observations. The dataset incorporates a correction for topographic effects and under-catch by deriving catchment-average precipitation from streamflow observations at 13762 stations around the world [3]. MSWEP can be downloaded in http://www.gloh2o.org.

1.3. PERSIANN-CDR product

PERSIANN-CDR is a product generated from the PERSIANN algorithm using the historical GridSat-B1 IRWIN data to obtain daily precipitation estimates with a resolution of 0.25°. The derived estimates are then bias corrected using monthly 2.5° data from the Global Precipitation Climatology Project (GPCP), which contain the Global Precipitation Climatology Centre (GPCC) gauge information [4]. The PERSIANN-CDR product is available to the public on the Data Portal of the Center for Hydrometeorology and Remote Sensing (CHRS) at The University of California, Irvine (UCI) (http://chrsdata.eng.uci.edu/ [5]).

1.4. CMORPH product

In the CMORPH product, global half-hourly rainfall estimates are derived from passive microwave satellite scans and through movement vectors obtained from infrared

data of geostationary satellites. The shape and intensity of precipitation characteristics are adjusted by performing a time-weighted linear interpolation in the time between microwave sensor scans to obtain complete spatiotemporal precipitation analyses independent of the infrared temperature field [6]. CMORPH data were accessed from WCI portal, an open-source project built by Plymouth Marine Laboratory's Remote Sensing Group (https://wci.earth2observe.eu/).

1.5. CHIRPS product

CHIRPS data was produced to assist the United States Agency for International Development Famine Early Warning Systems Network (FEWS NET) and consists of a precipitation grid with a spatial resolution of 0.05° merging data from satellites with data from in-situ rain gauge stations. This dataset uses different data sources in its creation: the Tropical Rainfall Measuring Mission (TRMM) 3B42 product from NASA, the monthly precipitation climatology (CHPClim), atmospheric model rainfall fields from the NOAA Climate Forecast System, version 2 (CFSv2), quasi-global geostationary thermal infrared (IR) satellite observations from two NOAA sources, and in situ rainfall observations collected from different sources including regional and national meteorological agencies [7]. The daily data of CHIRPS v2.0 can be obtained from the Climate Hazards Group website (https://www.chc.ucsb.edu/data/chirps).

References

1. Saha, S., Moorthi, S., Wu, X., Wang, J., Nadiga, S., Tripp, P., Behringer, D., Hou, Y.-T., Chuang, H.-Y., Iredell, M., Ek, M., Meng, J., Yang, R., Mendez, M.P.A. The NCEP Climate Forecast System Version 2. *J. Clim.* **2014**, *27*, 2185–2208. https://doi.org/10.1175/JCLI-D-12-00823.1
2. Saha, S., Moorthi, S., Pan, H.-L., Wu, X., Wang, Jiande, Nadiga, S., Tripp, P., Kistler, R., Woollen, J., Behringer, D., Liu, H., Stokes, D., Grumbine, R., Gayno, G., Wang, Jun, Hou, Y.-T., Chuang, H., Juang, H.-M.H., Sela, J., Iredell, M., Treadon, R., Kleist, D., Delst, P.V., Keyser, D., Derber, J., Ek, M., Meng, J., Wei, H., Yang, R., Lord, S., Kumar, A., Wang, W., Long, C., Chelliah, M., Xue, Y., Huang, B., Schemm, J.-K., Ebisuzaki, W., Lin, R., Xie, P., Chen, M., Zhou, S., Higgins, W., Zou, C.-Z., Liu, Q., Chen, Y., Han, Y., Cucurull, L., Reynolds, R.W., Rutledge, G., Goldberg, M.. The NCEP Climate Forecast System Reanalysis. *Bull. Amer. Meteor. Soc.* **2010**, 91, 1015–1058. https://doi.org/10.1175/2010BAMS3001.1
3. Beck, H.E.; van Dijk, A.I.J.M.; Levizzani, V.; Schellekens, J.; Miralles, D.G.; Martens, B.; de Roo, A. MSWEP: 3-Hourly 0.25° Global Gridded Precipitation (1979–2015) by Merging Gauge, Satellite, and Reanalysis Data. *Hydrol. Earth Syst. Sci.* **2017**, 21, 589–615, doi:10.5194/hess-21-589-2017.
4. Ashouri, H.; Hsu, K.-L.; Sorooshian, S.; Braithwaite, D.K.; Knapp, K.R.; Cecil, L.D.; Nelson, B.R.; Prat, O.P. PERSIANN-CDR: Daily Precipitation Climate Data Record from Multisatellite Observations for Hydrological and Climate Studies. *Bull. Amer. Meteorol. Soc.* **2015**, 96, 69–83, doi:10.1175/BAMS-D-13-00068.1.
5. Nguyen, P., Shearer, E.J., Tran, H., Ombadi, M., Hayatbini, N., Palacios, T., Huynh, P., Braithwaite, D., Updegraff, G., Hsu, K., Kuligowski, B., Logan, W.S., Sorooshian, S. The CHRS Data Portal, an easily accessible public repository for PERSIANN global satellite precipitation data. Sci Data **2019**, 6, 180296. https://doi.org/10.1038/sdata.2018.296
6. Joyce, R.J.; Janowiak, J.E.; Arkin, P.A.; Xie, P. CMORPH: A Method That Produces Global Precipitation Estimates from Passive Microwave and Infrared Data at High Spatial and Temporal Resolution. *J. Hydrometeorol.* **2004**, 5, 17.
7. Funk, C.; Peterson, P.; Landsfeld, M.; Pedreros, D.; Verdin, J.; Shukla, S.; Husak, G.; Rowland, J.; Harrison, L.; Hoell, A.; et al. The Climate Hazards Infrared Precipitation with Stations—a New Environmental Record for Monitoring Extremes. *Sci. Data* **2015**, 2, 150066, doi:10.1038/sdata.2015.66.

IV.4 SÍNTESIS DE RESULTADOS Y DISCUSIÓN

IV.4.1 Impacto del cambio climático en las componentes del balance hídrico

El modelo SWAT para la simulación de escorrentías en la cuenca del río Guajoyo (GRB) empleó la siguiente información de partida: (1) El DEM se obtuvo del Advanced Spaceborne Thermal Emission and Reflection Radiometer (ASTER) Global Digital Elevation Model (GDEM) versión 2 de la NASA (https://asterweb.jpl.nasa.gov/, consultado el 24/08/2021) con una resolución espacial de 30 x 30 m; (2) Los suelos provienen de la Harmonized World Soil Database (Fischer et al., 2008) y los usos del suelo fueron facilitados por el Ministerio de Medio Ambiente y Recursos Naturales (MARN) de la República de El Salvador, correspondiéndose con el Mapa de coberturas y usos del suelo nacional (2011) con una resolución espacial de 5 x 5 m; (3) Los datos climáticos fueron facilitados por el MARN, de la estación convencional Güija, aunque debido a la falta de información para el cálculo de la evapotranspiración se completó con el Climate Forecast System Reanalysis (CFSR) con una resolución espacial de 38 x 38 Km desarrollado por NCEP y obtenido de la aplicación desarrollada por la Texas A&M University (https://Globalweather.tamu.edu/, consultado el 24/08/2021); (4) Los caudales medios mensuales fueron facilitados por el MARN y se corresponden con los registros de la estación Piedra-Cargada en el periodo 2006-2012.

IV.4.1.1 Comportamiento del modelo SWAT

En base a los mapas de suelos, usos del suelo y DEM se construyó el modelo hidrológico en SWAT con ayuda de GIS, generando un total de 85 HRU y 11 subcuencas. Los principales datos climáticos introducidos fueron la precipitación y la temperatura y se emplearon los siguientes métodos de cálculo:

- Número de Curva del SCS para la estimación del proceso lluvia-escorrentía.
- La propagación del flujo se establece mediante el método de Muskingum.

- La velocidad del agua en el cauce a través de la ecuación de Manning.

Se empleó el algoritmo SUFI-2 de SWAT-CUP para la calibración de los parámetros considerando la información correspondiente a los cuatro años del periodo de calibración – i.e. 2006-2009. Después de 1,500 iteraciones se obtuvieron los siguientes resultados de los once parámetros más sensibles que fueron seleccionados:

Parameter [1]	Description	Final Range Used in Calibration	Fitted Value	Final Value
r_CN2.mgt	SCS runoff curve number	−0.2 to 0.2	−0.09	[63.40–75.17] [2]
v_ALPHA_BF.gw	Baseflow alpha factor (days−1)	0 to 0.65	0.09	0.09
a_GW_DELAY.gw	Groundwater delay time (days)	−10 to 60	−2.90	28.07
a_GWQMN.gw	Threshold depth of water in the shallow aquifer for return flow to occur (mm)	200 to 1500	1407.70	2407.70
v_GW_REVAP.gw	Groundwater revap coefficient	0.02 to 0.15	0.13	0.13
a_RCHRG_DP.gw	Deep aquifer percolation fraction	−0.02 to 0.03	0.02	0.07
a_REVAPMN.gw	Threshold depth of water in the shallow aquifer for revap or percolation to the deep aquifer to occur (mm)	−150 to 150	−85.50	664.5
v_CANMX.hru	Maximum canopy storage (mm)	1 to 10	4.47	4.47
v_EPCO.bsn	Plant uptake compensation factor	0.5 to 1	0.87	0.87
v_ESCO.bsn	Soil evaporation compensation factor	0.3 to 0.9	0.79	0.79
r_SOL_AWC.sol	Available water capacity of the soil layer (mm H_2O/mm soil)	−0.02 to 0.02	−0.01	[0.06–0.10] [3]

[1] The qualifier (r_) refers to relative change, i.e., the current parameter must be multiplied by (1 + the value obtained in calibration), (v_) means that the value of the existing parameter must be replaced by the value obtained in calibration, and (a_) refers to absolute change, i.e., the fitted value must be added to the existing value of the parameter. [2] Varies by HRU. [3] Varies by soil layer.

Tabla 1. *Parámetros de calibración del modelo SWAT en la cuenca GRB*

Se pudo comprobar la existencia de un error generalizado en la simulación de los caudales punta, tanto en la fase de calibración como en la de validación, siendo un error destacado en numerosos estudios hidrológicos (Jimeno–Sáez et al., 2018; Spellman, Webster y Watkins, 2018; Čerkasova, Umgiesser y Ertürk, 2019). La siguiente figura representa la comparación entre los caudales observados y simulados en las fases de calibración y validación.

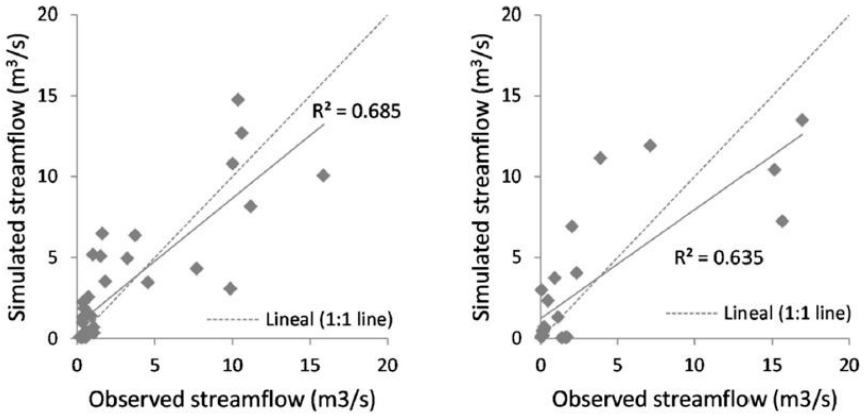

Figura 5. Regresión lineal de caudales observados y simulados para los periodos de (a) calibración (2006-2009), y (b) validación (2010-2012)

A pesar del referido contratiempo, los estadísticos de evaluación del desempeño del modelo calculados indican un comportamiento bueno en la fase de calibración y satisfactorio en la de validación, según los criterios establecidos por Moriasi et al. (2007). Teniendo en cuenta la escasez de datos en la cuenca, se puede considerar que estos resultados son adecuados para la evaluación de las respuestas a medio y largo plazo de la cuenca con la consideración de los escenarios de cambio climático.

Performance Metric	Calibration	Validation
NSE	0.67	0.63
R^2	0.69	0.64
PBIAS (%)	−9.04	−8.80
RMSE (m^3/s)	2.35	3.12
RSR	0.58	0.61

Tabla 2. Estadísticos de evaluación del modelo SWAT en las fases de calibración y validación

Una segunda evaluación del modelo calibrado fue realizada con los datos de precipitación de CHIRPS para el periodo completo – i.e. 2006-2012 – obteniendo un comportamiento bueno (según Moriasi et al. 2007): NSE de 0.74, R2 de 0.78, PBIAS de -23.55, RMSE de 2.29 y RSR de 0.51.

IV.4.1.2 Selección de los modelos de cambio climático

Se empleó el software CCT para la extracción, reducción de escala y corrección estadística del sesgo de cinco GCM – i.e. GFDL-ESM2M, HadGEM2-ES, IPSL-CM5A-LR, MIROC y NoerESM1-M – seleccionando el modelo que mejor representaba el año medio para los estadísticos mensuales clave.

En este caso se utilizó el índice Id, que se define como la suma del valor absoluto de la diferencia relativa entre la serie histórica y el escenario de control durante los 12 meses de un año medio. Se realizó el cálculo mensual para cada GCM en el periodo 1980-2004, considerando las variables precipitación y temperatura y para cada una de ellas el Id de la media (Δx) y el de la desviación típica (Δσ). El modelo con un valor inferior del índice Id es el que presenta un mejor ajuste con los datos observados.

	RCMs	Monthly Series				Id
		Precipitation		Temperature		
		Id (Δx)	Id (Δσ)	Id (Δx)	Id (Δσ)	
1	GFDL–ESM2M	2.14	11.18	1.22	3.76	18.30
2	HadGEM2–ES	1.78	5.95	1.63	2.74	12.10
3	IPSL–CM5A–LR	1.51	10.93	1.23	4.15	17.82
4	MIROC	2.65	9.30	1.21	9.17	22.33
5	NoerESM1–M	1.52	8.13	1.23	5.45	16.33

Tabla 3. Cálculo del índice Id para cada RCM

En base al criterio descrito se seleccionó el modelo HadGEM2-ES por ser el que presenta un menor índice Id.

IV.4.1.3 Cambios en las variables climáticas en los distintos escenarios RCP

La siguiente figura representa los cambios experimentados por las variables climáticas de precipitación y temperatura en la cuenca GRB para los escenarios de emisiones seleccionados – i.e. RCP 4.5 y 8.5 – del modelo HadGEM2-ES para los horizontes de mediados y finales del SiGlo XXI.

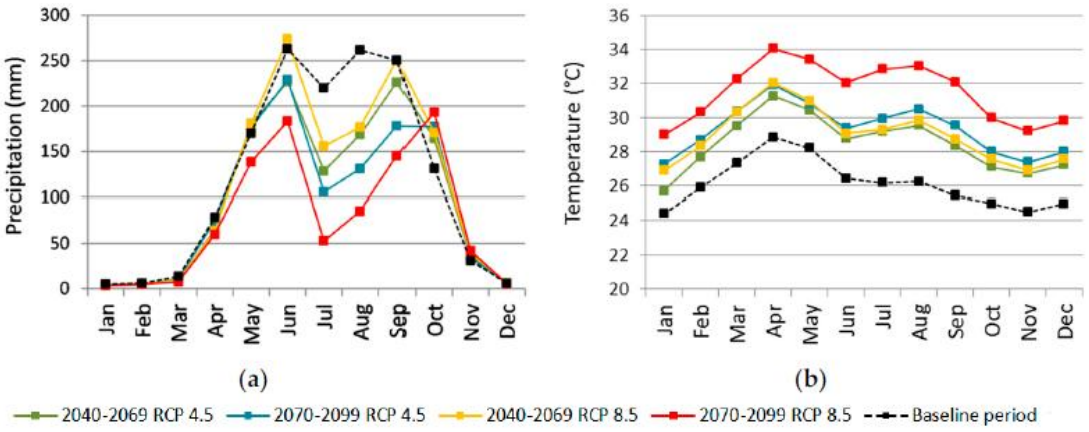

Figura 6. Comparativa de los valores medios mensuales de (a) precipitación y (b) temperatura entre el periodo histórico (1975-2005) y los escenarios de medio y largo término para RCP 4.5 y 8.5 del GCM HadGEM2-ES

En el gráfico de precipitación puede apreciarse para los distintos escenarios considerados la presencia de la canícula (MSD, por sus siglas en inglés), referida por Magaña, Amador y Medina (1999), que constituye un descenso local en las precipitaciones mensuales entre Julio y Agosto, presentando valores máximos tanto en el mes de Junio como entre Septiembre y Octubre. Este fenómeno se verá intensificado en los escenarios de cambio climático considerados, especialmente en los valores previstos para final de SiGlo.

De manera genérica las precipitaciones disminuyen en el periodo húmedo, produciéndose un aumento de las mismas en los meses finales del año – i.e. Noviembre y Diciembre –, dentro del periodo seco.

Por otro lado, en cuanto a temperaturas puede apreciarse un aumento generalizado de las mismas, siendo más acusado en los meses de verano (Julio, Agosto y Septiembre).

Los valores medios anuales para los diferentes periodos y escenarios quedan resumidos en la siguiente tabla, donde cabe destacar la correspondencia de resultados con estudios antecedentes – i.e. CEPAL (2010) estima un descenso en la precipitación similar al obtenido para finales de SiGlo y Conde-Álvarez y Saldaña-Zorrilla establecieron un rango del incremento de temperaturas de entre 1 y 6 °C para final del periodo de estudio, consistente con los resultados del presente estudio.

Model	Scenario	Time Period	Precipitation (mm)		Temperature (°C)	
			Value	Change with Respect to Baseline	Value	Change with Respect to Baseline
Baseline		1975–2004	1435.60	–	26.12	–
HadGEM2–ES	RCP 4.5	2040–2069	1219.12	−216.48 (−15%)	28.45	+2.33 (+9%)
		2070–2099	1129.62	−305.98 (−21%)	29.30	+3.19 (+12%)
	RCP 8.5	2040–2069	1332.64	−102.96 (−7%)	28.95	+2.84 (+11%)
		2070–2099	919.07	−516.53 (−36%)	31.49	+5.38 (+21%)

Tabla 4. Variación de precipitación y temperatura respecto del periodo histórico para los escenarios RCP 4.5 y 8.5

Finalmente se realizó un análisis de tendencia de las variables climáticas para el periodo 2040-2099 aplicando el test de Mann-Kendall y el método de Sen mediante el uso de la hoja de cálculo MS Excel con la aplicación MAKESENS (Versión 1.0) descrita por Salmi et al. (2002).

Month	Precipitation RCP 4.5			Temperature RCP 4.5			Precipitation RCP 8.5			Temperature RCP 8.5		
	Test Z	Sig.	Q_i	Test Z	Sig.	Q_i	Test Z	Sig.	Q_i	Test Z	Sig.	Q_i
January	−0.49		−0.01	3.78	***	0.03	0.16		0.00	7.79	***	0.07
February	0.10		0.00	4.98	***	0.03	−0.56		−0.01	7.57	***	0.07
March	−0.17		−0.01	4.02	***	0.02	−0.84		−0.03	8.12	***	0.07
April	0.91		0.27	3.31	***	0.02	−0.43		−0.10	7.53	***	0.07
May	−0.07		−0.05	1.10		0.01	−2.38	*	−1.19	6.96	***	0.07
June	−0.12		−0.09	2.98	**	0.02	−3.50	***	−2.46	7.67	***	0.09
July	−1.91	+	−0.90	2.56	*	0.03	−5.83	***	−2.53	8.41	***	0.11
August	−1.55		−0.94	3.91	***	0.03	−5.35	***	−2.92	9.29	***	0.10
September	−2.53	*	−1.34	4.46	***	0.03	−5.02	***	−3.66	9.00	***	0.11
October	0.94		0.42	4.11	***	0.03	1.24		0.75	8.09	***	0.08
November	−0.47		−0.04	3.17	**	0.02	1.17		0.18	7.83	***	0.07
December	1.00		0.02	4.45	***	0.02	−0.32		−0.01	7.69	***	0.07
Annual	−1.79	+	−3.70	5.24	***	0.02	−6.8	***	−13.17	9.34	***	0.08

Test Z is the Mann–Kendall (MK) test statistic; Q_i is the Sen's slope estimator; + indicates a significance level of 0.1; * indicates a significance level of 0.05; ** indicates a significance level of 0.01; *** indicates a significance level of 0.001.

Tabla 5. Análisis de tendencia para resultados mensuales y anuales de precipitación y temperatura para el periodo 2040-2099

Se observa como la mayoría de resultados para la precipitación son negativos, a excepción de los valores de final de año (meses de Octubre a Diciembre) en los que la tendencia es positiva, tal y como se había concluido con el análisis anterior. En cuanto a temperaturas, se observa una tendencia al alza en la serie completa para ambos escenarios de emisiones.

IV.4.1.4 Cambios en el balance hídrico en los distintos escenarios RCP

En el presente estudio se asumieron constantes todas las variables hidrológicas – e.g. usos del suelo – a excepción de las variables climáticas de precipitación y temperatura. Tal y como se ha visto con anterioridad, el modelo SWAT fue calibrado y validado con las variables observadas en la cuenca y posteriormente, con ayuda del software CCT, se emplearon las predicciones del modelo GCM seleccionado, HadGEM2-ES para los escenarios RCP 4.5 y 8.5, como datos de entrada en el balance hídrico para explorar la respuesta en la generación de caudales por efecto del cambio climático.

De los resultados del modelo SWAT para los distintos periodos estudiados se obtienen los siguientes valores de la respuesta hidrológica (precipitación, evapotranspiración, producción total de agua y recarga acuífera) de la cuenca GRB en valores totales (y variación en %).

Scenario	Time Period	P (mm)	ET (mm)	ET/P	WYLD (mm)	DA_RCHG (mm)
Baseline	1975–2004	1435.6	523.9	0.36	720.72	27.95
RCP 4.5	2040–2069	1219.12 (−15%)	608.70 (+16%)	0.50	450.33 (−37%)	15.85 (−43%)
	2070–2099	1129.62 (−21%)	613.80 (+17%)	0.54	359.47 (−50%)	12.55 (−55%)
RCP 8.5	2040–2069	1332.64 (−7%)	626.40 (+19%)	0.47	522.18 (−27%)	18.66 (−33%)
	2070–2099	919.07 (−36%)	547.00 (+4%)	0.60	268.87 (−63%)	8.19 (−71%)

P = precipitation, ET = evapotranspiration, ET/P = evapotranspiration/precipitation, WYLD = the net amount of water that contributes to streamflow (surface runoff contribution to streamflow + lateral flow + groundwater contribution to streamflow − transmission losses) and DA_RCHG = amount of water entering deep aquifer from root zone.

Tabla 6. Componentes del balance hídrico con SWAT para los distintos escenarios y periodos considerados

Se observa como el incremento en la temperatura y el descenso en la precipitación conllevan una tendencia al alza en la evapotranspiración y un descenso de la producción de agua y la recarga acuífera. Estas conclusiones y sus valores cuantitativos son concordantes con los resultados de CEPAL (2010), Maurer, Adam y Wood (2009) e Imbach et al. (2012).

IV.4.1.5 Proyecciones futuras de sequía

Se calcularon los índices SPI (de precipitación) y SRI (de escorrentía) para caracterizar las sequías meteorológica e hidrológica, respectivamente, a partir de la precipitación observada y de la escorrentía calculada en SWAT, tanto para el periodo histórico (1975-2004) como para las simulaciones futuras (2006-2099).

Characteristics of drought	Baseline (1975–2004)		RCP 4.5				RCP 8.5			
			2040–2069		2070–2099		2040–2069		2070–2099	
	SPI	SRI	SPI	SRI	SPI	SRI	SPI	SRI	SPI	SRI
Number of drought events	9	5	4	4	10	6	7	7	3	3
Longest duration of drought events (months)	26	36	47	46	34	34	22	24	54	53
Average duration of drought events (months)	12	14	22	27	13	14	15	14	36	36
Average drought intensity	1.60	1.95	2.15	2.01	1.47	1.85	1.93	1.53	1.98	1.90
Maximum drought intensity	2.52	2.64	2.68	2.49	2.44	2.15	2.42	2.68	2.74	2.58

Tabla 7. Análisis de sequías en la cuenca GRB

De la serie histórica se observa que la situación actual está caracterizada por 9 y 5 eventos , con una duración de 12 y 14 meses y una intensidad media de 1.60 y 1.95 para SPI y SRI, respectivamente. Del análisis de los resultados se observa como el número de eventos disminuye ara los periodos de mitad de SiGlo en el caso del escenario de emisiones RCP 4.5 y el de final de SiGlo para el escenario RCP 8.5. En ambos casos, la duración de los eventos se verá incrementada de manera considerable, así como la intensidad media de precipitación. Estos resultados son consistentes con los reportados en IPCC-AR5 (2014) e IPCC-AR6 (2021) en el que se reporta un incremento en los periodos de sequía para las proyecciones climáticas futuras.

IV.4.2 Uso de la serie de caudales de GloFAS-ERA5 para calibrar el modelo SWAT

Para el establecimiento del modelo SWAT en la cuenca del río Grande de San Miguel (GSM) se empleó el mismo modelo digital del terreno (DEM), el mapa

de suelos y el mapa de los usos del suelo que en el estudio realizado en la cuenca GRB.

De manera adicional, existen aforos mensuales en el desagüe de la cuenca modelada para el periodo 1970-2012.

IV.4.2.1 Comparación entre datos observados y los provenientes de reanálisis

En primer lugar se llevó a cabo la comparativa entre la precipitación proveniente de los productos de reanálisis de datos satelitales con la proveniente de las estaciones de la cuenca del río GSM – i.e. Chapeltique (CHA), El Delirio (DEL), Villerías (VIL) y San Miguel (MIG). Para ello se seleccionaron las celdas de la malla raster más próximas a las estaciones, los datos extraídos se corresponden con el periodo en el que existen registros de caudal en la cuenca – i.e. 2005-2010 – y los días que no presentan datos fueron omitidos del análisis comparativo.

Para realizar dicho análisis se emplearon los índices estadísticos referidos en Jiang et al. (2018): (1) Probabilidad de detección (POD, por sus siglas en inglés), indicativo de la cantidad total de eventos de precipitación identificados por los datos provenientes de reanálisis, POD varía entre 0 y 1, siendo 1 el valor referido a la coincidencia exacta entre las series de datos; (2) Ratio de Falsa Alarma (FAR, por sus siglas en inglés), indica el porcentaje de avisos falsos de precipitación entre todos los avisos de precipitación, FAR varía entre 0 y 1, siendo 0 el valor óptimo; (3) El Índice de Éxito Crítico (CSI, por sus siglas en inglés), es función de POD y FAR con lo que se trata de un índice más completo, al igual que POD, su rango varía entre 0 y 1 y su valor óptimo es 1.

En base a este análisis se pudo comprobar como CHIRPS fue el producto que presentaba la mejor capacidad de detección de eventos de precipitación (con valores de CSI de entre 0.52 y 0.63 para las cuatro estaciones hidrometeorológicas existentes en la cuenca), obteniendo resultados aceptables y valores muy similares los otros dos productos satelitales (ERA5 varía entre 0.45 y 0.55; CFSR entre 0.43 y 0.51).

Posteriormente se analizó la función de densidad de probabilidad para eventos de precipitación a escala diaria, quedando patente el hecho de que los distintos productos satelitales analizados no eran capaces de identificar todos los eventos de precipitación ocurridos.

En este sentido, nuevamente CHIRPS resultó el producto que se comportaba de una manera más parecida a los registros de las distintas estaciones. Tanto CFSR como ERA5 sobreestiman los valores de precipitación de los rangos [1,20] mm. Sin embargo, en el caso de CFSR es el producto, de los tres evaluados, que mejor representa los datos del rango [5,20] mm. Finalmente, respecto al rango de mayor precipitación – i.e. por encima de 20 mm –, los tres productos obtuvieron valores muy similares a los observados.

De igual modo se analizaron los patrones mensuales de precipitación y temperatura, en este caso mediante se representaron gráficos de violín, que combinan diagramas de caja con la representación de la densidad kernel para observar de manera conjunta la distribución de los datos y la densidad de probabilidad; la distribución mensual de precipitaciones; y un gráfico de dispersión.

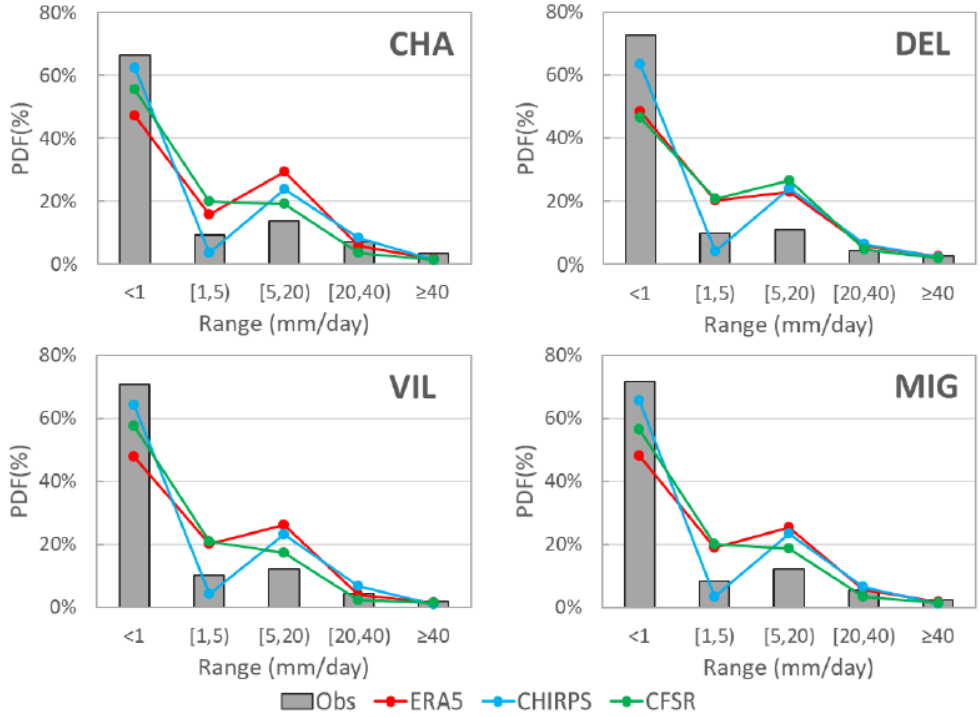

Figura 7. Distribución de la función de densidad de probabilidad por rangos para los productos satelitales y estaciones consideradas en el proyecto

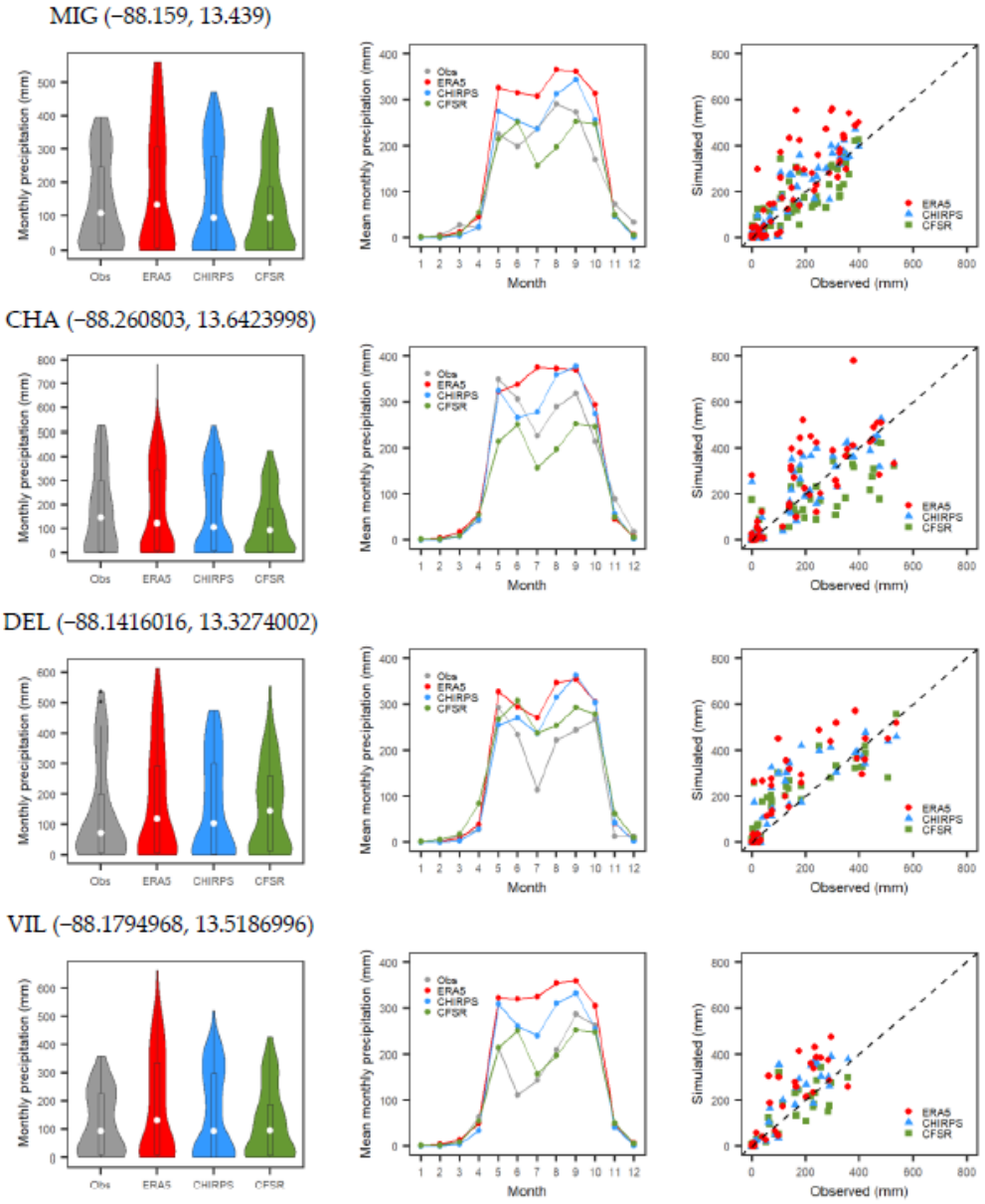

Figura 8. Comparación entre valores mensuales de precipitación de los productos ERA5, CHIRPS y CFSR y los valores observados, mediante gráficos de violín (izquierda), variaciones mensuales (centro) y dispersión (derecha)

Excepto para la estación MIG, los datos de CHIRPS fueron los que representaron de manera más precisa la distribución de los datos y la densidad de probabilidad, quedando ERA5, de manera genérica con valores más altos y una

mediana más alta en las cuatro estaciones evaluadas. Los tres productos identificaron de manera correcta los períodos húmedo (de Mayo a Octubre) y seco (de Noviembre a Abril), incluso la presencia de la característica canícula (MSD, por sus siglas en inglés), a excepción de ERA5 en los casos de CHA y VIL. Adicionalmente, cabe destacar la sobreestimación de valores máximos de los datos de ERA5 y CHIRPS en la época lluviosa; aunque según los gráficos de dispersión y los resultados del estadístico R^2, CHIRPS es el producto que mejor ajuste presenta entre los datos simulados y los observados.

Respecto a la temperatura, los productos comparados fueron ERA5, CHIRTS y CFSR con los valores observados en la estación MIG – por ser la única que contaba con registro de temperatura. ERA5 es el producto que presenta una mejor representación, destacando igualmente la sobreestimación generalizada de 2-3 C que presentan los datos de CHIRTS.

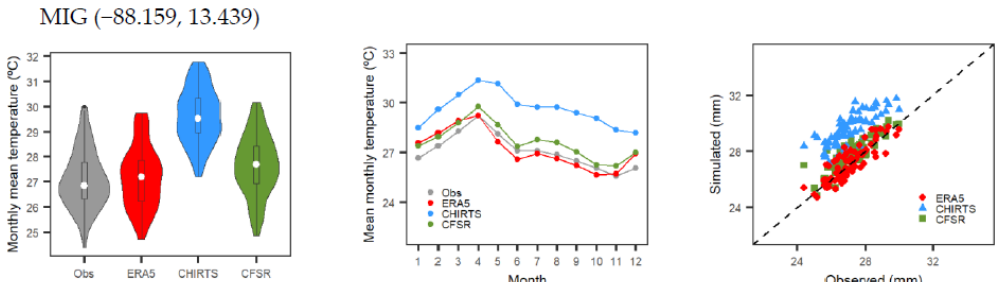

Figura 9. Comparación entre valores mensuales de temperatura de los productos ERA5, CHIRTS y CFSR y los valores observados en MIG, mediante gráficos de violín (izquierda), variaciones mensuales (centro) y dispersión (derecha)

IV.4.2.2 Comportamiento del modelo antes de la calibración

Según Peterson y Hamlett (1998), ante la falta de datos observados el comportamiento de un modelo sin calibrar es un buen indicador del comportamiento del modelo. De hecho, el modelo SWAT fue concebido para modelar cuencas rurales sin estaciones climáticas (Arnold et al., 1998).

En este sentido, se evaluó el comportamiento de los distintos productos de reanálisis con los parámetros por defecto del modelo SWAT, obteniendo los resultados de la siguiente figura.

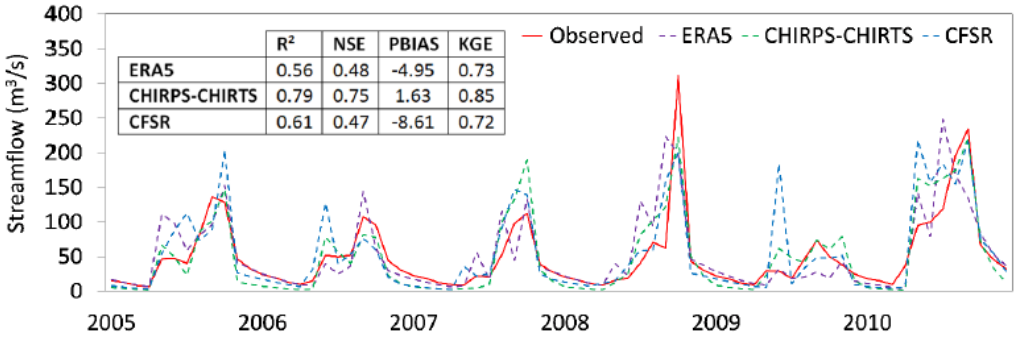

	R^2	NSE	PBIAS	KGE
ERA5	0.56	0.48	-4.95	0.73
CHIRPS-CHIRTS	0.79	0.75	1.63	0.85
CFSR	0.61	0.47	-8.61	0.72

Figura 10. Comportamiento de los modelos sin calibrar con datos de ERA5, CHIRPS-CHIRTS y CFSR con los caudales mensuales observados

De los estadísticos calculados y mostrados en la figura se observa como el mejor modelo es el realizado a partir de los datos de CFSR, lo cual es consistente con el análisis anterior en el que se observó que CFSR presentaba el menor sesgo. En cualquier caso, a escala mensual todos los productos analizados presentan resultados adecuados, tal y como indican los resultados de R^2. Por tanto, es esperable que tras la calibración de los parámetros más sensibles del modelo SWAT el comportamiento de los modelos sea aceptable.

IV.4.2.3 Calibración del modelo con la serie de caudales de GloFAS

El modelo se calibró usando la serie de caudales procedentes de reanálisis de imagen satelital GloFAS con los datos climáticos de los tres productos climáticos satelitales evaluados. Para ello se empleó el algoritmo SUFI-2 con ayuda del software SWATCUP, referido en el estudio anterior, para la optimización de doce parámetros hidrológicos del modelo SWAT.

Del estudio de sensibilidad de los parámetros llevado a cabo con 500 simulaciones del modelo SWAT para cada producto satelital se obtuvo que CN2, GWQMN y ESCO obtuvieron los menores valores del estadístico *p*-value en los tres modelos, lo cual es indicativo de que se trata de los parámetros más sensibles (Abbaspour et al., 2017).

CN2 es uno de los parámetros más sensibles puesto que directamente corrige la generación de escorrentía (Arnold et al., 2000; Marin et al., 2020), por lo que las reducciones obtenidas tras la calibración para corregir la sobreestimación de la precipitación que había sido detectada en la comparativa de las series, era

esperada. Por su parte, la reducción sufrida por ESCO se ajusta a los valores obtenidos en otros estudios en zonas tropicales (Blanco-Gómez et al., 2019; da Silva et al., 2018).

Las mayores discrepancias se presentaron en los parámetros relacionados con la recarga acuífera debido a la complejidad que presenta la alta permeabilidad y fisuración de los acuíferos volcánicos existentes en la región Centroamericana.

La siguiente tabla muestra los resultados del modelo SWAT correspondiente a cada producto satelital, obteniendo valores de los estadísticos compatibles con una representación razonablemente buena de los modelos, tanto para el periodo de calibración (2005-2008) como el de validación (2009-2010).

Parameter	Dataset					
	ERA5		CHIRPS-CHIRTS		CFSR	
	Calibration	Validation	Calibration	Validation	Calibration	Validation
R^2	0.88	0.82	0.78	0.78	0.82	0.60
NSE	0.87	0.81	0.77	0.70	0.81	0.54
PBIAS (%)	−11.68	−13.36	7.34	−30.70	−3.29	−32.31
KGE	0.86	0.81	0.85	0.65	0.88	0.47

Tabla 8. Comportamiento del modelo SWAT comparado con los datos de caudal de GloFAS

IV.4.2.4 Evaluación de la serie de caudales mensuales para varios escenarios

Finalmente, se compararon los modelos calibrados con los caudales de GloFAS con los de los caudales observados, obteniendo un ajuste aceptable en todos los casos aunque destacando entre todos ellos el modelo elaborado a partir de los datos climáticos de CHIRPT-CHIRTS.

Estos resultados demuestran la hipótesis de partida establecida en la que si

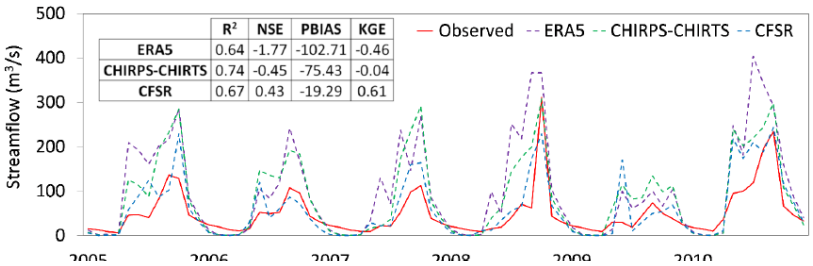

Figura 11. Comportamiento de los modelos calibrados con datos de ERA5, CHIRPS-CHIRTS y CFSR con los caudales mensuales observados

el producto de reanálisis de imagen satelital ERA5 presenta un ajuste adecuado, los caudales de GloFAS pueden ser empleados en la simulación hidrológica de cuencas con escasez de información hidrometeorológica a escala mensual.

Este hallazgo permitiría el empleo de modelos hidrológicos como SWAT para el estudio de los impactos derivados de los cambios en los usos del suelo o del clima. En esta línea Eini et al. (2019) estableció que cuando la precipitación satelital presentaba una buena correlación (R^2 mayor de 0.6) se obtenían resultados razonables en la simulación de los caudales, todo ello en una cuenca semiárida de Irán. Aunque estos resultados deben valorarse con cautela porque depende de la calidad del ajuste de GloFAS con los caudales observados. En este sentido, Harrigan et al. (2020) demostró que la calidad del ajuste de GloFAS aumenta sustancialmente con el tamaño de la cuenca, por lo que se recomienda que la metodología descrita en la presente investigación sea empleada en cuencas de gran tamaño.

IV.4.3 Impacto de los productos satelitales de precipitación en la simulación de caudales en cuencas con escasez de datos de aforo

En este caso se estudiaron cinco productos satelitales de precipitación – i.e. CFSR, MSWEPv1.1, PERSIANN-CDR, CMORPH y CHIRPSv2.0 – y se contaba con dos estaciones hidrometeorológicas – i.e. PS-1 y PS-2 – para poder evaluar el desempeño de los mismos.

IV.4.3.1 Comparación y evaluación de los productos satelitales de precipitación

Para evaluar la capacidad de detección de precipitaciones mayores a 1 mm/día se emplearon los siguientes índices:

- Probabilidad de detección (POD), establece la capacidad de los GP para capturar de manera precisa la precipitación observada.
- Ratio de falsa alarma (FAR), evalúa la fracción de alarmas falsas detectadas por los GP.
- Índice de éxito crítico (CSI), establece la habilidad de los GP para detectar eventos reales de precipitación. Está basado en POD y FAR.

- Puntuación de sesgo (BS), es la relación entre la precipitación estimada y la observada.

Todos ellos son adimensionales y sus valores oscilan entre [0,1] – a excepción de BS, donde los valores por encima de 1 son indicativos de que el producto de referencia sobrestima a la precipitación observada –, siendo 1 el valor óptimo de POD, CSI y BS; y 0 el valor óptimo de FAR.

La siguiente tabla muestra los valores obtenidos en las dos estaciones estudiadas.

Precipitation Dataset	PS-1 Station				PS-2 Station			
	POD	FAR	CSI	BS	POD	FAR	CSI	BS
CFSR	0.78	0.40	0.51	1.31	0.79	0.48	0.46	1.53
MSWEPv1.1	0.93	0.41	0.57	1.57	0.91	0.46	0.51	1.69
PERSIANN-CDR	0.93	0.41	0.57	1.58	0.92	0.47	0.51	1.74
CMORPH	0.80	0.31	0.59	1.16	0.79	0.30	0.59	1.13
CHIRPSv2.0	0.81	0.27	0.62	1.11	0.79	0.35	0.55	1.22

Tabla 9. Índices de detección para los distintos GP en las estaciones hidrometeorológicas de referencia de la cuenca

Se observa como MSWEPv1.1 y PERSIANN-CDR obtienen los valores más altos de POD, mientras que CMORPH y CHIRPSv2.0 obtienen los más cercanos a 0 en FAR. De igual modo se observa como los valores de CSI se mantienen alejados de 1 en todos los casos, oscilando entre [0.46,0.62]. Finalmente, el hecho de que todos los GP presenten valores superiores a 1 en BS es indicativo de que sobreestiman la precipitación observada. Por tanto, ninguno de los productos destaca por su habilidad en la detección de precipitación.

Seguidamente se realizó un análisis estadístico de la comparativa entre los cinco GP y la precipitación observada, tanto a escala diaria como mensual, así como de la precipitación media anual, en ambas estaciones de referencia.

Station/Precipitation Dataset	CC		RSR		ME		BIAS [1]		M_A (mm)
	Daily	Monthly	Daily	Monthly	Daily	Monthly	Daily	Monthly	
PS-1									
Gauge observations	-	-	-	-	-	-	-	-	1833.55
CFSR	0.32	0.84	1.05	0.60	−1.15	−34.64	−19.83	−19.83	1526.50
MSWEPv1.1	0.51	0.82	0.88	0.59	0.11	3.39	1.94	1.94	1867.66
PERSIANN-CDR	0.48	0.83	0.89	0.56	−0.03	−1.09	−0.58	−0.63	1813.24
CMORPH	0.50	0.87	0.96	0.50	−0.03	−0.96	−0.55	−0.55	1805.05
CHIRPSv2.0	0.55	0.89	0.88	0.50	0.50	15.05	8.62	8.62	2058.75
PS-2									
Gauge observations	-		-	-	-	-	-	-	1553.04
CFSR	0.27	0.86	1.10	0.52	−0.25	−5.38	−5.49	−5.38	1537.81
MSWEPv1.1	0.52	0.88	0.90	0.57	0.55	12.26	12.13	12.26	1752.64
PERSIANN-CDR	0.47	0.90	0.91	0.53	0.82	17.98	17.88	17.98	1827.73
CMORPH	0.47	0.84	1.03	0.60	0.02	0.85	0.73	0.85	1588.88
CHIRPSv2.0	0.53	0.94	0.91	0.45	0.61	13.48	13.34	13.48	1847.27

[1] Note: Differences between daily and monthly BIAS are due to gaps in gauge observation datasets. Only months with all daily data available were compared.

Tabla 10. Estadísticos diarios y mensuales de la comparativa entre GP y la precipitación observada en las estaciones PS-1 y PS-2

Se pudo comprobar que los estadísticos mensuales eran mucho mejores que los diarios y, nuevamente, que según el estadístico que se observe, el GP que mejor representa a los valores observados varía. En este sentido, se observa como para ambas estaciones los mejores valores de CC y RSR corresponden a CHIRPSv2.0, tanto a escala diaria como mensual; al igual que pasa con CMORPH para ME y BIAS; sin embargo, PERSIANN-CDR presenta unos valores adecuados en todos los estadísticos para PS-1, pero presenta las mayores discrepancias en ME y BIAS en PS-2; algo parecido pasa con CFSR en PS-1, aunque en este caso, sus resultados en PS-2 son menos relevantes. En cuanto a la precipitación media anual, nuevamente CMORPH destaca por su proximidad en la predicción en ambas estaciones.

Se evaluó la variación mensual de los distintos productos comparada con la observada en las estaciones de referencia, obteniendo los siguientes diagramas de caja para cada uno de los casos.

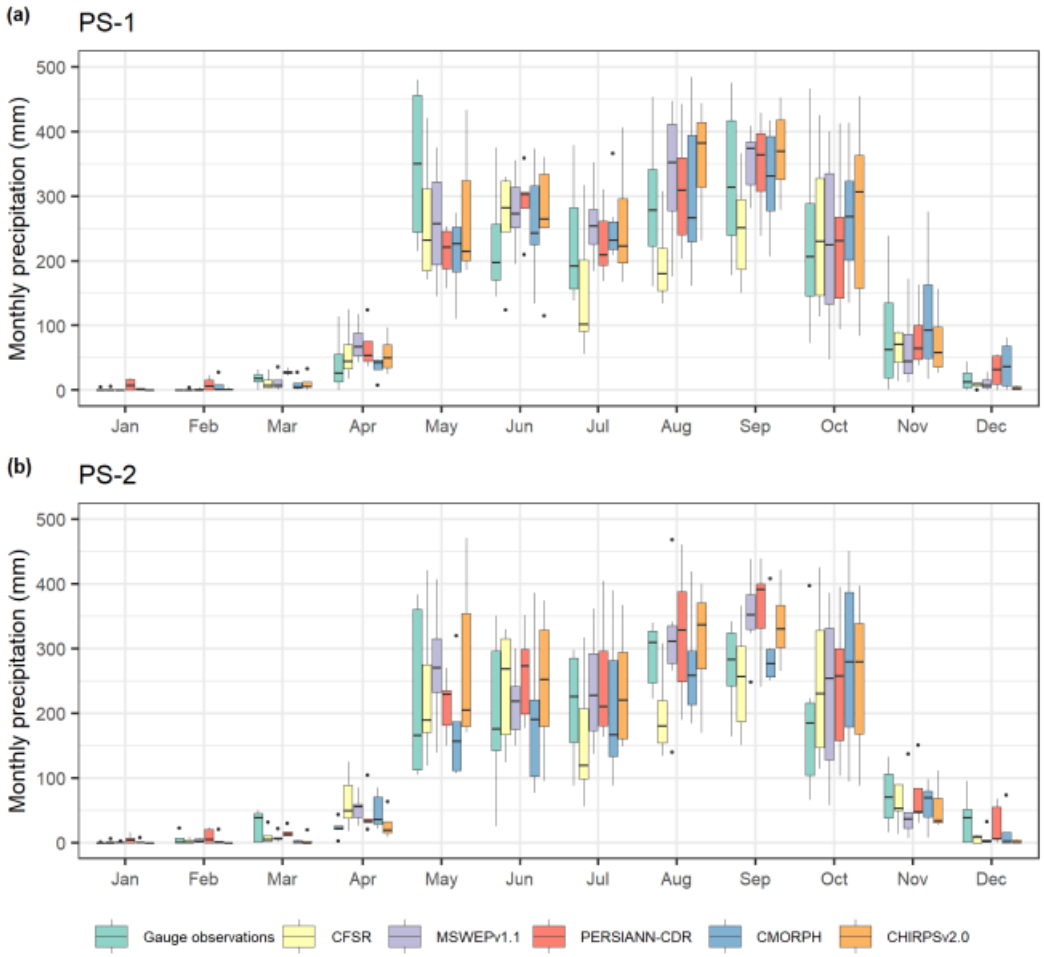

Figura 12. Comportamiento de los modelos calibrados con datos de ERA5, CHIRPS-CHIRTS y CFSR con los caudales mensuales observados

Los productos satelitales de precipitación presentan un comportamiento similar a los valores observados en ambas estaciones – lo cuál es consistente con los estadísticos obtenidos en el análisis anterior –, reflejando claramente los períodos húmedo (de Mayo a Octubre) y seco (de Noviembre a Abril) y la aparición de la canícula en mitad de la temporada lluviosa. Todos los productos, a excepción de CFSR sobreestiman de manera general el valor medio mensual de precipitación durante la temporada húmeda.

Por otro lado, se evaluó la función de densidad acumulada (CDF, por sus siglas en inglés) de la precipitación diaria en las dos estaciones de referencia,

pudiendo comparar seis series de datos en cada una de ellas – i.e. los 5 GP y la precipitación observada. Para ello, se categorizó la precipitación conforme a los criterios establecidos por la Organización Meteorológica Mundial (WMO, 2012a).

Type of Event	Daily Rainfall Intensity (mm/Day)
Tiny rain	<1
Light rain	[1, 2)
Low modeerate rain	[2, 5)
High moderate rain	[5, 10)
Heavy rain	[10, 50)
Violent rain	≥50

Tabla 11. Clasificación de eventos de precipitación en función de su intensidad diaria (DRI, mm/día)

En cuanto a la probabilidad de encontrar días secos (DRI = 0 mm/día) CHIRPSv2.0 obtuvo resultados similares a los de las dos estaciones. CMORPH obtuvo los mejores ajustes con ambas estaciones por encima de 1 mm/día. Para lluvias moderadas y fuertes, [2,50) mm/día, los productos PERSIANN-CDR, CHIRPSv2.0 y MSWEPv1.1 sobreestiman la precipitación. Por su parte, el producto CFSR no sigue un patrón de precipitación comparable con los de las estaciones en toda la serie.

Finalmente, se comparó la variabilidad anual de los distintos productos respecto a lo observado en las estaciones, pudiendo concluir que CMORPH es el producto que más se ajustaba a lo observado en ambas estaciones y que CFSR el que menor precipitación presentaba.

IV.4.3.2 Comportamiento de los productos satelitales de precipitación en la simulación de caudales

En la segunda etapa de la investigación se evaluó la respuesta del modelo hidrológico SWAT para simular los caudales en las estaciones de aforos SG-1, SG-2 y SG-3 empleando como precipitación de entrada tanto la registrada en las estaciones hidrometeorológicas de la cuenca como los cinco productos satelitales de precipitación estudiados en la presente tesis.

En primera instancia se ajustaron los parámetros de entrada del modelo hidrológico con los registros de precipitación de las estaciones y se evaluó el comportamiento de los modelos así calibrados empleando las precipitaciones de

los distintos GP. El resultado en cada una de las estaciones de aforo de referencia se muestra en la siguiente tabla.

Stream Gauge/Criteria	CFSR	MSWEPv1.1	PERSIANN-CDR	CMORPH	CHIRPSv2.0
			SG-1 calibration (validation)		
R^2	0.54 (0.68)	0.75 (0.65)	0.76 (0.72)	0.63 (0.60)	0.80 (0.82)
NSE	0.39 (0.63)	0.67 (0.64)	0.69 (0.71)	0.36 (0.58)	0.51 (0.80)
PBIAS	31.97 (25.56)	11.92 (11.57)	18.71 (6.03)	1.70 (0.78)	−10.49 (−6.30)
RSR	0.78 (0.61)	0.57 (0.60)	0.56 (0.54)	0.80 (0.65)	0.70 (0.45)
			SG-2 calibration (validation)		
R^2	0.60 (0.69)	0.77 (0.66)	0.78 (0.70)	0.63 (0.60)	0.80 (0.82)
NSE	0.42 (0.62)	0.67 (0.63)	0.68 (0.68)	0.34 (0.58)	0.50 (0.80)
PBIAS	33.99 (26.73)	15.49 (16.46)	24.43 (12.31)	8.24 (7.21)	−5.06 (−3.20)
RSR	0.76 (0.62)	0.57 (0.61)	0.57 (0.56)	0.81 (0.65)	0.70 (0.45)
			SG-3 calibration (validation)		
R^2	0.62 (0.67)	0.78 (0.65)	0.79 (0.71)	0.65 (0.59)	0.82 (0.81)
NSE	0.44 (0.61)	0.67 (0.63)	0.68 (0.69)	0.34 (0.57)	0.53 (0.79)
PBIAS	34.19 (25.79)	16.08 (16.58)	25.56 (12.63)	9.53 (7.46)	−3.47 (−3.24)
RSR	0.75 (0.63)	0.57 (0.61)	0.57 (0.56)	0.82 (0.66)	0.69 (0.46)

Tabla 12. Resultados del modelo SWAT calibrado con las estaciones hidrometeorológicas en las tres estaciones de aforos (SG-i) para los distintos GP evaluados

De acuerdo a los criterios de evaluación de modelos establecidos en Moriasi et al.(2007) los modelos simulados con la precipitación de MSWEPv1.1, PERSIANN-CDR y CHIRPSv2.0 fueron satisfactorios – a excepción de PERSIANN-CDR en la estación SG-3 por obtener un PBIAS superior al 25% en la fase de calibración. Mientras que los modelos simulados con CFSR y CMORPH no satisficieron las condiciones en términos de NSE y RSR – todo ello a pesar de los buenos resultados que CMORPH presentó en la fase de comparación de los datos con los de las estaciones de la cuenca.

Posteriormente se llevó a cabo una segunda evaluación de los modelos hidrológicos, ajustando en este caso los parámetros para cada uno de los GP. En términos generales, las simulaciones mejoraron en términos de R^2, NSE, PBIAS y RSR respecto a las obtenidas con los parámetros calibrados para las estaciones hidrometeorológicas de la cuenca – estos resultados son consistentes con los obtenidos en Bitew et al. (2012) en cuencas montañosas de Etiopia. Los estadísticos obtenidos se presentan en la siguiente tabla.

Stream Gauge/Criteria	Precipitation Gauge Data	CFSR	MSWEPv1.1	PERSIANN-CDR	CMORPH	CHIRPSv2.0
			SG-1 calibration (validation)			
R^2	0.73 (0.61)	0.68 (0.79)	0.76 (0.59)	0.83 (0.71)	0.58 (0.62)	0.82 (0.90)
NSE	0.70 (0.60)	0.62 (0.77)	0.71 (0.57)	0.82 (0.69)	0.56 (0.57)	0.79 (0.87)
PBIAS	−7.48 (10.37)	−1.03 (−6.41)	−16.63 (−15.10)	−4.76 (−13.66)	−13.36 (−13.58)	−14.52 (−12.15)
RSR	0.55 (0.63)	0.62 (0.48)	0.54 (0.66)	0.43 (0.56)	0.67 (0.66)	0.46 (0.37)
			SG-2 calibration (validation)			
R^2	0.77 (0.63)	0.74 (0.79)	0.78 (0.57)	0.85 (0.70)	0.60 (0.62)	0.84 (0.91)
NSE	0.76 (0.61)	0.67 (0.76)	0.72 (0.56)	0.84 (0.69)	0.60 (0.58)	0.83 (0.88)
PBIAS	1.13 (16.85)	0.20 (−6.26)	−13.82 (−11.52)	1.03 (−7.75)	−5.60 (−7.37)	−8.50 (−12.53)
RSR	0.49 (0.63)	0.58 (0.49)	0.53 (0.66)	0.39 (0.55)	0.63 (0.65)	0.41 (0.35)
			SG-3 calibration (validation)			
R^2	0.77 (0.62)	0.76 (0.78)	0.78 (0.57)	0.85 (0.71)	0.62 (0.61)	0.85 (0.91)
NSE	0.76 (0.59)	0.67 (0.73)	0.72 (0.56)	0.84 (0.70)	0.62 (0.58)	0.84 (0.88)
PBIAS	3.11 (17.34)	−0.10 (−8.11)	−13.59 (−12.31)	2.14 (−7.67)	−3.99 (−7.20)	−6.39 (−14.24)
RSR	0.49 (0.64)	0.57 (0.52)	0.53 (0.67)	0.39 (0.54)	0.62 (0.65)	0.40 (0.34)

Tabla 13. Resultados del modelo SWAT calibrado para cada GP en las tres estaciones de aforos (SG-i)

Los modelos a escala mensual simulados a partir de las precipitaciones de PERSIANN-CDR y CHIRPSv2.0 obtuvieron un comportamiento excelente – i.e. NSE > 0.75 – mejorando incluso los realizados a partir de los datos de las estaciones hidrometeorológicas. En cualquier caso, todos los modelos evaluados obtuvieron un comportamiento satisfactorio – i.e. NSE > 0.5, PBIAS < ±25% y RSR < 0.7, según Jang, Engel y Ryu (2018) – tanto en la fase de calibración (2005-2007) como en la de validación (2008-2009).

Analizando los resultados del balance hídrico, se pudo comprobar como los resultados de CHIRPSv2.0 no consideraban la recarga del acuífero, lo cual es inconsistente con el tipo de terreno existente en la cuenca. Por tanto, PERSIANN-CDR resultó el producto más apropiado para llevar a cabo la simulación de caudales en la cuenca del río GSM.

Por último, cabe destacar los motivos por los que los productos satelitales son capaces de reproducir mejor la hidrología de una cuenca que los propios registros de precipitación de la misma (Senent-Aparicio et al., 2018b): (1) los datos observados eran escasos y con pocos registros en la cuenca; (2) es posible que los equipos no estén recibiendo un mantenimiento adecuado y, en consecuencia, no estén funcionando debidamente; y (3) hay diferencias significativas entre la precipitación puntual y la distribuida en una cuenca, por lo que ante la existencia de pocos registros puede ser conveniente el empleo de un GP distribuido.

IV.5 CONCLUSIONES Y LÍNEAS DE INVESTIGACIÓN FUTURA

El uso del modelo SWAT en la modelación hidrológica está ampliamente extendido entre la comunidad científica y sus resultados son relevantes para la toma de decisiones en la gestión de los recursos hídricos, especialmente en contextos en los que el cambio climático genera incertidumbres en cuanto a la capacidad de producción de los cultivos, el abastecimiento a poblaciones o la sostenibilidad de los ecosistemas medioambientalmente protegidos. Del mismo modo, el uso de datos climáticos provenientes de reanálisis de imágenes satelitales y la extracción de datos de los GCM permite elaborar modelos para la evaluación de recursos hídricos en cuencas con escasa cobertura de estaciones meteorológicas y foronómicas.

Se ha empleado la República de El Salvador como caso de estudio en la presente tesis, debido a un convenio de colaboración con el Ministerio de Medio Ambiente y Recursos Naturales (MARN) en el que se ponía a disposición de la investigación la información hidrometeorológica existente en las áreas de estudio seleccionadas – i.e. cuencas de los ríos Guajoyo (GRB) y Grande de San Miguel (GSM).

La **Publicación 1** evalúa el impacto del cambio climático en la gestión de recursos hídricos y sequías en la cuenca del río GRB. Se trata de un entorno de estudio con distintas figuras de protección medioambiental y necesidad de uso del agua para el abastecimiento de las comunidades locales y el desarrollo de actividades primarias como el cultivo de café.

Para ello, se tuvieron en cuenta las proyecciones futuras de cinco GCM – i.e. GFDL-ESM2M, HadGEM2-ES, IPSL-CM5A-LR, MIROC y NoerESM1-M – y se seleccionó el modelo de circulación Global que representa de mejor manera los datos históricos, HadGEM2-ES, en el entorno de estudio. Los escenarios de cambio climático considerados fueron RCP 4.5 y RCP 8.5.

El modelo SWAT fue calibrado con éxito a pesar de la escasez de datos en la cuenca, prevenientes de la estación hidrometeorológica del lago Güija y de la medición de aforos en el desagüe de la cuenca – i.e. Piedra-Cargada – y se realizó una comparativa entre el modelo a partir de datos históricos (1975-2004) y las proyecciones futuras (2040-2069 y 2070-2099). Se pudo observar un decremento en la precipitación anual y un aumento de las temperaturas, más acusados en las

proyecciones de final de siglo y para los escenarios de emisiones más severos. Del mismo modo, la disponibilidad de agua va a verse reducida, pudiendo comprobarse que las sequías futuras serán más pronunciadas que las actuales, presentando una mayor intensidad y duración.

La **Publicación 2** pone a prueba el potencial que los caudales provenientes de reanálisis de imagen satelital del producto GloFAS tienen para la calibración de modelos hidrológicos en regiones con escasez de información hidrometeorológica y foronómica, empleando para ello el caso de estudio de la cuenca del río GSM en El Salvador.

GloFAS emplea los datos climáticos provenientes del producto satelital de precipitación ERA5 para la determinación de caudales a escala Global. Sin embargo, el presente trabajo parte de la premisa de que emplear GloFAS en la calibración es adecuado siempre que exista un buen ajuste estadístico entre las variables de precipitación y temperatura provenientes de reanálisis satelital y los datos climáticos observados, en línea con lo establecido por Eini et al. (2019); por lo que de manera adicional a los datos climáticos provenientes de ERA5, se evaluaron los de CHIRPS-CHIRTS y CFSR.

Se pudieron extraer las siguientes conclusiones: (1) De la evaluación estadística de los datos se observa que CHIRPS es el que mejor reproduce la precipitación observada, a pesar de la sobreestimación de los valores de precipitación del rango [5,20] mm; (2) CHIRPS es el que presenta la mejor capacidad de detección de los sucesos de precipitación, presentando los tres productos capacidad suficiente de detección; (3) En cuanto a temperatura, CHIRTS sobreestima los valores de manera generalizada en 2-3 °C, presentando el resto de productos una correlación excelente con los datos observados; (4) Los modelos calibrados con los caudales provenientes de GloFAS presentaron un comportamiento aceptable, independientemente del origen de los datos climáticos.

La sobreestimación del número de eventos de precipitación y el volumen de precipitación puede ser debida a la habilidad que presentan los productos satelitales de detectar los eventos de mayor altura de precipitación, frente a la dificultad relativa para discernir la producción en los eventos de menor entidad – i.e. [5,20] mm. Adicionalmente, la corrección estadística del sesgo empleada

normalmente para corregir los datos satelitales eleva los valores de precipitación detectada para compensar el volumen de los eventos no identificados (Tian et al., 2007).

De manera general, se observa como los productos satelitales de precipitación y temperatura son una solución para la evaluación de recursos hídricos con escasez de datos climáticos. De igual modo, se subraya el potencial de los caudales provenientes de GloFAS para la calibración de modelos en cuencas no aforadas.

Se establecen como líneas de investigación futura el uso de otras variables hidrológicas provenientes de reanálisis satelital, tales como la evapotranspiración; el uso de otros modelos hidrológicos distintos a SWAT que puedan contrastar la validez de la hipótesis de partida – i.e. el producto GloFAS es adecuado para la calibración de modelos hidrológicos siempre y cuando exista correlación entre los valores climáticos observados y los provenientes de reanálisis –; en caso de existencia de registros continuos de caudal aforado, la evaluación de GloFAS a escala diaria o infradiaria.

Finalmente, la **Publicación 3** concluye que la precisión espacio-temporal de la precipitación es crucial para la fiabilidad de los procesos hidrológicos y que el estudio de aportaciones en los ríos de El Salvador es complejo por la falta de estos datos. En este estudio se evalúa la capacidad de cinco productos satelitales de precipitación para simular de manera fiable los caudales en la cuenca del río GSM.

Del estudio realizado se pudieron extraer las siguientes conclusiones:

- Respecto de la comparativa entre los GP no se puede asegurar que alguno de los productos destaque en la representación de la lluvia observada.
- Los modelos hidrológicos alimentados con los cinco GP obtuvieron resultados aceptables y arrojaron información realista de los caudales.
- Los modelos alimentados con la precipitación de PERSIANN-CDR y de CHIRPSv2.0 obtuvieron mejores resultados que los alimentados con la precipitación observada en las estaciones hidrometeorológicas de la cuenca.

- El producto más estable y adecuado para la simulación de caudales fue PERSIANN-CDR.
- Los productos satelitales de precipitación demuestran un potencial uso en la simulación hidrológica, aunque los resultados de modelación varían sustancialmente entre los distintos productos analizados.
- Los modelos se comportan mejor cuando son calibrados con los datos de precipitación del GP que se use en lugar de con los datos de precipitación observada en las estaciones de la cuenca.

A pesar de las conclusiones satisfactorias del presente estudio, es recomendable evaluar hidrológicamente los resultados de estos u otros productos satelitales de precipitación antes de su uso. De igual modo, en futuros trabajos se puede evaluar el uso de nuevos productos GP, así como la capacidad que tendrían para la simulación de caudales con escalas diarias o infradiarias.

Se trata del primer estudio realizado en El Salvador sobre la precisión de los productos satelitales de precipitación en la simulación hidrológica, y queda demostrada la capacidad de replicación en otras áreas que, de manera similar, tengan falta de datos de precipitación. De igual modo, se demuestra el potencial de uso de estos productos en los estudios de gestión de agua y cambio climático.

V – REFERENCIAS BIBLIOGRÁFICAS

V- REFERENCIAS BIBLIOGRAFICAS

Abbaspour, K.C., Johnson, C.A. & van Genuchten, M.Th., 2004. Estimating uncertain flow and transport parameters using a sequential uncertainty fitting procedure. J. Vadouse Zone 3 (4), 1340–1352.

Abbaspour, K.C., 2007. User Manual for SWAT-Cup, SWAT Calibration and Uncertainty Analysis Programs; Swiss Federal Institute of Aquatic Science and Technology, Eawag: Duebendorf, Switzerland, 2007.

Abbaspour, K.C., Vejdani, M. & Haghighat, S., 2007. SWAT–CUP calibration and uncertainty programs for SWAT. In Proceedings of the Modsim 2007: International Congress on Modelling and Simulation, Christchurch, New Zealand, 3–8 December 2007; pp. 1603–1609.

Abbaspour, K.C., Yang, J., Maximov, I., Siber, R., Bogner, K., Mieleitner, J., Zobrist, J. & Srinivasan, R., 2007. Modelling hydrology and water quality in the pre-alpine/alpine Thur watershed using SWAT. J. Hydrol. 2007, 333, 413–430.

Abbaspour, K.C., 2012. SWAT Calibration and Uncertainty Program—A User Manual. SWAT-CUP-2012, 2012th ed.; Swiss Federal Institute of Aquatic Science and Technology: Dubendorf, Switzerland, 2012.

Abbaspour, K.C., Rouholahnejad, E., Vaghefi, S., Srinivasan, R., Yang, H. & Kløve, B., 2015. A continental-scale hydrology and water quality model for Europe: Calibration and uncertainty of a high-resolution large-scale SWAT model. J. Hydrol. 2015, 524, 733–752. https://doi.org/10.1016/j.jhydrol.2015.03.027.

Abbaspour, K.C., Vaghefi, S.A., Yang, H. & Srinivasan, R., 2019. Global soil, landuse, evapotranspiration, historical and future weather databases for SWAT Applications. Sci. Data 2019, 6, 1–11.

Abbott, M.B., Bathurst, J.C., Cunge, J.A. & O´Conell, P.E., 1986. An introduction to the European Hydrological System-Systeme Hydrologique European 'SHE' 1: Hystory and Philosophy of a Physically-Based Distributed Modeling System. J. Hydrol. 87:45-59.

Aguilar, M.Y., Pacheco, T.R., Tobar, J.M. & Quiñónez, J.C., 2009. Vulnerability and adaptation to climate change of rural inhabitants in the central coastal plain of El Salvador. Clim. Res. 2009, 40, 187–198.

Ahmed, K.F., Wang, G.L., Silander, J., Wilson, A.M., Allen, J.M., Horton, R. Anyah, R., 2013. Statistical downscaling and bias correction of climate model outputs for climate change impact assessment in the US northeast. Glob. Planet. Change 100, 320-332.

Ahmed, K., Sachindra, D.A., Shahid, S., Demirel, M.C. & Chung, E.S., 2019. Selection of multi-model ensemble of GCMs for the simulation of precipitation based on spatial assessment metrics. Hydrol. Earth Syst. Sci. 2019, 23, 4803–4824, https://doi.org/10.5194/hess-23-4803-2019

Akoko, G., Kato, T. & Tu, L.H., 2020. Evaluation of Irrigation Water Resources Availability and Climate Change Impacts – A Case Study of Mwea Irrigation Scheme, Kenya. Water 2020, 12, 2330. https://doi.org/10.3390/w12092330.

Alemayehu, T., van Griensven, A. & Bauwens, W., 2016. Evaluating CFSR and WATCH data as input to swat for the estimation of the potential evapotranspiration in a data–scarce Eastern–African catchment. J. Hydrol. Eng. 2016, 21, 16.

Alfieri, L., Lorini, V., Hirpa, F.A., Harrigan, S., Zsoter, E., Prudhomme, C. & Salamon, P., 2020. A global streamflow reanalysis for 1980–2018. J. Hydrol. X 2020, 6, 100049.

Allen, R.G., Pereira, L.S., Raes, D. & Smith, M., 1998. Crop Evapotranspiration: Guidelines for Computing Crop Water Requirements; Food and Agriculture Organization of the United Nations: Rome, Italy, 1998.

Arnold, J.G., Allen, P.M., & Bernhardt, G., 1993. A comprehensive surface-groundwater flow model. Journal of hydrology, 142(1-4), 47-69. https://doi.org/10.1016/0022-1694(93)90004-S.

Arnold, J.G., Srinivasan, R., Muttiah, R.S. & Williams, J.R., 1998. Large area hydrologic modeling and assessment part I: Model development. JAWRA J. Am. Water Resour. Assoc. 1998, 34, 73–89.

Arnold, J., Muttiah, R., Srinivasan, R. & Allen, P., 2000. Regional estimation of base flow and groundwater recharge in the Upper Mississippi river basin. J. Hydrol. 2000, 227, 21–40.

Arnold, J.G., Kiniry, J.R., Srinivasan, R., Williams, J.R., Haney, E.B. & Neitsch, S.L., 2012a. Soil & Water Assessment Tool—Input/Output Documentation; Version 2012; TexasWater Resources Institute: College Station, TX, USA, 2012; p. 650. Available online: https://swat.tamu.edu/docs/ (accessed on 12 September 2021).

Arnold, J.G., Moriasi, D.N., Gassman, P.W., Abbaspour, K.C., White, M.J., Srinivasan, R., Santhi, C., Harmel, R.D., van Griensven, A., Van Liew, M.W., et al., 2012b. SWAT: Model Use, Calibration, and Validation. Trans. ASABE 2012, 55, 1491–1508.

Ashouri, H., Hsu, K.H., Sorooshian, S., Braithwaite, D.K., Knapp, K.R., Cecil, L.D., Nelson, B.R. & Prat, O.P., 2015. PERSIANN-CDR: Daily precipitation climate data record from multisatellite observations for hydrological and climate studies. Bull. Amer. Meteor. Soc., https://doi.org/10.1175/BAMS-D-13-00068.1.

ASTER Global Digital Elevation Map. Available online: https://asterweb.jpl.nasa.gov/gdem.asp (accessed on 12 September 2021).

Aznarez, C., Jimeno-Sáez, P., López-Ballesteros, A., Pacheco, J. & Senent-Aparicio, J., 2021. Analysing the impact of climate change on hydrological ecosystem services in Laguna del Sauce (Uruguay) using the SWAT model and remote sensing data. Remote Sens. 2021, 13, 2014.

Baez-Villanueva, O.M., Zambrano-Bigiarini, M., Ribbe, L., Nauditt, A., Giraldo-Osorio, J.D. & Thinh, N.X., 2018. Temporal and Spatial Evaluation of Satellite Rainfall Estimates over Different Regions in Latin-America. Atmos. Res. 2018, 213, 34–50.

Balsamo, G., Pappenberger, F., Dutra, E., Viterbo, P. & Hurk, B.V.D., 2011. A revised land hydrology in the ECMWF model: A step towards daily water flux prediction in a fully-closed water cycle. Hydrol. Process. 2011, 25, 1046–1054.

Beck, H.E., van Dijk, A.I.J.M., Levizzani, V., Schellekens,J., Miralles, D.G., Martens, B. & de Roo, A., 2017. MSWEP: 3-hourly 0.25◦ global gridded

precipitation (1979–2015) by merging gauge, satellite, and reanalysis data, Hydrol. Earth Syst. Sci.,21, 589–615, https://doi.org/10.5194/hess-21-589-2017.

Beven, K.J. & Kirkby, M.J., 1979. A physically-based variable contributing area model of basin hydrology. Hydrol. Sci. Bull. 24(1):43-69.

Bhatta, B., Shrestha, S., Shrestha, P.K. & Talchabhadel, R., 2019. Evaluation and application of a SWAT model to assess the climate change impact on the hydrology of the Himalayan River Basin. Catena 2019, 181, 104082.

Bitew, M.M. & Gebremichael, M., 2011. Evaluation of satellite rainfall products through hydrologic simulation in a fully distributed hydrologic model. Water Resour. Res. 2011, 47, W06526.

Bitew, M.M., Gebremichael, M., Ghebremichael, L.T. & Bayissa, Y.A., 2012. Evaluation of High-Resolution Satellite Rainfall Products through Streamflow Simulation in a Hydrological Modeling of a Small Mountainous Watershed in Ethiopia. J. Hydrometeorol. 2012, 13, 338–350.

Blacutt, L.A., Herdies, D.L., de Gonçalves, L.G.G., Vila, D.A. & Andrade, M., 2015. Precipitation Comparison for the CFSR, MERRA, TRMM3B42 and Combined Scheme Datasets in Bolivia. Atmos. Res. 2015, 163, 117–131.

Blanco-Gómez, P., Jimeno-Sáez, P., Senent-Aparicio, J. & Pérez-Sánchez, J., 2019. Impact of climate change on water balance components and droughts in the Guajoyo River Basin (El Salvador). Water 2019, 11, 2360, https://doi.org/10.3390/w11112360.

Brighenti, T.M., Bonumá, N.B., Grison, F., Mota, A.D.A., Kobiyama, M. & Chaffe, P.L.B., 2019. Two calibration methods for modeling streamflow and suspended sediment with the SWAT model. Ecol. Eng. 2019, 127, 103–113.

Burek, P., van der Knijff, J.M., & de Roo, A.P.J.D., 2013. LISFLOOD – Distributed Water Balance and Flood Simulation Model – Revised User Manual, Publications Office of the European Union, https://doi.org/10.2788/24719.

Burnash, R.J.C., Ferral, R.L. & McGuire. R.A., 1973. A general streamflow simulation system – Conceptual modelling for digital computers. Report by the Joint Federal State River Forecasts Center, Sacramento, California.

Cabezas, F., 2015. Análisis estructural de modelos hidrológicos y de sistemas de recursos hídricos en zonas semiáridas. Tesis Doctoral. Univ. Murcia. pp. 290. Disponible en: http://hdl.handle.net/10201/48218.

Campos, M., Herrador, D., Manuel, C. & McCall, M.K., 2013. Estrategias de adaptación al cambio climático en dos comunidades rurales de México y El Salvador. BAGE 2013, 61, 329–349.

CEPAL, 2010. La Economía del Cambio Climático en Centroamérica—Síntesis 2010; Comisión Económica para América Latina y El Caribe (CEPAL): Naciones Unidas, México, 2010.

Centella-Artola, A., Bezanilla-Morlot, A., Taylor, M.A., Herrera, D.A., Martinez-Castro, D., Gouirand, I., Sierra-Lorenzo, M., Vichot-Llano, A., Stephenson, T., Fonseca, C., Campbell, J. & Alpizar, M., 2020. Evaluation of Sixteen Gridded Precipitation Datasets over the Caribbean Region Using Gauge Observations. Atmosphere. 2020; 11(12):1334. https://doi.org/10.3390/atmos11121334

Čerkasova, N., Umgiesser, G. & Ertürk, A., 2019. Assessing climate change impacts on streamflow, sediment and nutrient loadings of the Minija River (Lithuania): A hillslope watershed discretization application with high–resolution spatial inputs. Water 2019, 11, 676.

Chattopadhyay, S. & Jha, M.K., 2016. Hydrological response due to projected climate variability in Haw River watershed, North Carolina, USA. Hydrol. Sci. J. 2016, 61, 495–506.

Chen, J., Brissette, F.P., Chaumont, D. & Braun, M., 2013. Performance and uncertainty evaluation of empirical downscaling methods in quantifying the climate change impacts on hydrology over two North American river basins. J. Hydrol. 2013, 479, 200–214.

Conde–Álvarez, C. & Saldaña–Zorrilla, O., 2007. Cambio climático en América Latina y el Caribe: Impactos, vulnerabilidad y adaptación. Revista Ambiente y Desarrollo 2007, 23, 23–30.

da Silva, R.M., Dantas, J.C., Beltrão, J.D.A. & Santos, C.A.G., 2018. Hydrological simulation in a tropical humid basin in the Cerrado biome using the SWAT model. Hydrol. Res. 2018, 49, 908–923.

Darbandsari, P. & Coulibaly, P., 2020. Inter-comparison of lumped hydrological models in data-scarce watersheds using different precipitation forcing data sets: Case study of Northern Ontario, Canada. J. Hydrol. Reg. Stud. 2020, 31, 100730.

Deng, P.X., Zhang, M.Y., Bing, J.P., Jia, J.W. & Zhang, D.D., 2019. Evaluation of the GSMaP_Gauge products using rain gauge observations and SWAT model in the Upper Hanjiang River Basin. Atmos. Res. 2019, 219, 153–165

Dhanesh, Y., Bindhu, V.M., Senent-Aparicio, J., Brighenti, T.M., Ayana, E., Smitha, P.S., Fei, C. & Srinivasan, R. A., 2020. Comparative Evaluation of the Performance of CHIRPS and CFSR Data for Different Climate Zones Using the SWAT Model. Remote Sens. 2020, 12, 3088.

Dile, Y.T. & Srinivasan, R., 2014. Evaluation of CFSR climate data for hydrologic prediction in data-scarce watersheds: An application in the Blue Nile River Basin. JAWRA J. Am. Water Resour. Assoc. 2014, 50, 1226–1241.

Dile, Y.T., Daggupati, P., George, C., Srinivasan, R. & Arnold, J., 2016. Introducing a New Open Source GIS User Interface for the SWAT Model. Environ. Modell. Softw. 2016, 85, 129–138.

Dinh, K.D., Anh, T.N., Nguyen, N.Y., Bui, D.D. & Srinivasan, R., 2020. Evaluation of grid-based rainfall products and water balances over the Mekong River basin. Remote Sens. 2020, 12, 1858.

Dinku, T., Ruiz, F., Connor, S.J. & Ceccato, P., 2010. Validation and Intercomparison of Satellite Rainfall Estimates over Colombia. J. Appl. Meteorol. Climatol. 2010, 49, 1004–1014.

Duan, Z., Tuo, Y., Liu, J., Gao, H., Song, X., Zhang, Z., Yang, L. & Mekonnen, D.F., 2019. Hydrological Evaluation of Open-Access Precipitation and Air Temperature Datasets Using SWAT in a Poorly Gauged Basin in Ethiopia. J. Hydrol. 2019, 569, 612–626.

Dufresne, JL., Foujols, MA., Denvil, S. et al. Climate change projections using the IPSL-CM5 Earth System Model: from CMIP3 to CMIP5. Clim Dyn 40, 2123–2165 (2013). https://doi.org/10.1007/s00382-012-1636-1.

Dunne, J.P., John, J.G., Adcroft, A.J., Griffies, S.M., Hallberg, R.W., Shevliakova, E., Stouffer, R.J., Cooke, W., Dunne, K.A., Harrison, M.J., Krasting,

J.P., Malyshev, S.L., Milly, P.C.D., Phillips, P.J., Sentman, L.T., Samuels, B.L., Spelman, M.J., Winton, M., Wittenberg, A.T. and Zadeh, N., 2012. GFDL's ESM2 Global Coupled Climate–Carbon Earth System Models. Part I: Physical Formulation and Baseline Simulation Characteristics. Journal of Climate, Vol. 25:19, 6646-6665, https://doi.org/10.1175/JCLI-D-11-00560.1.

Dunne, J.P., John, J.G., Shevliakova, E., Stouffer, R.J., Krasting, J.P., Malyshev, S.L., Milly, P.C.D., Sentman, L.T., Adcroft, A.J., Cooke, W., Dunne, K.A., Griffies, S.M., Hallberg, R.W., Harrison, M.J., Levy, H., Wittenberg, A.T., Phillips, P.J. & Zadeh, N., 2013. GFDL's ESM2 Global Coupled Climate–Carbon Earth System Models. Part II: Carbon System Formulation and Baseline Simulation Characteristics. Journal of Climate, Vol. 26:7, 2247-2267, https://doi.org/10.1175/JCLI-D-12-00150.1.

Dutta, P. & Sarma, A.K., 2020. Hydrological modeling as a tool for water resources management of the data-scarce Brahmaputra basin. J. Water Clim. Change 2020, 12, 152–165.

Eini, M.R., Javadi, S., Delavar, M., Monteiro, J. & Darand, M., 2019. High accuracy of precipitation reanalyses resulted in good river discharge simulations in a semi-arid basin. Ecol. Eng. 2019, 131, 107–119.

Elgamal, A., Reggiani, P. & Jonoski, A., 2017. Impact Analysis of Satellite Rainfall Products on Flow Simulations in the Magdalena River Basin, Colombia. J. Hydrol. Reg. Stud. 2017, 9, 85–103.

Emami, F. & Koch, M., 2019. Modeling the impact of climate change on water availability in the Zarrine River Basin and inflow to the Boukan Dam, Iran. Climate 2019, 7, 51.

Esquivel, M., Grünwaldt, A., Paredes, J.R. & Rodríguez–Flores, E., 2016. Vulnerabilidad al Cambio Climático de los Sistemas de Producción Hidroeléctrica en Centroamérica y sus Opciones de Adaptación, Resumen Ejecutivo; Sector de Cambio Climático y Sector de Energía, Banco Interamericano de Desarrollo (BID): Madrid, Spain, 2016; Available online: http://expertosenred.olade.org/wp-content/uploads/sites/8/2017/01/Vulnerabilidad-alcambio-climatico-de-los-sistemas-de-produccion-hidroelectrica-en-Centroamerica-y-sus-opciones-deadaptacion-1.pdf (accessed on 23 August 2019).

Falck, A.S., Maggioni, V., Tomasella, J., Vila, D.A. & Diniz, F.L.R., 2015. Propagation of satellite precipitation uncertainties through a distributed hydrologic model: A case study in the Tocantins-Araguaia basin in Brazil. J. Hydrol. 2015, 527, 943–957

FAO, 2008. Base referencial mundial del recurso suelo. Un marco conceptual para clasificación, correlación y comunicación internacional. Organización de las Naciones Unidas para la Agricultura y la Alimentación (FAO). pp. 128.

Fischer, G., Shah, M., Tubiello, F.N. & Van Velhuizen, H., 2005. Socio–economic and climate change impacts on agriculture: An integrated assessment, 1990–2080. Philos. T. Roy. Soc. B 2005, 360, 2067–2083.

Fischer, G., Nachtergaele, F., Prieler, S., Velthuizenvan, H., Verelst, L. & Wiberg, D., 2008. Agro–Ecological Zones Assessment for Agriculture (GAEZ 2008); IIASA: Laxenburg, Austria; FAO: Rome, Italy, 2008.

Flato, G.M., 2011: Earth system models: an overview. WIREs Climate Change, 2(6), 783–800, https://doi.org/10.1002/wcc.148

Fukunaga, D.C., Cecílio, R., Zanetti, S.S., Oliveira, L.T. & Caiado, M.A.C., 2015. Application of the SWAT hydrologic model to a tropical watershed at Brazil. Catena 2015, 125, 206–213.

Funk, C., Peterson, P., Landsfeld, M., Pedreros, D., Verdin, J., Shukla, S., Husak, G., Rowland, J., Harrison, L. & Hoell, A., 2015. The climate hazards infrared precipitation with stations—A new environmental record for monitoring extremes. Sci. Data 2015, 2, 150066.

Gao, J., Sheshukov, A.Y., Yen, H. & White, M.J., 2017. Impacts of Alternative Climate Information on Hydrologic Processes with SWAT: A Comparison of NCDC, PRISM and NEXRAD Datasets. Catena 2017, 156, 353–364.

Ghiggi, G., Humphrey, V., Seneviratne, S.I. & Gudmundsson, L., 2021. G-RUN ensemble: A multi-forcing observation-based global runoff reanalysis. Water Resour. Res. 2021, 57.

Good, P., Jones, C., Lowe, J., Betts, R. & Gedney, N., 2013. Comparing Tropical Forest Projections from Two Generation of Hadley Centre Earth System

Models, HadGEM2-ES and HadCM3LC. Journal of Climate, vol. 26, 495-511. https://doi.org/10.1175/JCLI-D-11-00366.1.

Green, W.H. & Ampt, G.A. (1911). Studies on soil physics, 1. The flow of air and water through soils. Journal of Agricultural Sciences 4:11-24.

Gulakhmadov, A., Che, X., Gulahmadov, N., Liu, T., Anjum, M.N. & Rizwan, M., 2020. Simulation of the Potential Impacts of Projected Climate Change on Streamflow in the Vakhsh River Basin in Central Asia under CMIP5 RCP Scenarios. Water 2020, 12, 1426. https://doi.org/10.3390/w12051426.

Gupta, H.V., Kling, H., Yilmaz, K.K. & Martinez, G.F., 2009. Decomposition of the mean squared error and NSE performance criteria: Implications for improving hydrological modelling. J. Hydrol. 2009, 377, 80–91.

Hargreaves, G. L., Hargreaves, G. H., & Riley, J. P. (1985). Agricultural benefits for Senegal River basin. Journal of irrigation and Drainage Engineering, 111(2), 113-124. https://doi.org/10.1061/(ASCE)0733-9437(1985)111:2(113).

Hargreaves, G.H., 1994. Defining and Using Reference Evapotranspiration. J. Irrig. Drain. Eng. 1994, 120, 1132–1139.

Harrigan, S., Zsoter, E., Alfieri, L., Prudhomme, C., Salamon, P., Wetterhall, F., Barnard, C., Cloke, H. & Pappenberger, F., 2020. GloFAS-ERA5 operational global river discharge reanalysis 1979–present. Earth Syst. Sci. Data 2020, 12, 2043–2060.

He, X., Pan, M., Wei, Z., Wood, E.F. & Sheffield, J., 2020. A global drought and flood catalogue from 1950 to 2016. Bull. Am. Meteorol. Soc. 2020, 101, E508–E535.

HEC, 1981. HEC-1, Flood Hydrograph Package – Users Manual. U.S. Army Corps of Engineers, Davis, California.

Hempel, S., Frieler, L., Warszawski, J., Schewe, J. & Piontek, F., 2013. A trend-preserving bias correction – the ISI-MIP approach. Earth Syst. Dynam., 4, 219–236, 2013. https://doi.org/10.5194/esd-4-219-2013.

Hersbach, H., Bell, B., Berrisford, P., Hirahara, S., Horanyi, A., Muñoz-Sabater, J., Nicolas, J., Peubey, C., Radu, R. & Schepers, D., 2020. The ERA5 global reanalysis. Q. J. R. Meteorol. Soc. 2020, 146, 1999–2049.

Hidalgo, H.G., Amador, J.A., Alfaro, E.J. & Quesada, B., 2013. Hydrological climate change projections for Central America. J. Hydrol. 2013, 495, 94–112.

Hirpa, F.A., Gebremichael, M. & Hopson, T., 2010. Evaluation of High-Resolution Satellite Precipitation Products over Very Complex Terrain in Ethiopia. J. Appl. Meteorol. Climatol. 2010, 49, 1044–1051.

Huffman, G.J., Bolvin, D.T., Nelkin, E.J., Wolff, D.B., Adler, R.F., Gu, G., Hong, Y., Bowman, K.P. & Stocker, E.F., 2007. The TRMM Multisatellite Precipitation Analysis (TMPA): Quasi-Global, Multiyear, Combined-Sensor Precipitation Estimates at Fine Scales. J. Hydrometeorol. 2007, 8, 38–55.

Hughes, D.A., 2006. Comparison of satellite rainfall data with observations from gauging station networks. J. Hydrol. 2006, 327, 399–410.

Imbach, P., Molina, L., Locatelli, B., Roupsard, O., Mahé, G., Neilson, R., Corrales, L., Scholze, M. & Ciais, P., 2012. Modeling potential equilibrium states of vegetation and terrestrial water cycle of mesoamerica under climate change scenarios. J. Hydrometeorol. 2012, 13, 665–680.

IPCC-AR5, 2014. Climate change 2013, The Physical Science Basis, Working Group I Contribution to the Fifth Assessment Report of the Intergovernmental Panel on Climate Change; Cambridge University Press: Cambridge, UK, 2014; ISBN 978-1-107-66182-0.

IPCC-AR6, 2021: Climate Change 2021: The Physical Science Basis. Contribution of Working Group I to the Sixth Assessment Report of the Intergovernmental Panel on Climate Change [Masson-Delmotte, V., P. Zhai, A. Pirani, S. L. Connors, C. Péan, S. Berger, N. Caud, Y. Chen, L. Goldfarb, M. I. Gomis, M. Huang, K. Leitzell, E. Lonnoy, J. B. R. Matthews, T. K. Maycock, T. Waterfield, O. Yelekçi, R. Yu and B. Zhou (eds.)]. Cambridge University Press. In Press.

Iversen, T., Bentsen, M., Bethke, I., Debernard, J.B., Kirkevåg, A., Seland, Ø., Drange, H., Kristjansson, J.E., Medhaug, I., Sand, M., & Seierstad, I.A., 2013. The Norwegian Earth System Model, NorESM1-M – Part 2: Climate response and scenario projections, Geosci. Model Dev., 6, 389–415, https://doi.org/10.5194/gmd-6-389-2013.

Jang, W.S., Engel, B. & Ryu, J., 2018. Efficient Flow Calibration Method for Accurate Estimation of Baseflow Using a Watershed Scale Hydrological Model (SWAT). Ecol. Eng. 2018, 125, 50–67.

Ji, L. & Duan, K., 2019. What is the main driving force of hydrological cycle variations in the semiarid and semi–humid Weihe River Basin, China? Sci. Total Environ. 2019, 684, 254–264.

Jiang, S., Ren, L., Xu, C.-Y., Yong, B., Yuan, F., Liu, Y., Yang, X. & Zeng, X., 2018. Statistical and hydrological evaluation of the latest Integrated Multi-satellitE Retrievals for GPM (IMERG) over a midlatitude humid basin in South China. Atmos. Res. 2018, 214, 418–429.

Jiang, D. & Wang, K., 2019. The Role of Satellite-Based Remote Sensing in Improving Simulated Streamflow: A Review. Water 2019, 11, 1615. https://doi.org/10.3390/w11081615.

Jiang, Q., Li, W., Fan, Z., He, X., Sun, W., Chen, S., Wen, J., Gao, J. & Wang, J., 2021. Evaluation of the ERA5 reanalysis precipitation 45dataset over Chinese Mainland. J. Hydrol. 2021, 595, 125660.

Jimeno–Sáez, P., Senent–Aparicio, J., Pérez–Sánchez, J. & Pulido–Velazquez, D., 2018. A Comparison of SWAT and ANN models for daily runoff simulation in different climatic zones of Peninsular Spain. Water 2018, 10, 192.

Jimeno-Sáez, P., Pulido-Velazquez, D.;, Collados-Lara, A.-J., Pardo-Igúzquiza, E., Senent-Aparicio, J. & Baena-Ruiz, L.A., 2020. Preliminary Assessment of the "Undercatching" and the Precipitation Pattern in an Alpine Basin. Water 2020, 12, 1061.

Jodar-Abellán, A., Pla-Bru, C. & Valdés-Abellán, J., 2019. Los modelos hidrológicos como sistemas de soporte en la toma de decisiones. Evolución histórica. Congreso Nacional del Agua 2019: innovación y sostenibilidad. Temática: aguas superficiales y subterráneas. ISBN: 978-84-1302-034-1. pp. 1269-1285

Jones, C.D., Hughes, J.K., Bellouin, N., Hardiman, S.C., Jones, G.S., Knight, J., Liddicoat, S., O´Connor, F.M., Andre, R.J., Bell, C., Boo, K.-O., Bozzo, A., Butchart, N., Cadule, P., Corbin, K.D., Doutriaux-Boucher, M., Friedlingstein, P., Gornall, J., Gray, L., Halloran, P.R., Hurtt, G., Ingram, W.J., Lamarque, J.-F., Law,

R.M., Meinshausen, M., Osprey, S., Palin, E.J., Parsons Chini, L., Raddatz, T., Sanderson, M.G., Sellar, A.A., Schurer, A., Valdes, P., Wood, N., Woodward, S., Yoshioka, M. and Zerroukat, M., 2011. The HadGEM2-ES implementation of CMIP5 centennial simulations. Geosci. Model Dev., 4, 543-570, 2011, https://doi.org/10.5194/gmd-4-543-2011.

Jones, P.D., Harpham, C., Harris, I., Goodess, C.M., Burton, A., Centella-Artola, A., Taylor, M.A., Bezanilla-Morlot, A., Campbell, J.D., Stephenson, T.S., et al., 2016. Long-term trends in precipitation and temperature across the Caribbean. Int. J. Climatol. 2016, 36, 3314–3333

Joyce, R. J., Janowiak, J.E., Arkin, P.A. and Xie, P., 2004. CMORPH: A method that produces global precipitation estimates from passive microwave and infrared data at high spatial and temporal resolution. J. Hydromet., 5, 487-503.

Jury, M.R., 2009. An Intercomparison of Observational, Reanalysis, Satellite, and Coupled Model Data on Mean Rainfall in the Caribbean. J. Hydrometeorol. 2009, 10, 413–430.

Kiros, G., Shetty, A. & Nandagiri, L., 2015. Performance evaluation of SWAT model for land use and land cover changes under different climatic conditions: A review. J. Waste Water Treat. Anal. 2015, 6, 1–6.

Knisel, W.G., 1980. CREAMS, a field scale model for chemicals, runoff and erosion from agricultural management systems. U.S. Dept. Agric. Conserv. Res. Report No. 26.

Knutti, R., Furrer, R., Tebaldi, C., Cermak, J. & Meehl, G.A., 2010. Challenges in combining projections from multiple climate models. J. Clim. 2010, 23, 2739–2758.

Kok, K. & Winograd, M., 2002. Modelling land-use change for Central America, with special reference to the impact of hurricane mitch. Ecol. Model. 2002, 149, 53–69.

Kolluru, V., Kolluru, S. & Konkathi, P., 2020. Evaluation and integration of reanalysis rainfall products under contrasting climatic conditions in India. Atmos. Res. 2020, 246, 105121.

Krysanova, V. & Arnold, J.G., 2008. Advances in ecohydrological modelling with SWAT—A review. Hydrol. Sci. J. 2008, 53, 939–947.

Krysanova, V. & Srinivasan, R., 2014. Assessment of climate and land use change impacts with SWAT. Reg. Environ. Chang. 2014, 15, 431–434.

Krysanova, V. & White, M., 2015. Advances in water resources assessment with SWAT— an overview. Hydrological Sciences Journal, 60(5), 771-783. https://doi.org/10.1080/02626667.2015.1029482.

Lakew, H.B., Moges, S.A., Anagnostou, E.N., Nikolopoulos, E.I. & Asfaw, D.H., 2019. Evaluation of global water resources reanalysis runoff products for local water resources applications: Case study-upper blue Nile basin of Ethiopia. Water Resour. Manag. 2019, 34, 2157–2177.

Lane, L.J., Ferreira, V.A. & Shirley, E.D., 1980. Estimating transmission losses in ephemeral stream channels. In Hydrology and Water Resources in Arizona and the Southwest; Arizona-Nevada Academy of Science: Las Vegas, NV, USA, 1980.

Laurenson, E.M. & Mein, R.G., 1983. RORB-Version 3: Runoff Routing Program – User Manual (2nd Edition). Department of Civil Engineering, Monash University, Monash, Australia.

Le, M.-H., Lakshmi, V., Bolten, J. & Bui, D.D., 2020. Adequacy of Satellite-Derived Precipitation Estimate for Hydrological Modeling in Vietnam Basins. J. Hydrol. 2020, 586, 124820.

Levard, C. & Basile–Doelsch, I., 2016. Geology and mineralogy of imogolite–type materials. In Nanosized Tubular Clay Minerals; Elsevier: Amsterdam, The Netherlands, 2016; pp. 49–65.

Li, D., Christakos, G., Ding, X.X. & Wu, J.P., 2018. Adequacy of TRMM satellite rainfall data in driving the SWAT modeling of Tiaoxi catchment (Taihu lake basin, China). J. Hydrol. 2018, 556, 1139–1152.

Liu, R., Xu, F., Zhang, P., Yu,W. & Men, C., 2016. Identifying Non-Point Source Critical Source Areas Based on Multi-Factors at a Basin Scale with SWAT. J. Hydrol. 2016, 533, 379–388.

Liu, Y., Wang, R., Guo, T., Engel, B.A., Flanagan, D.C., Lee, J.G., Li, S., Pijanowski, B.C., Collingsworth, P.D. & Wallace, C.W., 2019. Evaluating Efficiencies and Cost-Effectiveness of Best Management Practices in Improving

AgriculturalWater Quality Using Integrated SWAT and Cost Evaluation Tool. J. Hydrol. 2019, 577, 123965.

López-Ballesteros, A., Senent-Aparicio, J., Martínez, C. & Pérez-Sánchez, J., 2020. Assessment of Future Hydrologic Alteration Due to Climate Change in the Aracthos River Basin (NW Greece). Sci. Total Environ. 2020, 733, 139299.

Magaña, V., Amador, J.A. y Medina, S., 1999. The midsummer drought over Mexico and Central America. J. Clim. 1999, 12, 1577–1588.

Maggioni, V. & Massari, C., 2018. On the performance of satellite precipitation products in riverine flood modeling: A review. J. Hydrol. 2018, 558, 214–224.

Magris, R.A., Marta-Almeida, M., Monteiro, J.A.F. & Ban, N.C., 2019. A modelling approach to assess the impact of land mining on marine biodiversity: Assessment in coastal catchments experiencing catastrophic events (SW Brazil). Science of The Total Environment 659 (2019) 828-840. https://doi.org/10.1016/j.scitotenv.2018.12.238.

Mararakanye, N., Le Roux, J.J. & Franke, A.C., 2020. Using Satellite-BasedWeather Data as Input to SWAT in a Data Poor Catchment. Phys. Chem. Earth 2020, 117, 102871.

Marin, M., Clinciu, I., Tudose, N.C., Ungurean, C., Adorjani, A., Mihalache, A.L., Davidescu, A.A., Davidescu,S, .O., Dinca, L. & Cacovean, H., 2020. Assessing the vulnerability of water resources in the context of climate changes in a small forested watershed using SWAT: A review. Environ. Res. 2020, 184, 109330.

MARN, 2017a. Plan Nacional de Gestión Integrada del Recurso Hídrico de El Salvador, con Énfasis en Zonas Prioritarias, 1st ed.; Ministerio de Medio Ambiente y Recursos Naturales: San Salvador, El Salvador, 2017. Available online: https://cidoc.marn.gob.sv/documentos/plan-nacional-de-gestion-integrada-del-recurso-hidrico-de-el-salvador-con-enfasis-en-zonas-prioritarias/ (accessed on 19 August 2021).

MARN, 2017b. Modelos de Simulación y Escenarios Climáticos para El Salvador (Nacional, Regional y Local); Ministerio de Medio Ambiente y Recursos Naturales, Centro del Agua del Trópico Húmedo para América Latina y el Caribe:

San Salvador, El Salvador, 2017. Available online: http://rcc.marn.gob.sv/xmlui/handle/123456789/347 (accessed on 12 September 2021).

Maurer, E.P., Adam, J.C. & Wood, A.W., 2009. Climate model based consensus on the hydrologic impacts of climate change to the Rio Lempa basin of Central America. Hydrol. Earth Syst. Sci. 2009, 13, 183–194.

Mazzoleni, M., Brandimarte, L. & Amaranto, A., 2019. Evaluating precipitation datasets for large-scale distributed hydrological modelling. J. Hydrol. 2019, 578, 124076.

McKee, T.B., Doesken, N.J. & Kleist, J., 1993. The relationship of drought frequency and duration to time scales. In Proceedings of the 8th Conference on Applied Climatology, Anaheim, CA, USA, 17–22 January 1993; pp. 179–184.

McSweeney, C.F., Jones, R.G., Lee, R.W. & Rowell, D.P., 2015. Selecting CMIP5 GCMs for downscaling over multiple regions. Clim. Dyn. 2015, 44, 3237–3260.

Melo, D.d.C.D., Xavier, A.C., Bianchi, T., Oliveira, P.T.S., Scanlon, B.R., Lucas, M.C. & Wendland, E., 2015. Performance Evaluation of Rainfall Estimates by TRMM Multi-satellite Precipitation Analysis 3B42V6 and V7 over Brazil. J. Geophys. Res. Atmos. 2015, 120, 9426–9436.

Monteith, J.L., 1965. Evaporation and the environment. p. 205-234. In The state and movement of water in living organisms. 19th Symposia of the Society for Experimental Biology. Cambridge Univ. Press, London, U.K.

Moriasi, D.N., Arnold, J.G., van Liew, M.W., Bingner, R.L., Harmel, R.D. & Veith, T.L., 2007. Model evaluation guidelines for systematic quantification of accuracy in watershed simulations. Trans. ASABE 2007, 50, 885–900.

Moss, R.H., Edmonds, J.A., Hibbard, K.A., Manning, M.R., Rose, S.K., van Vuuren, D.P., Carter, T.R., Emori, S., Kainuma, M., Kram, T., Meehl, G.A., Mitchell, J.F.B., Nakicenovic, N., Riahi, K., Smith, S. J., Stouffer, R.J., Thomson, A.M., Weyant, J.P. & Wilbanks, T.J., 2010.: The next generation of scenarios for climate change research and assessment, Nature, 463, 747–756, https://doi.org/10.1038/nature08823.

Muche, M.E., Sinnathamby, S., Parmar, R., Knightes, C.D., Johnston, J.M., Wolfe, K., Purucker, S.T., Cyterski, M.J. & Smith, D., 2020. Comparison and Evaluation of Gridded Precipitation Datasets in a Kansas AgriculturalWatershed Using SWAT. J. Am. Water Resour. Assoc. 2020, 56, 486–506.

Musie, M., Sen, S. & Srivastava, P., 2019. Comparison and evaluation of gridded precipitation datasets for streamflow simulation in data scarce watersheds of Ethiopia. J. Hydrol. 2019, 579, 124168.

Nash, J.E. & Sutcliffe, J.V., 1970. River Flow Forecasting through Conceptual Models Part I—A Discussion of Principles. J. Hydrol. 1970, 10, 282–290.

NDMC, 2021. SPI Generator Software. University of Nebraska–Lincoln, USA. 2019. Available online: https://drought.unl.edu/droughtmonitoring/SPI/SPIProgram.aspx (accessed on 12 September 2021).

Neitsch, S. L., Arnold, J. G., Kiniry, J. R., & Williams, J. R. (2011). Soil and water assessment tool theoretical documentation version 2009. Texas Water Resources Institute.

Nguyen, P., Shearer, E.J., Tran, H., Ombadi, M., Hayatbini, N., Palacios, T., Huynh, P., Braithwaite, D., Updegraff, G., Hsu, K., 82 Kuligowski, B., Logan, W.S. & Sorooshian, S., 2019. The CHRS Data Portal, an easily accessible public repository for PERSIANN global 83 satellite precipitation data. Sci Data 2019, 6, 180296. https://doi.org/10.1038/sdata.2018.296.

Oliveira, P.T.S., Nearing, M.A., Moran, M.S., Goodrich, D.C.,Wendland, E. & Gupta, H.V., 2014. Trends inWater Balance Components across the Brazilian Cerrado. Water Resour. Res. 2014, 50, 7100–7114.

Opere, A.O. & Okello, B.N., 2011. Hydrologic analysis for river Nyando using SWAT. Hydrol. Earth Syst. Sci. Discuss. 2011, 8, 1765–1797.

Overland, J.E., Wang, M., Bond, N.A., Walsh, J.E., Kattsov, V.M. & Chapman, W.L., 2011. Considerations in the selection of global climate models for regional climate projections: The Arctic as a case study. J. Clim. 2011, 24, 1583–1597.

Parajuli, P.B., 2010. Assessing sensitivity of hydrologic responses to climate change from forested watershed in Mississippi. Hydrol. Process. 2010, 24, 3785–3797.

Parry, M.L., Canziani, O.F., Palutikof, J.P., Van der Linden, P.J. & Hanson, C.E., 2007. IPCC, 2007. Climate Change 2007: Impacts, Adaptation and Vulnerability. Contribution of Working Group II to the Fourth Assessment Report of the Intergovernmental Panel on Climate Change; Cambridge University Press: Cambridge, UK, 2007; p. 976.

Partal, T. & Kahya, E., 2006. Trend analysis in Turkish precipitation data. Hydrol. Process. 2006, 20, 2011–2026.

Paul, P.K., Kumari, N., Panigrahi, N., Mishra, A. & Singh, R., 2018. Implementation of cell-to-cell routing scheme in a large scale conceptual hydrological model. Environ. Model. Softw. 2018, 101, 23–33.

Pérez-Sánchez, J., Senent-Aparicio, J., Martínez Santa-María, C. & López-Ballesteros, A., 2020. Assessment of Ecological and Hydro-Geomorphological Alterations under Climate Change Using SWAT and IAHRIS in the Eo River in Northern Spain. Water 2020, 12, 1745.

Peterson, J.R. & Hamlett, J.M., 1998. Hydrologic calibration of the SWAT model in a watershed containing fragipan soils. JAWRA J. Am. Water Resour. Assoc. 1998, 34, 531–544.

Pfannerstill, M., Guse, B. & Fohrer, N., 2014. Smart low flow signature metrics for an improved overall performance evaluation of hydrological models. Journal of Hydrology, 510, 447-458. https://doi.org/10.1016/j.jhydrol.2013.12.044.

Poméon, T., Diekkrüger, B., Springer, A., Kusche, J. & Eicker, A., 2018. Multi–objective validation of SWAT for sparsely–gauged West African River basins—A remote sensing approach. Water 2018, 10, 451.

Priestley, C.H.B., & Taylor, R.J., 1972. On the assessment of surface heat flux and evaporation using large-scale parameters. Monthly weather review, 100(2), 81-92.

Pulido–Velazquez, D., García–Aróstegui, J.L., Molina, J.L. & Pulido–Velazquez, M., 2015. Assessment of future groundwater recharge in semi–arid

regions under climate change scenarios (Serral–Salinas aquifer, SE Spain). Could increased rainfall variability increase the recharge rate? Hydrol. Process. 2015, 29, 828–844.

Radcliffe, D.E. & Mukundan, R., 2017. PRISM vs. CFSR Precipitation Data Effects on Calibration and Validation of SWAT Models. J. Am. Water Resour. Assoc. 2017, 53, 89–100.

Randall, D.A., R.A. Wood, S. Bony, R. Colman, T. Fichefet, J. Fyfe, V. Kattsov, A. Pitman, J. Shukla, J. Srinivasan, R.J. Stouffer, A. Sumi & K.E. Taylor, 2007: Climate Models and Their Evaluation. In: Climate Change 2007: The Physical Science Basis. Contribution of Working Group I to the Fourth Assessment Report of the Intergovernmental Panel on Climate Change [Solomon, S., D. Qin, M. Manning, Z. Chen, M. Marquis, K.B. Averyt, M.Tignor and H.L. Miller (eds.)]. Cambridge University Press, Cambridge, United Kingdom and New York, NY, USA.

Revilla-Romero, B., Beck, H.E., Burek, P., Salamon, P., de Roo, A. & Thielen, J., 2015. Filling the gaps: Calibrating a rainfall-runoff model using satellite-derived surface water extent. Remote Sens. Environ. 2015, 171, 118–131.

Rienecker, M.M., Suarez, M.J., Gelaro, R., Todling, R., Bacmeister, J., Liu, E., Bosilovich, M.G., Schubert, S.D., Takacs, L., Kim, G.-K., et al., 2011. MERRA: NASA's Modern-Era Retrospective Analysis for Research and Applications. J. Clim. 2011, 24, 3624–3648.

Rockwood, D.M., Davis, E.D. & Anderson, J.A., 1972. User Manual for COSSARR Model. U.S. Army Engineering Division, North Pacific, Portland, Oregon.

Saha, S., Moorthi, S., Pan, H.-L., Wu, X., Wang, J., Nadiga, S., Tripp, P., Kistler, R., Woollen, J., Behringer, D., et al., 2010. The NCEP climate forecast system reanalysis. Bull. Am. Meteorol. Soc. 2010, 91, 1015–1058.

Saha, S., Moorthi, S., Wu, X., Wang, J., Nadiga, S., Tripp, P., Behringer, D., Hou, Y.-T., Chuang, H.-Y. & Iredell, M., 2014. The NCEP climate forecast system version 2. J. Clim. 2014, 27, 2185–2208.

Salmi, T., Maatta, A., Anttila, P., Airola, T.R. y Amnell, T., 2002. Detecting Trends of Annual Values of Atmospheric Pollutants by the Mann–Kendal Test

and Sen's Slope Estimates—The Excel Template Application MAKESENS; User Manual; Air Quality, Finish Meteorological Institute: Helsinki, Finland, 2002; p. 35.

Sánchez-Murillo, R., Esquivel-Hernández, G., Corrales-Salazar, J.L., Castro-Chacón, L., Durán-Quesada, A.M., Guerrero- Hernández, M., Delgado, V., Barberena, J., Montenegro-Rayo, K., Calderón, H., et al., 2020. Tracer Hydrology of the Data-scarce and Heterogeneous Central American Isthmus. Hydrol. Process. 2020, 34, 2660–2675.

Sen, P.K., 1968. Estimates of the regression coefficient based on Kendall's tau. J. Am. Stat. Assoc. 1968, 63, 1379–1389.

Senent–Aparicio, J., Pérez–Sánchez, J., Carrillo–García, J. & Soto, J., 2017. Using SWAT and fuzzy TOPSIS to assess the impact of climate change in the headwaters of the segura river Basin (SE Spain). Water 2017, 9, 149.

Senent-Aparicio, J., Liu, S., Pérez-Sánchez, J., López-Ballesteros, A. & Jimeno-Sáez, P., 2018a. Assessing impacts of climate variability and reforestation activities on water resources in the headwaters of the Segura River Basin (SE Spain). Sustainability 2018, 10, 3277.

Senent-Aparicio, J., López-Ballesteros, A., Pérez-Sánchez, J., Segura-Méndez, F. & Pulido-Velazquez, D., 2018b. Using Multiple Monthly Water Balance Models to Evaluate Gridded Precipitation Products over Peninsular Spain. Remote Sens. 2018, 10, 922.

Senent-Aparicio, J., Alcalá, F.J., Liu, S. & Jimeno-Sáez, P., 2020. Coupling SWAT Model and CMB Method for Modeling of High-Permeability Bedrock Basins Receiving Interbasin Groundwater Flow. Water 2020, 12, 657.

Senent-Aparicio, J., Jimeno-Sáez, P., López-Ballesteros, A., Giménez, J.G., Pérez-Sánchez, J., Cecilia, J.M. & Srinivasan, R., 2021. Impacts of SWAT weather generator statistics from high-resolution datasets on monthly streamflow simulation over Peninsular Spain. J. Hydrol. Reg. Stud. 2021, 35, 100826.

Sevruk, B., 1996. Adjustment of Tipping-Bucket Precipitation Gauge Measurements. Atmos. Res. 1996, 42, 237–246.

Shukla, S. & Wood, A.W., 2008. Use of a standardized runoff index for characterizing hydrologic drought. Geophys. Res. Lett. 2008, 35, L02405.

Sierra Alcocer, R., Zenteno-Jimenez, E.D. & Barrios, J., 2015. Automatic Land Use and Land Cover Classification Using RapidEye Imagery in Mexico. In Proceedings of the AAAIWorkshops Workshops at the Twenty-Ninth AAAI Conference on Artificial Intelligence, Austin, TX, USA, 25–26 January 2015.

Sikder, S., David, C., Allen, G.H., Qiao, X., Nelson, E.J. & Matin, M.A., 2019. Evaluation of available global runoff datasets through a river model in support of transboundary water management in South and Southeast Asia. Front. Environ. Sci. 2019, 7, 171.

Singh, V., Bankar, N., Salunkhe, S.S., Bera, A.K. & Sharma, J.R., 2013. Hydrological stream flow modelling on Tungabhadra catchment: Parameterization and uncertainty analysis using SWAT CUP. Curr. Sci. India 2013, 104, 1187–1199.

Singh, V. & Woolhiser, D.A., 2002. Mathematical modeling of watershed hydrology. J. Hydrol. Eng. 2002. 7:270-292. https://doi.org/10.1061/(ASCE)1084-0699(2002)7:4(270).

Skinner, C.J., Bellerby, T.J., Greatrex, H. & Grimes, D.I.F., 2015. Hydrological modelling using ensemble satellite rainfall estimates in a sparsely gauged river basin: The need for whole-ensemble calibration. J. Hydrol. 2015, 522, 110–122.

Sloan, P.G., Morre, I.D., Coltharp, G.B., & Eigel, J.D., 1983. Modeling surface and subsurface stormflow on steeply-sloping forested watersheds. Water Resources Inst. Report 142. Univ. Kentucky, Lexington.

Sofaer, H.R., Barsugli, J.J., Jarnevich, C.S., Abatzoglou, J.T., Talbert, M.K., Miller, B.W. & Morisette, J.T., 2017. Designing ecological climate change impact assessments to reflect key climatic drivers. Glob. Change Biol. 2017, 23, 2537–2553.

Soo, E.Z.X., Jaafar, W.Z.W., Lai, S.H., Islam, T. & Srivastava, P., 2019. Evaluation of Satellite Precipitation Products for Extreme Flood Events: Case Study in Peninsular Malaysia. J. Water Clim. Chang. 2019, 10, 871–892.

Spellman, P., Webster, V. & Watkins, D., 2018. Bias correcting instantaneous peak flows generated using a continuous, semi–distributed hydrologic model. J. Flood Risk Manag. 2018, 11, e12342.

Srivastava, A., Sahoo, B., Raghuwanshi, N.S. & Singh, R., 2017. Evaluation of variable-infiltration capacity model and modis-terra satellite-derived grid-scale evapotranspiration estimates in a river basin with tropical monsoon-type climatology. J. Irrig. Drain. Eng. 2017, 143, 04017028.

Srivastava, A., Deb, P. & Kumari, N., 2020. Multi-Model approach to assess the dynamics of hydrologic components in a tropical ecosystem. Water Resour. Manag. 2020, 34, 327–341.

Stisen, S. & Sandholt, I., 2010. Evaluation of remote-sensing-based rainfall products through predictive capability in hydrological runoff modeling. Hydrol. Process. 2010, 24, 879–891.

Sugawara, M., Ozaki, E., Wantanabe, I. & Katsuyama, 1976. Tank model and its application to Bird Creekm Wollombi Brook, Bihin River, Sanaga River and Nam Mune. Research Note 11, National Center for Disaster Prevention, Tokio, Japan.

Tan, M.L., Gassman, P.W. & Cracknell, A.P., 2017. Assessment of three long-term gridded climate products for hydro-climatic simulations in tropical river basins. Water 2017, 9, 229.

Tan, M.L. & Yang, X., 2020. Effect of Rainfall Station Density, Distribution and Missing Values on SWAT Outputs in Tropical Region. J. Hydrol. 2020, 584, 124660.

Tan, M.L., Gassman, P.W., Liang, J. & Haywood, J.M., 2021. A Review of Alternative Climate Products for SWAT Modelling: Sources, Assessment and Future Directions. Sci. Total Environ. 2021, 795, 148915.

Tang, X., Zhang, J., Gao, C., Ruben, G.B. & Wang, G., 2019. Assessing the uncertainties of four precipitation products for swatmodeling in Mekong River basin. Remote Sens. 2019, 11, 304.

Tarawneh, E., Bridge, J. & Macdonald, N., 2016. A pre–calibration approach to select optimum inputs for hydrological models in data–scarce regions. Hydrol. Earth Syst. Sci. 2016, 70, 4391–4407.

Tarek, M., Brissette, F.P. & Arsenault, R., 2020. Evaluation of the ERA5 reanalysis as a potential reference dataset for hydrological modelling over North America. Hydrol. Earth Syst. Sci. 2020, 24, 2527–2544.

Tian, Y., Peters-Lidard, C.D., Choudhury, B.J. & Garcia, M., 2007. Multitemporal Analysis of TRMM-based satellite precipitation products for land data assimilation applications. J. Hydrometeorol. 2007, 8, 1165–1183.

Todini, E., 1996. The ARNO Rainfall-Runoff Model. Journal of Hydrology 175(1996):339-382.

Tolera, M., Chung, I.-M. & Chang, S., 2018. Evaluation of the Climate Forecast System Reanalysis Weather Data for Watershed Modeling in Upper Awash Basin, Ethiopia. Water 2018, 10, 725.

Tubiello, F.N. & Rosenzweig, C., 2008. Developing climate change impact metrics for agriculture. Integrat. Assess. 2008, 8, 165–184.

Tuo, Y., Duan, Z., Disse, M. & Chiogna, G., 2016. Evaluation of Precipitation Input for SWAT Modeling in Alpine Catchment: A Case Study in the Adige River Basin (Italy). Sci. Total Environ. 2016, 573, 66–82.

USDA-SCS (1972). National Engineering Handbook. Section 4. Hydrology. Department of Agriculture. Soil Conservation Service. Washington.

USDA-SCS (2007). National Engineering Handbook. Chapter 19. Transmission Losses. Department of Agriculture. Soil Conservation Service. Washington.

Usman, M., Ndehedehe, C.E., Ahmad, B., Manzanas, R. & Adeyeri, O.E., 2021. Modeling streamflow using multiple precipitation products in a topographically complex catchment. Model. Earth Syst. Environ. 2021, 1–11.

Vaghefi, S.A., Abbaspour, N., Kamali, B. & Abbaspour, K.C., 2017. A toolkit for climate change analysis and pattern recognition for extreme weather conditions – Case study: California-Baja California Peninsula. Environmental Modelling & Software, Volume 96, 2017, 181-198, ISSN 1364-8152, https://doi.org/10.1016/j.envsoft.2017.06.033.

Vaghefi, S.A., Iravani, M., Sauchyn, D., Andreichuk, Y., Goss, G. & Faramarzi, M., 2019. Regionalization and parameterization of a hydrologic model significantly a ect the cascade of uncertainty in climate–impact projections. Clim. Dyn. 2019, 53, 2861–2886.

van der Knijff, J., Younis, J. & De Roo, A.P.J., 2010. LISFLOOD: A GIS-based distributed model for river basin scale water balance and flood simulation. Int. J. Geogr. Inf. Sci. 2010, 24, 189–212.

van Vuuren, D.P., Edmonds, J., Kainuma, M., Riahi, K., Rhomson, A., Hibbarb, K., Hurtt, G.C., Kram, T., Krey, V., Lamarque, J.-F, Masui, T., Meinshausen, M., Nakicenovic, N., Smith, S.J. & Rose, S.K., 2011. The representative concentration pathways: an overview. Climatic Change (2011) 109:5-31, https://doi.org/10.1007/s10584-011-0148-z.

van Vuuren, D.P. & Carter, T.R., 2014. Climate and socio-economic scenarios for climate change research and assessment: reconciling the new with the old. Clim. Change 122 (3), 415-429.

Verdin, A., Funk, C., Peterson, P., Landsfeld, M., Tuholske, C. & Grace, K., 2020. Development and validation of the chirts-daily quasi-global high-resolution daily temperature data set. Sci. Data 2020, 7, 1–14.

Verma, S., Bhattarai, R., Bosch, N.S., Cooke, R.C., Kalita, P.K. & Markus, M., 2015. Climate change impacts on flow, sediment and nutrient export in a Great Lakes watershed using SWAT. Clean Soil Air Water 2015, 43, 1464–1474.

Wada, K., 1985. The distinctive properties of Andosols. In Advances in Soil Science; Springer: New York, NY, USA, 1985; pp. 173–229.

Wang, N., Liu, W., Sun, F., Yao, Z., Wang, H. & Liu, W., 2020. Evaluating Satellite-Based and Reanalysis Precipitation Datasets with Gauge-Observed Data and Hydrological Modeling in the Xihe River Basin, China. Atmos. Res. 2020, 234, 104746.

Warszawski, L., Frieler, K., Huber, V., Piontek, F., Serdeczny, O. & Schewe, J., 2014. The Inter-Sectoral Impact Model Intercomparison Project (ISI–MIP): Project framework. PNAS March 4, 2014 111 (9) 3228-3232; https://doi.org/10.1073/pnas.1312330110.

Watanabe, S., Hajima, T., Sudo, K., Nagashima, T., Takemura, T., Okajima, H., Nozawa, T., Kawase, H., Abe, M., Yokohata, T., Ise, T., Sato, H., Kato, E., Takata, K., Emori, S. & Kawamiya, M., 2011. MIROC-ESM 2010: model description and basic results of CMIP5-20c3m experiments. Geosci. Model Dev. Discuss., 4, 1063–1128, https://doi.org/10.5194/gmd-4-845-2011.

Williams, J.R. & Hann, R.W., 1978. HYMO: Problem-Oriented Language for Hydrologic Modelling – User´s Manual. USDA, ARS-S-9.

Woldemeskel, F.M., Sivakumar, B. & Sharma, A., 2013. Merging Gauge and Satellite Rainfall with Specification of Associated Uncertainty across Australia. J. Hydrol. 2013, 499, 167–176.

Woldesenbet, T.A., Elagib, N., Ribbe, L. & Heinrich, J., 2017. Hydrological responses to land use/cover changes in the source region of the upper blue Nile Basin, Ethiopia. Sci. Total Environ. 2017, 575, 724–741.

Worku, T., Khare, D., Tripathi, S.K., 2017. Modeling Runoff–Sediment Response to Land Use/Land Cover Changes Using Integrated GIS and SWAT Model in the Beressa Watershed. Environ. Earth Sci. 2017, 76, 550.

World Meteorological Organization, 2012a. Chapter 14; Observation of present and past weather; state of the ground. In Guide to Meteorological Instruments and Methods of Observation; WMO: Geneva, Switzerland, 2012; pp. I.14–I.19. Available online: http://www.posmet.ufv.br/wp-content/uploads/2016/09/MET-474-WMO-Guide.pdf (accessed on 12 August 2021).

World Meteorological Organization, 2012b. Standardized Precipitation Index User Guide; WMO–No. 1090; WMO: Geveva, Switzerland, 2012; Available online: https://library.wmo.int/doc_num.php?explnum_id=7768 (accessed on 12 September 2021).

Wozab, D. & Jovel, J.R., 1970. Hydrological analysis of volcanic terrane: Lower basin of the rio Grande de San Miguel El Salvador. Int. Assoc. Sci. Hydrol. Bull. 1970, 15, 47–66, https://doi.org/10.1080/02626667009493953.

Yang, L., Feng, Q., Yin, Z.,Wen, X., Si, J., Li, C. & Deo, R., 2017. Identifying separate impacts of climate and land use/cover change on hydrological processes in upper stream of Heihe River, Northwest China. Hydrol. Process. 2017, 31, 1100–1112.

Yasir, M., Hu, T. & Hakeem, S.A., 2021. Impending hydrological regime of lhasa river as subjected to hydraulic interventions—a SWAT model manifestation. Remote Sens. 2021, 13, 1382.

Yatagai, A., Kamiguchi, K., Arakawa, O., Hamada, A., Yasutomi, N. & Kitoh, A., 2012. Aphrodite: Constructing a long-term daily gridded precipitation dataset for Asia based on a dense network of rain gauges. Bull. Am. Meteorol. Soc. 2012, 93, 1401–1415.

Yen, H., Wang, R., Feng, Q., Young, C.-C., Chen, S.-T., Tseng, W.-H., Wolfe III, J.E., White, M.J. & Arnold, J.G., 2018. Input uncertainty on watershed modeling_ evaluation of precipitation and air temperature data by latent variables using SWAT. Ecol. Eng. 2018, 122, 16–26.

Yin, J., Guo, S., Gu, L., Zeng, Z., Liu, D., Chen, J., Shen, Y. & Xu, C.-Y., 2021. Blending multi-satellite, atmospheric reanalysis and gauge precipitation products to facilitate hydrological modelling. J. Hydrol. 2021, 593, 125878.

Zambrano-Bigiarini, M., Nauditt, A., Birkel, C., Verbist, K. & Ribbe, L., 2017. Temporal and Spatial Evaluation of Satellite-Based Rainfall Estimates across the Complex Topographical and Climatic Gradients of Chile. Hydrol. Earth Syst. Sci. 2017, 21, 1295–1320.

Zhang, Y., You, Q., Chen, C. & Ge, J., 2016. Impacts of climate change on streamflows under RCP scenarios: A case study in Xin River Basin, China. Atmos. Res. 2016, 178, 521–534.

Zhang, X., Xu, Y., Hao, F., Li, C. & Wang, X., 2019. Hydrological components variability under the impact of climate change in a semi–arid river basin. Water 2019, 11, 1122.

Zhu, H., Li, Y., Huang, Y., Li, Y., Hou, C. & Shi, X., 2018. Evaluation and Hydrological Application of Satellite-Based Precipitation Datasets in Driving Hydrological Models over the Huifa River Basin in Northeast China. Atmos. Res. 2018, 207, 28–41.

APÉNDICE: CALIDAD DE LAS PUBLICACIONES

APÉNDICE: CALIDAD DE LAS PUBLICACIONES

Publicación 1 y 3: Water

Estadísticas de la Revista Water:

- ISSN: 2073-4441
- Fundada en 2009 (Volúmenes: 13)
- 13,088 artículos publicados
- 25,371 citas totales

Factor de impacto:

- Factor de impacto actual: 3.103
- Factor de impacto de 5 años: 3.229
- Rango de la categoría JCR 2020: 39/98 (Q2) en *Water Resources*

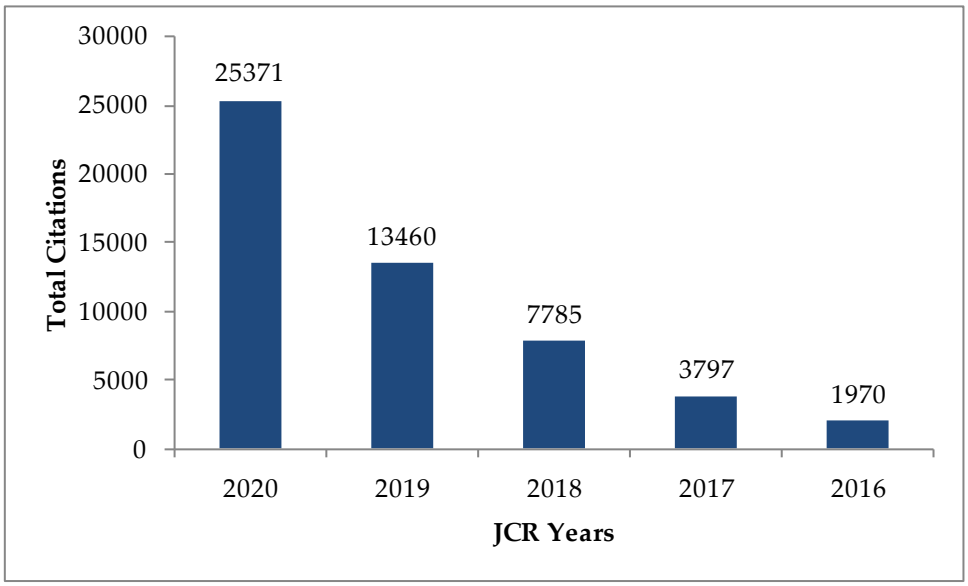

Publicación 2: Remote Sensing

Estadísticas de la Revista Remote Sensing:

- ISSN: 2072-4292
- Fundada en 2009 (Volúmenes: 13)
- 17,554 artículos publicados
- 56,704 citas totales

Factor de impacto:

- Factor de impacto actual: 4.848
- Factor de impacto de 5 años: 5.353
- Rango de la categoría JCR 2020: 27/199 (Q1) en *Geosciences*